

**Effect of In-situ CO<sub>2</sub> Sorption and Chemical Looping  
on Steam Reforming of Unconventional Gaseous  
Feedstocks**

Zainab Ibrahim Sarkin Gobir Adiya

Submitted in accordance with the requirements for the degree of  
Doctor of Philosophy

The University of Leeds  
School of Chemical and Process Engineering,

March 2017

## List of publications

The candidate confirms that the work is her own, except where work which has formed part of jointly-authored publications has been included. The contribution of the candidate and the other authors to this work has been explicitly indicated below. The candidate confirms that appropriate credit has been given within the thesis where reference has been made to the work of others.

The below jointly authored publications are based on Chapter 3, 4, 5 and 6 within this thesis. All work contained in the publications are directly attributed to the candidate. All authors are involved in editing works.

1. Zainab Ibrahim S G Adiya, Valerie Dupont and Tariq Mahmud. Chemical equilibrium analysis of hydrogen production from shale gas using sorption enhanced chemical looping steam reforming. *Fuel Processing Technology*, (2017)159, 128-144.
2. Zainab Ibrahim S G Adiya, Valerie Dupont and Tariq Mahmud. Effect of hydrocarbon fractions, N<sub>2</sub> and CO<sub>2</sub> in feed gas on hydrogen production using sorption enhanced steam reforming: Thermodynamic analysis. *International Journal of Hydrogen Energy*, (2017). [Under review].
3. Zainab Ibrahim S G Adiya, Valerie Dupont and Tariq Mahmud. Shale gas steam reforming in a packed bed reactor with and without chemical looping of nickel. [To be submitted]
4. Zainab Ibrahim S G Adiya, Valerie Dupont and Tariq Mahmud. Effect of calcium based in-situ CO<sub>2</sub> sorption and nickel chemical looping on steam reforming of shale gas. [To be submitted]
5. Zaheer Syed Abbas, Zainab Ibrahim S. G. Adiya, Robert Bloom, Valerie Dupont, Tariq Mahmud, Steve J. Milne. Novel Materials and Reforming Process Route for the Production of Ready-Separated CO<sub>2</sub>/N<sub>2</sub>/H<sub>2</sub> from Natural Gas Feedstocks. Final UKCCSRC Call Projects Showcase, London 27th June 2016.
6. Robert Bloom, Zainab Ibrahim S G Adiya, Steve J. Milne, Tariq Mahmud, Valerie Dupont. Production of Ready-Separated CO<sub>2</sub>/N<sub>2</sub>/H<sub>2</sub> from Natural Gas Feedstocks. 3rd International Conference on Chemical Looping, 8th-11th September 2014, Gothenburg, Sweden.

This copy has been supplied on the understanding that it is copy right material and that no quotation from the thesis may be published without proper acknowledgement.

©2017 The University of Leeds Zainab Ibrahim Sarkin Gobir Adiya

The right of Zainab Ibrahim Sarkin Gobir Adiya to be identified as Author of this wok has been asserted by her in accordance with the Copyright, Designs and Patents Act 1988

## Dedication

I dedicated this thesis to my parents

## Acknowledgement

In the Name of Allah (SWT), the Most Beneficent, the Most Mercifully.

All thanks and praise to Allah (SWT), The Bestower of Honours, the source of my success and happiness throughout my studies and my entire life.

I would like to express my sincere appreciation to my supervisors Dr. Valerie Dupont and Dr. Tariq Mahmud who provides constant guidance and encouragement throughout my PhD program. Your valuable comments and optimistic behaviour even when am on the wrong track have greatly contributed to the success of this work.

The support and encouragement of my colleagues and friends: Dr Gurav Nahar, Dr. Cheng Feng, Dr. Zaheer Abbas, Oluwafemi A Omoniyi, Hafizah Yun, Sergio Ramirez, Lifita Tande and Bintu Grema (including those not mention) is greatly appreciated. Great kudos to the technicians and the entire staffs of SCAPE. I am very grateful to them for taking their time to see that I learn and understand through them.

The Petroleum Technology Development Fund (PTDF Nigeria) is gratefully acknowledged for the two years scholarship. I wish to also thank Twigg Scientific & Technical Ltd (UK) for providing catalyst used in this research. I also thank the UKCCSRC EPSRC consortium ([EP/K000446/1](#)) for call 2 grant 'Novel Materials and Reforming Process Route for the Production of Ready-Separated CO<sub>2</sub>/N<sub>2</sub>/H<sub>2</sub> from Natural Gas Feedstocks'.

Lastly, my gratitude goes to family. Especially my parents, Alh Ibrahim S G Adiya and Hajiya Aishatu Ibrahim S G Adiya who through them I am what I am today. Words can't do justice to how supportive and encouraging you both were. Your love, care, support and advice in those difficult moments are unforgettable. I have nothing to pay back your kind gesture but to pray that Allah (SWT) grant you both Jannatul Firdausi. The support and encouragement from my siblings Bashar, Fah'd, Badiya and Fauziyyah S G Adiya are indeed appreciated and memorable. Great kudos to my extended family and family friends. Your prayers and good wishes are really valued.

## Abstract

Detailed chemical equilibrium analysis based on minimisation of Gibbs Energy is conducted to illustrate the benefits of integrating sorption enhancement (SE) and chemical looping (CL) together with the conventional catalytic steam reforming (C-SR) process for hydrogen production from a typical shale gas feedstock.  $\text{CaO}_{(s)}$  was chosen as the  $\text{CO}_2$  sorbent and Ni/NiO is the oxygen transfer material (OTM) doubling as steam reforming catalyst. Results are presented and compared for the separate processes of C-SR, SE-SR, CL-SR and finally the coupled SE-CLSR. Up to 49 % and 52 % rise in  $\text{H}_2$  yield and purity respectively were achieved with SE-CLSR with a lower enthalpy change compared to C-SR at S:C 3 and 800 K. A minimum energy of 159 kJ was required to produce 1 mol of  $\text{H}_2$  at S:C 3 and 800 K in C-SR process, this significantly dropped to 34 kJ/mol of produced  $\text{H}_2$  in the  $\text{CaO}_{(s)}/\text{NiO}$  system at same operating condition without regeneration of the sorbent. When the energy of regenerating the sorbent at 1170 K was included, the enthalpy rose to 92 kJ/mol  $\text{H}_2$ , i.e., significantly lower than the Ca-free system. The presence of inert bed materials in the reactor bed such as catalyst support or degraded  $\text{CO}_2$  sorbent introduced a very substantial heating burden to bring these materials from reforming temperature to sorbent regeneration temperature or to Ni oxidation temperature. The choice of S:C ratio in conditions of excess steam represents a compromise between the higher  $\text{H}_2$  yield and purity and lower risk of coking, balanced by the increased enthalpy cost of raising excess steam.

Furthermore, the effect of gas composition, inert  $\text{N}_2$  gas and  $\text{CO}_2$ , on the SE steam reforming process was also investigated. It was found that  $\text{H}_2$  yield and purity from sorption enhanced steam reforming (SE-SR) are determined by temperature S:C ratio in use, and feed gas composition in hydrocarbons  $\text{N}_2$  and  $\text{CO}_2$ . Gases with high hydrocarbons composition had the highest  $\text{H}_2$  yield and purity. The magnitude of SE effects compared to C-SR, i.e. increases in  $\text{H}_2$  yield and purity, drop in  $\text{CH}_4$  yield were remarkably insensitive to alkane (C1-C3) and  $\text{CO}_2$  content (0.1-10 vol%), with only  $\text{N}_2$  content (0.4-70 vol%) having a minor effect. Although the presence of inert ( $\text{N}_2$ ) decreases the partial pressure of the reactants which is beneficial in steam reforming, high inert contents increase the energetic cost of operating the reforming plants.

A high operating temperature and low pressure favours the C-SR and CL-SR processes while conversely a low/medium operating temperature favours the SE processes. The aim of the thermodynamic equilibrium study is to demonstrate the effect of coupling SE and CL in C-SR process as well as identify the optimum operating conditions of the studied processes.

Experimental studies to demonstrate the theoretical benefits identified in the thermodynamic equilibrium study were performed in a bench scale fixed bed reactor. The experimental study evaluates the performance of NiO based oxygen carriers on Al<sub>2</sub>O<sub>3</sub> and CaO/Al<sub>2</sub>O<sub>3</sub> support as C-SR and SE-SR catalyst as well as OTM for CL-SR and SE-CLSR processes when using a model shale gas as the feedstock. Ca based CaO sorbent was used as adsorbent for the SE processes.

High operating temperatures were found to be in favour of the strong endothermic steam reforming reaction but to the detriment of the water gas shift reaction. The effect of Ni loading and catalyst support on C-SR process comparing 18 wt. % NiO on Al<sub>2</sub>O<sub>3</sub> and 15 wt. % NiO on CaO/Al<sub>2</sub>O<sub>3</sub> was not evident in low/medium temperature range (600-650 °C). However, at higher temperature (700 and 750 °C), the NiO on CaO/Al<sub>2</sub>O<sub>3</sub> support catalyst showed better performance than the Ni on Al<sub>2</sub>O<sub>3</sub> support owing to the alkalinity of CaO suppressing solid carbon formation. The effect of SE using Ca based CaO sorbent and CL using NiO based oxygen carriers as OTM/catalyst on C-SR process was separately investigated and discussed in detail prior to coupling both processes together in a single process termed SE-CLSR process. The process (SE-CLSR) was investigated at 1 bar, GHSV 0.498, S:C 3 and 650 °C for 20 redox-oxidation-calcination cycles using CaO and 18 wt. % NiO on Al<sub>2</sub>O<sub>3</sub> as sorbent and OTM/catalyst respectively. The feedstock (shale gas) showed good reduction/reforming properties in the presence of the CaO sorbent and Ni based OTM/catalyst, with high H<sub>2</sub> yield and purity for example H<sub>2</sub> yield of 31 wt. % and purity of 92 % was obtained in the 4<sup>th</sup> cycle during the pre-breakthrough period. This was equivalent to 80 and 43 % enhancement compared to the C-SR process respectively. The experimental results were found to be away from equilibrium results which could be mainly attributed to reaction kinetics and mass transfer limitation. Comparison of the SE-CLSR process post breakthrough period with the C-SR process, shows that the SE-CLSR did not degenerate back fully to the C-SR process due to OTM/catalyst bed dilution with the sorbent material. The CaO sorbent demonstrated significant decrease in CO<sub>2</sub> adsorption capacity after the first 9 cycles due to sintering and agglomeration of particles, before stabilizing at a certain point limit to the end of the 20 cycles. An increase in the oxidation/regeneration temperature (10-25°C roughly) during the air feed was observed due to the exothermic nature of the oxidation reaction. This was accompanied with burning off of the solid carbon (coke) that had deposited on surface of the OTM/catalyst, coincidental with evolution of CO<sub>2</sub> and CO.

# Table of Contents

<b>LIST OF PUBLICATIONS</b> .....	<b>I</b>
<b>DEDICATION</b> .....	<b>III</b>
<b>ACKNOWLEDGEMENT</b> .....	<b>IV</b>
<b>ABSTRACT</b> .....	<b>V</b>
<b>TABLE OF CONTENTS</b> .....	<b>VII</b>
<b>LIST OF FIGURES</b> .....	<b>XI</b>
<b>LIST OF TABLES</b> .....	<b>XVI</b>
<b>ABBREVIATIONS</b> .....	<b>XIX</b>
<b>NOMENCLATURE</b> .....	<b>XXI</b>
<b>CHAPTER 1 INTRODUCTION</b> .....	<b>1</b>
1.1 GENERAL OVERVIEW ON HYDROGEN .....	1
1.2 HYDROGEN WITHIN PETROLEUM REFINERIES .....	6
1.3 RESEARCH BACKGROUND AND RATIONALE/MOTIVATION.....	9
1.3.1 Feedstock.....	9
1.3.2 An alternative to the conventional steam reforming process (SE-CLSR).....	11
1.3.3 Applications and maturity of research .....	16
1.4 AIMS AND OBJECTIVES.....	17
1.5 SCOPE OF RESEARCH .....	18
<b>CHAPTER 2 LITERATURE REVIEW</b> .....	<b>20</b>
2.1 HYDROGEN CONSUMERS WITHIN A REFINERY .....	20
2.1.1 Hydrotreating .....	21
2.1.2 Hydrocracking.....	33
2.1.3 Isomerization process.....	40
2.1.4 Fluid catalytic cracking .....	42
2.2 SOURCES OF HYDROGEN WITHIN THE REFINERY .....	43
2.2.1 Catalytic reforming reactions .....	44
2.2.2 Conventional Steam Methane Reforming (C-SMR) .....	50
2.2.3 Partial Oxidation (POX) .....	54
2.2.4 Auto-thermal reforming (ATR) .....	58
2.2.5 Hydrogen recovery .....	59
2.3 OTHER AVAILABLE METHODS AND FUTURE TRENDS IN HYDROGEN PRODUCTION .....	62
2.3.1 Chemical looping steam reforming (CL-SR) process .....	62
2.3.2 Sorption enhanced steam reforming process (SE-SR) .....	68
2.3.3 Sorption enhanced water gas shift (SE-WGS).....	70
2.3.4 Sorption enhanced chemical looping reforming process (SE-CLR).....	72

2.3.5 Sorption enhanced chemical looping steam reforming (SE-CLSR) .....	74
2.3.6 Hydrocarbon gasification.....	74
2.3.7 Synthesis gas .....	75
2.3.8 Pyrolysis.....	75
2.3.9 Electrolysis.....	75
2.3.10 Aqueous phase reforming .....	75
2.3.11 Photochemical water splitting.....	76
2.3.12 Thermochemical cycles (sulphur-iodine, copper-chlorine) .....	77
2.4 PREVIOUS RESEARCH ON HYDROGEN PRODUCTION.....	77
2.4.1 Conventional steam reforming.....	77
2.4.2 Chemical looping steam reforming .....	79
2.4.3 Sorption enhanced steam reforming and sorption enhanced reforming .....	80
2.4.4 Sorption enhanced chemical looping reforming and Sorption enhanced chemical looping steam reforming.....	82
2.5 SUMMARY OF LITERATURE REVIEW .....	84
<b>CHAPTER 3 RESEARCH MATERIALS AND METHODOLOGIES .....</b>	<b>87</b>
3.1 METHODOLOGY OF THERMODYNAMIC EQUILIBRIUM CALCULATION .....	87
3.1.1 Chemical equilibrium application (CEA) software .....	87
3.1.2 Methodology .....	88
3.2 MATERIALS AND METHODOLOGY OF LABORATORY EXPERIMENTS .....	98
3.2.1 Materials.....	98
3.2.2 Experimental rig .....	100
3.2.3 Standard operational procedure of the rig .....	103
3.2.4 Analysis Methods .....	104
3.2.5 Experimental procedure.....	110
3.2.6 Definition of process outputs (analysis of experimental data) .....	111
<b>CHAPTER 4 THERMODYNAMIC EQUILIBRIUM STUDIES .....</b>	<b>115</b>
4.1 INTRODUCTION AND CHEMICAL REACTIONS INVOLVED IN STEAM REFORMING .....	115
4.2 EFFECT OF TEMPERATURE AND PRESENCE OF C2-C3 FEEDSTOCK IN BOTH C-SR AND SE-SR PROCESSES .....	118
4.3 EFFECT OF STEAM TO CARBON RATIO IN STEAM REFORMING PROCESSES .....	120
4.4 SORPTION ENHANCEMENT WITH CAO SORBENT (SE-SR PROCESS).....	122
4.5 CHEMICAL LOOPING WITH NIO COUPLED WITH STEAM REFORMING (CL-SR) OF SHALE GAS .....	125
4.6 EFFECT OF STEAM TO CARBON RATION WITH GIVEN CA:C AND NIO:C RATIO IN SORPTION ENHANCED CHEMICAL LOOPING STEAM REFORMING (SE-CLSR).....	127
4.6.1 H <sub>2</sub> yield, H <sub>2</sub> purity and selectivity to carbonate.....	127
4.6.2 Enthalpy balance of SE-CLSR .....	130
4.6.3 Effect of inert materials on enthalpy balance of the cyclic processes .....	133

4.7 CARBON PRODUCT .....	136
4.8 EFFECT OF PRESSURE ON C-SR AND SE-CLSR.....	137
4.9 CONCLUSION.....	139
<b>CHAPTER 5 EXPERIMENTAL STUDIES .....</b>	<b>141</b>
5.1 INTRODUCTION TO STEAM REFORMING EXPERIMENTS.....	141
5.2 CONVENTIONAL STEAM REFORMING (C-SR) OF SHALE GAS.....	143
5.2.1 Effect of gas hourly space velocity (GHSV) on C-SR process.....	143
5.2.2 Effect of temperature on C-SR process .....	144
5.2.3 Effect of catalyst support on C-SR process .....	149
5.2.4 Characterization of fresh and reacted catalyst .....	150
5.3 SORPTION ENHANCED STEAM REFORMING (SE-SR) PROCESS OF SHALE GAS .....	154
5.3.1 Effect of temperature on SE-SR process.....	154
5.3.2 Comparison of SE-SR with C-SR process and chemical equilibrium results.....	158
5.3.3 Characterization of fresh and reacted catalyst 18 wt. % NiO on Al <sub>2</sub> O <sub>3</sub> support and sorbent during SE-SR process .....	160
5.4 CHEMICAL LOOPING STEAM REFORMING (CL-SR) PROCESS OF SHALE GAS .....	163
5.4.1 Effect of chemical looping on steam reforming process .....	163
5.4.2 Cyclic stability of output during CL-SR process.....	169
5.4.3 Catalyst/Oxygen transfer material (OTM) characterization .....	171
5.5 SORPTION ENHANCED CHEMICAL LOOPING STEAM REFORMING (SE-CLSR) .....	174
5.5.1 Effect of sorbent and chemical looping on steam reforming process.....	174
5.5.2 Comparison of SE-CLSR at post CO <sub>2</sub> breakthrough period with C-SR process.....	179
5.5.3 Cyclic stability and behavior of sorbent and OTM/catalyst during SE-CLSR process .....	180
5.5.4 SE-CLSR process materials characterization .....	181
5.6 CONCLUSION.....	183
<b>CHAPTER 6 EFFECT OF HYDROCARBON FRACTIONS, N<sub>2</sub> AND CO<sub>2</sub> IN FEED GAS ON HYDROGEN PRODUCTION .....</b>	<b>186</b>
6.1 INTRODUCTION.....	186
6.2 EFFECT OF VARYING COMPOSITION IN FEEDSTOCK ON SE-SR PROCESS OUTPUTS .....	188
6.2.1 H <sub>2</sub> yield, H <sub>2</sub> purity and selectivity to calcium carbonate product.....	188
6.2.2 Magnitude of sorption enhancement effects due to hydrocarbon content in feed gas .....	190
6.2.3 Magnitude of sorption enhancement effects due to N <sub>2</sub> and CO <sub>2</sub> content in the feed gas ....	192
6.2.4 Enhancement effects of SE-SR vs. C-SR for SG1-4 .....	195
6.2.5 Effect of temperature on SE-SR process output.....	195
6.2.6 Effect of steam to carbon ratio on process outputs.....	196
6.3 EFFECT OF INERT BED MATERIALS, HYDROCARBON FRACTIONS, INERT N <sub>2</sub> AND CO <sub>2</sub> AND ON ENTHALPY BALANCE ....	198
6.3.1 Effect of inert bed materials on energy balance .....	198

6.3.2 Effect of hydrocarbon fractions on enthalpy balance .....	199
6.3.3 Effect of N <sub>2</sub> and CO <sub>2</sub> content in the feed gas on enthalpy balance .....	201
6.4 CONCLUSION AND FINAL REMARKS.....	202
<b>CHAPTER 7 CONCLUSION AND FUTURE WORK.....</b>	<b>204</b>
7.1 CONCLUSION AND FINAL REMARKS.....	204
7.2 RECOMMENDATION AND FUTURE WORK.....	208
<b>REFERENCES .....</b>	<b>209</b>
<b>APPENDIX .....</b>	<b>226</b>
<b>APPENDIX A1: SUPPLEMENTARY DATA FOR THERMODYNAMIC EQUILIBRIUM ANALYSIS.....</b>	<b>226</b>
<b>APPENDIX A2: VALIDATION OF CEA SOFTWARE RESULTS WITH ASPEN PLUS RESULTS.....</b>	<b>228</b>
<b>APPENDIX B1: CALIBRATION RESULTS FOR MICRO GC .....</b>	<b>230</b>
<b>APPENDIX B2: ICDD REFERENCE CODE .....</b>	<b>234</b>
<b>APPENDIX B3: EDX IMAGES.....</b>	<b>235</b>
<b>APPENDIX B4: CARBON BALANCE CALCULATION .....</b>	<b>237</b>
<b>APPENDIX B5: C-SR PROCESS MAXIMUM AND AVERAGE PROCESS OUTPUTS .....</b>	<b>239</b>
<b>APPENDIX B6: SE-SR PROCESS MAXIMUM AND AVERAGE PROCESS OUTPUTS .....</b>	<b>240</b>
<b>APPENDIX B7: CL-SR PROCESS MAXIMUM AND AVERAGE PROCESS OUTPUTS .....</b>	<b>241</b>
<b>APPENDIX B8: SECL-SR PROCESS MAXIMUM AND AVERAGE PROCESS OUTPUTS.....</b>	<b>245</b>
<b>APPENDIX B9: C-SR PROCESS OUTPUTS (REPEAT EXPERIMENTS) .....</b>	<b>248</b>
<b>APPENDIX B10: SE-SR PROCESS OUTPUTS (REPEAT EXPERIMENT) .....</b>	<b>249</b>
<b>APPENDIX B11: CL-SR PROCESS OUTPUTS (REPEAT EXPERIMENTS).....</b>	<b>250</b>
<b>APPENDIX B12: SECL-SR PROCESS OUTPUTS (REPEAT EXPERIMENT) .....</b>	<b>252</b>
<b>APPENDIX C1: PROCESS DESCRIPTION DIAGRAMS .....</b>	<b>253</b>

## List of Figures

Figure 1.1 Global hydrogen consumption by sector (Lan et al., 2012) .....	2
Figure 1.2 Present hydrogen production technologies (Ewan and Allen, 2005) .....	5
Figure 1.3 Flow diagram of a high conversion refinery (Rabiei, 2012) .....	7
Figure 1.4 Schematic description of (a) C-SR, (b) SE-CLSR steps 1 & 2 Blacked out valve symbols (if any) represent closed to flow. Size of flame in furnace are commensurate to heat input from relevant combustible flow (fresh fuel vs. separation unit tail gas) (S G Adiya et al., 2017). .....	12
Figure 1.5 Industrial steam reformer tubes Left: New tubes, Middle: Fractured tubes caused by gas supply cut off after power failure, Right: Failed and damaged tubes caused by overheating (Swaminathan et al., 2008) .....	15
Figure 2.1 Schematic diagram of a typical hydrogen consumer displaying the correct source and sink position (Hallale and Liu, 2001) .....	20
Figure 2.2 Significant of feeds quality on hydrogen consumption (Anon, c2000).....	23
Figure 2.3 Naphtha hydrotreating process description (catalytic desulphurization) (Anon, c2000) .....	28
Figure 2.4 light distillate hydrotreating process description ( catalytic desulphurization) (Anon, c2000) .....	31
Figure 2.5 Typical hydrocracker operating cost (long et al., 2011).....	34
Figure 2.6 Single stage hydrocracking process(Anon, c2000).....	37
Figure 2.7 Two stage hydrocracking process (Anon, c2000) .....	39
Figure 2.8 Naphtha catalytic reformer unit semi regenerative process (Anon, c2000) .....	48
Figure 2.9 Continuous catalyst regeneration reformer (Rahimpour et al., 2013) .....	50
Figure 2.10 Present distribution of the primary energy source for hydrogen production (Ewan and Allen, 2005) .....	51
Figure 2.11 Simplified schematic of C-SR system (Barelli et al., 2008).....	52
Figure 2.12 General process flow for industrial hydrogen and syngas production (Zakkour and Cook, 2010) .....	57
Figure 2.13 Sources of refinery off gases and hydrogen purge streams (Lee et al., 2013) .....	60
Figure 2.14 Chemical looping combustion (Left) and chemical looping reforming (Right) (Pröll and Hofbauer, 2011) .....	63
Figure 2.15 Schematic illustration of chemical looping steam reforming (Ryden and Ramos, 2012) .....	65
Figure 2.16 Schematic diagram of the SE-WGS (Storset et al., 2013).....	71
Figure 2.17 Sorption Enhanced Chemical Looping reforming (Ryden and Ramos, 2012) .....	73
Figure 3.1 CEA operational procedure (Note: the red star signifies mandatory database. ‘Only’ and ‘Omit’ database are mutually exclusive).....	98
Figure 3.2 Left: Catalyst pellet Right: catalyst particles grain size 1.2 mm.....	99
Figure 3.3 Left: Calcined calcium carbonate at 915 °C for 6 hours (CaO sorbent) particle grain size 1.2 mm Right: CaO sorbent and OTM/catalyst mixture particle grain size 1.2 mm .....	100
Figure 3.4 Schematic diagram of the rig .....	101
Figure 3.5 Picture of the experimental rig .....	101
Figure 3.6 Components of the experimental rig parts (a) Gas flow controller (b) water pump (c) condenser (d) spiral condenser (e) 1 <sup>st</sup> silica gel trap (f) 2 <sup>nd</sup> silica gel trap (g) chiller .....	102
Figure 3.7 Schematic of operational procedure .....	103

Figure 3.8 Micro gas chromatography .....	105
Figure 3.9 Left: XRD equipment Right: BET equipment .....	107
Figure 3.10 Left: SEM-EDX equipment Right: CHNS equipment .....	108
Figure 3.11 Total organic carbon analyser.....	109
Figure 4.1 (a) H <sub>2</sub> yield vs temperature at 1 bar, Ca:C 1 and varied S:C ratio 0-6, Table 1 inputs (b) H <sub>2</sub> purity vs temperature at 1 bar, Ca:C 1 and varied S:C ratio 0-6, Table 1 inputs (Note: the straight line in H <sub>2</sub> yield represent the theoretical maximum) .....	119
Figure 4.2 (a) Effect of S:C ratio on H <sub>2</sub> yield and $\Delta H$ ratio vs reaction temperature at 1 bar and S:C 3, without Ca in the system, Table 1 inputs, (b) Enthalpy terms vs. temperature at 1 bar and S:C 3, without Ca in the system, Table 1 inputs (c) Selectivity of carbon to calcium carbonate vs temperature at 1 bar, Ca:C 1, and S:C 0-3, Table 1 inputs.....	121
Figure 4.3 (a) $\Delta H$ ratio vs temperature at 1 bar, Ca:C 1, and S:C 3, Table 1 inputs (b) Total enthalpy terms vs. temperature at 1 bar, Ca:C 1, and S:C 3, Table 1 inputs (c) Enthalpy terms vs. temperature at 1 bar, Ca:C 1, and S:C 3, Table 1 inputs (Note: A and B mean without and with sorbent regeneration respectively while the number 1 and 2 denotes reaction process relevant to step 1 and step 2 respectively).....	123
Figure 4.4 (a) H <sub>2</sub> yield vs temperature at 1 bar, S:C 3 and varied NiO:C 0.5-1.0, Table 1 inputs (b) H <sub>2</sub> purity vs temperature at 1 bar, S:C 3 and varied NiO:C 0.5-1.0, Table 1 inputs (c) H <sub>2</sub> yield vs temperature at 1 bar, NiO:C of 1.0 and varied S:C 0- 3, Table 1 inputs (d) H <sub>2</sub> purity vs temperature at 1 bar, NiO:C of 1.0 and varied S:C 0-3, Table 1 inputs (Note: NiO:C 0.0 denote C-SR process and the straight line in H <sub>2</sub> yield represents the theoretical maximum).....	125
Figure 4.5 (a) $\Delta H$ ratio of CL-SR vs. temperature at 1 bar, S:C 3 and NiO:C 0.0-1.0, Table 1 inputs (b) Reaction enthalpy terms and (c) Sensible enthalpy terms (gases: 298 K $\rightarrow$ T(K) under stage 1, solid: T(K) $\rightarrow$ 1100 K under stage 2) vs. temperature at 1 bar, S:C 3 and NiO:C 1.0, Table 1 inputs (Note: the numbers 1 and 2 denote reaction processes stages 1 (reductive & reforming under fuel and steam feed) and 2 (oxidative under air feed) respectively). Temperature T(K) refers to reforming temperature. (Oxidation temperature is assumed to be 1100 K in all CL-SR cases)	126
Figure 4.6 (a) H <sub>2</sub> yield vs temperature with CaO <sub>(s)</sub> sorbent at 1 bar, Ca:C 1, NiO:C 1.0 and S:C 2 and 3, Table 1 inputs (b) H <sub>2</sub> purity vs temperature with CaO <sub>(s)</sub> sorbent at 1 bar, Ca:C 1, NiO:C 1.0 and S:C 2 and 3, Table 1 inputs (Note: the straight line in H <sub>2</sub> yield represent the theoretical maximum) .....	129
Figure 4.7 Selectivity of carbon to calcium carbonate vs temperature at 1 bar, Ca:C 1, NiO:C 1.0 and S:C 2 and 3 with CaO <sub>(s)</sub> sorbent, Table 1 inputs .....	130
Figure 4.8 $\Delta H$ ratio and enthalpy terms vs. reforming temperature for SE-CLSR at 1 bar, Ca:C 1, NiO:C 1.0 and S:C 3, Table 1 inputs (a) $\Delta H$ ratio vs reforming temperature (b) Total enthalpy terms vs. reforming temperature (c) Sensible enthalpy terms vs. reforming temperature (Note: A and B mean without and with CaCO <sub>3(s)</sub> regeneration to CaO <sub>(s)</sub> at 1170 K, respectively, while the numbers 1 and 2 denote reaction process stages 1 (reductive/reforming) and 2 (oxidative/regenerating) respectively at 1170 K) .....	131
Figure 4.9 SE-CLSR: process 2 at 1170 K, active Ca:C = 1, CL-SR: process 2 at 1100 K, S:C=3, NiO:C=1, no support: NiO 100 wt%, with support: 18 wt% NiO/Al <sub>2</sub> O <sub>3</sub> , active sorbent 100% CaO, degraded sorbent: 10% CaO active, 90% inert CaO.....	134
Figure 4.10 Carbon yield at 1 bar and S:C 0-1, Table 1 inputs (a) Ca free and Ca sorbent system at Ca:C 1.0, (b) Ca free and CL-SR system at NiO:C 1.0.....	137

Figure 4.11 Effect of pressure at Ca:C 1.0, NiO:C 1.0 and S:C 3, Table 1 inputs (a) H <sub>2</sub> yield vs temperature with CaO sorbent (b) H <sub>2</sub> purity vs temperature with CaO sorbent (c) selectivity of carbon to calcium carbonate vs temperature with CaO sorbent .....	138
Figure 5.1 Effect of GHSV on H <sub>2</sub> yield and purity, fuel and H <sub>2</sub> O conversion using 18 wt. % NiO on Al <sub>2</sub> O <sub>3</sub> support at 1 bar, 650 °C and S:C 3 (average values) .....	144
Figure 5.2 Comparative analysis between experimental (average) process output and chemical equilibrium results at 1 bar, GHSV 0.498 and S:C 3 (a) using 18 wt. % NiO on Al <sub>2</sub> O <sub>3</sub> support catalyst (b) using 15 wt. % NiO on CaO/Al <sub>2</sub> O <sub>3</sub> support catalyst (Note: Solid lines are for experimental results and dashed lines for chemical equilibrium results).....	145
Figure 5.3 Comparative analysis between experimental (average) process output and chemical equilibrium results at 1 bar, GHSV 0.498 and S:C 3 (a) outlet moles using 18 wt. % NiO on Al <sub>2</sub> O <sub>3</sub> support (b) Clearer graph of CO <sub>2</sub> and CO moles out using 18 wt. % NiO on Al <sub>2</sub> O <sub>3</sub> support (c) outlet moles using 15 wt. % NiO on CaO/Al <sub>2</sub> O <sub>3</sub> support (d) Clearer graph of CO <sub>2</sub> and CO moles out using 15 wt. % NiO on CaO/Al <sub>2</sub> O <sub>3</sub> support (Note: Solid lines are for experimental results and dashed lines for chemical equilibrium results) .....	146
Figure 5.4 Process output vs time at 750 °C 1 bar, GHSV 0.498 and S:C 3 (a) H <sub>2</sub> yield and purity, fuel and H <sub>2</sub> O conversion vs time using 18 wt. % NiO on Al <sub>2</sub> O <sub>3</sub> support catalyst (b) moles out vs time using 18 wt. % NiO on Al <sub>2</sub> O <sub>3</sub> support catalyst (c) H <sub>2</sub> yield and purity, fuel and H <sub>2</sub> O conversion vs time using 15 wt. % NiO on CaO/Al <sub>2</sub> O <sub>3</sub> support catalyst (d) moles out vs time using 15 wt. % NiO on CaO/Al <sub>2</sub> O <sub>3</sub> support catalyst.....	148
Figure 5.5 Maximum process output vs temperature at 1 bar, GHSV 0.498 and S:C 3 (a) Using 18 wt. % NiO on Al <sub>2</sub> O <sub>3</sub> support catalyst (b) Using 15 wt. % NiO on CaO/Al <sub>2</sub> O <sub>3</sub> support catalyst .....	149
Figure 5.6 XRD patterns of 18 wt. % NiO on Al <sub>2</sub> O <sub>3</sub> support catalyst; peaks with circle on top represent Ni peaks, peaks with triangle on top represent superimposed NiO and Al <sub>2</sub> O <sub>3</sub> peaks, peaks with square on top represent NiO peaks while the unidentified peaks represents Al <sub>2</sub> O <sub>3</sub> .....	150
Figure 5.7 FESEM images of 18 wt. % NiO on Al <sub>2</sub> O <sub>3</sub> support catalyst (a) Fresh catalyst (b) H <sub>2</sub> reduced catalyst at 700 °C (c) reacted at 600 °C (d) reacted at 650 °C (e) reacted at 700 °C (f) reacted at 750 °C .....	152
Figure 5.8 FESEM images of 15 wt. % NiO on CaO/Al <sub>2</sub> O <sub>3</sub> catalyst (a) Fresh catalyst (b) H <sub>2</sub> reduced catalyst at 700 °C (c) reacted at 600 °C (d) reacted at 650 °C (e) reacted at 700 °C (f) reacted at 750 °C .....	153
Figure 5.9 H <sub>2</sub> yield and purity vs temperature in the pre breakthrough period at 1 bar, GHSV 0.498 and S:C 3 using 18 wt. % NiO on Al <sub>2</sub> O <sub>3</sub> support catalyst (average values).....	155
Figure 5.10 Molar production rate of CH <sub>4</sub> and H <sub>2</sub> in the pre breakthrough period at 1 bar, GHSV 0.498 and S:C 3 using 18 wt. % NiO on Al <sub>2</sub> O <sub>3</sub> support catalyst (average values).....	156
Figure 5.11 Process output vs time at 600 °C , 1 bar, GHSV 0.498 and S:C 3 (a) H <sub>2</sub> yield and purity, fuel and H <sub>2</sub> O conversion vs time using 18 wt. % NiO on Al <sub>2</sub> O <sub>3</sub> support catalyst (b) moles out vs time using 18 wt. % NiO on Al <sub>2</sub> O <sub>3</sub> support catalyst (c) clearer graph of moles out vs time using 18 wt. % NiO on Al <sub>2</sub> O <sub>3</sub> support catalyst.....	157
Figure 5.12 Comparison of SE-SR during the pre-breakthrough period with C-SR and chemical equilibrium results at 1 bar, GHSV 0.498 and S:C 3 using 18 wt. % NiO on Al <sub>2</sub> O <sub>3</sub> support catalyst (a) comparison of SE-SR and C-SR process, H <sub>2</sub> yield and purity vs temperature (average values) (b) comparison of SE-SR and chemical equilibrium, H <sub>2</sub> yield and purity vs temperature (average	

values) (Note: Solid lines are for experimental results and dashed lines for C-SR process and chemical equilibrium results as applicable)..... 158

Figure 5.13 Comparison of SE-SR process during the post breakthrough period with C-SR process at 1 bar, GHSV 0.498 and S:C 3 using 18 wt. % NiO on Al<sub>2</sub>O<sub>3</sub> support (a) average H<sub>2</sub> yield and purity, fuel and H<sub>2</sub>O conversion (b) average outlet moles vs temperature (Note: Solid lines are for experimental results and dashed lines for C-SR process) ..... 159

Figure 5.14 XRD patterns of fresh, reduced and reacted catalyst (18 wt. % NiO on Al<sub>2</sub>O<sub>3</sub> support) and sorbent mixture; peaks with cycle on top represent Ni peaks, peaks with square on top represent NiO peaks, peaks with triangle on top represent superimposed NiO and Al<sub>2</sub>O<sub>3</sub> peaks, peaks with arrow on top represent superimposed CaO and Al<sub>2</sub>O<sub>3</sub> peaks, while the unidentified peaks represents Al<sub>2</sub>O<sub>3</sub>..... 160

Figure 5.15 FESEM images of Ni on Al<sub>2</sub>O<sub>3</sub> and CaO sorbent mixture (a) Fresh catalyst and sorbent mixture (b) H<sub>2</sub> reduced catalyst and sorbent mixture at 700 °C (c) reacted mixture at 600 °C (d) reacted mixture at 650 °C (e) reacted mixture at 700 °C ..... 162

Figure 5.16 Moles out at 1 bar, GHSV 0.498 and S:C 3 (average values). (a) Reforming/reduction reaction at 650 °C and oxidation reaction at 750 °C with 18 wt. % NiO on Al<sub>2</sub>O<sub>3</sub> support as OTM/catalyst, (b) Reforming/reduction reaction at 750 °C and oxidation reaction at 750 °C with 15 wt. % NiO on CaO/Al<sub>2</sub>O<sub>3</sub> support as OTM/catalyst..... 164

Figure 5.17 Comparison of CL-SR and C-SR process H<sub>2</sub> yield and purity, fuel and water conversion at 1 bar, GHSV 0.498, S:C 3 (average values) (a) Reforming/reduction reaction at 650 °C and oxidation reaction at 750 °C with 18 wt. % NiO on Al<sub>2</sub>O<sub>3</sub> support as OTM/catalyst, (b) Reforming/reduction reaction at 750 °C and oxidation reaction at 750 °C with 15 wt. % NiO on CaO/Al<sub>2</sub>O<sub>3</sub> support as OTM/catalyst (Note: Solid lines are for experimental results and dashed lines for C-SR process) ..... 165

Figure 5.18 Comparison of CL-SR and chemical equilibrium results H<sub>2</sub> yield and purity, fuel and water conversion at 1 bar, GHSV 0.498, S:C 3 (average values) (a) Reforming/reduction reaction at 650 °C and oxidation reaction at 750 °C with 18 wt. % NiO on Al<sub>2</sub>O<sub>3</sub> support, (b) Reforming/reduction reaction at 750 °C and oxidation reaction at 750 °C with 15 wt. % NiO on CaO/Al<sub>2</sub>O<sub>3</sub> support (Note: Solid lines are for experimental results and dashed lines for chemical equilibrium results)..... 168

Figure 5.19 7<sup>th</sup> cycle process output vs time 1 bar, GHSV 0.498 and S:C 3 (a) H<sub>2</sub> yield and purity, fuel and H<sub>2</sub>O conversion vs time using 18 wt. % NiO on Al<sub>2</sub>O<sub>3</sub> support as OTM/catalyst reforming/reduction reaction at 650 °C and oxidation reaction at 750 °C (b) moles out vs time using 18 wt. % NiO on Al<sub>2</sub>O<sub>3</sub> support as OTM/catalyst reforming/reduction reaction at 650 °C and oxidation reaction at 750 °C (c) H<sub>2</sub> yield and purity, fuel and H<sub>2</sub>O conversion vs time using 15 wt. % NiO on CaO/Al<sub>2</sub>O<sub>3</sub> support as OTM/catalyst reforming/reduction reaction at 750 °C and oxidation reaction at 750 °C (d) moles out vs time using 15 wt. % NiO on CaO/Al<sub>2</sub>O<sub>3</sub> support as OTM/catalyst reforming/reduction reaction at 750 °C and oxidation reaction at 750 °C..... 170

Figure 5.20 18 wt. % NiO on Al<sub>2</sub>O<sub>3</sub> support XRD patterns; peaks with cycle on top represent NiO peaks, peak with triangle on top represent a superimposed NiO and Al<sub>2</sub>O<sub>3</sub> peak while the unidentified peaks represents Al<sub>2</sub>O<sub>3</sub> peaks. Reforming/reduction reaction at 650 °C and oxidation reaction at 750 °C ..... 171

Figure 5.21 FESEM images (a) Fresh 18 wt. % NiO on Al<sub>2</sub>O<sub>3</sub> support OTM/catalyst (b) Reacted 18 wt. % NiO on Al<sub>2</sub>O<sub>3</sub> support OTM/catalyst at 650 °C (c) Fresh 15 wt. % NiO on CaO/Al<sub>2</sub>O<sub>3</sub>

support OTM/catalyst (d) Reacted 15 wt. % NiO on CaO/Al <sub>2</sub> O <sub>3</sub> support OTM/catalyst at 750 °C .....	173
Figure 5.22 Comparison of SE-CLSR process outputs with C-SR at 1 bar, GHSV 0.498, S:C 3, reforming/reduction temperature at 650 °C and oxidation at 850 °C with CaO and NiO on Al <sub>2</sub> O <sub>3</sub> support as sorbent and OTM/catalyst respectively (average process outputs) (Note: Solid lines are for experimental results and dashed lines for C-SR process).....	175
Figure 5.23 Comparison of SE-CLSR process outputs with chemical equilibrium results at 1 bar, GHSV 0.498, S:C 3, reforming/reduction temperature at 650 °C and oxidation at 850 °C with CaO and NiO on Al <sub>2</sub> O <sub>3</sub> support as sorbent and OTM/catalyst respectively (average process outputs) (Note: Solid lines are for experimental results and dashed lines for chemical equilibrium results).....	176
Figure 5.24 Process outputs for the 4 <sup>th</sup> cycle at 1 bar, GHSV 0.498, S:C 3, reforming/reduction temperature at 650 °C and oxidation at 850 °C with CaO and NiO on Al <sub>2</sub> O <sub>3</sub> support as sorbent and OTM/catalyst respectively (a) H <sub>2</sub> yield and purity, fuel and H <sub>2</sub> O conversion vs time using 18 wt. % NiO on Al <sub>2</sub> O <sub>3</sub> support catalyst (b) moles out vs time using 18 wt. % NiO on Al <sub>2</sub> O <sub>3</sub> support catalyst (c) clearer graph of moles out vs time using 18 wt. % NiO on Al <sub>2</sub> O <sub>3</sub> support catalyst	177
Figure 5.25 Comparison of post breakthrough period of SE-CLSR with the C-SR process at 1 bar, GHSV 0.498, S:C 3, reforming/reduction temperature at 650 °C and oxidation at 850 °C with CaO and NiO on Al <sub>2</sub> O <sub>3</sub> support as sorbent and OTM/catalyst respectively (Note: Solid lines are for experimental results and dashed lines for C-SR process) .....	179
Figure 5.26 Left: Pure CaCO <sub>3</sub> Right: pure CaO sorbent (calcined at 915 °C for 4 hours) .....	181
Figure 5.27 CaO sorbent and NiO on Al <sub>2</sub> O <sub>3</sub> support OTM/catalyst mixture Left: Fresh mixture Right: mixture after 20 redox-calcination-oxidation cycles at 1 bar, GHSV 0.498, S:C 3 reforming/reduction temperature at 650 °C and oxidation at 850 °C. ....	182
Figure 5.28 18 wt. % NiO on Al <sub>2</sub> O <sub>3</sub> support XRD patterns; peaks with triangle on top represent CaO peaks, peak with square on top represent NiO peaks, peak with arrow represent superimposed NiO, CaO and Al <sub>2</sub> O <sub>3</sub> peaks, peaks with cycle on top represent superimposed NiO and Al <sub>2</sub> O <sub>3</sub> peaks, while the unidentified peaks are Al <sub>2</sub> O <sub>3</sub> peaks.....	183
Figure 6.1 Equilibrium H <sub>2</sub> yield vs temperature at 1 bar, Ca:C 1 and S:C 3 for SG1-4 using CaO <sub>(s)</sub> sorbent. Maximum H <sub>2</sub> yield by complete reaction to CaCO <sub>3(s)</sub> given in Table 1. ....	189
Figure 6.2 (a) H <sub>2</sub> purity vs temperature at 1 bar, Ca:C 1 and S:C 3 for shale gases 1-4, using CaO <sub>(s)</sub> sorbent (b) selectivity of carbon to CaCO <sub>3</sub> vs temperature at 1 bar, Ca:C 1 and S:C 3 for shale gases 1-4, using CaO <sub>(s)</sub> sorbent. Maximum H <sub>2</sub> purity by complete reaction to CaCO <sub>3(s)</sub> given in Table 1. ....	190
Figure 6.3 Enhancement effects at 1 bar, S:C 3 and Ca:C 1 compared to C-SR when using feedstocks of single alkane content (CH <sub>4</sub> / C <sub>2</sub> H <sub>6</sub> / C <sub>3</sub> H <sub>8</sub> ) at 99.5 vol.%, with 0.1 vol.% CO <sub>2</sub> and 0.4 vol.% N <sub>2</sub> (same inerts as in SG1). (a) % increase in H <sub>2</sub> yield (b) % increase in H <sub>2</sub> purity, (c) % drop in CH <sub>4</sub> yield. ....	191
Figure 6.4 Enhancement effects at 1 bar, S:C 3 and Ca:C 1 compared to C-SR when using feedstocks of single alkane content CH <sub>4</sub> , with 0.1 vol.% CO <sub>2</sub> and varying N <sub>2</sub> content between 0.4 and 70 vol.% (a) % increase in H <sub>2</sub> yield (b) % increase in H <sub>2</sub> purity,(c) % drop in CH <sub>4</sub> yield	193
Figure 6.5 Enhancement effects at 1 bar, S:C 3 and Ca:C 1 compared to C-SR when using feedstocks of single alkane content CH <sub>4</sub> , with 0.4 vol.% N <sub>2</sub> and varying CO <sub>2</sub> content between 0.1 and 40 vol.% (a) % increase in H <sub>2</sub> yield (b) % increase in H <sub>2</sub> purity, (c) % drop in CH <sub>4</sub> yield .....	194

Figure 6.6 Magnitude of enhancement effects between SE-SR and C-SR as function of N <sub>2</sub> content in the shale gases SG1-4, represented by percent increases in H <sub>2</sub> yield and purity at 800 K and % drop in CH <sub>4</sub> yield at 550 K. ....	195
Figure 6.7 Enthalpy terms for SG3, catalyst 18 wt.% NiO/Al <sub>2</sub> O <sub>3</sub> , active Ca:C 1, S:C 3 (a) ΔH ratio vs temperature, (b) and (c) enthalpy terms vs temperature: process 2 at 1170 K, “active Sorb.”: 100 % CaO, “degr. Sorb.”: 10 % active CaO and 90 % inert CaO. ....	199
Figure 6.8 ΔH total vs. temperature for 18 wt.% NiO/Al <sub>2</sub> O <sub>3</sub> catalyst, active Ca:C 1, S:C 3 and SG1-4: process 2 at 1170 K, , “active Sorb.”: 100 % CaO, “degr. Sorb.”: 10 % active CaO and 90 % inert CaO. ....	200
Figure 6.9 ΔH ratio vs temperature comparing SG1-4: for 18 wt.% NiO/Al <sub>2</sub> O <sub>3</sub> catalyst, active Ca:C 1, S:C 3 and process 2 at 1170 K; “active sorbent”: 100 % CaO, “degraded sorbent”: 10 % active CaO and 90 % inert CaO. ....	201

## List of Tables

Table 1.1 Properties of hydrogen (Cecere et al., 2014) .....	4
Table 1.2 World hydrogen demand by source (Freedonia, 2014) .....	7
Table 1.3 World hydrogen demand by market (Freedonia, 2014) .....	8
Table 1.4 Hydrogen balance for a typical refinery cases .....	8
Table 1.5 Composition of shale gas used for studies (vol. %) (Bullin and Krouskop, 2008) .....	10
Table 1.6 Estimated hydrogen production by business sector (Anon, 2008c) .....	14
Table 1.7 Commercial chemical looping combustion plants (Fan, 2014) .....	17
Table 2.1 Hydrogen consumption data for various refinery processes (Rabiei, 2012).....	21
Table 2.2 Hydrogen consumption during hydrotreating of various feedstocks (Speight and Ozum, c2002) .....	25
Table 2.3 Supplementary hydrogen consumption caused by nitrogen compound during hydrodesulphurization (Speight and Ozum, c2002) .....	25
Table 2.4 Supplementary hydrogen consumption caused by metals during hydrodesulphurization (Speight and Ozum, c2002) .....	26
Table 2.5 Representative metal content of catalyst (Speight and Ozum, c2002) .....	26
Table 2.6 Composition and properties of hydrotreating catalyst (Speight, c2007).....	27
Table 2.7 Naphtha hydrotreating operating conditions (Parkash, c2003) .....	28
Table 2.8 Naphtha hydrotreating feed (sulphur run) and product properties (Parkash, c2003) .....	29
Table 2.9 : Naphtha hydrotreating units yield (Parkash, c2003) .....	29
Table 2.10 : Naphtha hydrotreating unit utility consumption per ton of feed (Parkash, c2003) .....	30
Table 2.11 : Kerosene hydrotreating operating conditions (Parkash, c2003) .....	31
Table 2.12 Kerosene hydrotreating unit utility consumption per ton of feed (Parkash, c2003).....	31
Table 2.13 Kerosene hydrotreating unit overall yield (Parkash, c2003).....	32
Table 2.14 Purge needed for hydrotreating processes (Parkash, c2003).....	33
Table 2.15 Range of hydrocracking process conditions (Speight, 1997) .....	35
Table 2.16 Operating conditions of single-stage hydrocracker (Parkash, c2003) .....	38
Table 2.17 Utility consumption per ton of feed (Parkash, c2003) .....	38
Table 2.18 Operating conditions of mild hydrocracker (Parkash, c2003).....	39
Table 2.19 Generalizations on the effect operating conditions severity (Anon, c2000) .....	40

Table 2.20 Typical hydrogen production data for different refinery processes (Lambert et al., 1994) .....	43
Table 2.21 Typical hydrogen concentration in refinery off gases (Rabiei, 2012) .....	44
Table 2.22 Composition of catalytic reformer product gas (Speight and Ozum, c2002).....	44
Table 2.23 Catalytic reformer operating conditions (Parkash, c2003) .....	48
Table 2.24 Catalytic reformer yield (Parkash, c2003).....	48
Table 2.25 Catalytic reformer product yield, W/W (Parkash, c2003).....	49
Table 2.26 Catalytic reformer utility consumption per ton of feed (Parkash, c2003).....	49
Table 2.27 Typical operating conditions (Parkash, c2003) .....	55
Table 2.28 Partial oxidation process, overall yield (Parkash, c2003).....	56
Table 2.29 Utility consumption per ton of feed (Parkash, c2003).....	56
Table 2.30 Off gas sources and composition (Lee et al., 2013) .....	61
Table 2.31 Hydrogen recovery technologies (Patel et al., 2006).....	61
Table 2.32 Oxygen carrying capacity for different metal/metal oxide pairs (Adanez et al., 2012) .....	66
Table 2.33 Oxygen carrying capacity (RO, oxygen ratio) of various oxygen carriers (Adanez et al., 2012) .....	67
Table 2.34 Characteristics of CO <sub>2</sub> sorbent materials (Chaubey et al., 2013).....	70
Table 2.35 Comparison/properties of sorbents (Ochoa-Fernandez et al., 2007).....	70
Table 2.36 Summary on some previous work on conventional steam reforming.....	78
Table 2.37 Summary of some previous work on chemical looping steam reforming .....	80
Table 2.38 Summary of some previous work on sorption enhanced steam reforming and sorption enhanced reforming (Note: references with subscribe b denote sorption enhanced reforming process).....	82
Table 2.39 Summary of some previous work on Sorption enhanced chemical looping reforming and Sorption enhanced chemical looping steam reforming (Note: references with subscribe b denote sorption enhanced chemical looping steam reforming process).....	84
Table 3.1 Composition of shale gas used for simulation in moles, based on vol % from (Bullin and Krouskop, 2008) .....	91
Table 3.2 Characteristics of fresh catalyst .....	99
Table 4.1 Composition of shale gas used for stimulations (Bullin and Krouskop, 2008).....	115
Table 4.2 Main reactions identified in the gas-water-Ni-Ca equilibrium system (S G Adiya et al, 2017) .....	117
Table 4.3 C-SR process maximum equilibrium output (H <sub>2</sub> yield, H <sub>2</sub> purity in the dry gas, and water conversion at 1 bar and S:C 0-3, Table 1 inputs) .....	119
Table 4.4 SE-SR process maximum equilibrium outputs (H <sub>2</sub> yield, H <sub>2</sub> purity in the dry gas, selectivity of C to CaCO <sub>3(S)</sub> and water conversion at 1 bar, Ca:C 1 and S:C 0-3, Table 1 inputs).....	124
Table 4.5 Maximum equilibrium outputs of CL-SR (H <sub>2</sub> yield, H <sub>2</sub> purity in the dry gas and H <sub>2</sub> O conversion at 1 bar, NiO:C 0.5-1.0 and S:C 0-3, Table 1 inputs) .....	127
Table 4.6 Maximum equilibrium outputs of SE-CLSR (H <sub>2</sub> yield, H <sub>2</sub> purity in the dry gas, water conversion and selectivity of C to CaCO <sub>3(S)</sub> at 1 bar, Ca:C 1, NiO:C 1.0 and S:C of 2 and 3, Table 1'inputs) .....	129
Table 4.7 Equilibrium outputs comparing C-SR and SE-CLSR (H <sub>2</sub> yield, H <sub>2</sub> purity in the dry gas, water conversion and selectivity of C to CaCO <sub>3(S)</sub> at 1 bar, 800 K, Ca:C 1, NiO:C 1.0 and S:C of 2 and 3, Table 1 inputs).....	130

Table 4.8 Equilibrium outputs comparing C-SR and SE-CLSR at 800 K, Table 1 inputs ( $\Delta H$ total and $\Delta H$ ratio at 1 bar, Ca:C 1, NiO:C 1.0, and S:C 2 and 3. A and B mean without sorbent regeneration and with sorbent regeneration respectively) .....	133
Table 5.1 Composition of shale gas used for experiments (Bullin and Krouskop, 2008) .....	142
Table 5.2 Comparison between the experimental (average values) and chemical equilibrium results at 1 bar, 650 °C and GHSV of 0.498-1.393, using 18 wt. % NiO on Al <sub>2</sub> O <sub>3</sub> support catalyst .....	144
Table 5.3 C-SR process characterisation results at 1 bar, GHSV 0.498, and S:C 3 (Table 5.1 inputs) .....	151
Table 5.4 Percentage (%) enhancement of SE-SR process over C-SR process (H <sub>2</sub> yield and purity) .....	160
Table 5.5 SE-SR process characterisation results at 1 bar, GHSV 0.498 and S:C 3 using Ni on Al <sub>2</sub> O <sub>3</sub> support catalyst (table 5.1 inputs) .....	161
Table 5.6 Percentage (%) enhancement of CL-SR process with C-SR process reforming/reduction reaction at 650 °C and oxidation reaction at 750 °C using 18 wt. % NiO on Al <sub>2</sub> O <sub>3</sub> support as OTM/catalyst (H <sub>2</sub> yield and purity, fuel and water conversion). .....	166
Table 5.7 Percentage (%) enhancement of CL-SR process with C-SR process reforming/reduction reaction at 750 °C and oxidation reaction at 750 °C using 15 wt. % NiO on CaO/Al <sub>2</sub> O <sub>3</sub> support as OTM/catalyst (H <sub>2</sub> yield and purity, fuel and water conversion). .....	167
Table 5.8 CL-SR process characterisation results at 1 bar, GHSV 0.498 and S:C 3. Reforming/reduction reaction at 650 °C and oxidation reaction at 750 °C (Table 5.1 inputs) .....	172
Table 5.9 Percentage (%) enhancement of SECL-SR process over C-SR process reforming/reduction at 650 °C and oxidation at 850 °C using CaO and 18 wt. % NiO on Al <sub>2</sub> O <sub>3</sub> support as sorbent and OTM/catalyst respectively (H <sub>2</sub> yield and purity).....	178
Table 5.10 SE-CLSR process characterisation results at 1 bar, GHSV 0.498, S:C 3, reforming/reduction temperature at 650 °C and oxidation at °C 850 using CaO and Ni on Al <sub>2</sub> O <sub>3</sub> support as sorbent and OTM/catalyst respectively (Table 5.1 inputs).....	182
Table 6.1 Composition in mol % for shale gases SG1-4 used in the simulation (Bullin and Krouskop, 2008), maximum H <sub>2</sub> yield (Eq.4) and corresponding H <sub>2</sub> purity (Eq.5) in conditions of max. H <sub>2</sub> yield (Eq.4), assuming C-SR and SE-SR.....	187
Table 6.2 Maximum equilibrium outputs .....	197

## Abbreviations

API	American petroleum institute
ATR	Auto-thermal reforming
ATK	Aviation turbine kerosene
CAGR	Compound annual growth
Ca:C	Calcium to carbon ratio
CCR	Continuous catalyst regeneration reformer
CCR plant	Catalytic cracking reformer plant
CNHT	Cracked naphtha hydrotreater
CLC	Chemical looping combustion
CL-SR	Chemical looping steam reforming
CP	Chemically pure
C-SMR	Conventional steam methane reforming
C-SR	Conventional steam reforming
GWP	Global warming potential
DHT	Diesel hydrotreater
EOR	End of run
FCC	Fluid catalytic cracking
HC	Hydrocracker
HDS	Hydrotreating
HE	Heat exchanger
HP gas	Hindustan petroleum gas
HP separator	High pressure separator
IS4	Isomerisation unit
KHT	Kerosene hydrotreater
LPG	Liquefied petroleum gas

Mole %	Mole percentage
MMcf	One million Cubic feet
MMsfd	Million standard cubic feet per day
mt	Mega ton
NiO:C	Nickel oxide to carbon ratio
NHT	Naphtha hydrotreater
OTM	Oxygen transfer material
POX	Partial oxidation
ppm	Parts-per-million
PSA	Pressure swing absorption
RON	Research octane number
RO	Oxygen ratio
S:C	Steam to carbon ratio
SSCM	Standard cubic centimetre per minute
Scf/bbl	Standard cubic feet per barrel
SE-SMR	Sorption enhance steam methane reforming
SE-CLR	Sorption enhance chemical looping reforming
SE-SR	Sorption enhance steam reforming
SMR	Steam methane reforming
SOR	Start of run
SRR	Semi-regenerative catalytic reformer
TBP	True boiling point
W.A.B.T	Weighted average bed temperature
Wt.	Weight
Wt. %	Weight percentage
Vol. %	Volume percentage

## Nomenclature

Symbol	Definition	Unit
T	Temperature	K
p	Pressure	Bar
E	Energy	J
V	Volume	L
u/v	Velocity	m/s
t	Time	h
A	Specific area	m <sup>2</sup> /g
$\dot{V}$	Specific volume	cm <sup>3</sup> /g
m	Mass	kg
d	Reactor diameter	mm
$\rho$	Density	kg/m <sup>3</sup>

# Chapter 1 Introduction

*This chapter gives detail back ground and context of the research study, including rationale of research, its scope, as well as aims and objectives of the research. General overview of production and use of hydrogen (H<sub>2</sub>) within and outside petroleum refinery is given, including why there is a need for more hydrogen, hydrogen use as the fuel of future and also hydrogen general applications. In addition to these, research applications and maturity was fully and clearly discuss.*

## 1.1 General overview on hydrogen

Hydrogen is the lightest known element with the chemical symbol H and atomic number of one. At standard temperature and pressure, hydrogen is a diatomic gas with the chemical molecular formula H<sub>2</sub>. Hydrogen gas is colourless, odourless, tasteless, non-toxic, non-metallic and highly combustible (Cecere et al., 2014). Hydrogen has the best energy-to-weight ratio of any fuel and the only by product of its combustion is water without any greenhouse gas or pollutant emission in the environments (Ryden and Ramos, 2012). Hydrogen is a very important element with a vast range of application and use (Ramachandran and Menon, 1998, Anon, 2008a). It is at present being utilised in many industries, from petroleum refining and chemicals production of methanol, HCl and polypropylene, to food (production of hydrogenated vegetable oils such as butter and margarine), metallurgical, glass (to form the rim on glass) as well as electronics industries (rotor coolant for turbo generators) (Ramachandran and Menon, 1998, Anon, 2008a). Hydrogen is mainly used as a chemical feedstock in the production of, for example, petrochemicals (such as methanol and HCl), ammonia (Haber-Bosch process) in synthetic fertilizer industries (Ramachandran and Menon, 1998, Hamad et al., 2014, Cecere et al., 2014).

Ammonia is the backbone of the fertilizer industry and is manufactured by the reaction between hydrogen and nitrogen at a high pressure (50-200 bar) and temperature (650-750 °C) in the presence of a metal catalyst (usually iron promoted with K<sub>2</sub>O, CaO, SiO<sub>2</sub>, or Al<sub>2</sub>O<sub>3</sub>). The process had been suggested to be the most significant invention of the 20th century and named the 'Bellwether reaction in heterogeneous catalysis' (Vojvodic et al., 2014), also known as Haber-Bosch process. Ammonia production individually represents the largest demand of hydrogen consuming about 50 % of all the hydrogen produced in the globe (Ramachandran and Menon, 1998, Chiron et al., 2011, Harrison and Peng, 2003). Rapid growth in world population is

generating increased demand for food and providing a continued demand for agrochemicals, especially fertilizers (Anon, 2014). World-wide demand of ammonia is anticipated to raise 16 % above 2013, reaching 245 Mt in 2018 (Heffer and Prud'homme, 2014). Figure 1.1 below shows estimated world hydrogen consumption by sector depicting ammonia production as the major consumer.

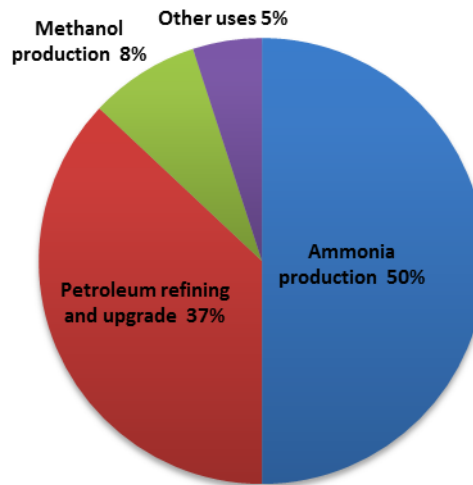


**Figure 1.1 Global hydrogen consumption by sector (Lan et al., 2012)**

Presently, over 50 million tons of hydrogen is produced worldwide with a global market value of more than 40 billion US dollars (PATH, 2011). It is estimated that the market value might increase to around 180 billion dollars owing to the advent of fuel cell technologies (PATH, 2011). This increasing market value is no doubt due to its increased utilisation in numerous industrial processes particularly in refining and petrochemical industries (PATH, 2011).

Hydrogen is also a significant reagent in petroleum refinery operations (Harrison and Peng, 2003, Ramachandran and Menon, 1998). Hydrogen production, management and recovery within petroleum refineries (area of interest in this research) is increasingly becoming important particularly in the production of low-sulphur and diesel fuels using hydrotreating and hydrocracking processes. The increasing stringent requirements on refinery products quality have effect on both hydrogen production and demand (Speight, c2007, Borges et al., 2012). 'Demand for hydrogen in the global petroleum refining market is forecast to rise 3.2% per annum to 232 billion cubic meters in 2018, remaining the dominant market segment' (Freedonia, 2014). However detail overview on hydrogen within the petroleum refinery will be discussed later in the next section.

Hydrogen is also used as raw fuel for fuel cells, which have the power to produce electricity. Low temperature fuel cells are very proficient and eco-friendly, they have increased the significance of hydrogen because they continuously need the pure supply of hydrogen and air (Kumar et al., 2002). The most vital capability of the fuel cell is that it generates pollution-free energy. A roadmap has been set by the European Union with the target of 1 GW energy generated from fuel cells by 2015 (Edwards et al., 2008). The Ministry of Economy, Trade and Industry of Japan, in June 2014 announced a “Strategic Road Map for Hydrogen and Fuel Cells” targeting to realize a carbon dioxide-free “hydrogen society” in three phases: intense expansion of hydrogen use; creation of a large-scale system for supplying hydrogen; and creation of a zero-carbon emission hydrogen supply system throughout the production process (D’Orazio et al., 2015).

Growing energy demands and pollution growth are also making hydrogen an attractive alternative energy carrier. Hydrogen is extensively regarded as the fuel of the future (Ramage, 2008, Holladay et al., 2009, N. Jhaveri et al., 2014), with ability to fuel the generation of electricity without releasing detrimental pollutants such as (CO<sub>2</sub> and hydrocarbons) (Chiron et al., 2011). As time passes by, hydrogen might turn out to be the general purpose carrier of energy for electricity and power generation, and in vehicles as transportation fuel (Abrardo et al., 1995, Liguras et al., 2003, Cecere et al., 2014). Hydrogen energy systems are directly connected to the development of a few key sectors (D’Orazio et al., 2015). For example, ‘in India, the National Hydrogen Energy Board and the Ministry of New and Renewable energy lunched in 2006 the national hydrogen energy road map for 2007-2020, covering the fields of hydrogen production, hydrogen storage, hydrogen application in power generation, hydrogen application in automobiles, and hydrogen system integration (D’Orazio et al., 2015). In January 2012, New Delhi launched the first fleet of hydrogen-fueled 3-wheeler rickshaws. Where the 3-wheeler rickshaw fleet operates, a hydrogen refuelling station has been also established. It was a cooperative project developed by Indian partners for the Indian transport sector, costing about 1 million US dollar, with 0.5 million US dollar of co-funding coming from the United Nations Industrial Development Organization’ (D’Orazio et al., 2015). China also launched the world's first hydrogen powered tram in April 2015. It is powered completely by hydrogen fuel cells and it takes just 3 minutes to refuel to cover 100 km (D’Orazio et al., 2015). In Africa the efforts of hydrogen research are getting tangible results (D’Orazio et al., 2015). To name an example, in November 2014 the University of Western Cape, in cooperation with a local company, launched a prototype hydrogen fuel cell power generator which has the ability to provide electricity for the whole university building (D’Orazio et al., 2015). The Tokyo Metropolitan Government in

January 2015 declared an investment plan for 40 billion yen (400 million US dollars) for renewable-based hydrogen fuel infrastructure and fuel cell buses with 35 hydrogen stations operative for the 2020 Tokyo Olympics (D'Orazio et al., 2015).

'Increased manufacturing output in countries such as China and India will drive demand for hydrogen in such industries as metal processing and glass production' (Freedonia, 2014). Increasing incomes expected in all the developing economies will promote growth in the world-wide electronics industry, as well as the demand for hydrogen employed in electronics production (Freedonia, 2014). Thus, shortage of hydrogen and construction of new hydrogen plants will become more severe and important in the future to come (Aitani, 1996, Alves and Towler, 2002).

It is also worth mentioning that hydrogen is also being used as a fuel in aerospace applications, as oxygen scavenger in metallurgical processes, and also as an electron donor in various oxide materials (Cecere et al., 2014). Hydrogen properties such as its viscosity and thermal conductivity designates good heat transfer attributes, while there are also indications of good combustion characteristics from the use of hydrogen in spark ignition engines (Yamin, 2007, Cecere et al., 2014). However, the low density of hydrogen indicates that its heating or calorific value would be low on a volumetric basis (Eziroglu and Barbir, 1998).

**Table 1.1 Properties of hydrogen (Cecere et al., 2014)**

<b>Properties</b>	
Molecular weigh	2.016
Density at 1 atm and 300 K (kg/m <sup>3</sup> )	0.082
Stoichiometric composition in air (% Volume)	29.53
Boiling Temperature (K)	20.3
Research Octane Number	130
Thermal conductivity at 300 K (mW/m K)	182
Flammability Limits (% Volume)	4-75
Minimum Ignition Energy (mJ)	0.02
Auto-ignition Temperature (K)	858
Specific Heat (kJ/(KgK))	14.89
Critical Point Temperature (K)	32.94
Critical point Pressure (Bar)	12.84

There are various ways of producing hydrogen, however Steam methane reforming (SMR) is the most established and commonly used process to produce hydrogen on a large scale (Rostrup-Nielsen et al., 2000). Approximately, 48 % of the world's overall hydrogen production is by SMR

of fossils fuels (Lan et al., 2012). The process (SMR), consist of mainly two basic steps followed by separation. In the first stage; water (in the form of high-temperature steam) reacts with feedstock (mainly natural gas) to generate syngas ( $\text{CO}$ ,  $\text{CO}_2$ ,  $\text{H}_2\text{O}$ ,  $\text{H}_2$ ) in the presence of nickel oxide catalyst at elevated temperature (almost  $800\text{--}950\text{ }^\circ\text{C}$ ) and medium pressure (at  $20\text{--}35\text{ atm}$ ) (Rosen, 1991, Pasel et al., 2015). In the second stage, the exothermic water gas shift (WGS) reaction runs at a lower temperature (almost  $200\text{--}400^\circ\text{C}$ ) (Adris et al., 1996, Fernández et al., 2012). Although the latter reaction is exothermic, the overall energy demand of the process is significantly endothermic, requiring part of the natural gas to burn in a furnace which houses the reformer reactors. Separation of the hydrogen from the syngas leaving the water–gas shift reactor (mostly unreacted  $\text{CH}_4$ ,  $\text{CO}$ ,  $\text{H}_2\text{O}$ , and  $\text{CO}_2$ ) is the final stage (S G Adiya et al., 2017). Numerous techniques can be used to undertake separation. Three of the most common techniques used are; pressure swing absorption (PSA), membranes, and cryogenics (Patel et al., 2006, Lee et al., 2013). Chemical absorption for example  $\text{CO}_2$  scrubbing using methyldiethanolamine (MDEA) and monoethanolamine (MEA) are also used for separation (Yildirim et al., 2012).

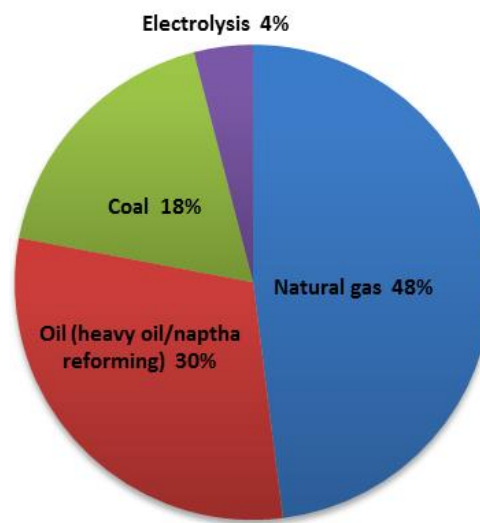


**Figure 1.2 Present hydrogen production technologies (Ewan and Allen, 2005)**

Steam reforming can also form the first step in the Fischer Tropsch process, which converts natural gas to gasoline-like liquid fuel (Pérez-Moreno et al., 2013). Other trends and available methods of hydrogen production include partial oxidation, auto-thermal reforming, electrolysis, gasification process, sorption enhanced steam reforming, and chemical looping steam reforming (Chaubey et al., 2013). Full details of hydrogen production technologies can be found in Chapter 2 of this thesis. Figure 1.2 present hydrogen production technologies depicting conventional steam reforming (C-SR) as the major hydrogen production route.

## 1.2 Hydrogen within petroleum refineries

Hydrogen production, management and recovery within petroleum refineries is increasingly becoming important particularly in the production of low-sulphur and diesel fuels using hydrotreating and hydrocracking processes (Speight, c2007, Borges et al., 2012, Antzaraa et al., 2015). Due to the increasing use of heavier crude oils, containing greater quantity of sulphur and nitrogen and the need to meet strict emission standards, hydrogen requirement is undergoing a very rapid increase in refineries. The increasing stringent requirements of refinery products quality have effect on both hydrogen demand and production. As more severe product specifications come into effect, a typical refinery is either been 'bottlenecked' due to lack of hydrogen or will be in the future (Simonsen et al., 1992). Perhaps hydrogen is the most significant utility in a modern petroleum refinery (Castañeda et al., 2011). Fluctuations in crude and product slates (refinery products) from the original design can make it challenging for even a new refinery to function proficiently. For existing refineries, it is predominantly vital to enhance hydrogen utilization (because of refiners' desire to maximize the yield of fuels from heavier crude oil) and improve existing transformation facilities (catalytic reforming and SMR units). Based on the findings from a literature review conducted in this project, (more details in Chapter 2 of this thesis), hydrotreating and hydrocracking are not the only consumers of hydrogen in the refinery, other hydrogen consumers include crude distillation unit (CDU), vacuum distillation unit (VDU), fluid catalytic cracking (FCC), coker, sweetening, lubricants plants, petrochemical processes and isomerization processes that can be incorporated into the refinery hydrogen network (Rabiei, 2012). Figure 1.3 is a simplified flow diagram of a refinery highlighting the hydrogen consuming processes. Hydrogen consumption during hydroprocessing (hydrotreating and hydrocracking processes) is reliant upon the feedstock properties, impurities to be removed (e.g sulphur, aromatic, and olefin molecules), conversion level, and catalyst properties (Ancheyta and Speight, 2007, Castañeda et al., 2011).

'Demand for hydrogen in the global petroleum refining market is forecast to rise 3.2% per annum to 232.0 billion cubic meters in 2018, remaining the dominant market segment' (Freedonia, 2014). This will be driven by the growing need for hydrogen in hydroprocessing processes (hydrocracking and hydrotreating), and other processes resulting from deteriorating crude oil quality; refiners desire to maximize the yield of fuels from heavier crude oil, and the requirement for low-sulfur and ultra-low sulfur diesel (ULSD) fuels in various regions of the world (Freedonia, 2014). Demand will also increase owing to the fact that new refineries are

constructed with hydrocrackers, and upgrades at some existing refineries are anticipated to include them (Freedonia, 2014).

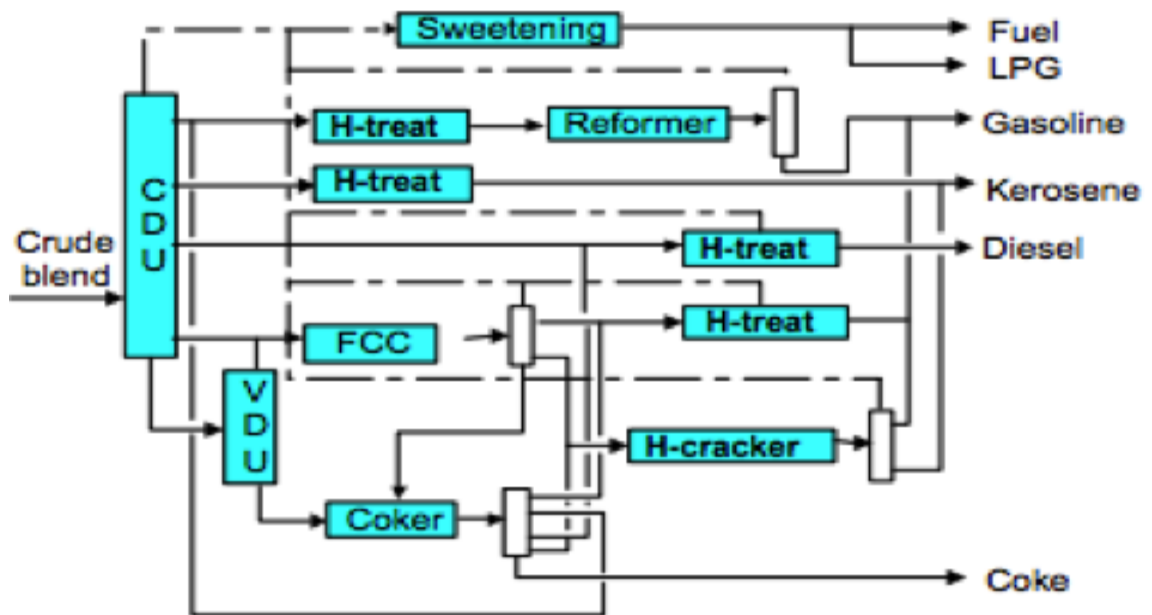


Figure 1.3 Flow diagram of a high conversion refinery (Rabiei, 2012)

Even though the 2018 increase from hydrotreating is the effect of rising demand for diesel fuel, clean fuel regulations will also increase demand, especially in countries that do not presently implement stringent regulations on sulphur in fuels (Freedonia, 2014). Global demand for merchant hydrogen (Hydrogen purchased from third parties or / industrial gas companies) is projected to advance 5.3 % annually through 2018 (Freedonia, 2014). Captive hydrogen (hydrogen produced and used within a facility, particularly in petroleum refineries) demand worldwide has reached 184.0 billion cubic meters in 2013, up from 159.7 billion cubic meters in 2008 (Freedonia, 2014). Table 1.2 and 1.3 below depicted world hydrogen demand by source and market respectively (Freedonia, 2014). (It is significant to point out that hydrogen consumed for ammonia and methanol production is excluded in this section. Section encompass petroleum refining mainly, chemical production, and other markets for example metal processing, glass production, and electronics).

Table 1.2 World hydrogen demand by source (Freedonia, 2014)

Item	2008	2013	2018	CAGR % 13/08	CAGR % 18/13
Hydrogen demand	218.0	254.5	302.5	3.1	3.5
Captive production	159.7	184.0	211.4	2.9	2.8
Merchant sales	58.3	70.5	91.1	3.9	5.3

**Table 1.3 World hydrogen demand by market (Freedonia, 2014)**

Item	2008	2013	2018	CAGR % 13/08	CAGR % 18/13
Hydrogen demand	218.0	254.5	302.5	3.1	3.5
Petroleum refining	172.5	198.0	232.0	2.8	3.2
Chemical manufacturing	24.8	30.7	38.8	4.4	4.8
Other markets	20.7	25.8	31.1	4.5	4.2

Hydrogen in refineries is produced in part by catalytic reforming of naphtha (main product: cracked fractions, by-product: H<sub>2</sub>) and by steam reforming (synthesis gas; main product: H<sub>2</sub>, by-product: CO, CO<sub>2</sub> and H<sub>2</sub>O), and to a much smaller extent by partial oxidation and autothermal reforming are used (Speight, c2007, Rabiei, 2012). Feedstocks for steam reforming in refineries vary from gases (associated gases, 'flare' gas, or natural gas) to naphtha (Hao, 1996, Turpeinen et al., 2008). Full details on the refinery hydrogen production route can be found in Chapter 2 of this thesis.

In order to leave no stone unturned with respect to hydrogen production and consumption in the refinery, three case studies that represent real refinery hydrogen networks from different plants were investigated, but certain information was disguised for confidentiality. Two cases from (Hallale and Liu, 2001) and (Birjandia et al., 2014) respectively showed that there are need for supplementary hydrogen in both refineries, obtained through hydrogen plant. The third case scenario from (Deng et al., 2014) demonstrated that in addition to the on-site hydrogen plant in the refinery, supplementary hydrogen requirement is also fulfilled via importation. Table 1.4 below depicts a hydrogen balance (current and maximum flow rate) of the refinery cases. More details can be found in the given references. Feedstocks used in the hydrogen plants were not given non was the technology of hydrogen production in case study 1 and 3 given. However, it is most likely that steam reforming of natural gas was employed in both cases.

**Table 1.4 Hydrogen balance for a typical refinery cases**

<b>Case study 1 (Hallale and Liu, 2001)</b>			
Process	Flow rate	Maximum flow rate	Purity (V % H <sub>2</sub> )
Catalytic reforming unit	23.50 (MMscfd)	23.50 (MMscfd)	75.0
Hydrogen plant	45.00 (MMscfd)	50.00 (MMscfd)	92.0
<b>Case study 2 (Deng et al., 2014)</b>			
Catalytic reforming unit	33,530 (Nm <sup>3</sup> /h)	33,530 (Nm <sup>3</sup> /h)	80
Steam reforming unit	50,303 (Nm <sup>3</sup> /h)	50,303 (Nm <sup>3</sup> /h)	93
Import	22,353 (Nm <sup>3</sup> /h)	27,942 (Nm <sup>3</sup> /h)	95
<b>Case study 3 (Birjandia et al., 2014)</b>			
Catalytic reforming unit	59,000 (Nm <sup>3</sup> /h)	65,000 (Nm <sup>3</sup> /h)	92
Hydrogen plant	40,500 (Nm <sup>3</sup> /h)	90,000 (Nm <sup>3</sup> /h)	76

## **1.3 Research Background and Rationale/Motivation**

### **1.3.1 Feedstock**

All hydrocarbon fuels from natural gases to shale gases, associated gases, or 'flare' gas can be used in hydrogen production. Gas feedstock compositions are characterised by a significant hydrocarbons content with carbon number from 2 to 6, in addition to the main component methane, as well as greatly varying contents in N<sub>2</sub>, CO<sub>2</sub>, H<sub>2</sub>S according to their source (Turpeinen et al., 2008). Natural gas has been recently publicised as a bridge fuel to a low carbon future due to its favourable hydrogen-to-carbon ratio and newly developed technologies to tap enormous amount of the gas, that was previously inaccessible worldwide reserves (Kargbo et al., 2010, Paltsev et al., 2011, Anderson et al., 2014). With the newly found abundance of natural gas, that is readily available and can be supplied at a competitive cost, natural gas will remain a very significant energy mix (Nicholls et al., 2012, Anderson et al., 2014). Natural gas is the one and only fossil fuel in which demand rose in all the three of the International Energy Agency's (IEA) (Nicholls et al., 2012). A boom in the shale gas (a form of natural gas found trapped within shale formation) production (Peng, 2014) in the world also foresees that gas will remain the main feedstock for steam reforming in the near term, in contrast to naphtha (Catalytic reforming feedstock) which is declining due to high availability of natural gas (Beyer et al., 2005, Peng, 2014). In 2013, the Annual Energy Outlook projected that the U.S (world largest producer of shale gas) natural gas production will increase by an estimate of 44 % over the next 30 years. Enormous amount of this projected increase is expected from shale gas extraction. Shale gas is also expected to grow from 7.8 million MMcf (million cubic feet) extracted in 2011, to 16.7 million MMcf in 2040. In future, shale gas production in the U.S is anticipated to rise, whereas all other extraction methods such as coal and natural gas extraction are likely to remain steady or decline (Anon, 2013, Anon, 2015). Furthermore, many developed countries have extensive natural gas storage and distribution networks which can act as energy storage and transport facilities of natural gas with lower losses than their electricity grids, which positions gas as an attractive energy carrier (e.g. UK). The use of natural gas fuelled vehicles and natural gas power stations is also increasing in the world.

Generally speaking, 90% of the global hydrogen originates from fossil fuels. At present, natural gas is the major feedstock of hydrogen production (Ding and Alpay, 2000, Johnsen and Rostrup-Nielsen, 2002). This perspective formulates the basis of using varied composition of shale gas as feedstock in this study. The selected feedstock model composition was based on values

found in the literature. Both compositions are actual shale gas composition from the United States (Bullin and Krouskop, 2008). Shale gas termed '1' is from a Marcellus shale which lies in western Pennsylvania, Ohio and West Virginia. The gas composition differs across the field, becomes richer from east to west. Shale gas termed '2', '3' and '4' are from Antrim shale (a shallow shale) in Michigan, U.S. The Antrim shale is unique due to the fact that its gas is predominately biogenic (methane is generated as a by-product of bacterial consumption of organic material in the shale) (Bullin and Krouskop, 2008). Full details on the gases can be found on Bullin and Krouskop (Bullin and Krouskop, 2008). In addition, Shale gas termed '1' was chosen because it represents a typical composition of natural gas, containing roughly up to 80 % of methane with roughly 20 % higher hydrocarbons (>C3), CO<sub>2</sub> and inert gas (Mokhatab and Poe, 2012), representing a mixture rich in ethane and propane. Shale gas '1' and '2' can also represent typical composition of Nigerian (Sonibare and Akeredolu, 2004) and UK North sea (Peebles, 1992) natural gas containing up to 80 % methane and Lacq France natural gas containing up to 70 % methane (Peebles, 1992) respectively. Shale gas '3' and '4' compositions correspond to typical composition of gases with relatively low hydrocarbon and high inert (N<sub>2</sub>) content. The later will also help in accessing the effect of inert gases in H<sub>2</sub> production.

Furthermore, to date, investigation on a typical/actual gas composition containing higher hydrocarbons, inert gas and CO<sub>2</sub> has not been investigated, including in the so called 'matured' C-SR process. Researchers, for example; Anderson et al (Anderson et al., 2014) and Ryden et al (Ryden and Ramos, 2012) mainly focused on methane or a single hydrocarbon gas such as propane by e.g. Wang et al (Wang et al., 2011). Table 1.5 depicts composition of shale gas used in the studies.

**Table 1.5 Composition of shale gas used for studies (vol. %) (Bullin and Krouskop, 2008)**

Composition	Shale gas '1'	Shale gas '2'	Shale gas '3'	Shale gas '4'
CH <sub>4</sub>	79.4	77.5	57.3	27.5
C <sub>2</sub> H <sub>6</sub>	16.1	4.0	4.9	3.5
C <sub>3</sub> H <sub>8</sub>	4.0	0.9	1.9	1.0
CO <sub>2</sub>	0.1	3.3	0.0	3.0
N <sub>2</sub>	0.4	14.3	35.9	65.0
Total	100	100	100	100

### 1.3.2 An alternative to the conventional steam reforming process (SE-CLSR)

Despite having reached technological maturity, steam reforming (major hydrogen production route) is one of the most energy consuming processes in hydrocarbon processing and ammonia production due to its heating requirement with additional disadvantages such as greenhouse gas emission, high operational and maintenance costs, low efficiency at small scales due to heat transfer limitations, and coke formation (Kumar et al., 2002).

The integration of steam reforming with Sorption enhancement (i.e., process with in situ CO<sub>2</sub> capture which shifts chemical equilibria) and chemical looping (i.e., oxygen for oxidative heat is provided by a solid material undergoing redox cycles as opposed to combustion) in one single process is called sorption enhanced chemical looping steam reforming (SE-CLSR). The material bed consists of a mixture of particles comprising solid oxygen carrier (e.g. NiO) and CO<sub>2</sub> sorbent (e.g. CaO). The reforming reactor normally operates at a low/medium temperature 527-627 °C (800-880 K), partially reducing the fuel with the oxygen provided by oxygen carrier and steam reforming most of the fuel, and at the same time any CO<sub>2</sub> produced during the process is captured by the CO<sub>2</sub> sorbent, causing sorption enhanced steam reforming. The overall reaction in the reduction/reforming reactor is thermo-neutral (Lyngfelt et al., 2001, Ryden and Ramos, 2012) owing to the strongly exothermic carbonation reaction. The SE-CLSR process could in principle be self-sufficient with regard to energy because the required heat for the endothermic steam reforming and reduction reactions could be provided by the exothermic sorbent carbonation reaction, while the heat from re-oxidation of the OTM is utilised for sorbent regeneration (Antzara et al., 2015) in a separate time step. Hence, this could mean near complete elimination of dependency on flue gas use to provide reformer heat at steady state operation. Figure 1.4 depicts the SE-CLSR process, with step 1 consisting of the combined OTM reduction, H<sub>2</sub> production under gas and steam flow with in situ CO<sub>2</sub> capture by the sorbent, and step 2 carrying out the coupled OTM oxidation under air flow and CO<sub>2</sub> sorbent calcination. It is suggested that a smaller scale separation process be used, owing to the fact that nearly pure H<sub>2</sub> can be generated in step 1 of the process under well chosen operating conditions. Another capital cost reducing aspect is that instead of needing to use an assembly of many long thin reformer tubes exposed to harsh combustion environments, the reformer could be a single reactor making little use of external heat (e.g. for startup only). The benefits of intensifying the C-SR process by using SE-CLSR technology are pointed out in Fig. 1.4 (a) in comparison to Fig. 1.4 (b), where the furnace and WGS reactor are no longer required, the energy content of the separation gases is used to run (as an example) a combustor/gas turbine-generator, the 'squat'

reformer aspect and the reduced separation stage all permit economical downsizing and potentially co-generation. In addition potentially sources of leakages between units is also eliminated.

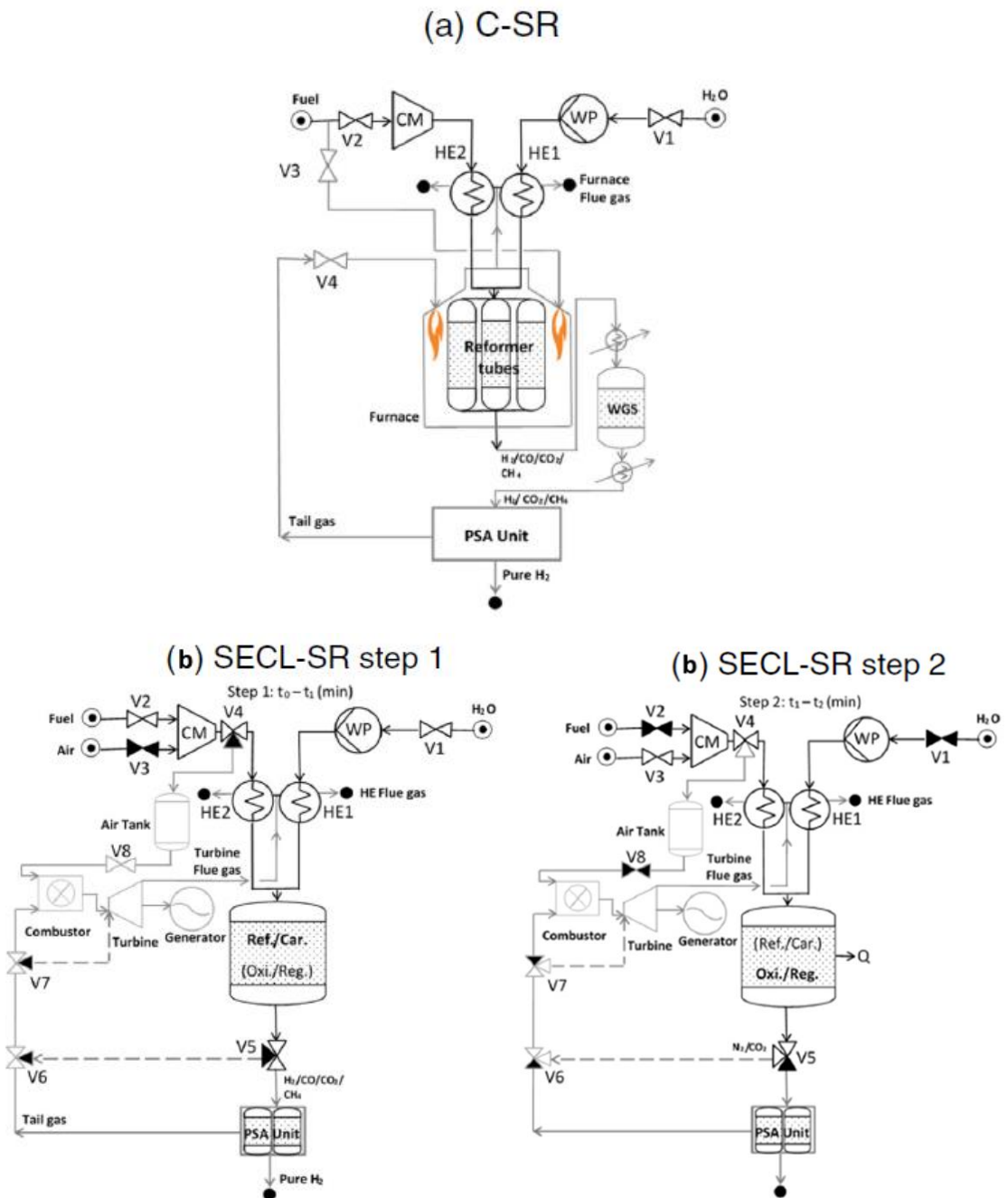


Figure 1.4 Schematic description of (a) C-SR, (b) SE-CLSR steps 1 & 2 Blacked out valve symbols (if any) represent closed to flow. Size of flame in furnace are commensurate to heat input from relevant combustible flow (fresh fuel vs. separation unit tail gas) (S G Adiya et al., 2017).

Global warming is presently one of the major concern in the world (Hafizi et al., 2016b). The C-SR process is one of leading causes of global warming by increasing the CO<sub>2</sub> (the primary (80 %)

greenhouse gas bringing about global warming (Gilassi and Rahmanian, 2015a)) concentration in the atmosphere. For every 4 mole of  $H_2$  produced by complete steam methane reforming process for example, a mole of  $CO_2$  is generated (S G Adiya et al., 2017). In addition to tons of  $CO_2$  generated and release into the atmosphere by furnace flue gas. Generally speaking, almost all the hydrogen production technologies released  $CO_2$ . Remember, throughout the nineteenth century the demand for ammonia for use as fertilizers and industrial feedstocks had been progressively increasing (James, c1993). This also mean increase in hydrogen demand. The deteriorating value of heavy fuel oil and move to heavier crude oils (e.g. tar sands from Alberta, heavy bitumen from Venezuela) has also increased the demand for hydrogen. "The US oil industry has increased its hydrogen production and recovery capacity from 3.156 Gmol/day (2499MMscf/day) to 3.703Gmol/day (2932 MMscf/day) since 1991. With a further 0.648 Gmol/day (513 MMscf/day) planned or under construction" (Thrash, 1991, Towler et al., 1996, Ratan and Uffelen, 2008, N. Jhaveri et al., 2014). The increasing demand for hydrogen, while good for the manufactures, causes a significant concern about  $CO_2$  emissions, because most hydrogen is generated using technologies that produce  $CO_2$  as mention earlier. This makes the capture and storage of  $CO_2$  from hydrogen production an interesting option for the reduction of  $CO_2$  emissions (Anon, c2015). Table 1.6 shows estimated hydrogen production by business sector and their  $CO_2$  emission. A typical quantity of  $CO_2$  emission from oil refineries owing to hydrogen generation is around 25 million metric tons per year (Anon, 2008c). Worldwide agreements such as the Kyoto and current Bali conventions has also call for 8 to 20% reduction in  $CO_2$  emissions from 1990 levels by 2010 and 2020, respectively (Ratan and Uffelen, 2008). Under the Kyoto Protocol, The Paris Agreement had advances; targeting to hold worldwide average temperature rise below  $2\text{ }^\circ\text{C}$  (275 K) and pursue efforts to reach a limit of  $1.5\text{ }^\circ\text{C}$  (274 K) (Gehring and Phillips, 2016). The refinery and power generation sectors are being targeted for such curtailment as they account for a significant portion of the present 25 GT/y of fossil based  $CO_2$  emissions (Ratan and Uffelen, 2008). Based on a refiner's perspective, viable and commercial  $CO_2$  management is a top challenge in light of increased hydrogen usage for complying with clean fuels product slate, along with "bottom of the barrel" strategies to deal with the significant  $CO_2$  release from the required hydrogen production (Ratan and Uffelen, 2008). Thus, making a case for the use of SE-CLSR technology even stronger, as the process do not only capture  $CO_2$  during steam reforming process but also completely eradicate the use of flue gas at steady state operation.

**Table 1.6 Estimated hydrogen production by business sector (Anon, 2008c)**

<b>Business Sector</b>	<b>Annual Hydrogen Production (million metric tons per year)</b>	<b>Estimated CO<sub>2</sub> Emissions (million metric tons per year)</b>
Merchant hydrogen	2.0	17
Oil refineries	2.6	25
Ammonia plants	2.1	18
Methanol plants	1.5	-
Chlorine plants	0.4	-
Other	0.3	<1

Regardless of feedstock used, the conventional steam reformer has poor heat exchange between the gas flames and solid catalysts inside the reformer tubes (irreversibilities produced by large temperature gradients/heat transfer limitation). Figure 1.5 (middle and right image) illustrates fractured reformer tubes caused by gas supplies cut off to the reformer after a power failure, and damaged reformer tubes caused by overheating, which is the major cause of the tubes failure (in addition to creep damage and CO diffusion) which induced cracking from the outside surface along the inter-dendritic carbide network (Swaminathan et al., 2008). This is relevant to hydrogen plants too (because reactors are subjected to external heating using burners/furnaces and it is common for plants to experience unexpected cut off/failure from the burners/furnaces while in operation) hence, the use of SE-CLSR is again made even stronger because of the mild reactor wall materials temperatures it allows to use and complete eradication of flue gas in steady state operation. The tubes fail more easily due to (1) their long narrow shape, hence large expansion under heating, and (2) the use of external heating via burners which has the largest temperatures at the reformer tube walls, not inside the reformer tubes where the endothermic reactions occur (Swaminathan et al., 2008). SE-CLSR eradicate both situations because external heating would only be required at start up (no external heating required at steady state) and by having the outer walls at a lower temperature than inside the reactor, hence less thermal expansion and lower thermal stress when there is a power failure. The possibility of having the walls at a lower temperature than inside the reactor is due to the fact that all the heat demand and release comes from inside the reactor not from outside, which occurs in conventional steam reformers where burners are firing over the reformer tube walls. Consequently, SE-CLSR process walls are most likely to be coolest as heat is lost from the reactor to the environment, whereas for conventional steam reforming, the walls are the hottest as they are subjected to the burners radiation flux.



**Figure 1.5 Industrial steam reformer tubes Left: New tubes, Middle: Fractured tubes caused by gas supply cut off after power failure, Right: Failed and damaged tubes caused by overheating (Swaminathan et al., 2008)**

The capital cost of C-SR plants are very high as well. 254.1 million dollar was estimated to be the capital cost of plant producing 341, 448 kg/day H<sub>2</sub> (Rutkowski, 2005). Practically, reformer tubes are designed to endure a period of 11. 4 years. However, due to extremely high temperature in the reformer furnace or burners firing on the reformer tubes, the tubes life cycle decreases from 11.4 to 2 years, necessitating immediate replacement (Ray et al., 2003). Despite the fact that reformer tubes are usually fabricated from centrifugally cast creep-resistant high carbon austenitic steel of ASTM A297 Grade HK (25 Cr, 20 Ni and C 0.4) or Grade HP (26 Cr, 35 Ni and C 0.4) or heat resistance alloys with composition derived from HP Grade (Ray et al., 2003). Again, this problem can be completely eliminate or at least significantly reduced owing to the mild temperature use SE-CLSR permit as explained earlier.

It is imperative that energy saving measures be devised to mitigate the economic and environmental impacts associated with the production of hydrogen to meet the forecasted large increases in hydrogen demand. SE-CLSR have drawn attention as promising modifications to the C-SR process. This is because of their potential for significant energy savings and lower environmental impacts brought about by process intensification features and milder reactive conditions (Ryden and Ramos, 2012).

The advantages of SE-CLSR over C-SR process are; potential to use a lower operating temperature, reduction of purification steps and extent of the reduction, minimization of reactor size and decrease in the quantity of steam to be used as opposed to C-SR (Chaubey et al., 2013, García-Lario et al., 2015). Brun-Tsekhovoi et al (Brun-tsekhovoi et al., 1988) revealed that the SE-SR process is able to reduce the overall energy required by the system with a potential of saving up to 20-25 % as opposed to the C-SR process. In addition to these benefits, the SE-SR process has the advantage of increasing feed conversion, producing high purity hydrogen with a minimum CO<sub>2</sub>, proficient CO<sub>2</sub> capture from the product as CaCO<sub>3(s)</sub>, and

potential to generate pure CO<sub>2</sub> during the sorbent calcination step that is suitable for subsequent use or sequestration (Chaubey et al., 2013, García-Lario et al., 2015, Wess et al., 2015, S G Adiya et al., 2017). These advantages are illustrated in Fig. 1.4 (b) in contrast to Fig. 1.4 (a) by the absence of WGS stage, a smaller PSA unit, and no large demand of fresh natural gas in the furnace.

### **1.3.3 Applications and maturity of research**

This research generally focuses on all hydrogen manufacturing plants (new and existing) and all hydrogen consuming processes. The present study (on SE-CLSR) can be used to stimulate and upgrade an existing hydrogen plant. Or alternatively be used to design and commission a new plant (further studies on SE-CLSR IS required as discussed in chapter 7). The pure hydrogen produced from SE-CLSR can be utilised in any industrial process that requires hydrogen such as ammonia production and refinery hydroprocessing processes to electronic, food and glass industries etc. The pure CO<sub>2</sub> capture can be diverted to other industrial uses such as: (1) carbonation of beverages, (2) production of dry ice, (3) fire extinguishing agent, refrigerant, or laboratory gas, and (4) grain disinfestation (Anon, 2008c). Or alternatively can be disposed underground or in the ocean depending on geographical location (Holloway, 1997).

In the past few years, various SE-SR pilot plants with capacity of 2-20 MW were built in Sweden, Australia, and Germany (Hufton et al., 1999, Ochoa-Fernandez et al., 2007, Chaubey et al., 2013). However, all of the plants used wood chips or woods pellets as fuel for syngas production and the process was demonstrated during gasification [43]. Presently, many research groups, both at research institutes and university levels, are investigating the performance of the SE-SR process [35] using various/diverse fuel and feedstocks ranging from methane [24], to propane [23], including hydroxyacetone [46], acetic acid [47], and urea [20]. On the other hand, chemical looping combustion can be called a fully matured technology (Storset et al., 2013). Table 1.7 summarizes commercial chemical looping combustion plants used for different purposes including the production of high purity hydrogen.

In order to carry out a preliminary technical and economic feasibility assessment of SE-CLSR as applied to the refinery and other commercial plants such as fertiliser and chemical industry, more research need to be carried not only on the sorbents and oxygen transfer materials but also on the optimisation of process flow sheet, process design calculations, equipment sizing

and layout and estimation of capital and operating costs as well as detailed studies on the safety and environmental aspects of the process.

**Table 1.7 Commercial chemical looping combustion plants (Fan, 2014)**

Organization	Process	Capacity	Features
Hunuosa, Spain	CaOling - CaO looping	2 MW <sub>th</sub>	Capture CO <sub>2</sub> from the flue gas from 50 MW coal power plant
Technical University of Darmstadt, Germany	LISA – limestone based absorption of CO <sub>2</sub>	1 MW <sub>th</sub>	Capture plant is an extension to a 1052 MW hard coal fired power plant
Industrial Technology Research Institute (ITRI), Taiwan	Carbonation-calcination and carbonation-calcination-hydration (Ohio State CCR process) looping reactions to capture CO <sub>2</sub> / Type II	2 MW <sub>th</sub>	Limestone sorbents are used with spent CaO fed to cement industry
Technical University of Darmstadt, Germany	ECLAIR - emission free chemical looping coal combustion process using ilmenite / Type	1 MW <sub>th</sub>	The pilot unit is for solid fuel conversion and designed based on CFB concept
Alstom, U.S.	Calcium sulfate chemical looping combustion / Type I	3 MW <sub>th</sub>	The oxygen carriers are CaS/CaSO <sub>4</sub>
Ohio State University, U.S.	High pressure syngas chemical looping (SCL) gasification process using iron based oxygen carrier / Type I	250 kW <sub>th</sub> - 3MW <sub>th</sub>	SCL enables high purity hydrogen production with in-situ CO <sub>2</sub> capture via countercurrent moving bed reactor design; Syngas is from KBR gasifier

## 1.4 Aims and objectives

The main purpose of this project is to demonstrate the effect of in situ CO<sub>2</sub> sorption and chemical looping on steam reforming of gaseous feedstock with compositions representative of various origins, from natural gas to shale including flared gas for the production of refinery hydrogen with an aim to demonstrate significant energy savings compared to the conventional process. The specific objectives of the study are:

- a. To perform a comprehensive literature review on refinery process that consumes hydrogen in significant amounts. This include quantification of data on required amount and cost associated with them, as well as detailed process conditions
- b. To determine the origins of hydrogen used in the above processes. Including process conditions of the hydrogen produced for refinery use, as well as any energy and costs associated with obtaining the hydrogen
- c. Perform chemical equilibrium calculations in order to compare the conventional steam reforming process of natural gas with sorption enhanced steam reforming, followed by chemical looping steam reforming, and finally sorption enhanced chemical looping steam reforming using gas feedstock with compositions representative of various origins.
- d. Conduct experimental studies in a bench scale packed bed reactor aiming at testing the theoretical gains observed in the thermodynamic equilibrium study (Increase in H<sub>2</sub> yield and purity, reduction in operation temperature and water gas shift stages brought about by in situ CO<sub>2</sub> sorption during steam reforming).
- e. Demonstration of cyclic operation of chemical looping steam reforming.
- f. To identify the optimum conditions for sorption enhance chemical looping steam reforming of the chosen gases based on the favourable conditions retrieved from thermodynamic equilibrium calculations and experimental results.
- g. To study the performance of nickel based catalyst via sorption enhanced chemical looping steam reforming of the chosen gas.
- h. Comparison of sorption enhanced chemical looping steam reforming to the equivalent conventional process in order to make prediction on viability and environmental impacts.

## **1.5 Scope of research**

The work in this research is divided into four main sections/areas: (i) literature review, (ii) chemical equilibrium calculations used to demonstrate the theoretical benefits of the proposed processes, (iii) experimental programme aimed at proving feasibility of achieving the outcomes of the chemical equilibrium concepts investigated earlier and finally (iv) characterisation of research materials (catalyst and sorbent) using know techniques such as SEM-EDX, XRD, BET, TOC and CHNS.

The background and literature review on refinery processes showed that they consume hydrogen in significant amounts. Quantification data on required amount and cost associated with them is covered, as well as the detailed process conditions on the origins of the hydrogen used in the above process. A review on process conditions for hydrogen produced within the refinery and future demand, as well as any energy and costs associated with obtaining the hydrogen is also conducted. Detailed literature review on the current and developing hydrogen technologies is also covered. Chemical equilibrium calculations that compare the conventional steam reforming process (C-SR) with the sorption enhanced steam reforming process (SE-SR), but also chemical looping steam reforming (CL-SR), and finally, sorption enhanced chemical looping steam reforming (SE-CLSR), are being performed using the CEA (Chemical Equilibrium Applications) software by NASA Glenn Research Centre. Aspen plus software using both ideal and Peng Robinson method was used to validate the results. The outputs from the thermodynamic equilibrium study were used as a reference for selecting the optimum and favourable conditions for the experimental work. The experimentation began with characterisation of the research materials (fresh sorbents and catalyst) and continued with a programme of experiments aiming at testing, verifying and quantifying the theoretical effects observed from the thermodynamic equilibrium study, using a bench scale packed bed reactor operating under the conditions identified in the theoretical study as optimum. Lastly, the research experimentation was rounded up with characterisation of used research materials to help in assessing and comparing sorption enhanced chemical looping steam reforming process to the equivalent conventional process in order to make predictions on process viability and ecological influences.

## Chapter 2 Literature Review

*This chapter comprises a comprehensive literature review on refinery processes that consume hydrogen in significant amounts. This includes quantification data on required amount and cost associated with the processes, as well as detailed process conditions of the hydrogen consumers. The sources of hydrogen used in the refinery processes; including process conditions of the hydrogen produced for refinery use, as well as any energy and costs associated with obtaining the hydrogen is also discussed. Future trend in hydrogen production and other available methods are discussed in detail too. A summary of the literature review is made at the end of the chapter.*

### 2.1 Hydrogen consumers within a refinery

Hydrotreating and hydrocracking units are the major consumers of hydrogen in the refinery. Additional hydrogen consuming processes in the refinery include isomerization, lubricant plant and petrochemical processes that can be incorporated into refinery hydrogen system (Aitani, 1996, Rabiei, 2012). Hydrogen consumption data for numerous refinery processes are given in Table 2.1 and a schematic diagram of a typical hydrogen consumer displaying the correct source and sink position is display in Figure 2.1. The quantity of hydrogen required for a particular process is determined by the hydrogen content of the feed and products, and the quantity of heteroatoms e.g. sulphur, nitrogen, etc. to be removed (Aitani, 1996, Alves and Towler, 2002).

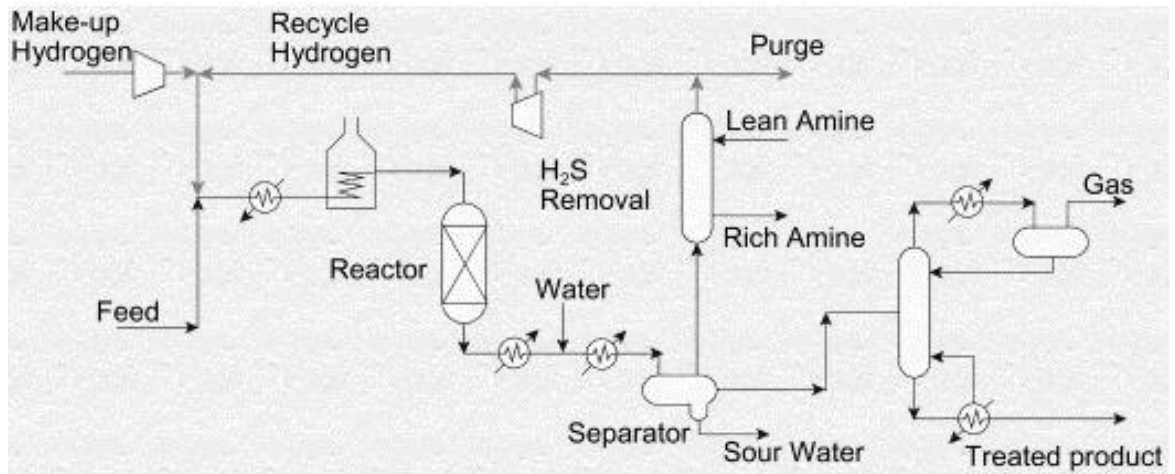


**Figure 2.1 Schematic diagram of a typical hydrogen consumer displaying the correct source and sink position (Hallale and Liu, 2001)**

**Table 2.1 Hydrogen consumption data for various refinery processes (Rabiei, 2012)**

<b>Process</b>	<b>Wt. % in feed</b>
<b>Hydrotreating</b>	
Straight run naphtha	0.05
Cracked naphtha	0.7-1.0
<b>Hydrodesulphurization</b>	
Low Sulphur gas-oil to 0.05% S	0.15
High Sulphur gas-oil to 0.05% S	0.35
Cycle oils hydrogenation	3
Hydrocracking vacuum gas-oil	2-3

### **2.1.1 Hydrotreating**

Hydrotreating is a refining process in which petroleum feedstock is thermally treated with hydrogen in the presence of a suitable catalyst under appropriate operating conditions to convert them to lower weight hydrocarbons and improved the quality of final products. In hydrotreating process, the feedstock reacts with hydrogen in the presence of a hydrogenation catalyst at high temperatures (300-500 °C (573-773 K)) and pressures 8.3-151.7 bar (Speight and Ozum, c2002). The operating conditions are a function of type of feedstock to be used and the desired level of desulfurization in the treated product. Hydrotreating feeds, operational conditions, products and yields that are mainly used in petroleum refining will be discussed later (2.1.13) with two different feedstock: naphtha hydrotreating and light distillate hydrotreating. The major impurities to be removed during hydrotreating are sulphur, nitrogen, oxygen, olefins and metals. (Speight and Ozum, c2002, Parkash, c2003).

The major purpose of hydrotreating is to process light streams (naphtha, distillate, gas oil) from atmospheric and vacuum tower. Common objectives and applications of hydrotreating include;

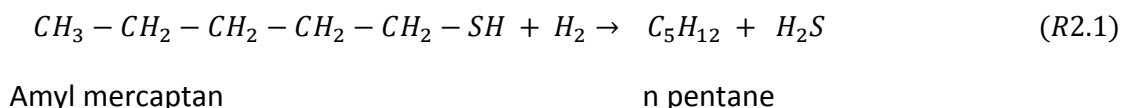
1. Improvement of exiting petroleum products by:
  - elimination of sulphur and to saturate aromatic and olefin molecules causing enhanced centane number, smoke point, storing stability and diesel index in kerosene, heating oil, jet fuel and diesel,
  - pre-treatment of catalytic reformer feed (naphtha) to eradicate sulphur, oxygen and metals that would damage catalyst,

- pre-treatment of fluid catalytic cracking (FCC) feed to reduce corrosion by decreasing the feed sulphur, nitrogen, metals and polynuclear aromatics content. Increase FCC yield, decrease FCC catalyst usage and stack emission,
  - increase the colour and colour stability, viscosity index, and storing stability to decrease gum formation and neutralization number of lube oil,
  - production of lower sulphur fuels oils (Leach, 1983, Anon, c2000, Anon, c2005).
2. Assurance of least possible cracking occurs as in hydrocracking, enabling petroleum products to reach market specification.
  3. Development of novel products or “even new uses for existing products”
  4. Solid residua conversion to liquid fuels.
  5. Conversion of substandard products into valued products (Leach, 1983, Speight and Ozum, c2002)

#### 2.1.1.1 Chemistry of hydrotreating

The quantity of hydrogen utilised during hydrotreating is a major function of bonds broken and hydrogen lost with products. Feed quality has a significant impact on the hydrogen chemical consumption (Stratiev et al., 2009). Figure 2.2 illustrates the significance of feed quality on hydrogen consumption. A qualitative generalisation on the chemistry of hydrotreating and hydrogen consumption is as follows;

1. Chemical consumption owing to hydrogenation reactions; such reactions are normally exothermic and their management is very significant for safety and operating constancy of a unit.
  - During desulfurization, sulphides, disulphides, polysulfides, thiophenes, and marcaptans are the main sulphur containing compound (Porgar and Rahmanian, 2015), they are eliminated in the form of hydrogen sulphide (H<sub>2</sub>S). Than most other type of sulphur the thiophenes are more difficult to remove. Carbon sulphur bonds are broken and the residual hydrocarbon chains are saturated, all as a result of hydrogen addition. This produces some light ends. By breaking more complex molecules, heavier distillates produce more light ends. Heavier feeds result in the formation of sulphur in the form of disulphides and thiopenes,



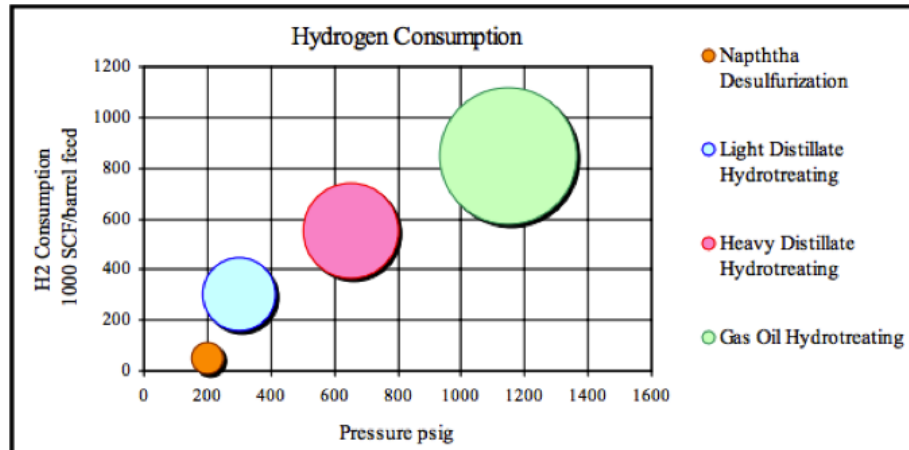


Figure 2.2 Significant of feeds quality on hydrogen consumption (Anon, c2000)

- During denitrogenation, nitrogen is converted to ammonia. Nitrogen removal requires four times as much hydrogen as the corresponding in sulphur removal roughly. Nitrogen containing compounds include pyrroles and pyridines. In naphtha hydrotreating, nitrogen removal is lesser than in heavier feeds. Denitrogenation is more significant during hydrotreating of distillate and gas oil,



Methyl pyrrol

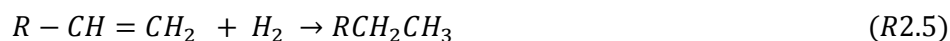
- Oxygen containing compounds such as phenols and peroxides are converted to water. Oxygen removal is more significant in heavy distillate hydrotreating than in naphtha hydrotreating. Removal of oxygen requires about two times as much hydrogen as the equivalent of sulphur removal,



- Organic chlorides are present in a small amount and are converted to hydrogen chloride. Hydrogen consumption per molecule is same case as desulphurization process,



- Olefins are removed by saturation to produce light hydrocarbons. Hydrogen consumption is stoichiometric. For each double bond, one hydrogen molecule is added. Olefins are usually found in cracked streams like naphtha streams from a Coker, catalytic cracker gasoline and catalytic cracker gas oil. Maintaining high octane level is significant as no selective catalyst is available for use in hydrotreating of saturated olefins,



- Aromatic rings are hydrogenated to cycloparaffins. Hydrogen consumption in this reaction is a strong function of convolution of the aromatics. Ring saturation occurs during gas oil hydrotreating and heavy distillate hydrotreating (Jones, c1995, Anon, c2000, Speight and Ozum, c2002, Parkash, c2003).



2. Hydrogen is absorbed in liquid products. This is usually low compared to hydrogen used during sulphur elimination.
3. Hydrogen is lost in balance with light gases. This quantity lost is usually twice the amount used for sulphur removal.
4. Hydrogen is also lost with purge gas utilised in maintaining a purify hydrogen, as the light ends produce dilute hydrogen concentration. Hydrogen consumption here is not as much as needed for typical sulphur elimination.
5. Metals are deposited on the catalyst directly. This reduces activity of the catalyst if in excess. Hence, stimulating dehydrogenation and production of coke and hydrogen. Metals removal is very significant in gas oil hydrotreating. Metals contained in the feed such as lead, arsenic, nickel and copper damaged the catalyst permanently. Significant quantity of nickel and vanadium can be found in vacuum gas oils and residue feeds. Compounds comprising those metals are demolished during hydrotreating process and metals get deposited on the hydrotreating catalyst. (Scott and Bridge, 1971, Leach, 1983, Jones, c1995, Anon, c2000, Parkash, c2003).

**Table 2.2 Hydrogen consumption during hydrotreating of various feedstocks (Speight and Ozum, c2002)**

Feedstocks	API	Sulphur (wt. %)	Carbon residue (conradson) (wt.%)	Nitrogen (wt. %)	Hydrogen (Scf/bbl)
Arabian light, vaccum	8.5	3.8	-	-	435-1180
Bachaquero, vaccum	5.8	3.7	23.1	0.56	1080-1260
Boscan (whole crude)	10.4	5.6	-	0.52	1100
Khafji, atmospheric	15.1-15.7	4.0-4.1	11.0-12.2	-	725-800
Khafji, vacuum	5.0	5.4	21.0	-	1000-1100
Kuwait, atmospheric	5.5-8.0	5.1-5.5	16.0	-	290-1200
Kuwait, vaccum	15.7-17.2	3.7-4.0	8.6-9.5	0.20-0.23	470-815
Tia Juana, Vacuum	7.8	2.5	21.4	0.52	490-770
Venezuela, atmospheric	15.3-17.2	2.1-2.2	9.9-10.4	-	425-730
Venezuela, vacuum	4.5-7.5	2.9-3.2	20.5-21.4	-	825-950
West Texas, atmospheric	17.7-17.9	2.2-2.5	8.4	-	520-670
West Texas, vacuum	10.0-13.8	2.3-3.2	12.2-14.8	-	675-1200

**Table 2.3 Supplementary hydrogen consumption caused by nitrogen compound during hydrodesulphurization (Speight and Ozum, c2002)**

Nitrogen compound	(Mole H <sub>2</sub> / compound)	(Scf/bbl feed)
Saturates amines	1	83
Pyrrolidine	2	167
Nitriles, pyrroline, alkyl cynides	3	250
Pyrrole, nitroparaffins	4	334
Analine, pyridine	5	417
Indole	7	584

### 2.1.1.2 Hydrotreating catalyst

Cobalt molybdenum and nickel molybdenum are the most commonly used catalysts for hydrotreating of any kind of feedstock from naphtha to residua. One of the most vital characteristics of the catalyst is resistance to poisoning. These catalyst also promote desulphurisation and demetallization. Nickel cobalt molybdenum is normally employed if nitrogen is in a very significant concentration (Jones, c1995). Hydrotreating catalyst is made up of two parts; the support and the active element. The support is a solid material with a high porosity and ability to resist pressure, temperature and environmental conditions encountered

in the reactor. The support used by hydrotreating catalyst is alumina in the form of balls. The metals deposited on the support in the form of oxide are the active element (Parkash, c2003, Speight, c2007). The catalysts are made with the metals in an oxide state and in sulfide state when in an active form produce by sulfiding the catalyst before use or with the feed during use. Every catalysts that has hydrogenation activity can be used as catalyst to some level. Although the group VIB metals; chromium, molybdenum and tungsten when promoted by the iron group; iron, cobalt and nickel are mainly active for desulfurization. Cobalt molybdenum catalyst is mainly ideal for olefins saturation and desulfurization as they required less hydrogen for mild process. Nickel molybdenum is used for saturation of aromatics and removal of hydrogen (Anon, c2000, Speight, c2007). Nickel-tungsten (Ni-W) is usually used only when a very high activity for aromatic saturation and activity for nitrogen and sulphur removal is required (Speight and Ozum, c2002). Table 2.4 shows Supplementary hydrogen consumption caused by metals during hydrodesulphurization while Tables 2.5 and 2.6 below depicts representative metal content of hydrotreating catalyst and composition and properties of hydrotreating catalyst respectively.

**Table 2.4 Supplementary hydrogen consumption caused by metals during hydrodesulphurization (Speight and Ozum, c2002)**

Vanadium + Nickel (ppm)	Correction (%) to hydrogen consumption
0-100	-2
200	1
300	2.5
400	4
500	6.5
600	9
700	12
800	16
900	21
1000	28
1100	38
1200	50

**Table 2.5 Representative metal content of catalyst (Speight and Ozum, c2002)**

Metal (wt. %)	Co-Mo	Ni-Mo	Ni-Co-Mo	Ni-W
Cobalt	2.5		1.5	
Nickel		2.5	2.3	4
Molybdenum	10	10	11	
Tungsten				16

**Table 2.6 Composition and properties of hydrotreating catalyst (Speight, c2007)**

<b>Composition</b>	
<b>Active phase (wt. %)</b>	<b>Range</b>
MoO <sub>3</sub>	13-20
CoO	2.5-3.5
NiO	2.5-3.5
SiO	1.0-10.0
<b>Properties</b>	
Surface area (m <sup>2</sup> /g)	150-500
Pore volume (cm <sup>3</sup> /g)	0.2-0.8
Mesopores (nm)	3.0-50.0
Macropores (nm)	100-5000
Extrudable diameter (mm)	0.8-4.0
Extrudable length/diameter (mm)	2.0-4.0
Bulk density (kg/m <sup>3</sup> )	500-1000

### **2.1.1.3 Hydrotreating feeds and products**

#### **2.1.1.3.1 Naphtha hydrotreating**

The main aim to naphtha hydrotreating is sulphur elimination. Sulphur can be found in naphtha as sulphides, disulphides, polysulfides, marcaptans and ring compound such as thiophenes. Hydrotreating transforms all of those compounds to hydrogen sulphide and saturated hydrocarbons. Hydrogen utilization varies from 50 – 250 standard cubic feet per barrel of feet (scf/bbl). For a feed containing 1 % sulphur i.e. simple desulphurization hydrogen consumption varies from 70 – 100 scf/bbf. The higher the sulphur contents in the feed the higher the level of hydrogen consumption proportionately. About 250 scf/bbl of hydrogen is consumed for a significant sulphur and nitrogen elimination. This is chemical hydrogen consumption; grant must be made for mechanical loss and hydrogen lost with lower hydrocarbon vapours (Jones, c1995, Anon, c2000).

The process begins by feeding naphtha and hydrogen into the fired furnace (heater). The heated feed goes into the hydrotreating reactor at a temperature of 371 °C (700 F). Desulphurization reactions occur over Co-Mo on alumina catalyst. The reactor products comprises desulphurized naphtha, hydrogen sulphide, excess hydrogen and light end elements.

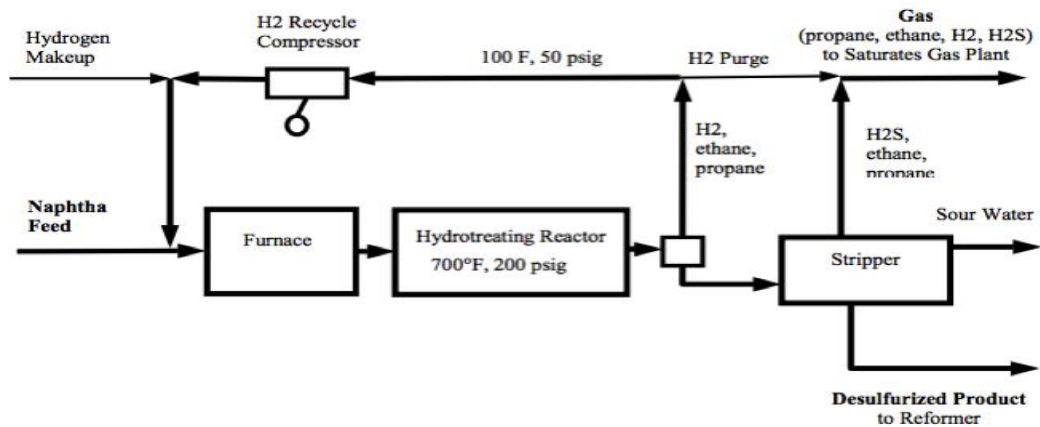


**Figure 2.3 Naphtha hydrotreating process description (catalytic desulphurization) (Anon, c2000)**

Depending on the operating pressures used a one-step flash is acceptable. Flashed liquid is fed into the stripper for removal of hydrogen sulphide, light end and sour water. One of the streams objective is to saturate gas plant for recapture of light hydrocarbons. Removal of hydrogen sulphide is carried in the stripper overhead. A splitter must be added to the process sequence to split the stripper bottoms between reformer feed and isomerization, if hydrodesulphurization unit is treating naphtha for reforming and light straight run feed (Anon, c2000, Parkash, c2003). Table 2.7 shows the naphtha hydrotreating operating conditions as reported by Parkash, c2003, while table 2.8, 2.9, and 2.10 shows naphtha hydrotreating feed and product properties, naphtha hydrotreating units yield and naphtha hydrotreating unit utility consumption respectively.

**Table 2.7 Naphtha hydrotreating operating conditions (Parkash, c2003)**

Operating parameters	Value
Reactor inlet temperature	
SOR	308 °C (581 K)
EOR	370 °C (643 K)
Hydrogen partial pressure	11 bar
Liquid hourly space velocity	4 hr
Hydrogen consumption	45 scf/bbl
Catalyst	Co-Mo on alumina
Surface area	225 m <sup>2</sup> /g
Pore volume	0.45 cm <sup>3</sup> /g
Crush strength	30 kg

**Table 2.8 Naphtha hydrotreating feed (sulphur run) and product properties (Parkash, c2003)**

Quality	Value
Sulphur gravity	0.734
<b>TBP Distillation</b>	
Initial boiling point distillation	98°C (371 K)
10 %	95 °C (368 K)
30 %	105 °C (378 K)
50 %	114 °C (387 K)
70 %	125 °C (398 K)
90 %	135 °C (408 K)
Final boiling point	140 °C (413K)
Paraffin's	69 Vol. %
Naphthenes	20 Vol. %
Aromatics	11 Vol. %
Total sulphur	0.015 wt. %
<b>Marcaptan</b>	
Total nitrogen	0.008 ppm
Molecular weight	111
Product sulphur	0.5 ppm

**Table 2.9 : Naphtha hydrotreating units yield (Parkash, c2003)**

	Yield weight fraction
<b>Feed</b>	
Naphtha feed	1.0000
Hydrogen	0.0080
Total feed	1.0080
<b>Products</b>	
Acid gas	0.0012
Hydrogen rich gas	0.0110
LPG rich gas	0.0058
Hydrotreated naphtha	0.9900
Total product	1.0080

**Table 2.10 : Naphtha hydrotreating unit utility consumption per ton of feed (Parkash, c2003)**

<b>Utility</b>	<b>Units</b>
Fuel gas	457191710 J
Steam	388560160 J
Power	36000000 J
Cooling water	4.81885 L
Distilled water	0.01136 L

#### **2.1.1.3.2 Distillate hydrotreating**

Normally, all liquid distillates contain sulphur compounds that must be removed. Light distillates hydrotreating limiting our discussion to kerosene required more hydrogen than naphtha hydrotreating. Heavy distillates hydrotreating consume substantial amount of hydrogen at great severity (Anon, c2000). Promotion of raw kerosene distillate to produce and meet specification products appropriate for marketing (kerosene and jet fuel) is the major objective of kerosene hydrotreating. Corrosion problems in the aircraft engines, fuel handling and storage facilities is a great obstacle caused by sulphur in the raw kerosene cuts existing from crude distillation unit. Presence of nitrogen in raw kerosene feed from certain crude oils can cause colour stability problems in the product. Aviation turbine fuels can only have straight run kerosene or hydrotreated blend components due to very stringent products specification. Hydrogen consumption in distillates hydrotreating is a strong function of stream being treated, level of desulphurisation and other aims and objectives like nitrogen removal, aromatic ring and olefins saturation (Speight and Ozum, c2002, Parkash, c2003).The process of distillate (kerosene) hydrotreating is the same as the naphtha hydrotreating process with major difference being in the feeds, product and operating conditions. Table 2.11, 2.12 and 2.13 display kerosene hydrotreating operating conditions, unit utility consumption per ton of feed, and unit overall yields respectively. While Figure 2.4 depicts light distillate hydrotreating process description.

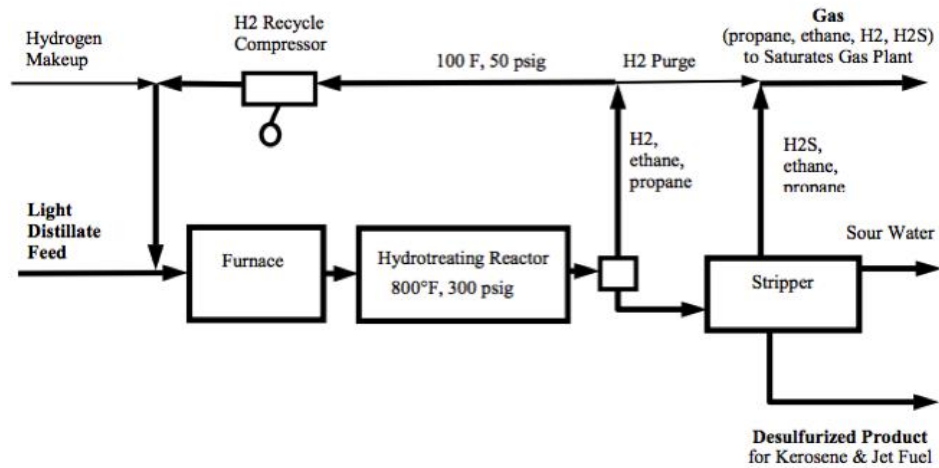


Figure 2.4 light distillate hydrotreating process description ( catalytic desulphurization) (Anon, c2000)

Table 2.11 : Kerosene hydrotreating operating conditions (Parkash, c2003)

Operating parameters	value
SOR	316 °C (589 K)
EOR	370 °C (643 K)
Reactor $\Delta T$	-1.1 °C (272 K)
Reactor $\Delta P$	2.4 bar
Total reactor pressure	93 bar
Hydrogen partial pressure	76 bar
Recycle ratio	3072 scf/bbl
Hydrogen consumption	555 scf/bbl
Desulfurization %	99.6 wt. %
Denitrification %	98.0 wt. %
Discharge pressure	96 bar
Discharge temperature	72 °C (345 K)

Table 2.12 Kerosene hydrotreating unit utility consumption per ton of feed (Parkash, c2003)

Utility	Consumption
Fuel	1794979000 J
Power	54000000 J
Steam	31676100 J
Cooling water	2.182124 L
Distilled water	1.545671 L

**Table 2.13 Kerosene hydrotreating unit overall yield (Parkash, c2003)**

<b>Stream</b>	<b>Weight fraction</b>
<b>Feed</b>	
Kerosene feed	1.0000
Hydrogen gas	0.0137
Total feed	1.0137
<b>Products</b>	
Gas from unfiner	0.0109
HP gas	0.0060
Acid gas	0.0018
Naphtha	0.1568
ATK	0.7582
Heavy kerosene	0.0800
Total product	1.0137

#### **2.1.1.4 Effect of process variables**

The total reactor pressure, temperature, hydrogen recycle rate, space velocity and partial pressure of hydrogen are the major variables during hydrotreating (Anon, c2000, Speight and Ozum, c2002, Parkash, c2003).

Temperature: increase in temperature favours hydrotreating reactions but at the expense of causing coking reactions and weakening the activity of the catalyst. Normally the reaction rate and the overall catalyst life need to be compromise. The temperature of the catalyst is gradually increase during the progress of runs to compensate for the decrease in activity because of coke deposit till the maximum acceptable temperature limit for the catalyst is reached. At this point the catalyst must be renewed or discarded (Parkash, c2003, Speight, c2007)

Pressure: increase in pressure raises the partial pressure of hydrogen, consequently, increasing the hydrotreating rate and reducing coke deposit on the catalyst. This increases the catalyst life and decreases the fouling rate. High pressure also raises desulphurization rate due to greater hydrogen partial pressure in the reactor, necessitating a small amount of catalyst. Furthermore, various unstable compounds are transformed to stable compounds. It is important to know that as the space velocity decreases, desulphurisation rate increases. The impact of increasing space

velocity can be balanced by increasing the reactor temperature or the partial pressure of hydrogen (Speight, c2007).

Recycle rate: using a compressor and furnace, hydrogen separated in a high pressure drum is recycled to the reactor. This stream joins the entering fresh feed. There must be high concentration of hydrogen at the outlet of hydrotreating reactors, thus the hydrogen quantity is much more than stoichiometry. To avoid poisoning of the catalyst and coke deposit on catalyst high concentration of hydrogen is needed especially for heavy distillates containing small amount of resins that are subjected to coking (Parkash, c2003, Speight, c2007).

Purge hydrogen: to avoid the accumulation of inert gases such as nitrogen and light hydrocarbons in the recycle gas purge hydrogen is required. The amount of purge directly impacts the purity of hydrogen in the recycle gas. Feeds containing low sulphur contents required a small purge ratio to maintain the purity of recycle hydrogen where as high purge ratio is needed for feeds with high sulphur contents. Table 2.14 shows a typical purge values used. Make up hydrogen replaces the hydrogen consumed during hydrotreating reactions. "The hydrogen is lost through solution losses in the liquid phase and purges for regulating unit pressure and maintaining recycle gas purity" (Parkash, c2003).

**Table 2.14 Purge needed for hydrotreating processes (Parkash, c2003)**

Process	Hydrogen in purge / hydrogen in make-up gas
Naphtha HDS	10 %
Kerosene HDS	15 %
Diesel HDS	20 %
VGO HDS	30 %

### **2.1.2 Hydrocracking**

A refining process that converts heavy gas oils into light distillates such as kerosene, diesel and naphtha etc. or base stocks for lubricating oil manufacture is called hydrocracking. Hydrocracking is a refining technology the like of hydrotreating discussed previously. They both fall under the same umbrella of hydroprocessing. Hydrocracking includes hydrogen addition (hydrogenation) and carbon-carbon scissions (cracking) of aromatic bonds. Hydrocracking is the prime consumer of hydrogen in the refinery and hydrogen normally account for more than 84% of the process operating cost (see figure 2.5). The process involves reacting feed with hydrogen

in the presence of a catalyst. The primary purpose of hydrocracking is to process heavy gas oil to crack carbon-carbon bonds of large aromatic composite and remove pollutants such as sulphur that ruined downstream catalyst. Hydrocracking reactions are similar to hydrotreating reactions. Once the feed is reacted with hydrogen sulphur is removed as hydrogen sulphide and metals deposited on the catalyst. Hydrogen also produce higher yield of products by breaking aromatic bonds to lower the averaged molecular weight (long et al., 2011, Speight and Ozum, c2002). Common objectives and applications of hydrocracking include;

1. Breaking down the high boiling range aromatic stocks created by catalytic cracking and coking.
2. Transformation of refinery feedstocks to gasoline and jet fuel.
3. Flexibility for diesel production (Speight, 1997, Speight, c2007).

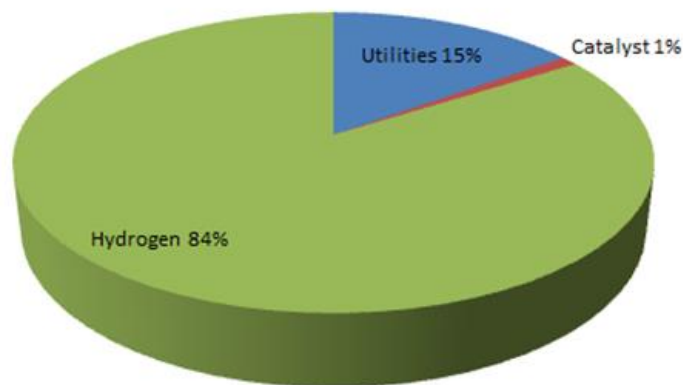


**Figure 2.5 Typical hydrocracker operating cost (long et al., 2011)**

### **2.1.2.1 Chemistry of hydrocracking**

As the name implies, hydrogenation and cracking are the major reactions taking place during hydrocracking. Isomerization also happens to some level. Dehydrogenation also known as condensation (undesirable reaction) also happens at some extent if not limited by hydrogenation. Hydrogenation reactions are highly exothermic reactions dependent on the condition of the operation, thus managing the heat of reaction is vital to safety and operational steadiness of the unit (Speight, 1997, Anon, c2000, Speight and Ozum, c2002, Parkash, c2003) . Below is a breakdown of the chemistry of hydrotreating process:

- Hydrogen is introduced to saturate the freshly made molecule from cracking of aromatic
- Aromatics rings are hydrogenated to naphthenes (cycloparaffins)

- Olefins are saturated to form light hydrocarbons
- Sulphur bonds are broken down to hydrogen sulphide, nitrogen to ammonia, oxygen to water and organic chlorides are transformed to hydrogen chlorides. They are normally in a minute quantity and hydrogen consumption is similar to desulphurization.

Cracking reactions are endothermic necessitating heat.

- Low molecular weight paraffins and olefins are formed by cracking of saturated paraffins ,
- Cracking of side chains off resins and asphaltenes leaving thermally steady polynuclear aromatics (PNAs) which are the enormous majority of the heteroatoms,
- Cracking of side chains off small ring aromatics and cycloparaffins (Speight, 1997, Anon, c2000, Speight and Ozum, c2002, Parkash, c2003).

Branching of alkyl groups of paraffins and opening of cycloparaffins is provided by isomerisation. Dehydrogenation reactions are suppressed by the presence of hydrogen in the reactor. When conditions are not severe or the molecules are complex, small ring aromatics and polynuclear aromatics are not hydrogenated. Hence, they start their cycle of condensations to form very complex asphaltene form structure, which precipitate and solidify as coke.

- Benzene and hydrogen may be formed by dehydrogenation of cyclohexane,
- Resins are formed by combination of small ring aromatics,
- After cracking of off side chains, resins combine with the remaining polynuclear aromatics and produced asphaltene,
- Asphaltene are left with enormous poly nuclear aromatics that are partly saturated with short side chains and entangled with heteroatoms after cracking of off side chains.

**Table 2.15 Range of hydrocracking process conditions (Speight, 1997)**

	<b>Diesel</b>	<b>Diesel</b>	<b>Gasoline</b>
Catalyst	CoMo/SiAl	Pd/zeolite	Pd/zeolite
Temperature (°C)	260-371	260-371	288-382
Hydrogen pressure (Bar)	103	55-103	152
Hydrogen consumption (scf/bbl)	400-1200	400-1200	> 2000
Hydrocracking stages	1	1	1
Hydrodenitrogenation pretreat	NiMo	Integral	NiMo

Chemical consumption due to hydrogenation reactions such as sulphur, nitrogen, oxygen, organic chlorides, olefins, and aromatic rings etc. removal are same with hydrotreating process discuss previously. Except that carbon-carbon bonds are cracked during hydrocracking which consumes a great quantity of hydrogen. Complexity of the aromatics is a great function of hydrogen consumption (Speight, 1997, Anon, c2000, Speight and Ozum, c2002, Parkash, c2003)

#### **2.1.2.2 Hydrocracking catalyst**

The cracking activity of hydrocracking catalyst is weakened by deposition of coke and metals on the catalyst. Elementary hydrogen plays the main part due to the susceptibility of such complex on the catalyst and their predisposition to form coke. The reactions of hydrocracking need a double function catalyst with a very great hydrogenation and cracking activities (Speight, 2000, Speight and Ozum, c2002). The hydrogenation function is provided by palladium sulphides and promoted group VI sulphides i.e. nickel molybdenum and nickel tungsten. These components safeguard the catalyst from poisoning by coke, saturate aromatics in the feed, and saturate olefins made during cracking. The cracking task is provided by zeolites or amorphous silica-alumina. At the molecular level both have analogous chemistry, but high activity is provided by the crystalline structure of the zeolites with controlled selectivity not established in the amorphous materials. The zeolites are crystalline aluminosilicates, the most universally used zeolite in virtually all commercial catalyst today is the faujasite. Pentasil zeolites are also utilised in certain catalyst for their capacity to selectively crack long chain paraffins. Typical range is 25 – 50 wt. % zeolites in the catalyst, the remainder being the hydrogenation catalyst and silica or alumina binder. "Exact recipes are guarded as trade secrets". Amorphous silica aluminas developments by Chevron and UOP permitted them to contend actively. Catalyst of this form contains 60 – 80 wt. % of the silica alumina, with the rest being the hydrogenation catalyst. The compositions of that catalyst are strictly detained as secrets. Silica is almost continuously used in excess for good acidity and steadiness. (Speight, 1997, Speight, c2007).

#### **2.1.2.3 Hydrocracking feeds and products**

Highly aromatic "cycle oil" and the bottoms of liquid stream from catalytic cracker are some of the feeds used in hydrocracker to produce high yields of diesel, kerosene, jet fuel and heating oil. Gas oil from visbreaker comprising aromatics and gas oil from the delayed coker containing olefins and sulphur are also typical feeds. Not always, as it is less economical, atmospheric and vacuum gas oils may be fed to hydrocracker when intention is to maximise diesel production over gasoline (Speight, 1997, Anon, c2000, Parkash, c2003).

#### 2.1.2.4 Hydrocracking process description

Hydrocracker can be operated in either of the following modes; single stage (once-through-mode) operation, single stage operation with total or partial recycle, and a two stage operation mode.

**Single stage operation:** it is the simplest mode of operation. A single reactor combines desulphurization with hydrocracking of gas oil. Fresh feed of gas oil and hydrogen are pre heated and fed into the reactor. The operating pressure ranges from 1200-2596 psi (83 -179 bar) and the process will consumed hydrogen at the rate of 1000 scf/bbl or more. At a very high pressure as possible the reactor products are flashed to recycle hydrogen to reduce recompression horsepower for recycle. At a low pressure the liquid is then flashed back once more to produce a flash gas for the gas plant. To generate straight run gas, distillates (jet fuel/kerosene or diesel/heating oil) and naphtha suitable for reforming and bottoms for recycle the liquid from the flash is fractionated at naphtha overhead (not showed in the PFD). The single stage process can be operated in either total or partial recycle of the feed, with partial recycling preferred over the total recycle. Total recycle outcomes in the build-up of highly refractory materials in the feed to the unit, consequently high catalyst fouling rate (Speight, 1997, Speight, 2000, Anon, c2000, Speight and Ozum, c2002). Figure 2.6 presents a single stage hydrocracking process and Table 2.16 and 2.17 shows the operating conditions of a single-stage hydrocracker and utility consumption per ton of feed respectively.

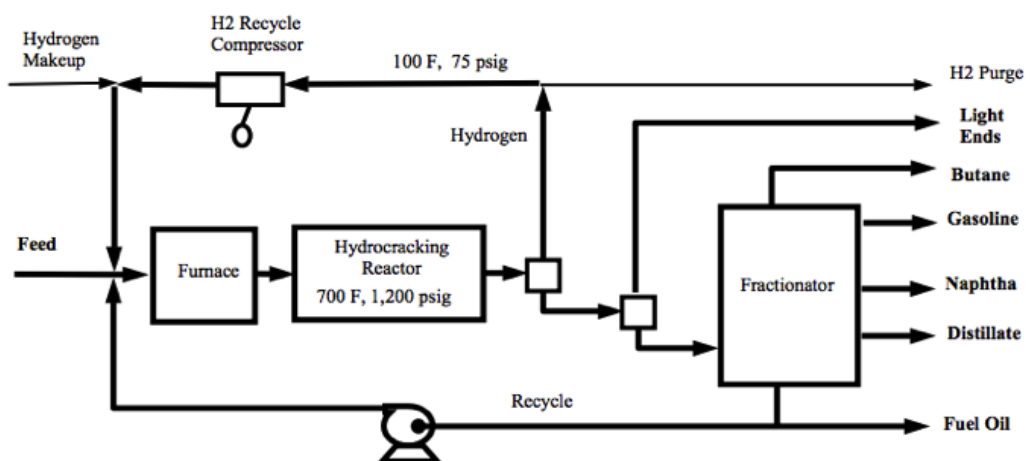


Figure 2.6 Single stage hydrocracking process(Anon, c2000)

**Table 2.16 Operating conditions of single-stage hydrocracker (Parkash, c2003)**

Operating parameters	Value
Catalyst or reactor averaged temperature	413 °C (686 K)
Space velocity	1.72 hr
Reactor inlet pressure	179 bar
Reactor pressure drop	3.4 bar
Hydrogen partial pressure, inlet	138 bar
Hydrogen chemical consumption	1150 scf/bbl
Makeup + recycle at reactor inlet	5000 scf/bbl
Makeup hydrogen purity	95 vol%
HP separator temperature	60 °C (333K)
HP separator pressure	138 bar
Bleed rate SOR (100%)	200 scf/bbl
Recycle compressor suction pressure	165 bar
Recycle compressor discharge pressure	187 bar

**Table 2.17 Utility consumption per ton of feed (Parkash, c2003)**

Utility	Single stage	Partial recycle mode
Fuel gas	633522000 J	802461200 J
Power	64800000 J	82800000 J
Steam	126704400 J	158380500 J
Distilled water	0.016 MIG	0.02 MIG
Cooling water	0.33 MIG	0.42 MIG

Where MIG = 1000 imperial gallons

**Two stage operation:** this mode of operation employs two separate reactors. Desulphurization and olefin saturation occur in the first reactor, while hydrocracking in the second reactor. The uncovered feed from the first reactor is fed into the second reactor. The feed is already purified by the removal of sulphur, nitrogen, and other impurities, and the second reactor can transform a large percentage of the feed with superior products quality. Less light gases production and less hydrogen consumption per barrel of feed is a major advantage of the two stage operation over one stage operation. Normally product with highest and best qualities, i.e. minimum mercaptans, lowest pour point and highest smoke, point, are produced in the second stage while products with lowest qualities are generated in the first stage. Adjustment of operating conditions (flexibility) is more feasible in the two stage process, distribution between the

naphtha and middle distillates is also more flexible (Speight, 1997, Speight, 2000, Anon, c2000, Speight and Ozum, c2002). Figure 2.7 and table 2.18 depicts Two stage hydrocracking process and operating conditions of mild hydrocracker respectively.

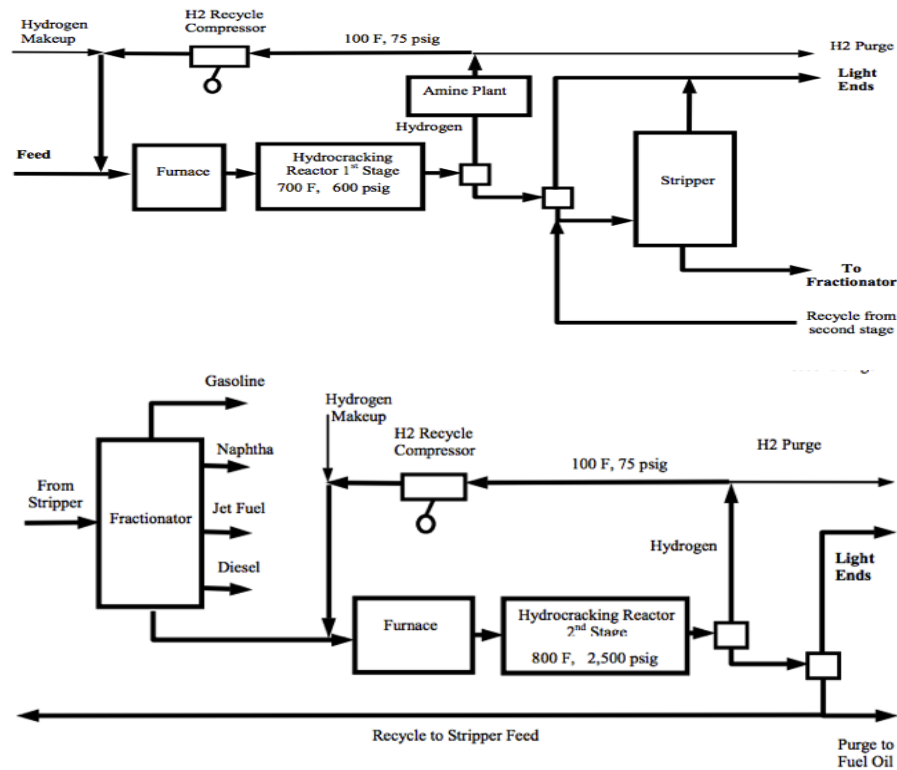


Figure 2.7 Two stage hydrocracking process (Anon, c2000)

Table 2.18 Operating conditions of mild hydrocracker (Parkash, c2003)

Operating parameters	Value
Catalyst averaged temperature	413 °C (686 K)
Space velocity	1.4 hr
Reactor inlet pressure	72 bar
Reactor pressure drop	3 bar
Hydrogen partial pressure, inlet	52 bar
Hydrogen chemical consumption	358 scf/bbl
Makeup + recycle at reactor inlet	2766 scf/bbl
Makeup hydrogen purity	92 vol. %
HP separator temperature	60 °C (333 K)
Hp separator pressure	59 bar
Bleed rate SOR (100%)	10.5 scf/bbl
Recycle compressor suction pressure	57 bar
Recycle compressor discharge pressure	74 bar

### 2.1.2.5 Effect of process variables

Operating conditions are a primary function of the catalyst, space velocity, total pressure and partial pressure of hydrogen. They determine the crackability of the feeds and the desired yield of product. Diesel or fuel oil from heavy gas oil is a mild operation while production of naphtha or kerosene for aromatic petrochemical feedstock from light gas oil could be a quite severe operation. In hydrocracking unit operation, the feed rate, recycle gas rate, and operating pressure are usually kept constant. The only variable is the reactor temperature necessitating close control to achieve the necessary feed transformation. High temperatures are needed for the catalyst to hydrocrack the feed. To control the temperature rise caused by exothermic hydrocracking reactions chilled hydrogen rich gas is injected between the catalyst beds in the reactor. Higher reactor pressure is required for catalyst life. High hydrogen content of the reactor feed and high reactor pressure are required to maintain the hydrogen partial pressure at a high level, thus increase the catalyst life. Table 2.19 below summarises impact of operating conditions on severity (Speight, 1997, Anon, c2000, Parkash, c2003).

**Table 2.19 Generalizations on the effect operating conditions severity (Anon, c2000)**

Operation	Severity	Pressure (Bar)	Reactor feed temperature °C	H <sub>2</sub> consumption (scf/bbl)
Production of diesel from heavy oil	Mild	83	371	1000-2000
Production of kerosene from light feed	Severe	172	427	2000-3000

### 2.1.3 Isomerization process

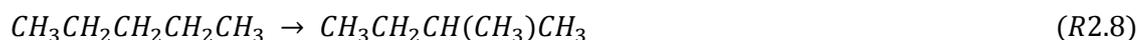
Isomerization converts n-paraffins (butane, hexane) to their isomers yielding gasoline components of high octane ratings in the lower boiling range. Conversion is attained in the presence of aluminium chloride catalyst activated with hydrochloric acid or a noble metal or zeolite catalyst (Speight and Ozum, c2002, Speight, c2007). The main objective of isomerization process is to improve the octane number of light naphtha fractions and at the same time also to decrease the quantity of benzene by saturation of the benzene fraction (Valavarasu and Sairam, 2013). The process is currently used to provide supplementary feedstock for alkylation unit (Speight and Ozum, c2002).

### 2.1.3.1 Isomerization feeds and product

Production of alkylation feed (isobutane) was the earliest significant process. The isomerization process can be conducted in liquid phase with dissolved catalyst or in the vapour phase with activated catalyst supported on a solid phase. A pure butane feed is mixed with hydrogen to prevent olefin formation and sent to the reactor at a temperature of 110-170 °C (383-443 K) and pressure of 20.7-68.9 bars. The product is chilled and gases are removed in a stabilizer column while hydrogen is separate. The bottom product of the stabilizer is sent to superfractionator, and n-butane and iso-butane are separated. With pentanes as feed, high temperatures favours the equilibrium and operating conditions of 250-500 °C (523-773) and 20.7-68.9 bars can be used (Speight and Ozum, c2002, Speight, c2007). Reaction 2.7 and 2.8 shows the isomerization of N-butane and N-pentane to isobutene and isopentane respectively.



N-butane                      Isobutane



N-pentane                      Isopentane

Aluminium chloride was used to isomerise butane, pentane and hexane during World War II. This catalyst is non-regenerable and has been and is still utilised with numerous carriers in fixed bed or liquid contactor, for the low temperature processes. Platinum or other metal regenerable or non-regenerable catalyst processes use a fixed bed reactor (Speight and Ozum, c2002).

### 2.1.3.2 Commercial isomerization processes

There are numerous commercially available isomerization processes depending on the specific design objectives. Few of those processes are summarise below.

Butomerate process is particularly aimed to isomerise n-butane to yield supplementary alkylation feedstock. The process runs with hydrogen recycle to eradicate coke deposition on the catalyst, but the isomerisation reaction can continue for prolonged period of time without

hydrogen. The catalyst consist of a small quantity of non-noble hydrogenation metal on a high surface area support.

The Penex process is a non-regenerative pentane and /or hexane commercial isomerization process. Platinum catalyst is use and reactions occur in the presence of hydrogen. The reactor conditions are selected to avert regeneration and ensure long catalyst life. The operating temperature and pressure ranges from 260-480 °C (533-753 K) and 20.7-68.9 bars respectively.

Isomerate process is a continuous isomerization process that employs a dual catalyst in a fixed bed reactor. Hydrogen is mixed with the feed along with the recycle gas, and the typical process comprises fractionation facilities to permit the recycling of n-paraffins almost to extinction. Operating conditions are mild 400 °C (673 k) and less than 51.7 bars. The process is particularly design to transform pentanes and hexanes into greatly branched isomers (Speight and Ozum, c2002).

#### **2.1.4 Fluid catalytic cracking**

The shell fluid catalytic cracking process (FCC) mixed preheated feedstock (heavy gas oil or vacuum gas oil) with hot regenerated catalyst. Volatile materials and catalyst are separated once reacted in a riser, and then the consumed catalyst is instantly stripped of entrained and hydrocarbons are absorbed in an active multistage stripper. A deNO<sub>x</sub>, deSO<sub>x</sub>, and particulate emission control device can be added in the flue gas train depending on the environmental conservation necessities (Speight and Ozum, c2002, Speight, c2007). Hydrogenation of pre-treatment of bitumen prior to FCC has been aimed to improve the yield of naphtha. To increases the quality and yield of distillate products, mild hydrotreating has been suggested to be carried out in the upstream of FCC unit (Speight and Ozum, c2002, Speight, c2007). The major aim of the FCC unit is to transform high boiling petroleum fractions (gas oil) to high value, high octane gasoline and heating oil. The objective of the unit is to upgrade low value feedstock's to more valued products.

Modern FCC catalyst are in the form of powder with four key constituents system; zeolite, matrix, binder, and filler. The zeolite also known as faujasite is the major ingredient of FCC

catalyst. It plays the vital role in selectivity and much of the catalytic activity. The catalysts performance is dependent on the nature and quality of the zeolite at large (Sadeghbeigi, 1995).

## 2.2 Sources of hydrogen within the refinery

The principal source of hydrogen within the refinery has been the catalytic reforming unit. This unit generates a large amount of hydrogen at 70-90 % purity that provides its requirements for hydrotreating and hydrocracking processes. Supplementary hydrogen needs might be provided by construction of a hydrogen plant that generates hydrogen gas by steam reforming of natural gas, naphtha or refinery off gases, if the hydrogen from the catalytic reforming is inadequate. Otherwise, partial oxidation of hydrocarbons or hydrogen importation via a pipeline is another alternative to steam reforming (Alves and Towler, 2002, Rabiei, 2012). The combination of steam reforming or partial oxidation facilities with pressure-swing adsorption (PSA) separation technology is a well know practice in novel designs, permitting the production of gas above 99 % hydrogen purity (Philcox and Fenner, 1997). A review of hydrogen production data for different refinery processes is given in table 2.20.

**Table 2.20 Typical hydrogen production data for different refinery processes (Lambert et al., 1994)**

Process	Wt. % on feed	Wt. % on crude
Semiregenerative Catalytic reforming	1.4-2.0	0.15-0.3
Continuous Catalytic reforming	3.5	0.35-0.6
Steam methane reforming	30	-
Partial oxidation	20-25	1.0-5.0
Catalytic cracking	0.01-0.5	0.01-0.04

Hydrogen is also recuperated from the off-gases of the hydrogen consuming processes in most refineries. These off-gases mostly comprise substantial quantity of hydrogen and light hydrocarbons such as methane, ethane etc.. The off-gases can be utilised directly as a source of hydrogen when there is a high concentration of hydrogen (usually, above 40 mol %). If the hydrogen concentration is very small (usually, below 40 mol %), it is vented into the refinery fuel system. For intermediate hydrogen concentrations, the hydrogen can be recuperated by purification if considered economical. The pressure-swing adsorption (PSA) separation technology, membrane permeation and cryogenic separation are the three purification technologies normally used for hydrogen purification in refineries (Abrardo et al., 1995, Wilcher et al., 1995). Table 2.21 shows the typical hydrogen concentration in refinery off gases.

**Table 2.21 Typical hydrogen concentration in refinery off gases (Rabiei, 2012)**

Processes	Hydrogen content (vol. %)	Initial pressure (Bar)
Catalytic reforming	40-85	28
Catalytic cracking (off-gas)	10-30	55
Hydrocracking	40-60	17-27.6
Hydrotreating (purge)	25-35	45
Thermalhydrodealkylation	50-75	28-26
Hydrogenation (purge)	85	-

### 2.2.1 Catalytic reforming reactions

Historically, hydrogen has been generated as a by-product from the catalytic reforming process of aromatic compounds used in gasoline and solvents. The major aim and objective of catalytic reforming is to improve the octane number quality of straight run naphtha and mixed naphtha comprising cracked materials. This is achieved by dehydrogenation (removal of hydrogen) from naphthenes to produce aromatics. In certain refineries (small scale) the hydrogen requirements may be fulfilled by hydrogen recovery from catalytic reformer product gases. However, it is not always necessary to have a catalytic reformer as part of refinery system, necessitating the need to build a hydrogen plant or import hydrogen. Table 2.22 shows a typical composition of catalytic reformer product gas. Naphtha without sulphur is best used as catalytic reformer feed. Naphtha from catalytic cracker containing olefins and aromatics are not suitable for catalytic reformer as it is more appropriate to increase gasoline octane by alkylation than reforming. Furthermore, reforming increases the quantity of gasoline in aromatics. Due to environmental regulations aromatics despite high octane values are not desired (Jones, c1995, Speight, 1997, Speight, 2000).

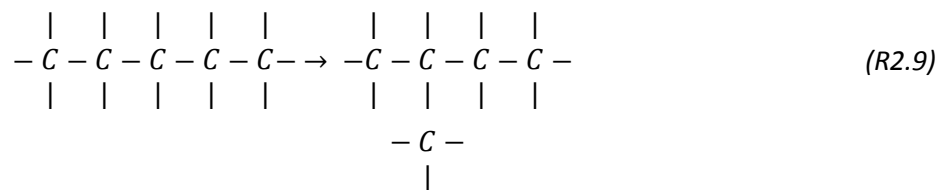
**Table 2.22 Composition of catalytic reformer product gas (Speight and Ozum, c2002)**

Constituent	Volume %
Hydrogen	75-85
Methane	5-10
Ethane	5-10
Propane	5-10
Butane	< 5
Pentane plus	> 2

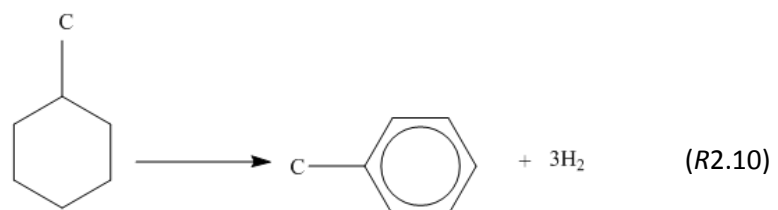
### 2.2.1.1 Reforming reactions and catalyst

The reactions are grouped in order of their respective hydrocarbon types and led by a catalyst under well-defined operating conditions.

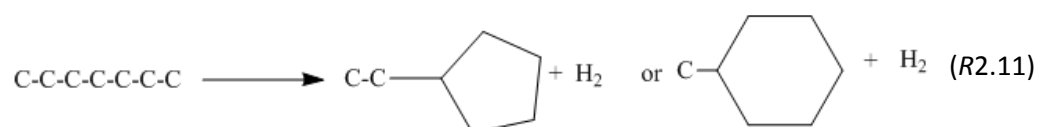
- Isomerization; this reaction is nearly thermoneutral heat release of  $\Delta H = 2$  kcal/mole with a insignificant effect on the final octane number. Normal paraffins are isomerise to isoparaffins, for example, pentane is rearrange to the isomer isopentane which increases the centane rating of gasoline feedstock (Parkash, c2003).



- Dehydrogenation; to produce aromatics, naphthenic hydrocarbons are dehydrogenated. The reaction is very fast and also endothermic  $\Delta H = 50$  kcal/mole. It is major advantage is that it produces hydrogen and also increases the octane number. Because of the endothermicity (large heat requirement) of the reaction the feed has to be reheated numerous times which is its main disadvantage. Example, methyl cyclohexane dehydrogenated to toluene (aromatic methyl benzene) (Nelson, c1958, Sinha, 2003, Parkash, c2003).

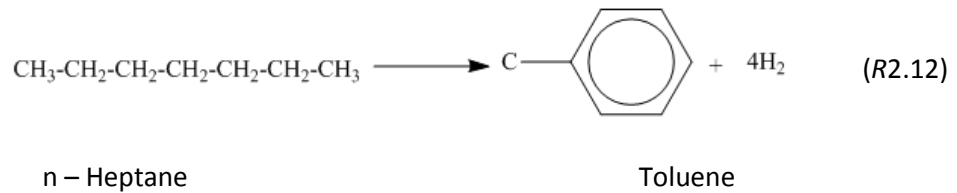


- Dehydrocyclization; the reaction is highly endothermic  $\Delta H = 60$  kcal/mole and it is the major reaction producing high octane gasoline. Example, normal heptane rearrangement to saturated ring structure of either ethyl cyclopentane or methyl cyclohexane (Nelson, c1958, Sinha, 2003, Parkash, c2003)



- Hydrocracking; an exothermic reaction with  $\Delta H = 10$  kcal/mole. This reaction breaks paraffins and removes alkyl side chains from aromatic and naphthenes. The reaction

rate and conversion rate is small at a low temperature compared to hydrodecyclization (Nelson, c1958, Sinha, 2003, Parkash, c2003)



Catalyst used for reforming comprise a high purity alumina base impregnated with platinum content of roughly about 0.35 % by weight and metallic activators. The catalyst is normally spheres of 2 mm diameter. More active catalyst at a low pressure is used as refiners develop their own process. Naphtha reforming catalyst are usually bimetallic catalyst comprising of a metal function mostly platinum and an acid function usually chloride alumina. The hydrogenation and dehydrogenation reactions are catalysed by the metal function and the acid function stimulates isomerization and cyclisation reactions (Anon, c2000, Parkash, c2003, Rahimpour et al., 2013).

#### 2.2.1.2 Catalytic reforming process

The most frequently used kind of catalytic reforming unit has three reactors each with a fixed bed of catalyst, heat exchangers, and auxiliary columns which utilises heat and the heaters in which heating the feedstock and intermediate product takes place. The process is operated in the temperature range of 350-500°C (623 – 773 K) and pressures of 1- 2.5 MN/m<sup>2</sup>. Product obtained includes; hydrogen, fuel gas, wet gas, light gasoline, light platformate and platformate (Ocic and Perisic, 2002, Ocic, 2005). Catalytic reformer energy characteristic are given below:

- Normally in a catalytic reforming process feedstock is preheated in heat exchangers using product stream of the process, before going into the process reactor.
- In the process heaters fuel gas is utilised as a fuel.
- Medium pressure steam is utilised to drive the ejector, to heat the bottommost of auxiliary column. One portion of the medium pressure steam is produced in the unit itself using the reboiler while use flue gases heat and the rest are provided externally.
- Pumps, fan (air cooling), auxiliary facilities and other equipment are driven by electric power (Ocic and Perisic, 2002, Ocic, 2005).

Many reforming processes are used differing only in the type of catalyst used and the manner in which they are regenerated. The diverse reforming processes used presently may be categorized as;

**Semi regenerative process:** this is the most common type of catalytic reforming unit; it leads reforming capacity to about 60 %. The unit is normally made up of three reactors each with a furnace preheater. The process is categorized by continuous operation over a long period of time, with drop in catalyst activity because of coking. With decreasing activity of the catalyst, aromatics yield and purity of the by-product hydrogen reduce. As catalyst activity declines the reactor temperature is raised in order to retain the conversion to almost constant.

The reformer is shut down to regenerate the catalyst in situ when the reactors reach the end of cycle levels. The Pt-Re catalyst is normally used for semi regenerative (SRR) due to its high tolerance level of coke deposition and it is easily regenerated. Research octane number of normally 85-100 can be archived in this process. (Rahimpour et al., 2013). Hydrotreated naphtha is mixed with a hydrogen rich recycle stream and pass over a low pressure feed effluent heat exchanger or heater. Then, the first reactor at about 482°C (755 K). The stream is reheated before entering the second reactor as reactions are endothermic (because of dehydrogenation of naphthenes to aromatics and dehydrocyclization of paraffins to aromatic carbons) (Anon, c2000, Sinha, 2003).

Equally the effluent of the second reactor is heated before entering the third reactor. The effluent from this reactor is cooled then separated into liquid products and hydrogen rich gas. Part of the hydrogen gas is bled off to uphold system pressure and part of it separated and recycle. Catalyst life is regulate by carbon laydown and usually expected to be one year (Anon, c2000, Sinha, 2003). Figure 2.8 show a schematic diagram of semi regenerative process, while table 2.23, 2.24, 2.25, and 2.26 shows a typical catalytic reformer operating conditions, yield product yield, and utility consumption respectively.

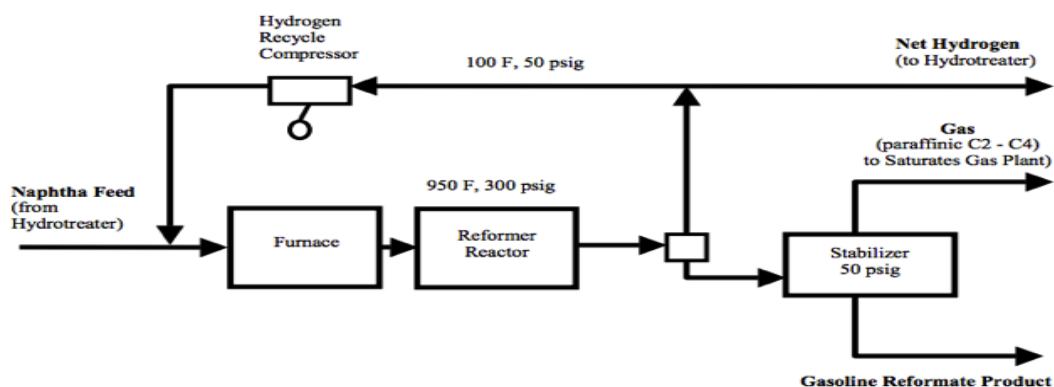


Figure 2.8 Naphtha catalytic reformer unit semi regenerative process (Anon, c2000)

Table 2.23 Catalytic reformer operating conditions (Parkash, c2003)

Operating variable	Value
Inlet temperature, SOR	501 °C (774 K)
Inlet temperature, EOR	545 °C (818 K)
Separator pressure	13 bar
Separator temperature	54 °C (327 K)
Moles of hydrogen/ moles of feed	4.5
Space velocity (liquid hourly space velocity on weight basis)	2.75

Table 2.24 Catalytic reformer yield (Parkash, c2003)

Component	96 RON W/W
<b>Feed</b>	
Heavy naphtha	1.0000
Total feed	1.0000
<b>Products</b>	
H <sub>2</sub>	0.0193
C <sub>1</sub>	0.0085
C <sub>2</sub>	0.0138
C <sub>3</sub>	0.0269
IC <sub>4</sub>	0.0180
NC <sub>4</sub>	0.0228
IC <sub>5</sub>	0.0276
NC <sub>5</sub>	0.0184
C <sub>6+</sub>	0.8447

**Table 2.25 Catalytic reformer product yield, W/W (Parkash, c2003)**

Feed	100 RON	102 RON
Heavy naphtha	1.0000	1.0000
Total feed	1.0000	1.0000
Products		
H <sub>2</sub>	0.0310	0.0320
C <sub>1</sub>	0.0120	0.0140
C <sub>2</sub>	0.0200	0.0230
C <sub>3</sub>	0.0290	0.0330
IC <sub>4</sub>	0.0170	0.0190
NC <sub>4</sub>	0.0230	0.0260
C <sub>5+</sub>	0.8680	0.8530
Total product	1.0000	1.0000

**Table 2.26 Catalytic reformer utility consumption per ton of feed (Parkash, c2003)**

Utility	Semi regenerative reformer	Continuous reformer
Fuel gas	2449618400 J	2449618400 J
Steam	496258900 J	496258900 J
Power	19080000 J	61200000 J
Cooling water	3.2 L	5.8 L

**Fixed bed catalytic reforming:** this type of catalytic process can be categorised based on the catalyst type namely; cyclic regenerative with platinum alumina catalyst and cyclic regenerative with non-precious metal oxide catalyst. Both processes use swing reactor to regenerate a portion of the catalyst while the leftovers stays on stream (Speight and Ozum, c2002). In cyclic reformers a swing reactor is present that can be isolated separately as the other reactors operate. Hence, in situ regeneration can be carried out in each reactor whereas the others reactors are in operation. In this method the reforming process continues while only one reactor at a time has to be taken out of operation for regeneration. Research octane number of normally 100-104 can be archived in this process. The main advantage of the process is the use of low operational pressure, insignificant change in total catalyst activity and hydrogen purity with time and conversion. On the other hand, the disadvantage of the process is that all reactors alternate often throughout regeneration. Hence, a complex process design is required with good safety precautions for the switching policy (Rahimpour et al., 2013)

**Continuous reforming (moving bed) process:** continuous reformers are the most modern kind of catalytic reformers. A step change in reforming technology (continuous process) is seen in this process compared to the other reforming technologies. The catalyst is regenerated in a special regenerator and added to the operating reactors. This process is characterised by reduced catalyst necessities, high catalyst activity, uniform reformate of higher aromatic content, and high hydrogen purity. Research octane number of normally 100-108 can be achieved in this process (Aitani, 1995). Figure 2.9 shows a typical continuous catalytic reformer equipment arrangement. The reactant passes radially through the catalyst to the inner channel and then to the succeeding bed and the catalyst flows down amid the concentric rings of screen (Anon, c2000).

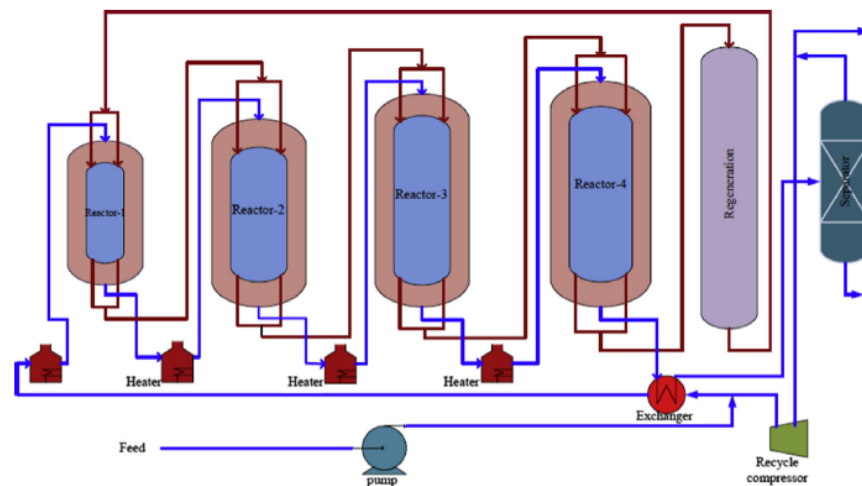
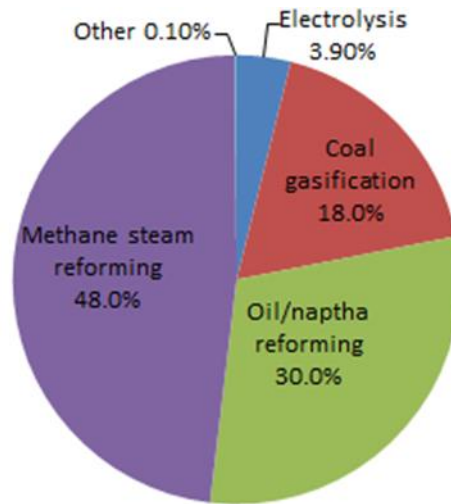


Figure 2.9 Continuous catalyst regeneration reformer (Rahimpour et al., 2013)

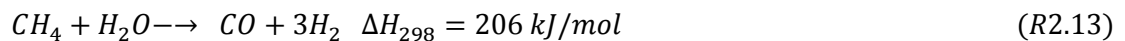
### 2.2.2 Conventional Steam Methane Reforming (C-SMR)

As mentioned earlier, hydrogen as the by-product of the catalytic reforming unit is not always sufficient to meet refinery needs; moreover not all refineries have a catalytic reforming unit; thus, there is a need for an alternative source of hydrogen. Steam methane reforming (SMR) is the most established and commonly used process to generate hydrogen on a large scale (Rostrup-Nielsen et al., 2000). Approximately, 90 % of the world's overall hydrogen generation is by SMR of fossils fuels (Rostrup-Nielsen et al., 2000, Simpson and Lutz, 2007, Chiron et al., 2011). Figure 2.10 shows the major production methods of hydrogen. Natural gas and naphtha are the most commonly used feed-stocks, but presently natural gas is the major source of hydrogen production (Ding and Alpay, 2000, Johnsen and Rostrup-Nielsen, 2002).

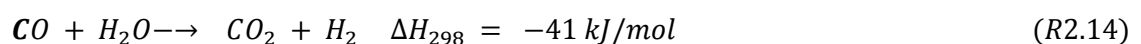


**Figure 2.10 Present distribution of the primary energy source for hydrogen production (Ewan and Allen, 2005)**

The SMR process used in industry consists of two main reaction steps followed by physical separation of the hydrogen from the product gases. The first step in this process is an endothermic steam methane reforming reaction (R2.13) that takes place at a very high temperature 800-1000°C (1073-1273 K) and pressure of 20.3-35.5 bars. In this step, natural gas containing mainly methane (for example, 89% CH<sub>4</sub>, 9% C<sub>2</sub>H<sub>6</sub>, C<sub>3</sub>H<sub>8</sub>, C<sub>4</sub>H<sub>10</sub>, N<sub>2</sub> and CO<sub>2</sub> roughly) reacts endothermically with steam (H<sub>2</sub>O) over a nickel based catalyst at an elevated temperature and pressure. Steam and Carbon ratio is an important factor to consider in reforming process; this is because it helps in determining the overall efficiency of the process. Basically, it is beneficial and more effective to have a higher steam to carbon ratio because; (1) it inhibits carbon formation, (2) favours hydrogen production, (3) decreases the quantity of unreacted hydrocarbon feed-stocks, (4) helps in the conversion and elimination of carbon monoxide.



The second step is the exothermic water gas shift reaction (R2.14) at a low temperature 200-400°C (473-673 K) (Adris et al., 1996, Boyano et al., 2012, Fernandez et al., 2012b).



The syngas existing the reformer is passed over a water-gas shift reactor that transforms the CO to CO<sub>2</sub> and H<sub>2</sub> consuming the available water (H<sub>2</sub>O) in the syngas or supplementary H<sub>2</sub>O added to system. Even though the reaction in equation (R2.14) is exothermic, the net reaction of

(R2.13) and (R2.14) is endothermic. In practice, the shift reaction takes place over two reactors that run within 200-400 °C (473–673 K) and 127- 177 °C (400–450 K) respectively. Figure 2.11 displays simple schematic of the conventional SMR system, depicting heat coming from an external source. Practically, the required heat is provided by combustion of supplementary methane or by using the available energy in the separated exhaust stream through combustion or simple heat exchanger (Simpson and Lutz, 2007, Pérez-Moreno et al., 2013). The C-SR unit comprises a furnace that is made up of tubes in it, with catalyst loaded in these tubes to increase the rate of reaction and heat transfer efficiency. The industrial process requires at least one reformer and one water gas shift (WGS) reactor and a separator. The WGS reactor may need two units with cooling amid them to maximise water conversion to hydrogen (Barelli et al., 2008).

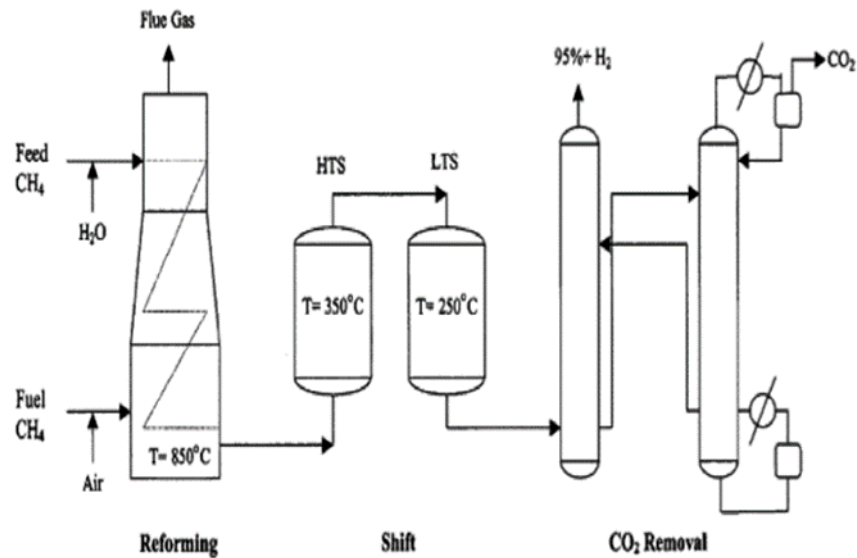


**Figure 2.11 Simplified schematic of C-SR system (Barelli et al., 2008)**

Separation of the hydrogen from the syngas leaving the WGS reactor (mostly H<sub>2</sub>, H<sub>2</sub>O and CO<sub>2</sub>) is the final step in the process. Numerous techniques can be utilised to accomplish the separation of hydrogen. Three of the most common techniques used are; pressure swing adsorption (PSA), membranes, cryogenics [38, 39] and chemical absorption for example CO<sub>2</sub> scrubbing using methyldiethanolamine (MDEA) and monoethanolamine (MEA) solution [40]. Hydrogen membrane separation is a promising and developing technology but also proficient in generating high end stream hydrogen purity (>99%) with moderate hydrogen recovery (85-90 %). PSA separation techniques are reasonably mature technologies that are energy intensive and deliver numerous degrees of end stream hydrogen purity (>99%) and moderate hydrogen

recovery (65-90 % dependent on the tail gas pressure) (Permanu et al., 1999, Whysall and Picioccio, 1999, Simpson and Lutz, 2007, Pérez-Moreno et al., 2013).

Sulphur free natural gas is not always available for many refiners to generate hydrogen. Thus, higher boiling hydrocarbons the like of propane, butane, or naphtha may be utilised as feedstock to produce hydrogen using the SMR process.

### **2.2.2.1 Effects of C-SMR process on hydrogen production and environments**

The steam methane reforming process would have been the most ideal method for hydrogen production if not for the fact that large amount of valuable resource (natural gas) is needed as both feed gas and combustion fuel. In fact, steam reforming of methane and other fossils based hydrocarbon is not in environmental equilibrium since the production and released of carbon dioxide and carbon monoxide into the atmosphere are involved. For every 4 mole of H<sub>2</sub> produced by complete steam methane reforming process For example, 1 mole of CO<sub>2</sub> is generated. In addition, tons of CO<sub>2</sub> are generated and release into the atmosphere by the reformer furnace flue gas (Gaudernack and Lynum, 1998, Speight, c2007).

The two key problems in the C-SR process can be summarised as follows:

- the reaction is endothermic and necessitates an external source of heat
- the nickel based catalysts need the use of high steam/carbon ratios (3-3.5) to evade coke deposition that causes the deactivation of the catalyst (Speight, c2007, Pérez-Moreno et al., 2013).
- Emission of CO<sub>2</sub> the major cause of global warming

Regardless of those obvious defects, the process has the following advantages;

- Readily available feedstocks (methane and water)
- For each mole of methane consumed, three moles of hydrogen are produced
- The process is flexible to variety of hydrocarbon feedstock
- The process operate at low pressures less than 31 bar (450 psi)
- Good use of input energy (reaching 93 %)
- Good process kinetics
- Catalyst that are stable and resist corrosion can be use (Speight, c2007).

Production costs are extremely reliant on the scale of production. Large, modern SMR hydrogen plants have been built with hydrogen production capacities beyond 480,000 kg/per day, or

about 200 million standard cubic feet per day. The technology is also scalable to smaller scale application (Anon, 2008f).

### **2.2.2.2 Maturity of C-SMR process**

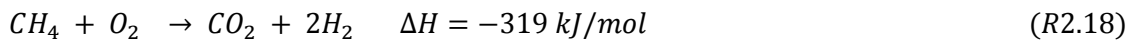
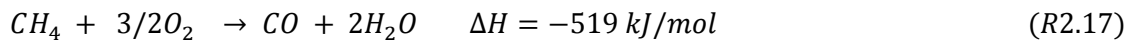
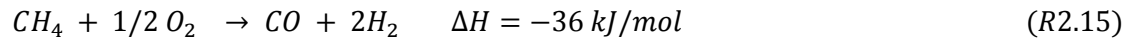
The C-SR is fully mature and developed technology (Momirlana and Veziroglu, 1999, Antzaraa et al., 2015). For years, it has been the leading technology for hydrogen production in refining and petrochemical complexes (Collodi and Wheeler, 2009). The technology has dominated syngas production for the past 70 years (Zhu et al., 2001) and still counting.

Numerous oil and gas companies (e.g. Linde engineering, with 'more than 200 constructed units producing capacities of synthesis gas from 1,000 to over 120,000 Nm<sup>3</sup>/h of') are involved in commissioning and R&D of the C-SR process. Institutes such as University of Leeds and university of Birmingham are also involved in R&D. 'Small-scale conventional (long tube, high temperature) steam methane reformers are also commercially available from a number of companies' (Ogden, 2001).

### **2.2.3 Partial Oxidation (POX)**

Another commercially available method for generating hydrogen from hydrocarbons is partial oxidation (POX). Natural gas mainly methane is usually oxidized to produce carbon monoxide and hydrogen (R2.15). The main reaction is accompanied with full oxidation of methane (R2.16) and with side reactions (R2.17 and R2.18) (Figen and Baykara, 2015). Reaction R2.15 is the main reaction and it generates synthesis gas CO and H<sub>2</sub>. Reaction R2.16 is a full combustion reaction of CH<sub>4</sub> while R2.17 is a side reaction that upsurges selectivity of CO and reduces selectivity of H<sub>2</sub>. Reaction R2.18 on the other hand upsurges selectivity of H<sub>2</sub> and reduces selectivity of CO (Engera et al., 2008, Figen and Baykara, 2015). The reaction is exothermic and no external heating is required. However, the yield per mole of methane input and system efficiency can be significantly improved by use of catalysts (Ogden, 2001). This process (POX in the presence of catalyst) is termed catalytic partial oxidation (CPOX). CPOX of methane reaction has been studied in the presence of heterogeneous catalysts with or without noble metal constituents (Figen and Baykara, 2015). Owing to the high cost and low accessibility of noble metal catalysts (despite having high activity and stability), non-precious metal catalysts are often preferred in industrial plants (Koh et al., 2007, Rogatisa et al., 2009). Even though nickel (Ni) containing catalysts is the most widely used due it is high activity, the exothermic CPOX reaction causes

solid carbon deposition, sintering of Ni owing to coke formation; and catalyst deactivation by forming  $\text{NiAl}_2\text{O}_4$  phase particularly when Ni is used with  $\text{Al}_2\text{O}_3$  support (Rogatisa et al., 2009, Figen and Baykara, 2015). The CPOX is operated at a relatively low temperature 600-900 °C (873-1173K) (Song, 2002).



Hydrogen production via POX from heavy feedstock such as vacuum residues and asphaltic pitch is non-catalytic process called thermal partial oxidation. Catalysts are not required due to the high temperature use 1100-1500 °C (1373-1773K) (Song, 2002). The heavy feedstock is partially burned using oxygen in a reactor, while the remaining part of the feed is cracked due to the high temperature. The composition of the hot synthesis gas leaving the reactor is primarily CO and  $\text{H}_2$  with small minor amounts of  $\text{CO}_2$ ,  $\text{CH}_4$ , argon (Ar), nitrogen (N), and hydrogen sulphide ( $\text{H}_2\text{S}$ ) along with some root and ash. Ash originates from the metals in the residual feed and Ar from air, from which oxygen is separated (Marion and Slater, 1963, Parkash, c2003). Table 2.27, 2.28, and 2.29 list the parameters of the reaction.

Cooling of the synthesis gas is done either by direct quenching or raising steam in waste heat boilers. The cooled synthesis gas is directed to a single stage shift converter that transform most of CO to  $\text{CO}_2$  by reacting with steam over Co-Mo catalyst (Auer, 1971, Parkash, c2003). Followed by removal and separation of acid gas.  $\text{H}_2\text{S}$  recuperated is used for elemental sulphur production (Parkash, c2003).

**Table 2.27 Typical operating conditions (Parkash, c2003)**

Parameter	Value
Temperature	1093-1538 °C (1366-1811 K)
Pressure	83-138 bar

**Table 2.28 Partial oxidation process, overall yield (Parkash, c2003)**

Property	
<b>Feed origin</b>	<b>Vacuum residue from wafra crude</b>
API	4.3
Specific gravity	1.0420
Sulphur wt.%	6.2
Viscosity, 99 °C CST	4000
<b>Stream feed</b>	<b>Yield wt. fraction</b>
Vacuum residue	1.0000
Boiler feed water	1.1140
Oxygen	1.7154
Total	3.8294
<b>Product</b>	
H <sub>2</sub>	0.2105
CH <sub>4</sub>	0.0504
A	0.0061
N <sub>2</sub>	0.0031
CO <sub>2</sub> + Water	3.4956
H <sub>2</sub> S	0.0637

**Table 2.29 Utility consumption per ton of feed (Parkash, c2003)**

Utility	O <sub>2</sub> import at 97 bar (1400 psig)	In plant generation of O <sub>2</sub> . Air separation unit on steam drive
Power	368640 kJ	0 kJ
Fuel	4434654 kJ	9819591 kJ
Steam	-390671.9 kJ	0 kJ
Cooling water	55 L	226 L

Hydrogen rich feedstock e.g. coal, petroleum coke, biomass or some other hydrocarbon feedstock such as oil can be used as an alternative to natural gas. With natural gas as a feedstock, the partial oxidation route normally generates hydrogen at a faster rate than conventional SMR. However, it generates less hydrogen from the same amount of feedstock (Anon, 2008f). A hydrogen plant constructed on partial oxidation consists of a partial oxidation reactor, trailed by a shift reactor and hydrogen purification equipment as shown in Figure 2.12 (Ogden, 2001).

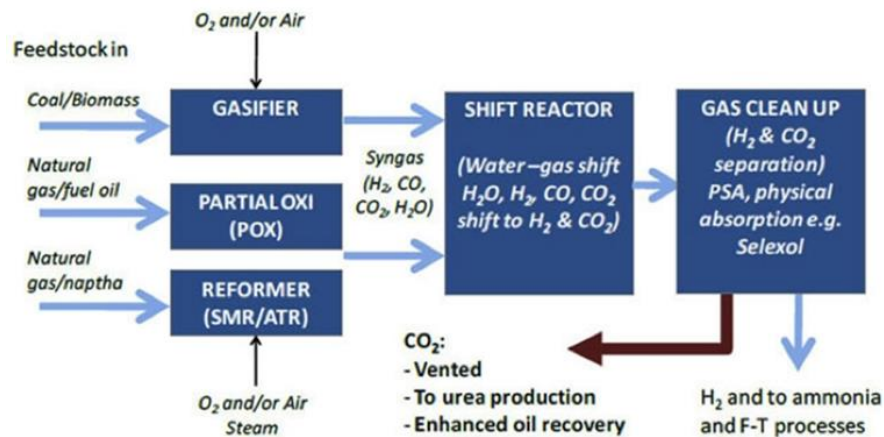


Figure 2.12 General process flow for industrial hydrogen and syngas production (Zakkour and Cook, 2010)

### 2.2.3.1 Effect of POX process on hydrogen production

Small-scale POX systems have lately become commercially available, but are still experiencing serious R&D. Such systems have a quicker response to time, making them suitable for following rapidly variable loads, and can handle numerous fuels, comprising methane, ethanol, methanol, and gasoline. POX systems do not require indirect heat exchangers like the case of steam methane reformers, thus it has been suggested that POX reactors could have lesser cost than steam methane reformers (Ogden et al., 1996, Ogden, 2001). Despite these obvious advantages, the process has the following disadvantages;

- normally less energy efficient than C-SR due to the higher temperatures involved (which worsens heat losses) and the problem of heat recovery (applicable to thermal partial oxidation)
- The downstream WGS reaction and purification steps are expected to be more costly even though the POX reactor is expected to be less costly than a steam methane reformer
- pure oxygen feed to the POX, causes great capital expenses for small scale oxygen generation (Ogden et al., 1996, Ogden, 2001).

Numerous companies are involved in developing small-scale POX systems. For example, variety of hydrogen generation systems based on partial oxidation has been developed by Hydrogen Burner Technology (HBT), Inc. This includes reformer that generates very pure hydrogen for cogeneration in buildings (Ogden, 2001). POX reformer suitable for use in vehicles has been developed by Argonne National Laboratory (Ahmed et al., 1998). A number of projects to use partial oxidation systems in stationary fuel cells has also been conducted and commissioned (Ogden, 2001). Institutes/universities are also involved in R&D of the process.

#### 2.2.4 Auto-thermal reforming (ATR)

The term Autothermal reforming (ATR) refers to combination of steam reforming with partial oxidation process in a single reactor. The process combines specific top features of these two processes (C-SR and POX). ATR process has attracted much more attention due to its great efficiency for hydrogen production and a lesser dependence on supplementary power sources (Dauenhauer et al., 2007, Chen et al., 2009a, Pasel et al., 2015). Hydrocarbons (e.g. methane, propane, and diesel fuel) or carbohydrates (e.g. cellulose and ethanol) are usually used as feedstocks for hydrogen production in this process (Ogden, 2001). Natural gas (mainly methane) or any feedstock used is first oxidized to syngas (CO and H<sub>2</sub>) in a catalytic furnace, followed by CO reaction in the presence of water to produce CO<sub>2</sub> and H<sub>2</sub> in a catalytic shift reaction (Chaubey et al., 2013, Pasel et al., 2015). The MEA solutions is then used to capture CO<sub>2</sub> in an absorption process. The ATR process does not require external source of energy due to the exothermic heat generated by POX directly fulfils the demand of SMR. The process consists of a thermal zone in which the temperature rises because of exothermic POX and also drops because of the endothermic SMR. The ratio of O<sub>2</sub> in feedstock/fuel and steam has to be regulated at all times in order to control the reaction temperature and product gas composition as well as inhibits by-products production (Aasberg-Petersen et al., 2004).

Catalysts play a vital role in the ATR process and although numerous types of catalysts have been studied nickel is still the most commonly used in commercial plants due to its low cost and excellent C–C bond cleavage activity (Min Hye Youna et al., 2006, Seo et al., 2007). The performance of nickel catalyst in ATR is determined by the nature of supporting material, this is because the supporting element affects the dispersion and stability of the catalyst (Youn et al., 2008). However, these catalysts are also extremely active in coke deposition. To avert coking, Ni crystallites in small size are highly required. The best possible conditions for hydrogen production require a high temperature at the exist of the reforming reactor 799 –910 °C (1072-1183 K) and high additional steam (molar carbon to steam ratio of 2.3-3), and fairly low pressure below 31 bar (Speight, c2007, Chen et al., 2009a). A number of studies have been carried out on the performance of noble metal catalysts to accomplish high yield of hydrogen at low temperature, but their high cost is the major problem for their effective use in the process (Chaubey et al., 2013). Noble metal catalysts the like of Rh–Ce/Al<sub>2</sub>O<sub>3</sub> (Deluga et al., 2004) and Ir/La<sub>2</sub>O<sub>3</sub> (Chen et al., 2009a) have been verified to be ideal for ATR of ethanol. Non- noble metal based catalysts have also been reported to exhibit fairly high catalytic performance in the ATR of ethanol (Velu et al., 2002, Fierroa et al., 2005, Zakkour and Cook, 2010).

#### **2.2.4.1 Effect of ATR process on hydrogen production**

ATR has benefits over the SMR process as no direct CO<sub>2</sub> emissions are made due to all of the heat release is internal (Metz et al., 2005). Conversely, these advantages are balanced by the investment and running costs of the ATR plant. The high cost of noble metals would limit their use in a large scale plant (Chen et al., 2009a). Hot spots formation in the initial parts of the reactor, formation of coke in the final part of the reactor and catalyst low activity due the oxidation of active metal phase are also major disadvantages of the ATR process

ATR are being developed by various research/industries usually for fuel processing of gasoline, diesel and logistics fuels and for natural gas fuelled PEMFC cogeneration systems (Ogden, 2001, Pasel et al., 2015). Priority is given to ATR at Juelich because it has been experimentally verified to be the most robust dynamic, and simple variant (Pasel et al., 2015).

Some research/industrial groups and companies involved include; (1) Johnson-Matthey: developed a Hot-Spot ATR capable of reforming methanol and methane (Reinkingh, 1998). (2) Hydrogen Burner Technologies, Inc: development of ATR system for use with fuel cells and for hydrogen production. (3) Analytic Power: assessment of multi-fuel reformer technology, including ATR (Ogden, 2001) etc.

ATR has the potential to produce high purity hydrogen and other chemical products such as methanol and synthetic fertiliser (ammonia) (Noelker and Johanning, 2010, Pasel et al., 2015). However, ATR syngas generator is ideal for Fischer-Tropsch syntheses as it provides the required gas composition straight away. In addition to using pure oxygen it is technically possible to operate the ATR on plain air and feed the nitrogen containing syngas to the Fischer-Tropsch synthesis (Noelker and Johanning, 2010).

#### **2.2.5 Hydrogen recovery**

Over years of operation, refinery fuel-gas systems the like fluidized catalytic cracking, delayed coking, catalytic reforming, hydrotreating, hydrocracking, and other process units such as blown-down gases of ammonia and methanol production have become the repository for purge gases. Numerous chemical and petrochemical industries are trying to evade capital investment in hydrogen generation facilities due to the fact that hydrogen is considered as a utility not a

profit centre (Lee et al., 2013, Shalygin et al., 2015). Even though hydrogen purification units such PSA and membrane are an attractive alternative to construction of new plants or upgrade, it includes complex decisions such as (Rabiei, 2012, Lee et al., 2013)

- stream to recuperate
- recovery technology to utilised
- Inlet and outlet pressure to use
- “that trade off to make between product purity, recovery, and capital cost” (Rabiei, 2012, Lee et al., 2013)

It is essential to clearly identify the price and incentives on which the comparisons will be established to justify hydrogen retrieval from off gas or purge gas. Any quantity of hydrogen recuperated will decrease the size of a new hydrogen plant, which can decrease capital cost of a new plant or decrease operating cost for feed. Hydrogen recovery from off gas or purge gas may suspend the required additional hydrogen plant or incremental hydrogen production facilities when the capacity of an existing hydrogen plant is limited. To decrease the compression cost, it is vital to recover hydrogen at the highest possible pressure (Rabiei, 2012, Lee et al., 2013). Figure 2.13 and Table 2.30 shows sources of refinery off gases and hydrogen purge streams and off gas sources and composition respectively.

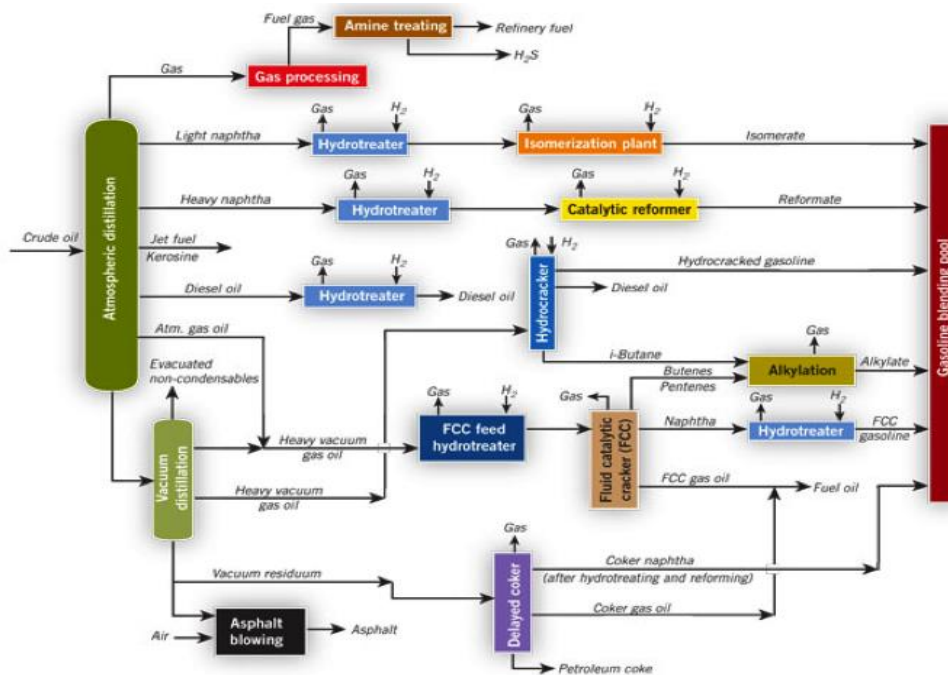


Figure 2.13 Sources of refinery off gases and hydrogen purge streams (Lee et al., 2013)

**Table 2.30 Off gas sources and composition (Lee et al., 2013)**

Off gas source	Crude distillation mole %	Hydrotreaters mole %	FCC/ coker mole %
Hydrogen	9.00	70.00	10.50
Nitrogen	2.50	-	5.00
Methane	5.50	15.00	40.50
Ethane	10.00	7.50	12.00
Ethylene	-	0.01	7.50
Propane	22.00	3.60	4.50
Propylene	-	0.06	6.50
Oxygen	-	-	0.20

### 2.2.5.1 Hydrogen recovery technologies

Pressure swing absorption process; this process work by adsorbing CO<sub>2</sub>, CO, CH<sub>4</sub>, N<sub>2</sub>, and H<sub>2</sub>O at normal pressure while letting hydrogen to pass through. The absorbents reliant on the particular use are made up of molecular sieve, activated silica, activated alumina or activated carbon. This process is the common purification technique of choice for steam reforming due to it generation of high purity hydrogen and similarly it is used for refinery off gases where it vies with membrane technology. Variance in impurity partial pressure between the feed and tail gas is the driving force in this process (Parkash, c2003) table 2.31 below show the features of the three commonly use hydrogen recovery technologies.

**Table 2.31 Hydrogen recovery technologies (Patel et al., 2006)**

Features	Adsorption	Membranes	Cryogenics
Hydrogen purity	99.9 %+	90-98 %	90-96 %
Hydrogen recovery	75-92 %	85-95 %	90-98 %
Feed pressure	10-40 bar	20-160 bar	> 5 – 75 bar
Feed hydrogen content	> 40 %	> 25 – 50 %	> 10 %
Hydrogen product pressure	Feed pressure	<< feed pressure	Feed/low pressure
Hydrogen capacity	1-200 MMscfd	< 50 MMscfd	5-60 MMscfd
Pre-treatment requirement	None	Minimum	CO <sub>2</sub> , H <sub>2</sub> O removal
Multiple products	no	no	Liquids hydrocarbons

Membrane technology; in this process gases are separated by differences in the rate of diffusion. Pressure drives the separation, therefore they are ideal for high-pressure feeds (>20 bar/ 300

psig) like hydroprocessing of purge gases. A preheater exchange and separator is needed to remove heavy constituent that could condense and damaged the membrane. Hydrogen sulphide must be removed from the feed gas as it can damaged the membrane (Speight, 1997, Speight, c2007, Rabiei, 2012, Lee et al., 2013). Presently, the membrane technology is widely used in many areas because of its simplicity, ease of operation and it cost effectiveness (Gilassi and Rahmanian, 2015b)

Cryogenic technology; this technology works by chilling the gas and condensing some or all of the components for the gas stream. Separation may include distillation or flashing depending on the product purity needed. Ability to separate diverse product from a single stream is one of the advantage of this process (Speight, 1997, Speight, c2007).

## **2.3 Other available methods and future trends in hydrogen production**

A number of methods are available for hydrogen production (C-SR, POX, ATR and hydrogen recovery) as mentioned previously in section 2.2. The C-SMR process is the most dominant and mature process for hydrogen production see section 2.2.2 for full details of the process. In this section, detail explanation on the available and future trend of hydrogen production are discussed.

### **2.3.1 Chemical looping steam reforming (CL-SR) process**

Chemical looping reforming (CL-SR) process was introduced to evade the gap in external heating source, process efficiency and cost in conventional steam reforming process. The term presently lacks any clear and even recognised meaning (Ryden and Ramos, 2012). CL-SR is described as a partial oxidation process where oxygen carriers are used as a source of undiluted oxygen (Ryden et al., 2008, Diego et al., 2008). Other researchers such as (Lyon, 1996, Ravi V. Kumar et al., 1999, Lyon and Cole, 2000) have defined CL-SR (also called unmixed steam reforming (USR)) as an auto-thermal cyclic steam reforming process for generating hydrogen from hydrocarbon fuels and specifically used it with a fixed bed reactor using alternating feed flows, generating different products. They basically considered the process as an auto-thermal reforming process. CL-SR have been utilised for hydrogen generation for ages, such as continuous hydrogen generation through steam-iron reaction coupled with chemical looping combustion (CLC) and hydrogen production through steam reforming also coupled with CLC (Rydén and Lyngfelt, 2006, Ryden and Ramos, 2012).

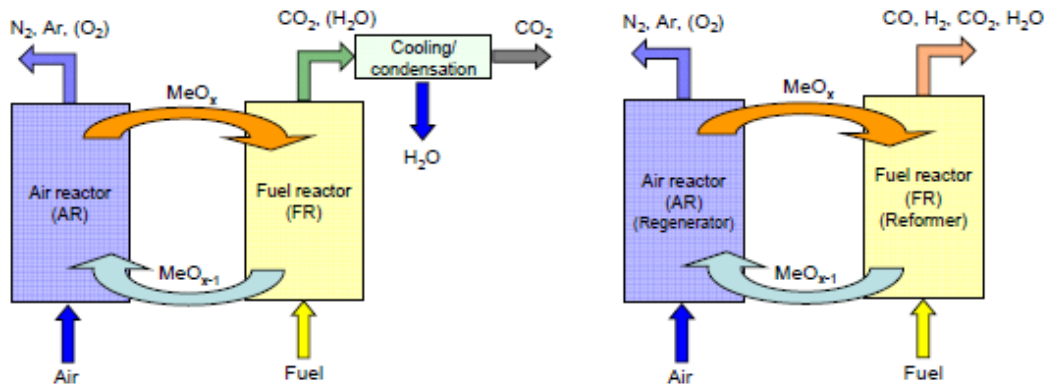
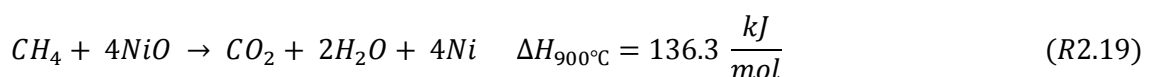


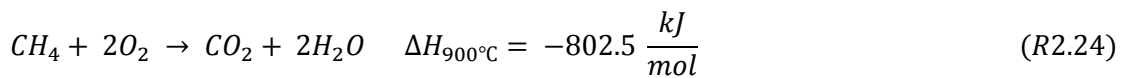
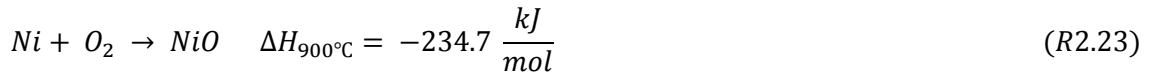
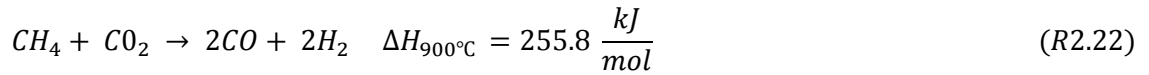
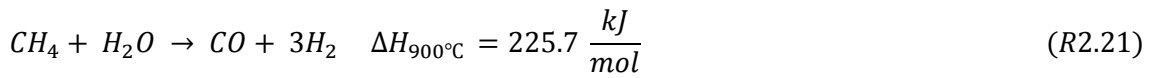
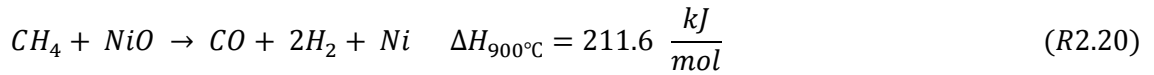
**Figure 2.14 Chemical looping combustion (Left) and chemical looping reforming (Right) (Pröll and Hofbauer, 2011)**

CLC is a combustion process with intrinsic CO<sub>2</sub> separation (evading the requirement of CO<sub>2</sub> separation units and lacking any penalty in energy). ‘Metal oxide is used to transport oxygen from air to fuel. If suitable metal oxide is used as the oxygen carrier, the CLC system can be operated in such a way that the exhaust gas consists of CO<sub>2</sub> and H<sub>2</sub>O only and allows for subsequent water condensation, compression and storage of CO<sub>2</sub>. The costly gas separation steps are inherently avoided. Therefore, CLC is one of the most energy efficient approaches to carbon capture from power production or fuel upgrading’ (Storset et al., 2013). CL-SR uses same basic principles as CLC with the major difference being in the desired product (H<sub>2</sub> and CO are the desired products for CL-SR not heat). This necessitates the need to keep the air to fuel ratio low to evade the fuel from being oxidised completely to H<sub>2</sub>O and CO<sub>2</sub> (Ryden and Ramos, 2012).

### 2.3.1.1 Principle of CL-SR process

The CL-SR process is based on the transfer of oxygen from air to the fuel via a solid oxygen-carrier eluding direct contact between fuel and air (Silvester et al., 2015). (Zafar et al., 2005) have investigated experimentally oxygen carriers specifically for CL-SR. The principle behind CL-SR process is to partially oxidise hydrocarbon in two different steps. The process gas is fed into the reactor where it may be oxidised to H<sub>2</sub>O and CO<sub>2</sub> but most of it should be oxidised to CO and H<sub>2</sub> by the metal oxide. With natural gas (mainly methane) as fuel and nickel oxide as catalyst, this will be in accordance with following reaction (R2.19) and (R2.20) respectively.





To improve the relative importance of steam reforming, steam could be added (R2.21) or CO<sub>2</sub> reforming reaction (R2.22). Reduced Oxygen carriers are taken to a second reactor (air reactor) where it is oxidised to its initial state with O<sub>2</sub> provided with air as displayed in equation (R2.23). When the fuel and oxygen carriers reacts according to reaction (R2.19) and (R2.23), heat corresponding to the lower heating value of the fuel is released (Ryden and Ramos, 2012). This is expected because the net reaction is combustion of the fuel with the oxygen that is reaction (R2.24); this reaction scheme is called CLC. Reaction (R2.21) and (R2.22) are strongly endothermic and do not offer reduced oxygen carriers that can be re-oxidised through equation (R2.23) for heat, hence only small quantity of steam and CO<sub>2</sub> could be added as fuel or else a process that need external heat is required which is technically unfavourable at relevant temperature (Ryden and Ramos, 2012).

The CL-SR concept shown in Figure 2.15 has been suggested by (Ryden and Ramos, 2012) to be proficient in diverse type of reactors and configurations, like; two interconnected moving or fluidized-bed reactors, alternated packed or fluidized-bed reactor, or a rotating reactor. Most CL-SR plants configuration worldwide at present consist of two interconnected fluidized-bed reactors, one of them being the fuel-reactor and the other the air-reactor. In addition, it has been recommended that two loop seal devices should be used to evade gas leakage between reactors. Although the reduction reaction is endothermic, the oxidation reaction is exothermic. Heat of reaction is dependent on oxygen carrier and fuel type (Hossain and de Lasa, 2008, Adanez et al., 2012).

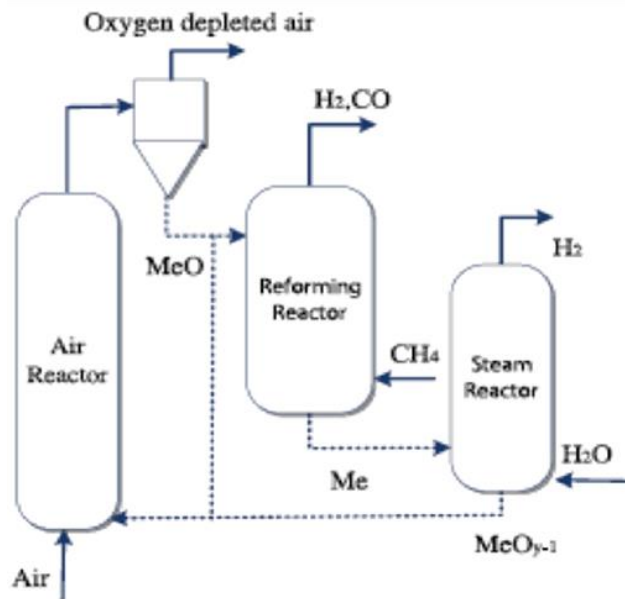


Figure 2.15 Schematic illustration of chemical looping steam reforming (Ryden and Ramos, 2012)

### 2.3.1.2 Oxygen carriers

The large scale application of CLC and CL-SR is still reliant upon the obtainability of appropriate oxygen carriers. A significant research effort on CLC has been on the development of feasible oxygen carrier materials (Källén et al., 2015). Transition metals (the like of nickel, copper, iron, cobalt, and manganese) are good oxygen carriers. The most commonly studied oxygen transfer materials are oxides of nickel, copper, iron and manganese. For years nickel was the most used oxygen carrier and considered as state of the art (Linderholm et al., 2009, Källén et al., 2015) because of its high reactivity, negligible volatility, and thermal steadiness which are favourable factors for elevated temperature and high gas turbine CLC (Mattisson et al., 2003, Adánez et al., 2004, Hossain and de Lasa, 2008, Adanez et al., 2012). Nevertheless, nickel is toxic, costly and has a thermodynamic constraint of 99–99.5 % fuel conversion, conditional on temperature and pressure (Källén et al., 2015). ‘Iron oxides have been more frequently studied as oxygen carriers for CLC’ (Källén et al., 2015). Its reactivity is normally enduring and the mechanical strength is considered to be good (Abada et al., 2007). The oxygen release properties of copper oxide oxygen carriers have made researchers interested to increase (Abad et al., 2012). Copper has good feed/fuel conversion and is highly reactive, but has the disadvantage of being expensive. The mechanical strength of copper materials is also indeterminate (Rydén et al., 2014). Manganese oxides have also been acknowledged as a suitable oxygen carrier material with a good oxygen uncoupling capacity; however, the relevant equilibrium concentrations for the oxygen release happen at moderately low temperatures (below 800 °C) (Mattisson et al., 2009).

The thermodynamic properties of manganese oxides can be improved by combining it with other metals (Rydén et al., 2013). The primary significant characteristic of a good oxygen carrier is its reactivity in both oxidation and reduction cycles. Oxygen carrier capability to entirely combust a fuel is another vital characteristic. In addition to that, oxygen carriers should also have the following characteristics; unchanging under repeated oxidation/reduction cycles at elevated temperatures, fluidizable, resist agglomeration and friction stress associated with high circulation of particles, good thermodynamics concerning the fuel conversion to CO<sub>2</sub> and H<sub>2</sub>O in CLC, and H<sub>2</sub> and CO in CL-SR, economically and environmentally friendly (Hossain and de Lasa, 2008, Adanez et al., 2012). Table 2.32 and 2.33 are list of oxygen carrying ability of metal oxides and oxygen carriers respectively. Amid the candidates Co<sub>3</sub>O<sub>4</sub> gives the highest quantity of oxygen (0.67 moles) per mole of metal.

Apart from thermodynamics, some physical properties such as active surface area, pore volume, particle size, density and crushing strength are also vital factors for an ideal oxygen carrier material. Reports from literature review confirmed that oxygen carriers with particle size ranging from 0.08 to 2 mm are appropriate for CLC while for most oxygen carriers, the crushing strength ranges from 3.7 to 5.2 N. Oxygen carrier's particles can be prepared by depositing the active metal oxide(s) phase on an inert support such as SiO<sub>2</sub>, TiO<sub>2</sub>, ZrO<sub>2</sub>, Al<sub>2</sub>O<sub>3</sub>, YSZ, and bentonite to escalate their reactivity, durability and fluidizability. " In the case of metal oxide oxygen carriers, the oxygen carrying capacity is a strong function of the metal loading and of the stability of the carrier over repeated reduction-oxidation cycles" (Adanez et al., 2012). Table 2.32 and 2.33 presents Oxygen carrying capacity for different metal/metal oxide pairs and Oxygen carrying capacity of various oxygen carriers respectively.

**Table 2.32 Oxygen carrying capacity for different metal/metal oxide pairs (Adanez et al., 2012)**

<b>Metal oxide</b>	<b>Moles of O<sub>2</sub> / mole of metal</b>
NiO/Ni	0.5
CuO/Cu	0.5
CuO <sub>2</sub> /Cu	0.25
Fe <sub>2</sub> O <sub>3</sub> /Fe <sub>3</sub> O <sub>4</sub>	0.083
Mn <sub>2</sub> O <sub>3</sub> /MnO	0.25
Mn <sub>3</sub> O <sub>4</sub> /MnO	0.17
Co <sub>3</sub> O <sub>4</sub> /CO	0.65
CoO/Co	0.5

**Table 2.33 Oxygen carrying capacity (RO, oxygen ratio) of various oxygen carriers (Adanez et al., 2012)**

Oxygen carriers	Metal loading (%)	Ro <sup>a</sup>
NiO/SiO <sub>2</sub>	35	0.074
NiO/Al <sub>2</sub> O <sub>3</sub>	20-60	0.043-0.16
NiO/NiAl <sub>2</sub> O <sub>4</sub>	40-60	0.09-0.13
NiO/MgAl <sub>2</sub> O <sub>4</sub>	37-60	0.09-0.13
NiO/TiO <sub>2</sub>	40-60	0.09-0.13
CuO/SiO <sub>2</sub>	41	0.083
CuO/Al <sub>2</sub> O <sub>3</sub>	14-35	0.027-0.08
CuO/MgAl <sub>2</sub> O <sub>4</sub>	43	0.087
Fe <sub>2</sub> O <sub>3</sub> /SiO <sub>2</sub>	39	0.012
Fe <sub>2</sub> O <sub>3</sub> /Al <sub>2</sub> O <sub>3</sub>	60	0.027
Fe <sub>2</sub> O <sub>3</sub> /MgAl <sub>2</sub> O <sub>4</sub>	32	0.0096
Mn <sub>2</sub> O <sub>3</sub> /SiO <sub>2</sub>	47	0.048
Mn <sub>2</sub> O <sub>3</sub> /MgAl <sub>2</sub> O <sub>4</sub>	46	0.047
Mn <sub>2</sub> O <sub>3</sub> /Al <sub>2</sub> O <sub>3</sub>	28-60	0.02-0.07
Mn <sub>2</sub> O <sub>3</sub> /MgZrO <sub>2</sub>	40	0.028
CoO/Al <sub>2</sub> O <sub>3</sub>	28-35	0.07

### 2.3.1.3 Maturity of CL-SR process

Significant studies have been carried out on testing numerous oxygen carrier materials from synthetic to natural materials (Storset et al., 2013, Källén et al., 2015, Pans et al., 2015). Production methodology has also been evaluated (Storset et al., 2013). However, because the oxygen carriers need to satisfy a number of certain criterions (Storset et al., 2013, Källén et al., 2015, Pans et al., 2015), there are challenges to prepare those materials. Despite the oxygen carrier challenges in needs to fulfill certain criteria the process is already on commercial scale. Table 1.7 provides a summary of commercial CLC plants.

A number of research groups, both at research institutes and university levels are involved in the process. Industries are also not left behind in CLC research. Participating industries include; Alstom (both EU and US), Total, Shell, and to a point Statoil and GE are also involved (Storset et al., 2013). Research institutes and universities levels involved include; IFP (Hoteit et al., 2011, Yazdanpanah et al., 2011), Chalmers, TU Vienna (Vienna university of technology), TU Darmstadt

(Technische Universität Darmstadt), SINTEF (Stiftelsen for industriell og teknisk forskning), Ohio State University, and University of Utah (Storset et al., 2013).

### **2.3.2 Sorption enhanced steam reforming process (SE-SR)**

The purpose of sorption enhanced steam reforming (SE-SR) is to enhance the well known conventional steam reforming process (C-SR) (Storset et al., 2013). In 1868, hydrogen production from hydrocarbon in the presence of  $\text{CaO}_{(s)}$  sorbent reportedly took place (Ryden and Ramos, 2012). However, patent for hydrogen production using SE-SR process was explained and issued as early as 1933 (Williams, 1933, Ryden and Ramos, 2012).

The C-SR process route has at least three basic steps; steam methane reforming (SMR) process, WGS reaction and finally the separation/purification step. The logic behind SE-SR process is to perform all these three steps (SMR, WGS and  $\text{CO}_2$  capture) simultaneously in a single reactor vessel in the presence of nickel based catalyst and calcium based sorbent (Ryden and Ramos, 2012). The process is usually operated using two packed bed reactors or two fluidized bed reactors; the reforming reaction reactor and the regeneration/calcination reactor. Although, it is feasible to perform reforming and calcination batch wise in a single reactor, a continuous operating process using two reactors seems to be more attractive (Ryden and Ramos, 2012). Thus, making the process cyclic and each reactor must undergo repetitive reforming reaction and calcination steps. The  $\text{CO}_2$  produced is captured by a sorbent, which once saturated with  $\text{CO}_2$ , is regenerated in situ by using steam or pressure swing absorption principle. As the  $\text{CO}_2$  is captured to  $\text{CaCO}_{3(s)}$  the equilibrium of the reforming and WGS reaction is shifted towards the right, increasing hydrogen generation at a low temperature (723-873 K) compared to the C-SR process (1073-1300 K) (Hufton et al., 1999, Ochoa-Fernandez et al., 2007, Ryden and Ramos, 2012, Dupont et al., 2013).

The advantages of SE-SR over C-SR process are; potential to use low operating temperature, reduction of purification steps, minimization of side reaction and decrease in the quantity of steam to be used as opposed to C-SR (Chaubey et al., 2013, García-Lario et al., 2015). (Bruntskhovoi et al., 1988) revealed that SE-SR process has the ability to save the overall energy required by the system with the potential of saving up to 20-25 % as opposed to the C-SR process. In addition to these benefits, the process has the advantage of increasing fuel/feed conversion, production of high purity hydrogen with minimum  $\text{CO}_2$ , proficient  $\text{CO}_2$  capture to  $\text{CaCO}_{3(s)}$  from

the product, and potentially to generate pure CO<sub>2</sub> that is suitable for subsequent use or sequestration during sorbent calcination step (Chaubey et al., 2013, García-Lario et al., 2015, Wess et al., 2015).

### **2.3.2.1 Sorbent characterization**

The sorbents/adsorbent plays a significant role in the SE-SR process. It is vital for the sorbent to have certain basic characteristics such as; high selectivity to desired products and adsorption ability at operating temperature and pressure, good and steady adsorption capability of CO<sub>2</sub> after repeated adsorption and desorption cycles, and good mechanical strength of adsorbent particles after cyclic exposure to high pressure streams (Chaubey et al., 2013, García-Lario et al., 2015). The most commonly used CO<sub>2</sub> sorbent is CaO (Ryden and Ramos, 2012), which is reduced with CO<sub>2</sub> in an exothermic reaction forming CaCO<sub>3(s)</sub> (Dupont et al., 2013). The carbonated CO<sub>2</sub> sorbent can be regenerated in order to be useable again by calcination (Ryden and Ramos, 2012, Dupont et al., 2013). Comparative analysis between few of the most frequently used sorbent for capturing CO<sub>2</sub> and their outcome were examined by various researchers, the results confirm that none of the sorbents fully satisfy all the requirements needed in them. CaO is the most ideal sorbent from the thermodynamic perspective leading to the maximum hydrogen yields and it is also the most commonly used as mentioned earlier. Yet, further improvement of the material is necessary in order to increase its stability (Ochoa-Fernandez et al., 2007). Dolomite, Calcite and CaCO<sub>3</sub> (from Ca acetate) are good sorbent for CO<sub>2</sub> and they showed very high capacity for CO<sub>2</sub> adsorption (Dupont et al., 2008). Table 2.34 and 2.35 presents characteristics of CO<sub>2</sub> sorbent materials and comparison/properties of sorbents respectively.

### **2.3.2.2 Maturity of SE-SR process**

In the past few years, various SE-SR pilot plants with capacity of 2-20 MW were built in Sweden, Australia, and Germany [49-51]. However, all of the plants used wood chips or wood pellets as fuel for syngas production and the process was demonstrated during gasification [49]. Presently, numerous research groups, both at research institutes and university levels such as Statoil, Institution of Fire Engineers (IFE), SINTEF, and Norwegian University of Science and Technology (NTNU) (Storset et al., 2013) are investigating the performance of the SE-SR process [41] using various/diverse fuel and feedstocks ranging from methane [24]–to propane [23], including hydroxyacetone [52], acetic acid [53], and urea [20].

**Table 2.34 Characteristics of CO<sub>2</sub> sorbent materials (Chaubey et al., 2013)**

Group	Representative member	Adsorption capacity	Stability	Kinetics
Metal oxides	CaO	Good	Poor	Good
Hydrotalcities	Mg <sub>6</sub> Al <sub>2</sub> (OH) <sub>16</sub> (CO) <sub>3</sub> x 4H <sub>2</sub> O/K <sub>2</sub> CO <sub>3</sub>	Poor	Good	Poor
Double salts	(K <sub>2</sub> CO <sub>3</sub> )(2KHCO <sub>3</sub> )(MgCO <sub>3</sub> )(MgO)x xH <sub>2</sub> O	Fair	Unknown	Fair
Li metal oxides	Li <sub>4</sub> SiO <sub>4</sub>	Fair	Fair	Good
Supported sorbents	CaO on cobot superior micropowder	Fair	Good	Good

**Table 2.35 Comparison/properties of sorbents (Ochoa-Fernandez et al., 2007)**

	CaO	Li <sub>2</sub> ZrO <sub>3</sub>	KLiZrO <sub>3</sub>	Li <sub>4</sub> SiO <sub>4</sub>	Na <sub>2</sub> ZrO <sub>3</sub>
Capacity	Good	Fair	Fair	Fair	Fair
Thermodynamics	Good	Fair	Fair	Fair	Fair
Stability	Poor	Good	Fair	Good	Good
Kinetics	Good	Fair/Poor	Fair	Fair	Good
Regeneration T	High	Medium	Medium	Medium	Medium

### 2.3.3 Sorption enhanced water gas shift (SE-WGS)

Sorption enhanced water gas shift (SE-WGS) also called sorption enhanced reforming (SE-R) is a enhanced reforming process similar to SE-SR except that only the water gas shift reaction (WGS) is enhanced in the process. In SE-WGS process a sorbent is used in the presence of WGS catalyst to adsorb CO<sub>2</sub> and shift the equilibrium towards higher hydrogen yield (Li et al., 2012, Lee and Lee., 2014). The process is a fixed bed multi-Column pressure swing adsorption (PSA) process where the WGS reaction is conducted at 400 °C and pressure of 40 bar. The process needs more than two columns to make it a continuous process (Storset et al., 2013). Figure 2.16 depicts a schematic diagram of the SE-WGS.



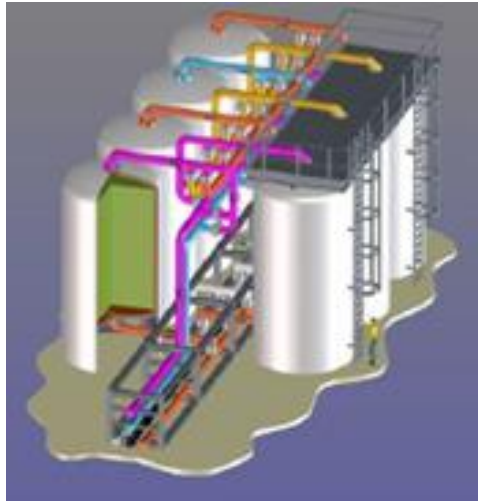


**Figure 2.16 Schematic diagram of the SE-WGS (Storset et al., 2013).**

### **2.3.3.1 Maturity of SE-WGS process**

Energy research Centre of the Netherlands ECN (NL) with 5 countries in Europe has been the major developer of SE-WGS (Allam et al., 2005, Cobden et al., 2007, Storset et al., 2013). They have been operating a six column laboratory scale SE-WGS process since 2009. Over 2000 cycles have been run indicating steady performances. The next step is the pilot scale plant commissioning (Storset et al., 2013). A novel thermal swing sorption-enhanced reaction process for continuous operation has been developed by Sircar and coworkers at Lehigh University. The SE-WGS reaction was studied using  $K_2CO_3$ -promoted hydrotalcite and  $Na_2O$ -promoted alumina (Jang et al., 2013). High temperature  $CO_2$  sorbents based on  $CaO$  and  $Na_2ZrO_3$  have been recently studied for prospective use in the SE-WGS reaction (Lee et al., 2007, Lee et al., 2008).

Energy research Centre of the Netherlands ECN (NL) has been the major developer of the process as mentioned earlier. They are also developing the sorbents material partly with SINTEF. Sasol, South Africa is producing K-promoted hydrotalcite at low cost. Educational institutes such as Lehigh University and Korea University, Seoul are also involved in R&D of the process (Storset et al., 2013).

Energy proficiency beyond 39 % can be archived in SE-WGS process in connection with integrated gasification combined cycle (IGCC) (Gazzani and Manzolini, 2013). Proficiency of 50.9 % and effective  $CO_2$  capture of 95.2 % have been achieved by Industrial Research and

Consultancy Centre (IRCC) (Manzolini et al., 2011). It has been found that when sorbents with good cyclic capability is used, substantial improvements in both proficiency and cost can be gained (Manzolini et al., 2012) (88).

### 2.3.4 Sorption enhanced chemical looping reforming process (SE-CLR)

Combination of sorption enhancement and CL-SR in one single process is called sorption enhanced chemical looping reforming (SE-CLSR). The material bed consists of a mixture of particles comprising of solid oxygen carrier and CO<sub>2</sub> sorbent. "A mixture of oxygen carrier such as NiO and CO<sub>2</sub> sorbent such as CaO is used as bed material" (Ryden and Ramos, 2012).

The reforming reactor normally operates at a low temperature, partially oxidizing hydrocarbon with the oxygen provided by oxygen carrier and steam reactions (R2.27 and R2.28), and at the same time any carbon dioxide produce during the process is captured by the CO<sub>2</sub> sorbent reaction (R2.30) causing sorption enhanced water gas shift reaction (R2.29), the over-all reaction in the reforming reactor is thermo neutral (Lyngfelt et al., 2001, Ryden and Ramos, 2012). As depicted in a schematic diagram (Figure 2.17) of the process, the reforming reactor produces hydrogen, the calcination reactor generates a stream of pure CO<sub>2</sub> which is released as the CO<sub>2</sub> sorbent is regenerated in accordance with reaction (R2.30). The regeneration reactor operates at an intermediate temperature and the over-all reaction is endothermic. The air reactor operates at a high temperature, re-oxidizing the oxygen carrier with air in accordance with reaction (R2.31), the over-all reaction in the air reactor is exothermic. In order to resolve the heat balance of the process, the solid circulation rate between the air reactor and the calcination reactor needs to be large. Hence, the solid flow from the calcination reactor is separated into two. Large share of the solids from the calcination reactor enters the air reactor while the required quantity of NiO and CaO along with some metallic Ni is extracted and goes to the reformer reactor. It is recommended that the process should be conducted in three fluidized bed reactors (Ryden and Ramos, 2012).



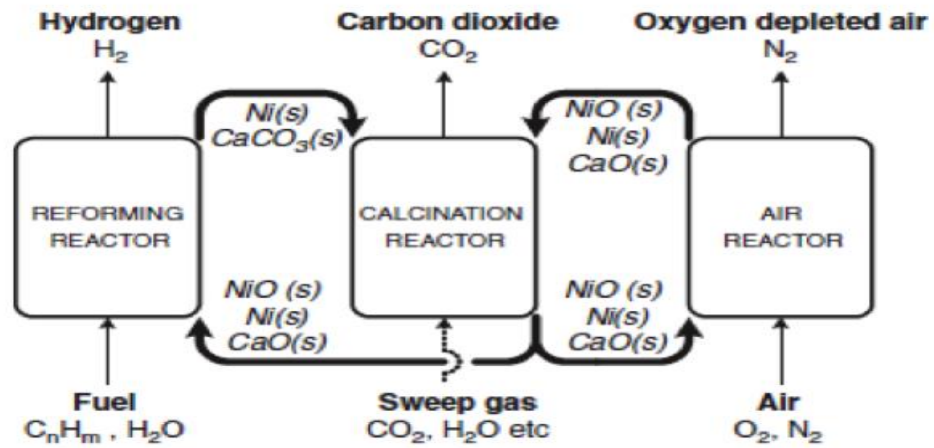
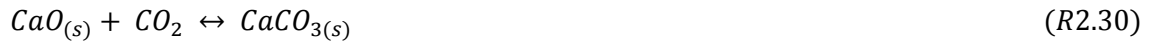


Figure 2.17 Sorption Enhanced Chemical Looping reforming (Ryden and Ramos, 2012)

The SE-CLR process is self-sufficient with heat due to the fact that part of the oxidation is executed with  $O_2$  supplied by the solid oxygen carrier rather than with water and subsequent re-oxidation of  $O_2$  carrier generates heat. Transferring enough amount of this heat from the air reactor to the calcination reactor through the solid circulation eradicates the need to cool or heat all the three reactors (Ryden and Ramos, 2012) making the process very novel. Another related process has been recommended by (Pimenidou et al., 2010) who examined hydrogen generation from waste cooking oil in packed bed reactor using NiO as oxygen carrier and CaO as  $CO_2$  sorbent.

#### 2.3.4.1 Factors affecting SE-CLR process

A large number of operating variables directly or indirectly affects the performance of the SE-CLR process and can have a strong impact on hydrogen production, conversion of water and fuel, hydrogen purity, and efficiency of  $CO_2$  capture. The effect of temperature, pressure, steam to carbon ratio (S:C) and oxygen to carbon ratio (O:C) on the performance of SE-CLR was investigated by (Ryden and Ramos, 2012). The results showed that increasing the oxygen to carbon ratio (O:C), at a constant temperature of 853 K and pressure of 1 atm reduced the hydrogen production since this would result in total oxidation of the fuel rather than the desired

partial oxidation. Conversely, increasing the steam to carbon ratio (S:C), at exactly the same operating conditions will result in increase in hydrogen production, methane conversion and decrease in water conversion. Increase in temperature of the system under well-chosen conditions will result in high yield of hydrogen, up to a certain temperature limit. As the temperature reaches certain limit (higher temperature above 1000 K) yield and purity of hydrogen will decrease, and CO<sub>2</sub> adsorption process will stop but methane conversion will increase (Rydén and Lyngfelt, 2006, Ryden and Ramos, 2012, Dupont et al., 2013). At temperature of 873 K, 1 bar pressure and steam to carbon ratio of 3 (Johnsen et al., 2006) obtained hydrogen with 98 % purity using NiO as a catalyst and OTM and CaO as sorbent in a fluidized bed reactor having 0.1 m/s superficial velocity.

### **2.3.5 Sorption enhanced chemical looping steam reforming (SE-CLSR)**

The sorption enhanced chemical looping steam reforming (SE-CLSR) process has same basic principles as the SE-CLR process discussed in section 2.3.4, except that, here steam is also a reactant in the process. Thus, both steam reforming and water gas shift reactions are enhanced. Therefore, higher hydrogen yield and purity, as well as a better CO<sub>2</sub> adsorption are expected compared to the SE-CLR process. In addition sorption enhanced reduction which is identified here (this research) for the first time is also achieved (S G Adiya et al., 2017). Limited studies have been carried on the SE-CLSR process. Researchers focused mainly on coupling of sorption enhanced water gas shift and chemical looping with partial oxidation (Ryden and Ramos, 2012). Previous studies by Antzara et al (Antzara et al., 2014, Antzara et al., 2016a) have investigated the thermodynamic and experimental analysis of the process respectively using methane as feedstock. This research focused mainly on the process.

### **2.3.6 Hydrocarbon gasification**

Production of hydrogen via hydrocarbon gasification is a continuous, non-catalytic process that includes partial oxidation of the feedstock. At a temperature of 1095-1480 °C (1368-1753 K) air or oxygen with carbon dioxide or steam is used as oxidant. During the process carbon produced is removed in a carbon separator as slurry, then pelletized as raw material for carbon based product or fuel (Speight and Ozum, 2002, Speight, 2007). Details of the process can be found in the mentioned references (Speight and Ozum, 2002, Speight, 2007).

### **2.3.7 Synthesis gas**

The process is also a non-catalytic process for synthesis gas production mainly hydrogen and carbon dioxide, for vital production of high purity hydrogen from liquid or gaseous hydrocarbons. A precise blend of preheated feedstock and oxygen is fed to the topmost of the generator where carbon monoxide and hydrogen arise as products. The reactor temperature from 1095-1490 °C (1395-1763 K) and pressure varies from approximately atmospheric pressure to nearly 138 bar (Speight and Ozum, c2002, Parkash, c2003, Speight, c2007). More details of the process conditions can be found in the mention references

### **2.3.8 Pyrolysis**

Interest has been developed in the use of pyrolysis process to produce hydrogen. Specifically, the attention has concentrated on the pyrolysis of hydrogen sulphide and natural gas. Hydrogen sulphide direct decomposition has been studied widely and has been reported to be highly endothermic with poor equilibrium yield. The thermodynamic equilibrium is not favourable toward hydrogen production at a temperature smaller than 1500 °C (1773K). Though in the presence of catalyst such as platinum-cobalt or other transition metals sulphides supported by alumina decomposition proceeds quickly (Speight and Ozum, c2002, Speight, c2007).

### **2.3.9 Electrolysis**

Presently, water electrolysis process for hydrogen production is not considered a competitive technology because of its poor kinetics for oxidation of hydroxyl ions to oxygen at anode, great electricity consumption and limitation to small scale settings. Nevertheless, the process is simple, ecologically clean and produces very high purity gases (hydrogen and oxygen) from water. The principle behind the process is that two electrodes (anodes and cathodes) are immersed into water; amid the two electrodes an electrolyte is placed. Direct voltage/current is provided in demand to retain the balance of electrons flow from the negative charged side to the cathode where negatively charged hydrogen ions are consumed for hydrogen production (Dubey et al., 2010, Zhang et al., 2010).

### **2.3.10 Aqueous phase reforming**

Aqueous-phase reforming is a remarkably flexible process that can be used for hydrogen production (Davda et al., 2005, El Doukkali et al., 2012). The process has received considerable attention; owing to its numerous advantages as compared to other reforming processes

(Cortright et al., 2002, Davda et al., 2005, El Doukkali et al., 2012). It can be conducted at fairly low temperatures (200–280 °C) and moderated pressure (15–70 bars) (Davda et al., 2005, El Doukkali et al., 2012). Moreover it is operated in liquid phase, thus the aqueous solution used as process feed must not be evaporated, consequently the corresponding energy saving is an attractive benefit. Besides, unwanted decomposition reactions can be narrowed. Furthermore, it is feasible to generate H<sub>2</sub> and CO<sub>2</sub> in a simple one step reaction process with very low CO contents. The product gas can purified via direct transfer to membrane systems taking advantage of the reaction pressure. The process also have the ability to produce 15 times more hydrogen per mass of catalyst than existing steam reforming processes (Cortright et al., 2002, Davda et al., 2005, El Doukkali et al., 2012).

Carbohydrates such as sugars (e.g. glucose) and polyols (e.g. methanol, ethylene glycol, glycerol and sorbitol) can be effectively transformed with water in the aqueous phase under suitable heterogeneous catalysts at temperatures near 500 K to produce primarily H<sub>2</sub> and CO<sub>2</sub> (Davda et al., 2005). Aqueous-phase carbohydrates found in waste-water from biomass processing (e.g., cheese whey, beer brewery waste-water, sugar processing), from carbohydrates streams extracted from agricultural products such as corn and sugar beets, and from aqueous carbohydrates extracted by steam-aqueous fractionation of lower-valued hemicellulose from biomass can also be used for the reforming process (Davda et al., 2005).

### **2.3.11 Photochemical water splitting**

Photo-catalytic water splitting to produce hydrogen and oxygen using semiconducting catalysts has received considerable attention owing to the potential of the technology, including the great economic and environmental concern for the generation of the clean fuel hydrogen from water using solar energy (Ni et al., 2007, Ahmada et al., 2015, Zhao and Yang, 2016). Hydrogen generation through water splitting with TiO<sub>2</sub> as the photo-catalyst was reported as early as 1972. Fujishima and Honda were the first to demonstrate the potential/ability of TiO<sub>2</sub> semiconductor materials to split water into hydrogen and oxygen (Ahmada et al., 2015, Zhao and Yang, 2016). The technology is an effective method for transforming solar energy or sunlight into clean and renewable hydrogen fuel (Ni et al., 2007, Ahmada et al., 2015, Zhao and Yang, 2016). However, the process is the 'most promising and renewable choice' for hydrogen production (Ahmada et al., 2015).

### **2.3.12 Thermochemical cycles (sulphur-iodine, copper-chlorine)**

Thermochemical cycles are used to accomplish water splitting since they permit considerable amounts of hydrogen and oxygen to be produced at much lower temperatures (usually below 1000 °C) than are required for direct one-step thermal water decomposition (Rosen, 2010). The technology utilised heat (thermo) with chemical reactions to split water into hydrogen and oxygen. Apart from water, hydrogen and oxygen produced are continuously recycled, thus the term 'cycle'. The sulphur-iodine and copper-chlorine cycle are type of thermochemical cycle process that produces hydrogen and oxygen, the sulphur-iodine or copper-chlorine used in the process are recovered and reused (not consumed in the process) (Steinfeld, 2005, Naterer et al., 2008, Rosen, 2010).

## **2.4 Previous research on hydrogen production**

### **2.4.1 Conventional steam reforming**

Hydrogen is presently one of many fuel options for the future, and is particularly attractive because it can be stored and transported effectively, and the only by-product of it burning is water. Conventional steam reforming (C-SR) has been the leading technology for hydrogen production in refining and petrochemical complexes (Collodi and Wheeler, 2009). The technology is fully mature and has dominated syngas production for the past 70 years (Zhu et al., 2001) and still counting. C-SR can be used with diverse feedstocks from methane to ethane, methanol, ethanol, including acetone and other higher hydrocarbons. Because the technology is fully developed, research has been dedicated to characterization of catalysts using these feedstocks (LeValley et al., 2014). Significant attention has been given to methane owing to its favourable hydrogen to carbon ratio in contrast to other feedstocks (Wei et al., 2012). A significant research has also been carried on methanol and ethanol with various reaction mechanisms proposed (Palo et al., 2007, LeValley et al., 2014). Research has showed that many catalysts have good activity in steam reforming reactions for numerous feedstock combinations/mixture. However, nickel is the most commonly studied and used metal for the steam reforming because of its cheapness, reactivity and thermal steadiness at elevated temperatures (Mattisson et al., 2003, Adánez et al., 2004, Hossain and de Lasa, 2008, Adanez et al., 2012, LeValley et al., 2014). Numerous studies have been carried to improve the performance of steam reforming process. For example, Christensen et al. (Christensen et al., 2006) investigated the effect of support and Ni crystal size on solid carbon formation and sintering during steam methane reforming process. Numaguchi and Kikuchi (Numaguchi and Kikuchi, 1988) studied the intrinsic kinetics and design stimulation of steam reforming process. Research

studies on the kinetics of the C-SR process dates back to the 18th century. Akers and Camp (Akers and Camp, 1955) performed the first extensive study in 1955 (Ding and Alpay, 2000). Van Hook (Van Hook, 1980) reviewed the work up to 1970, covering the kinetic studies over porous nickel catalysts and nickel foil at 260-1000 °C and 100-5000 kPa pressure. Adris et al. (Adris et al., 1996) investigated on how to improve the performance of steam methane reforming reactor etc. Table 2.36 present a summary on some previous work on C-SR process. Numerous reviewed papers on the progress of the C-SR process such as Sà et al. (Sá et al., 2010), LeValley et al. (LeValley et al., 2014) and Iulianelli et al. (Iulianelli et al., 2016) to mention few has also been written.

**Table 2.36 Summary on some previous work on conventional steam reforming**

References	Experimental work/condition	Feedstocks
(Rosen, 1991)	Investigation of favorable thermodynamic conditions of the process	Natural gas
(Simpson and Lutz, 2007)	Investigation into the energy analysis of hydrogen production with emphasis on energy flows and efficiencies	N/A
(Dou et al., 2010)	Experimental assessment at atmospheric pressure, with and without in situ CO <sub>2</sub> sorption, in a fixed-bed reactor	Crude glycerol (by-product of a biodiesel production plant)
(Roses et al., 2013)	The production of pure hydrogen in a fluidized bed membrane reactor. The operating temperature investigated varies from 773–903 K range and 2.0–5.3 bar reacting pressure.	Natural gas
(Nieva et al., 2014)	Experimental studies conducted at 500 and 600 °C using four nickel-based catalysts: (a) Ni/a-Al <sub>2</sub> O <sub>3</sub> and Ni/SiO <sub>2</sub> , prepared by incipient wetness impregnation method and (b) Ni–Zn–Al and Ni–Mg–Al, prepared by co-precipitation method.	Methane
(Sadooghi and Rauch, 2015)	Experimental and theoretical studies of SMR reactions with different amount of hydrogen sulfide in the feed gas are investigated in a packed bed reactor. The effect of different amount of hydrogen sulfide on methane conversion and temperature distribution within the reactor under different operating conditions such as space velocity, temperature, and steam to carbon ratio were investigated.	Methane
(Watanabe et al., 2016)	‘Effect of nitrogen impurity for steam methane reforming over noble metal catalysts’	Methane containing nitrogen feedstock for residential fuel cell

## 2.4.2 Chemical looping steam reforming

The CL-SR process was first proposed in 2001 by Mattisson and Lyngfelt (Mattisson and Lyngfelt, 2001). Rydén (Rydén, 2008) also proposed the process and concluded that it has 5 % overall more efficiency compared to conventional process. Using  $\alpha$ -Al<sub>2</sub>O<sub>3</sub> and  $\gamma$ -Al<sub>2</sub>O<sub>3</sub> OTM Diego et al. (Diego et al., 2008) studied CL-SR of CH<sub>4</sub>. They concluded that  $\alpha$ -Al<sub>2</sub>O<sub>3</sub> has better reactivity during the reduction reaction than the reactivity of  $\gamma$ -Al<sub>2</sub>O<sub>3</sub> OTM. They also conclude that Ni based OTM are more suitable for CL-SR process. They observed that Ni-based catalyst/OTM have long lifetime and can be used for longer period of time without any significant change in their reactivity. Johansson et al. (Johansson et al., 2008) investigated the CL-SR process using two different Ni-based OTM (NiO/NiAl<sub>2</sub>O<sub>3</sub> and NiO/MgAl<sub>2</sub>O<sub>4</sub>) in a continuous process. They found that NiO/MgAl<sub>2</sub>O<sub>4</sub> has higher fuel conversion (CH<sub>4</sub>) with low tendency for solid carbon formation on the surface of the catalyst/OTM. Lea-Langton et al. (Lea-Langton et al., 2012) investigated the feasibility of CL-SR using highly oxygenated and volatile pyrolysis oils from biomass wastes as sustainable liquid fuels for conversion to a hydrogen rich syngas. They concluded that, despite the feedstock high oxygen content, they were able to reduce close to 90 % of the NiO during CL-SR, signifying their potential to be used in the CL-SR process. Jiang et al. (Jiang et al., 2016) investigated CL-SR of glycerol using Al-MCM-41 based oxygen carriers with and without Ce promoter. They found that both the ordered mesoporous structure and Ce promoted oxygen carriers play a very significant role in the CL-SR process. The oxygen carriers derived from direct-synthesis method have the potential to enhance Ni loading and dispersion while the oxygen carriers promoted on Ce could effectively control nickel size, enhance the WGS reaction and reducibility of partial NiO species. A comprehensive review on chemical looping combustion and reforming technologies on the main advances of the process up to 2010 has been done by Adanez et al (Adanez et al., 2012). They compiled more than 700 different OTM based on Ni, Cu, Fe, Mn, Co including mixed oxides and low cost materials. Full details can be found at the given reference. Tang et al (Tang et al., 2015) also comprehensively reviews the recent advances for CL-SR of CH<sub>4</sub>. They compiled the major milestones in the process. Table 2.37 show a summary of some previous work on CL-SR process.

**Table 2.37 Summary of some previous work on chemical looping steam reforming**

References	Experimental work/condition	Feedstocks
(Adanez et al., 2012)	A comprehensive review of the CLC and CL-SR processes reporting the core developments in these technologies up to 2010	A review paper
(Li et al., 2013)	Syngas production from methane via a chemical looping concept: A review of oxygen carriers	A review paper
(Zheng et al., 2014)	'The reduction characteristics of Cu-based oxygen carrier with hydrogen, carbon monoxide and methane were investigated using a fixed bed reactor, TPR and TGA'. In order to lower the required reduction temperature of oxygen carriers, a new CLC process with methane steam reforming was investigated	Hydrogen, methane and carbon monoxide
(Jiang et al., 2015)	Hydrogen production from CL-SR of glycerol was studied using Ni-based oxygen carrier in a fixed-bed reactor. The Ni-based oxygen carrier was prepared by a liquid-state co-precipitation method with rising pH technique and the characterization was performed by XRD, SEM, TEM and N <sub>2</sub> adsorption-desorption	Glycerol
(Silvester et al., 2015)	Two nickel based OTM supported on alumina and zirconia (Ni-Zr and Ni-Al) were tested for their potential use in CL-SR. The study was conducted by performing 20 redox cycles in a TGA unit	Methane
(Hafizi et al., 2016b)	A comprehensive study of cerium and calcium promoted iron based oxygen carrier was proposed using CL-SR process. Loading weight percentage of 0, 5 and 10 and reaction temperature in the range of 823–1073 K was studied at constant H <sub>2</sub> O/CH <sub>4</sub> molar ratio of 1.5	Methane
(Antzara et al., 2016b)	This study evaluates the performance of NiO-based oxygen carriers supported on ZrO <sub>2</sub> , TiO <sub>2</sub> , SiO <sub>2</sub> , Al <sub>2</sub> O <sub>3</sub> and NiAl <sub>2</sub> O <sub>4</sub> as C-SR catalysts at low temperature (650 °C) as well as OTM for CL-SR	Methane

### 2.4.3 Sorption enhanced steam reforming and sorption enhanced reforming

Sorption enhanced steam reforming (SE-SR) has the potential to produce high purity hydrogen with CO<sub>2</sub> capture (Storset et al., 2013). The process has also been integrated with natural gas combined cycle and compared to ATR process couple with CO<sub>2</sub> capture using MDEA-solvent. The results verified that SE-SR has 50.2 % proficiency compared to the most advanced ATR- MDEA with 50.7 % proficiency (Romano et al., 2011). In addition to that, the efficiency of CO<sub>2</sub> capture was lower in the SE-SR process compared to the ATR- MDEA (Storset et al., 2013). The major challenge in the SE-SR process is operating with CaO/CaCO<sub>3</sub> particles for recirculation to the carbonator. Owing to degradation of solvent and residual activity large quantity of CaCO<sub>3</sub> would be required (Storset et al., 2013).

In literature, extensive work on SE-SR has been published considering the fixed bed reactor system. Balasubramanian et al. (Balasubramanian et al., 1999) investigated operating conditions

of 650 °C, 15 bar and S:C of 4 on the performance of the sorption enhanced process. Composition of product gases at the outlet of reactor as a function of time was studied. They divided the outlet results into three sections; pre-breakthrough period (active carbonation period), breakthrough period (sorbent reaching its full capacity) and post-breakthrough period (sorbent fully carbonated). During the pre-breakthrough period the composition of product gases on dry basis was reported as 94.7% H<sub>2</sub>, 5.2% CH<sub>4</sub>, and approximately 400 ppmv CO<sub>2</sub> and 600 ppmv CO. They compared the values with equilibrium results and were in good agreement with those of the experimental studies. They came to the conclusion that using Ca-based CO<sub>2</sub> sorbent can save about 20-25% energy as compared to C-SR process. The major disadvantage of the SE-SR process is the high regeneration temperature requirements. The performance of different sorbents on hydrogen yield was investigated by Ochoa-Fernandez et al. (Ochoa-Fernandez et al., 2007). When a Ca based CaO sorbent was used the process was found to be weakly exothermic, whereas Li<sub>2</sub>ZrO<sub>3</sub> makes the overall process weakly endothermic. They concluded that CaO sorbent is the most favourable sorbent from thermodynamics point of view and results in higher hydrogen yield and purity compared to other sorbents. Mathematical model of SE-SR process in a fixed bed reactor have been studied by Fernandez et al (Fernandez et al., 2012b). They studied the effect of operating variables such as steam to carbon ratio, catalyst to sorbent ratio, space velocity, including temperature and pressure on the composition of product gases. Ca based CaO sorbent was used in fixed bed reactor to study the performance of the process. They found that for a fixed temperature of 923 K, 3.5 MPa pressure, S:C ratio of 5 and 3.5 kg m<sup>-2</sup> s<sup>-1</sup> gas mass flux there is a reduction in H<sub>2</sub> purity from 92 % to 85 % and decrease in CH<sub>4</sub> conversion from 85 % to 60 % as the catalyst to sorbent ratio decreases from 0.3 to 0.1. Under exactly the same operating conditions, increasing the gas mass flux decreases H<sub>2</sub> purity and CH<sub>4</sub> conversion. 3.5 kg m<sup>-2</sup> s<sup>-1</sup> was found to be the optimum gas mass flux if the operating conditions are kept the same as those mentioned above previously. They also found that increasing the S:C ratio and decreasing the operating pressure has positive influence on hydrogen purity in accordance with the Le Chatelier's principle. High temperature favours CH<sub>4</sub> conversion and subsequently high hydrogen generation, however, as the temperature goes beyond certain limit the hydrogen purity starts decreasing. Researchers such as Ding and Alpay (Ding and Alpay, 2000), Johnsen et al (Johnsen et al., 2006) and (Chen et al., 2009b) has also investigated the performance of SE-SR process. A comprehensive review on the SE-SR process can be found at Barelli et al (Barelli et al., 2008), and Harrison (Harrison, 2008).

Han and Harrison (Han and Harrison, 1994) studied sorption enhanced reforming using CaO as a CO<sub>2</sub> sorbent in a tubular reactor. CO conversions were observed to surpass that of the thermodynamic equilibrium conversion under the specified operating conditions. Table 2.38 shows summary of some previous work on SE-SR and SE-R processes.

**Table 2.38 Summary of some previous work on sorption enhanced steam reforming and sorption enhanced reforming (Note: references with subscribe b denote sorption enhanced reforming process)**

References	Experimental work/condition	Feedstocks
(Broda et al., 2013)	High purity hydrogen production through SE-SR reaction over a Ni-hydrotalcite derived catalyst and a synthetic Ca-based, calcium aluminate supported CO <sub>2</sub> sorbent	Methane
(Anderson et al., 2014)	Thermodynamic analysis of hydrogen production through SE-SR of methane in a new class of variable volume batch-membrane reactor was investigation.	Methane
(Lysikov et al., 2015)	Experimentally studies on a periodically operated dual fixed bed reactor was conducted in cyclic mode with CaO Sorbents. Temperature swing adsorption and pressure swing adsorption (PSA) modes were used for periodic sorbent regeneration.	Ethanol
(Xu et al., 2016)	Ni/CaO-Ca <sub>5</sub> Al <sub>6</sub> O <sub>14</sub> bifunctional catalyst extrudates were prepared by extruding sol-gel-derived Ni/CaO-Ca <sub>5</sub> Al <sub>6</sub> O <sub>14</sub> powder, and use for SE-SR process. The later was compared with Ni/CaO	Methane
(van Selow et al., 2009) <sub>b</sub>	Carbon Capture by Sorption-Enhanced Water-Gas Shift Reaction Process using Hydrotalcite-Based Material	CO
(Martavaltzi and Lemonidou, 2010) <sub>b</sub>	Development and evaluation of a new hybrid material; NiO-CaO-Ca <sub>12</sub> Al <sub>14</sub> O <sub>33</sub> , with dual function as reforming catalyst and CO <sub>2</sub> sorbent for use in SE-R. CaO-Ca <sub>12</sub> Al <sub>14</sub> O <sub>33</sub> acts as an effective CO <sub>2</sub> sorbent and also as a support for the active metallic Ni particles.	CO
(Martínez et al., 2013) <sub>b</sub>	Development of a detailed and comprehensive simulation model of hydrogen generation plant centred on SE-R process of natural gas.	CO

#### 2.4.4 Sorption enhanced chemical looping reforming and Sorption enhanced chemical looping steam reforming

Ryden and Ramos (Ryden and Ramos, 2012) proposed SE-CLR process for hydrogen production using three fluidized interconnected bed reactors (reforming reactor, calcination reactor and air reactor). The reformer reactor was operated at a low temperature and feedstock were oxidized by the OTM. In the reformer reactor, CO<sub>2</sub> generated during the reforming reactions were capture by the CaO sorbent via the carbonation reaction. The carbonation reaction is a highly exothermic reaction, thus the heat released was utilized in for the endothermic reforming reactions. Consequently, the overall reformer reactor operated under thermo-neutral conditions. They obtained over 95 % hydrogen purity in the reformer reactor. The saturated

sorbent was regenerated by supplying the sweep gas for the regeneration purposes. The heat released during the OTM oxidation was used for regeneration of the sorbent in the air reactor. Detail description of their process can be found in (Ryden and Ramos, 2012). Application of  $22\text{Fe}_2\text{O}_3/\text{MgAl}_2\text{O}_4$  and  $22\text{Fe}_2\text{O}_3/\text{Al}_2\text{O}_3$  as oxygen carriers and cerium promoted CaO as  $\text{CO}_2$  sorbent on SE-CLR process was investigated by Hafizi et al (Hafizi et al., 2016a). They revealed that using synthesized Ce:Ca = 0.2 as  $\text{CO}_2$  sorbent can effectively increase the  $\text{H}_2:\text{CO}$  molar ratio reaching the ratio of 16.4 and 16.7 with  $22\text{Fe}_2\text{O}_3/\text{Al}_2\text{O}_3$  and  $22\text{Fe}_2\text{O}_3/\text{MgAl}_2\text{O}_4$  oxygen carrier respectively was possible. Higher fuel conversion and hydrogen yield was achieved with  $22\text{Fe}_2\text{O}_3/\text{MgAl}_2\text{O}_4$  OTM and synthesized Ce:Ca = 0.2 sorbent. This sorbent and OTM system revealed steady activity at 600 °C in nine reduction, calcination and oxidation cycles.

Udomchoke et al (Udomchoke et al., 2016) evaluate the performance of SE-CLSR for hydrogen production from biomass. They modified the catalyst and sorbent regeneration, full details can be found in Udomchoke et al (Udomchoke et al., 2016) and concluded that bio-oil conversion increases when the quantity of NiO OTM and CaO sorbent increases. The performance of SE-CLSR process was investigated by Pimenidou et al (Pimenidou et al., 2010) using waste cooking oil as feedstock in a packed bed reactor. They used 18 wt. % NiO on  $\alpha\text{-Al}_2\text{O}_3$  support as OTM and pre-calcined dolomite as  $\text{CO}_2$  sorbent. They conducted 6 cycles at 1 bar pressure, 600 °C and S:C ratio of 4. They found that higher fuel conversion and subsequently higher hydrogen yield and purity could be obtained compared to the case without sorbent. Hydrogen production by SE-CLSR of glycerol in a moving bed reactors was also investigated by Dou et al (Dou et al., 2014). They observe that at stoichiometric steam to carbon ratio of 1, the process has the efficiency to produce a hydrogen purity of only 80 %. Above 90 % hydrogen purity was auto-thermally produced at 1.5 to 3.0 times the stoichiometric steam requirement and at initial temperature of 500–600 °C. The hydrogen purity increased with increasing steam to carbon ratio and temperatures. They concluded that the process has a great potential for economical hydrogen production and good efficiency with overall low 'footprint by combining different units in one stage'. Table 2.39 presents a summary of some previous work on SE-CLR and SE-CLSR processes.

**Table 2.39 Summary of some previous work on Sorption enhanced chemical looping reforming and Sorption enhanced chemical looping steam reforming (Note: references with subscribe b denote sorption enhanced chemical looping steam reforming process)**

References	Experimental work/condition	Feedstocks
(Ryden and Ramos, 2012)	Hydrogen generation with CO <sub>2</sub> capture by SE-CLR using NiO as oxygen carrier and CaO as CO <sub>2</sub> sorbent with methane as fuel was investigated	Methane
(Broda et al., 2013)	SE-SR was investigated using a mixture containing a Ni-hydrotalcite-derived catalyst and a synthetic, Ca-based, calcium aluminate supported CO <sub>2</sub> sorbent. The fresh and cycled materials were characterized using N <sub>2</sub> physisorption, XRD, SEM and TEM	Methane
(Yahom et al., 2014)	Simulation and thermodynamic analysis of CL-SR and CO <sub>2</sub> enhanced CL-SR. The purpose of the work is to identify ideal operating conditions for obtaining optimum hydrogen yield and purity. The reactors were simulated using the Gibbs free energy minimisation technique. NiO was used as the OTM and CaO as the CO <sub>2</sub> adsorbent	Methane
(Zhu and Fan, 2015)	Thermodynamic analysis of hydrogen production from CaO SE-SR thermally coupled with CLC as a novel technology	Methane
(Antzara et al., 2014) <sub>b</sub>	A detailed thermodynamic analysis SE-CLSR, using CaO and NiO as CO <sub>2</sub> sorbent and OTM respectively, was carried out. SMR and SE-SR were also investigated for comparison reasons.	Methane
(Antzaraa et al., 2015) <sub>b</sub>	A detailed thermodynamic analysis of SE-CLSR, using CaO and NiO as CO <sub>2</sub> sorbent and OTM respectively was carried out. The effect of different parameters, such as reactor temperature, pressure, H <sub>2</sub> O/CH <sub>4</sub> ratio, CaO/CH <sub>4</sub> ratio and CaO/NiO ratio was also investigated	Methane
(Antzara et al., 2016a) <sub>b</sub>	The feasibility of the reforming process was demonstrated experimentally over a mixture of a bifunctional NiO-based OTM/reforming catalyst supported on ZrO <sub>2</sub> , and a ZrO <sub>2</sub> -promoted CaO-based CO <sub>2</sub> sorbent. The experiments were performed in a bench-scale fixed bed reactor unit. The effects of temperature, steam/methane, NiO/CaO molar ratios and space velocity of the feed stream, was investigated to define the optimum operating conditions and evaluate the full potential of the combined process over the two solids.	Methane

## 2.5 Summary of literature review

The major hydrogen consuming processes in the refinery are hydrotreating and hydrocracking processes. Other hydrogen consumers include lubricants plants, petrochemical processes and isomerization processes that can be incorporated into the refinery hydrogen network (Aitani, 1996, Rabiei, 2012). Hydrogen consumption in a refinery process depends on the feedstock properties, impurities to be removed, conversion level, and catalyst properties (Aitani, 1996, Alves and Towler, 2002). Apart from chemical consumption of hydrogen due to hydrogenation reactions such as sulphur, nitrogen, oxygen, organic chlorides, olefins, and aromatic rings etc.

removal, account has to be made for hydrogen consumption due mechanical processes such as hydrogen absorbed in liquid products, hydrogen lost in balance with light gases including hydrogen lost with purge gas utilised in maintaining a purify hydrogen (Jones, c1995, Anon, c2000, Speight and Ozum, c2002, Parkash, c2003).

The major source of hydrogen in petroleum refineries is the catalytic reforming units by product. Although, the unit can fulfil the hydrogen requirements of many refineries, the case is different for some large scale refineries and those without a catalytic reforming plant. This necessitates the needs to construct a supplementary hydrogen plant (when the by product from the catalytic reformer is inadequate) or a major hydrogen plant (in the absence of catalytic reforming plant) that generates hydrogen gas by steam reforming of natural gas, naphtha or refinery off gases, otherwise partial oxidation of hydrocarbons or hydrogen importation via a pipeline can be employed as an alternative to steam reforming (Alves and Towler, 2002, Rabiei, 2012).

Conventional steam reforming process is the major hydrogen producing technology. The technology is fully mature and has dominated the syngas production for the past 70 years (Zhu et al., 2001) and still counting. Despite having reached technological development and maturity, it is still one of the most energy intensive processes for syngas production through its heating requirement with a high operational and maintenance cost (Gil et al., 2016). The process is also one of the leading causes of global warming; by increasing the CO<sub>2</sub> concentration in the atmosphere. Equilibrium constraints is also a major drawback of the process to date owing to heat transfer limitations. Other challenges of the process include high chance of coke formation, limited catalyst effectiveness and overall efficiency of the process is poor. Researchers are presently focusing on novel technologies that generate hydrogen with minimum possible energy requirement and zero/low CO<sub>2</sub> released in the atmosphere.

Numerous methods are available for hydrogen production such as auto-thermal reforming, pyrolysis, sorption enhance steam reforming, and chemical looping steam reforming etc. as competitors/developing competitors to conventional steam reforming process. The combination of steam reforming or partial oxidation with pressure-swing adsorption (PSA) separation technology is a well know practice in novel designs, also permitting the production of hydrogen gas above 99 % purity (Philcox and Fenner, 1997).

The gaps in hydrogen requirement in some refineries such as, inadequate hydrogen generation from catalytic reformer or the absence of catalytic reforming unit, including, the key problems in the conventional steam reforming process (major route for hydrogen production) as well as limitation of other hydrogen producing processes for example partial oxidation process; (i) is normally less energy proficient than steam reforming due to the higher temperatures involved (which worsens heat losses) and the problem of heat recovery, (ii) purification steps are expected to be more costly in partial oxidation process, and (iii) the fact that pure oxygen feed to the partial oxidation system, causes great capital expenses for small scale oxygen generation (Ogden et al., 1996, Ogden, 2001) necessitates the need for further research and development of current processes for hydrogen production.

## Chapter 3 Research Materials and Methodologies

Chapter 3 provides a description of the thermodynamic and experimental procedure (methodology), including methods used to characterise catalyst and sorbent before and after experiments. Details of materials (gases, catalyst and sorbents) were also given in this chapter. Characterisation equipment, rig set up, and the analytical techniques used for the study were fully described. Methodology used to analyse both thermodynamic and experimental data are also provided.

### 3.1 Methodology of thermodynamic equilibrium calculation

#### 3.1.1 Chemical equilibrium application (CEA) software

The software comprises the thermodynamic properties for each species in the form of polynomials of temperature using nine coefficients; the first seven are for the temperature dependent polynomial fits of the heat capacity over two wide ranges of temperature and the final two coefficients are integration constants for calculation of enthalpy and entropy of formation respectively. The polynomial fits were derived from the following equations:

Heat capacity

$$\frac{C_p^o}{R} = a_1 T^{-2} + a_2 T^{-1} + a_3 + a_4 T + a_5 T^2 + a_6 T^3 + a_7 T^4 \quad (3.1)$$

Enthalpy

$$\frac{H^o(T)}{RT} = -a_1 T^{-2} + a_2 T^{-1} \ln T + a_3 + a_4 \frac{T}{2} + a_5 \frac{T^2}{3} + a_6 \frac{T^3}{4} + a_7 \frac{T^4}{5} + \frac{b_1}{T} \quad (3.2)$$

Entropy

$$\frac{S^o(T)}{R} = -a_1 \frac{T^{-2}}{2} - a_2 T^{-1} + a_3 \ln T + a_4 T + a_5 \frac{T^2}{2} + a_6 \frac{T^3}{3} + a_7 \frac{T^4}{4} + b_2 \quad (3.3)$$

Where T is the absolute temperature (K),  $C_p^o$  is the specific heat,  $H^o$  is the enthalpy of formation, and  $S^o$  is the entropy of formation for a given species (McBride and Gordon, 1996).

The programme calculates equilibrium compositions using a Gibbs free energy minimization method. Gibbs energy of a mixture system is at its minimum when the system reaches

equilibrium at constant temperature and pressure. It is a very significant criterion for forecasting the trend of a chemical processes featuring multiple reactions and the composition of the system at equilibrium. The higher the pressure of a gas the higher the free energy (free energy is reliant on pressure). The software is able to calculate the product compositions of each gas in the system at equilibrium state based on the Gibbs free energy theory. The software use input information; temperature, pressure, enthalpy, entropy, internal energy, specific heat and mole of the reactants for calculation of the output data at equilibrium for every mole of mixture. The Gibbs free energy is defined as:

$$G_{(\rho,T)} = H - TS \rho \text{ dependent is } RT \ln \rho \ (\rho \text{ at } 1 \text{ bar}) \quad (3.4)$$

There are two compulsory keywords for every problem to be run. These words with brief portrayal of any associated data (McBride and Gordon, 1996) are as follows; first, Problem type and associated input. The dataset problem comprises all the input parameters connected with any problem with the exclusion of reactant data. Various problem types such as ‘combustion’, ‘shock tube’ and ‘rocket’ etc. are present in the CEA software but the one chosen in this project was ‘constant temperature and pressure’ to best reflect the conditions in the packed bed reformer. The second mandatory step is the reactant identification and the number of moles of input, in combinations representing the numerous typical compositions of the gases under investigation. The quantity of water, NiO based OTM/catalyst and CaO sorbent used (in moles) was chosen to reflect the desired steam-to-carbon molar ratio, nickel oxide-to-carbon molar ratio and calcium oxide-to-carbon ratio in the reformer. Other keywords (optional) such as ‘only’ and ‘output’ etc. are also available; where the choice of which product species to consider at equilibrium is made before saving and executing the simulation. The result is displayed seconds after the execution command is made. However, in the present study, the equilibrium species to be considered at equilibrium were not specified, i.e. all possible equilibrium output species present in the program’s library (thermo.inp) were considered.

### 3.1.2 Methodology

Prior to simulation the thermodynamic and thermal property data for the species of interest were checked for their presence in the thermo.inp file (the text file containing elemental content as well as  $a_1$ - $a_7$ ,  $b_1$  and  $b_2$  for each species in the system) as downloaded directly from the NASA Glenn Research Centre website. It was found that only the data for NiO<sub>(s)</sub> was missing, so a research team member (Feng Cheng) incorporated this as an add-on to the original file. A set of  $C_p^\circ$  in J/mol K in the temperature range of 298-2000 K was obtained from Kelley (Kelley, 1960).

The reliability of the data was further verified with Keem and Honig (Keem and Honig, 1978) data and were found to be in good agreement with each other. The temperature range was divided into three segments (298-525 K, 525-565 K, 565-2000 K). For each segment, the plot of  $C_p^o$  against temperature was fitted into polynomials to obtain coefficients  $a_1$ - $a_7$  according to Eq. 3.1. Coefficients  $a_1$  and  $a_2$  that were not shown in the fitted polynomials were assumed to be zero.  $H^o$  (298 K),  $H^o$  (525 K), and  $H^o$  (565 K) were used in Eq. 3.2 to calculate coefficient  $b_1$  for each segment.  $S^o$  (298 K),  $S^o$  (525 K), and  $S^o$  (565 K) were used in Eq. 3.3 to calculate coefficient  $b_2$  for each segment. The thermodynamic and thermal property data was presented in the CEA software species databases according to NASA polynomial set-up as presented in table A1 (appendixes) of McBride and Gordon (McBride and Gordon, 1996).

The CEA (Chemical Equilibrium and Applications) software by NASA (Mcbride et al., 1993) was used to perform the thermodynamic equilibrium calculations of the gas-water-solid (Ca- based CO<sub>2</sub> sorbent/Ni-OTM) system of four different processes using model compositions of shale gases as the hydrocarbon feedstock. First, conventional steam reforming (C-SR), then sorption enhanced steam reforming (SE-SR), followed by chemical looping steam reforming (CL-SR) and finally, sorption enhanced chemical looping steam reforming (SE-CLSR) were simulated. The program uses a solution procedure based on minimisation of the Gibbs energy function of a feed mixture consisting of hydrocarbon gas, water, and solids (Ca-sorbent/Ni-OTM) to calculate the mole fractions of the equilibrium mixture of products. The CEA calculations were conducted at isothermal and isobaric conditions given the endothermicity of the main reaction of steam reforming, permitting changes in volume of the system and representing a reactor mostly necessitating external heat. However, the energy balance of the combined processes will show exothermic balance in some cases, whereby the isothermal conditions would have represented a cooled reactor. Included in the program outputs were specific enthalpy, internal energy, entropy and molar masses of the initial and equilibrium mixtures.

The species considered at equilibrium in the gas-water system in addition to all the gaseous reactants (CH<sub>4</sub>, C<sub>2</sub>H<sub>6</sub>, C<sub>3</sub>H<sub>8</sub>, N<sub>2</sub>, CO<sub>2</sub> and H<sub>2</sub>O) were: H<sub>2</sub>, CO, C<sub>(s)</sub>, and NH<sub>3</sub> when simulating the C-SR process. In addition, Ca containing solid species CaO<sub>(s)</sub> and Ca(OH)<sub>2(s)</sub> were included in the reactant mixtures of the sorption enhanced processes (SE-SR and SE-CLSR), with CaCO<sub>3(s)</sub> as additional product, while NiO<sub>(s)</sub> was included in the reactant mixture of the chemical looping processes (CL-SR and SE-CLSR), with Ni<sub>(s)</sub> as additional product species. Other related species such as CH<sub>2</sub>, CH<sub>3</sub>, CH<sub>2</sub>OH, C<sub>2</sub>H<sub>4</sub>, C<sub>2</sub>H<sub>5</sub>, and CH<sub>3</sub>COOH to mention few, were also included in the

equilibrium calculations but their molar fractions were less than  $5 \times 10^{-6}$  and considered negligible.

The thermodynamic properties (specific heats, enthalpies, entropies) for the initial feed mixture and the equilibrium mixture products were obtained from NASA (Mcbride et al., 1993). The NIST (National Institute of Standards and Technology) database, and Aspen Plus software's RGibbs model reactor with Ideal and Peng-Robinson thermodynamic properties were also used for the verification of results. The selected feedstock model composition presented in Table 3.1 was based on values found in the literature. Both compositions are actual shale gas composition from the United States (Bullin and Krouskop, 2008). Shale gas termed '1' is from a Marcellus shale, which lies in western Pennsylvania, Ohio and West Virginia. The gas composition differs across the field, becomes richer from east to west. Shale gas termed '2' '3' and '4' are from Antrim shale (a shallow shale) in Michigan, U.S. The Antrim shale is unique due to the fact that its gas is predominately biogenic (methane is generated as a by-product of bacterial consumption of organic material in the shale) (Bullin and Krouskop, 2008). Full details on the gases can be found on Bullin and Krouskop (Bullin and Krouskop, 2008). In addition, Shale gas termed '1' was chosen because it represents a typical composition of natural gas, containing roughly up to 80 % of methane with roughly 20 % higher hydrocarbons ( $>C_3$ ),  $CO_2$  and inert gas (Mokhatab and Poe, 2012), representing a mixture rich in ethane and propane. Shale gas '1' and '2' can also represent typical composition of Nigerian (Sonibare and Akeredolu, 2004) and UK North sea (Peebles, 1992) natural gas containing up to 80 % methane and Lacq France natural gas containing up to 70 % methane (Peebles, 1992) respectively. Shale gas '3' and '4' compositions correspond to typical composition of gases with relatively low hydrocarbon and high inert ( $N_2$ ) content. This will also help in accessing the effect of inert gases in  $H_2$  production. Conditions at equilibrium were provided on the basis of moles of each hydrocarbon gas input ( $CH_4$ ,  $C_2H_6$ ,  $C_3H_8$ ), as represented by content in higher hydrocarbon and inert ( $N_2$ ) in the various gases, with methane always being the main hydrocarbon component. The molar steam-to-carbon ratio (S:C), the molar calcium-to-carbon ratio (Ca:C), and the molar nickel oxide-to-carbon ratio (NiO:C), as well as system pressure and temperature. The four S:C equilibrium conditions of 0, 1, 2, and 3 were calculated in the study, where 'C' represents 'hydrocarbon' moles of carbon in the gas feed, and S the moles of water feed.

**Table 3.1 Composition of shale gas used for simulation in moles, based on vol % from (Bullin and Krouskop, 2008)**

Composition	Shale gas '1'	Shale gas '2'	Shale gas '3'	Shale gas '4'
CH <sub>4</sub>	79.4	77.5	57.3	27.5
C <sub>2</sub> H <sub>6</sub>	16.1	4.0	4.9	3.5
C <sub>3</sub> H <sub>8</sub>	4.0	0.9	1.9	1.0
CO <sub>2</sub>	0.1	3.3	0.0	3.0
N <sub>2</sub>	0.4	14.3	35.9	65.0
Total	100	100	100	100

Their choice is justified as follows: S:C of 0 represents the thermal decomposition of the gas. S:C of 1 is the stoichiometric S:C ratio for complete conversion of C<sub>n</sub>H<sub>2n</sub> feedstock to CO and H<sub>2</sub>, hence it represents the minimum S:C ratio of practical operation for H<sub>2</sub> generation. S:C of 2 is the condition of stoichiometry for complete conversion of C<sub>n</sub>H<sub>2n</sub> to CO<sub>2</sub> and H<sub>2</sub> formation, while S:C 3 is the condition of excess steam typically used in industrial steam methane reforming, aimed at H<sub>2</sub> production rather than syngas generation (Dupont et al., 2013). The excess steam also increases the yield and purity of H<sub>2</sub> via the Le Chatelier's principle, and in practice inhibits carbon deposition on the catalyst as well as consumes already formed carbon deposits, if any, via steam gasification.

A post processing procedure was applied allowing the calculations of reactants conversions, molar yields of product and enthalpy balances, including the enthalpy terms associated with bringing to the reaction temperature the reactants from initial room temperature of 298 K and natural phase of feed (gas, liquid water, solid sorbent (CaO<sub>(s)</sub>), and NiO<sub>(s)</sub>). Additional enthalpy term associated with regeneration of the sorbent, was also incorporated in the energy balance calculation when CaO<sub>(s)</sub> was present in the initial mixture. A carbon balance was used to facilitate the calculation of the equilibrium total moles produced for the initial mixture chosen ('Neq') and derive products yields and reactants conversions 'X<sub>i</sub>' using Eqs. (3.5-3.11). Presentation and discussion of results was based on the following definitions:

$$N_{eq} = \frac{\sum_{i,in} \alpha_i n_{C_{i,in}}}{\sum_{j,eq} \alpha_j y_{C_{j,eq}}} \quad (3.5a)$$

where  $n_c$  represents number of moles of carbon species represented by the subscript indices  $i$  in the initial 'in' mixture, and  $j$  in the equilibrium 'eq' mixtures.  $\alpha$  is the number of carbon atoms in the relevant carbon species. Henceforth, molar amounts  $n_{j,eq}$  obey the equation:

$$n_{j,eq} = y_{j,eq} \times N_{eq} \quad (3.5b)$$

where  $y$  stands for mol fraction of a particular species in the relevant mixture. Reactants gas and steam conversions (percent or fraction) were defined based on Eqs. (3.6-3.7)

$$X_{gas}(\%) = \frac{\sum_{i,in} \alpha_i n_{C_{i,in}} - \sum_{j,eq} \alpha_j n_{C_{j,eq}}}{\sum_{i,in} \alpha_i n_{C_{i,in}}} \times 100 \quad (3.6)$$

$$X_{H_2O}(\%) = \frac{n_{H_2O,in} - n_{H_2O,eq}}{n_{H_2O,in}} \times 100 \quad (3.7)$$

where  $n$  stands for number of moles for the relevant species (e.g. 'H<sub>2</sub>O' is the sum of moles of water) in the relevant conditions (e.g. 'in' or 'eq').

Two definitions of H<sub>2</sub> yield were used: on mass basis (Eq. 3.8) and molar basis (Eq. 3.9)

$$H_2 \text{ yield (wt. \%)} = \frac{100 \times 2.02 \left( \frac{g \text{ of } H_2}{mol \text{ of } H_2} \right) \times n_{H_2,eq}}{MW_{gas} \left( \frac{g \text{ of } gas}{mol \text{ of } gas} \right) \times n_{gas \text{ in}}} \quad (3.8)$$

$$H_2 \text{ yield (mole basis)} = y_{H_2,eq} \times N_{eq} \quad (3.9)$$

And H<sub>2</sub> purity was defined using Eqn. 3.10.

$$H_2 \text{ purity (dry basis)} = \frac{n_{H_2,eq}}{\sum n_{j,eq}} \times 100 \quad (3.10)$$

Where  $j$  is the sum of all gaseous moles at equilibrium excluding steam (i.e. CH<sub>4</sub>, CO, CO<sub>2</sub>, N<sub>2</sub>, NH<sub>3</sub>, H<sub>2</sub>). A Ca:C ratio of 1 was used in the SE processes, representing the stoichiometry of the calcium oxide and calcium hydroxide carbonation reactions. The regeneration temperature of 1170 K (~900 °C) was selected to represent temperatures used in practice for decarbonation (calcination) of calcium carbonate in mixtures that may have significant CO<sub>2</sub> content (MacDowell et al., 2010, Dupont et al., 2013). Calculations were made based on the following outputs, where  $T_R$  is the reaction temperature:

Carbon products selectivity to CaCO<sub>3</sub> :

$$S_{C \text{ to } CaCO_3} = \frac{n_{CaCO_3,eq}}{Tn_{C,eq}} \times 100 \quad (3.11)$$

The enthalpy balances were performed by summing up the ‘reactants’ terms to the ‘reaction’ term, where the former is the enthalpy change of bringing individual reactants from ambient temperature (25 °C) and in their natural phase to a given reaction temperature and potentially new phase (e.g. liquid water to water vapour), and the latter is the enthalpy change of conversion to products isothermally at the given reaction temperature. Thermal efficiency of the process is assessed via the ‘ΔH ratio’. ‘ΔH ratio’ is the total enthalpy change of generating 1 mol of H<sub>2</sub> via the equilibrium process considered (e.g. C-SR, SE-SR, CL-SR and SE-CLSR), divided by that of generating 1 mol of H<sub>2</sub> via thermal water splitting. Total enthalpy change assumes reactants in their natural state at 298 K (25 °C) and ending with products at reaction temperature. In other words, it can also be defined as the measure of energy expenditure of generating H<sub>2</sub> via the gas-water system compared to the energy gain by evolution of heat from combusting this H<sub>2</sub> with oxygen, representing its final use in a fuel cell or combustion process (Dupont et al., 2013). ΔH ratio greater than one (>1) signifies a non-efficient process from energy perspective since it would require more energy to generate H<sub>2</sub> than the energy released after its oxidation or combustion in a heat or power generating device. On the other hand, ΔH ratio <1 signifies a proficient process and potentially economic from energy perspective. The further the ΔH ratio is from one, the more proficient and feasible the process should be considered. As a measure of theoretical thermal efficiency, The ΔH ratio provides a basis for comparison between feedstocks for a same process, or same feedstock for different processes with same outcome (e.g. 1 mol of H<sub>2</sub> produced). Calculations were made based on the enthalpy terms presented in equation 3.12-3.25.

Individual reactants enthalpy change terms: The subscript ‘1’ denotes reaction process 1, i.e., the first time step of the reforming process under consideration (steam reforming, carbonation, NiO reduction), and the subscript ‘2’ is used when there is a second time step in the process, i.e., the oxidation of Ni and regeneration of CO<sub>2</sub> sorbent, and ‘H’ is enthalpy of formation of relevant species at the indicated temperature. Two scenarios were considered in the processes that featured solids: ‘A’ is used for a total energy balance which does not account for the energy of regeneration of the CO<sub>2</sub> sorbent and ‘B’ includes the sorbent regeneration energy. The enthalpy terms with the index ‘1’ apply to step 1 of the process considered, and ‘2’ to step 2. These terminologies are used in the figures legends and their relevant equations are presented in equation 3.12 to 3.25.

**Reaction process 1 (steam reforming, Ni reduction); at temperature  $T_{R1}$**

$$\Delta H_{gas\ 1} = H_{feed\ gas\ at\ T_{R1}} - H_{feed\ gas\ at\ 298\ K} \text{ (kJ)} \quad (3.12)$$

$$\Delta H_{H2O\ 1} = H_{feed\ H2O\ Vap\ at\ T_{R1}} - H_{feed\ H2O\ Liq\ at\ 298\ K} \text{ (kJ)} \quad (3.13)$$

Assuming cyclic operation where solid bed materials remain in the reformer:

$$\Delta H_{Reactants\ 1} = \Delta H_{gas\ 1} + \Delta H_{H2O\ 1} \quad (3.14)$$

Reaction Enthalpy change  $\Delta H_{Reaction}$ :

$$\Delta H_{Reaction\ 1} = H_{Product\ mixture\ 1\ at\ T_{R1}} - H_{Reactants\ mixture\ 1\ at\ T_{R1}} \text{ (kJ)} \quad (3.15a)$$

Alternatively, it can be rewritten as follows for C-SR, SE-SR, CL-SR and SE-CLSR process respectively

$$\begin{aligned} \Delta H_{Reaction\ 1} = & \left( (H_{CH_4} + H_{H_2} + H_{CO_2} + H_{CO} + H_{NH_3} + H_{N_2} + H_{H_2O}) \right. \\ & \left. - (H_{feed\ gas} + H_{feed\ H_2O}) \right) \text{ at } T_{R1} \text{ (kJ)} \end{aligned} \quad (3.15b)$$

for SE-SR,

$$\begin{aligned} \Delta H_{Reaction\ 1} = & \left( (H_{CH_4} + H_{H_2} + H_{CO_2} + H_{CO} + H_{NH_3} + H_{N_2} + H_{H_2O} + H_{Ca(OH)_2} + H_{CaCO_3} \right. \\ & \left. + H_{CaO}) - (H_{feed\ gas} + H_{feed\ H_2O} + H_{feed\ CaO}) \right) \text{ at } T_{R1} \text{ (kJ)} \end{aligned} \quad (3.15c)$$

For CL-SR,

$$\begin{aligned} \Delta H_{Reaction\ 1} = & \left( (H_{CH_4} + H_{H_2} + H_{CO_2} + H_{CO} + H_{NH_3} + H_{N_2} + H_{H_2O} + H_{Ni}) \right. \\ & \left. - (H_{feed\ gas} + H_{feed\ H_2O} + H_{feed\ NiO}) \right) \text{ at } T_{R1} \text{ (kJ)} \end{aligned} \quad (3.15d)$$

And finally for SE-CLSR,

$$\begin{aligned} \Delta H_{Reaction\ 1} = & \left( (H_{CH_4} + H_{H_2} + H_{CO_2} + H_{CO} + H_{NH_3} + H_{N_2} + H_{Ca(OH)_2} + H_{CaCO_3} \right. \\ & \left. + H_{H_2O} + H_{CaO} + H_{Ni}) - (H_{feed\ gas} + H_{feed\ H_2O} + H_{feed\ CaO} \right. \\ & \left. + H_{feed\ NiO}) \right) \text{ at } T_{R1} \text{ (kJ)} \end{aligned} \quad (3.15e)$$

The presence of inert solid materials (support or degraded sorbent or both) does not affect the  $\Delta H_{Reaction\ 1}$  term (Eqn. 3.15 e) as the reaction term represents an isothermal process at  $T_{R1}$  (equilibrium enthalpies of inerts equal initial enthalpies).

Total enthalpy change of process 1 for C-SR process  $\Delta H_T$  and SE-SR process without sorbent regeneration  $\Delta H_{T\ w/o\ sorb\ reg}$  is

$$\Delta H_{T\ 1} = \Delta H_{Reactants\ 1} + \Delta H_{Reaction\ 1} \text{ (kJ)} \quad (3.16a)$$

$$\Delta H_{T\ w/o\ sorb\ reg.1} = \Delta H_{Reactants\ 1} + \Delta H_{Reaction\ 1} \text{ (kJ)} \quad (3.16b)$$

### Process 2; oxidation of Ni at $T_{R2}$

As previously, the total enthalpy of process 2 can be broken down into the two terms, one associated with sensible enthalpy change (heating/cooling of reactants to oxidation temperature  $T_{R2}$ ), and another associated with isothermal reaction enthalpy change at  $T_{R2}$ .

#### **Sensible enthalpy change of process 2:**

Sensible enthalpy change consists of the gas reactant air heating up all the way from ambient temperature 298 K to oxidation temperature  $T_{R2}$  ( $\Delta H_{feed\ air\ 2}$ ), and of the solid materials present in the bed heating up from reformer temperature  $T_{R1}$  to oxidation temperature  $T_{R2}$  ( $\Delta H_{solids\ 2}$ )

$$\Delta H_{feed\ air\ 2} = (H_{O_2,TR2} + H_{N_2,TR2}) - (H_{O_2,298K} + H_{N_2,298K}) \text{ (kJ)} \quad (3.17)$$

$$\Delta H_{solids\ 2} = \Delta H_{Ni,TR2-TR1} + \Delta H_{NiO,TR2-TR1} + \Delta H_{Al_2O_3,TR2-TR1} + \Delta H_{CaO,TR2-TR1} + \Delta H_{CaCO_3,TR2-TR1} \quad (3.18)$$

Equation 3.18 simplifies to a shorter version according to absence of support or sorbent or both.

In Chapter 4  $TR2$  was chosen as 1100 K for CL-SR, which is sufficiently high to oxidise any carbon deposits if there were any from the previous reduction/reforming stage. In the SE-CLSR case we chose  $TR2$  to be 1170 K, sufficiently high to achieve decarbonation of the  $CaCO_3$ . Energy savings can occur if, in the case of absence of sorbent (CL-SR case), the Ni oxidation reaction of process 2 is conducted at as low as possible.

#### **Process 2 reaction enthalpy at $T_{R2}$**

Reaction enthalpy changes only involve the reacting species, as it considered an isothermal process at  $T_{R2}$ .

$$\Delta H_{Reaction\ 2} = H_{Product\ mixture\ 2\ at\ T_{R2}} - H_{Reactants\ mixture\ 2\ at\ T_{R2}} \text{ (kJ)} \quad (3.19a)$$

The reaction is  $Ni + 0.5O_2 = NiO$ , therefore, alternatively it can be re-written as:

$$\Delta H_{Reaction\ 2} = (H_{NiO} - (H_{feed\ Ni} + H_{feed\ O_2})) \text{ at } T_{R2} \text{ (kJ)} \quad (3.19b)$$

#### **Total enthalpy change for process 2**

Total enthalpy change of process, for Ni oxidation  $\Delta H_{TF\ Ni\ oxi.}$

$$\Delta H_{TF\ Ni\ oxi.\ 2} = \Delta H_{feed\ air\ 2} + \Delta H_{solids\ 2} + \Delta H_{Reaction\ 2} \text{ (kJ)} \quad (3.20)$$

**Sorbent regeneration either stand alone (SE-SR) or integrated with process 2 (SE-CLSR)**

Regeneration of the sorbent involves heating the reformer solid bed to a temperature high enough to induce decarbonation of the  $\text{CaCO}_{3(s)}$ , this temperature is assumed to be 1170 K based on the literature. Solid reactor bed consists of both reforming catalyst and sorbent, therefore there will be again two terms in the enthalpy change associated with regeneration of the sorbent: sensible and reaction enthalpy changes respectively.

***Sensible enthalpy change of sorbent regeneration***

For the SE-SR process, this can be effected by heat transfer from the furnace to the reformer tubes, hence does not involve a gas flow through the reformer tubes, or perhaps a negligible amount of carrier gas. The sensible enthalpy change is therefore that of solids which are the Ni-catalyst materials and the sorbent materials:

$$\text{SE-SR: } \Delta H_{\text{solids, reg}} = \Delta H_{\text{Ni, 1170-TR1}} + \Delta H_{\text{Al}_2\text{O}_3, 1170-TR1} + \Delta H_{\text{CaO, 1170-TR1}} + \Delta H_{\text{CaCO}_3, 1170-TR1} \quad (3.21)$$

Equation 3.21 simplifies according to absence of catalyst support ( $\text{Al}_2\text{O}_3$ )

In the case of the SE-CLSR process, the sorbent regeneration takes place during process 2, and the sensible enthalpy change has been described in Eqn. 3.18

***Reaction enthalpy change of sorbent regeneration at 1170 K***

Reaction Enthalpy change of regeneration  $\Delta H_{\text{reaction reg.}}$  is with example of CaO as sorbent:

The decarbonation reaction is  $\text{CaCO}_{3(s)} \rightarrow \text{CaO}_{(s)} + \text{CO}_2$

$$\Delta H_{\text{reaction,reg.}} = X_{\text{Ca}} n_{\text{CaO}_{\text{act}}} \left( (h_{\text{CaO}} + h_{\text{CO}_2}) - h_{\text{CaCO}_3} \right) \text{ at } 1170 \text{ K (kJ)} \quad (3.22)$$

Where  $X_{\text{Ca}}$  is the conversion fraction of active CaO in the reformer to active carbonate. The term ‘active’ is used here to differentiate from total CaO inlet which may consist of active CaO and degraded CaO (i.e. unable to recarbonate)

***Total enthalpy change of sorbent regeneration at 1170 K***

Total enthalpy of process with sorbent regeneration  $\Delta H_{\text{sorb reg.}}$  for SE-SR and SE-CLSR process are as follows, respectively

$$\Delta H_{\text{sorb reg.}} = \Delta H_{\text{solids,reg}} + \Delta H_{\text{reaction,reg}} \quad (3.23)$$

**Total Enthalpy change of combined processes  $\Delta H_{\text{tot}}$  and  $\Delta H$  ratio**

***Total enthalpy change of combined processes***

Total enthalpy change of combined processes ( $\Delta H_{tot}$ ) is then the sum of the enthalpies associated with each process. i.e.:obtained by the sum of the relevant enthalpy terms equations as follows:

$$\text{SE-SR without regeneration: } \Delta H_{tot} = (3.14)+(3.15c)$$

$$\text{SE-SR with regeneration; } \Delta H_{tot} = (3.14)+(3.15c) + (3.21) + (3.22) = (3.15c) + (3.23)$$

$$\text{CLSR: } \Delta H_{tot} = (3.14)+(3.15d) + (3.17) + (3.18) + (3.19b) = (3.15d) + (3.20)$$

$$\text{SE-CLSR: } \Delta H_{tot} = (3.14)+(3.15e) + (3.17) + (3.18) + (3.19b) + (3.22) = (3.15e) + (3.20) + (3.22)$$

Terms featuring sensible enthalpy changes of Eqns (3.18) and (3.21) will vary according to the solid bed material content (with or without support, with or without degraded sorbent). In addition, in case of degraded sorbent present, Eq. 3.22 will see its molar term adjust according to active moles of Ca. Therefore, each combined process can take three or four  $\Delta H_{tot}$  and  $\Delta H_{ratio}$  values:

SE-SR: without ('w/o') degraded CaO sorbent & w/o regeneration

w/o degraded CaO sorbent, with regeneration

with degraded CaO sorbent, with regeneration

CLSR: w/o Ni support,  $T_{R2} = 1100$  K

with Ni support  $Al_2O_3$ ,  $T_{R2} = 1100$  K

SE-CLSR: w/o Ni support, w/o degraded CaO sorbent,  $T_{R2} = 1170$  K

With Ni support  $Al_2O_3$ , w/o degraded CaO sorbent,  $T_{R2} = 1170$  K

w/o Ni support, with degraded CaO sorbent,  $T_{R2} = 1170$  K

with Ni support, with degraded CaO sorbent,  $T_{R2} = 1170$  K

### **$\Delta H$ ratio**

$\Delta H$  ratio measures the energy cost of the combined processes ( $\Delta H_{tot}$ ) per mol of  $H_2$  product, relative to the energy return upon oxidation of 1 mol of hydrogen at  $T_R$ , generating condensed water at 298 K as product, or relative to the energy cost of thermal water splitting one mol of  $H_2O$ , according to reaction:  $H_2O \text{ liq, } 298 \text{ K} \rightleftharpoons (H_2 + 0.5O_2)_{TR}$

$$\Delta H_{Ratio} = \left( \frac{\Delta H_{tot}}{n_{H_2}} \right) / \Delta H_{WSP} \quad (3.24)$$

$$\Delta H_{WSP} = (0.5 h_{O_2} + h_{H_2}) \text{ at } T_R - h_{H_2O \text{ liquid at } 298 \text{ K}} \left( \frac{\text{kJ}}{\text{mol } H_2} \right) \quad (3.25)$$

A  $\Delta H_{\text{ratio}}$  below 1 represents an energetically viable process because of lower heat demand than thermal water splitting, values above 1 indicate a nonviable process, as thermal water splitting would be a less costly process of hydrogen production.

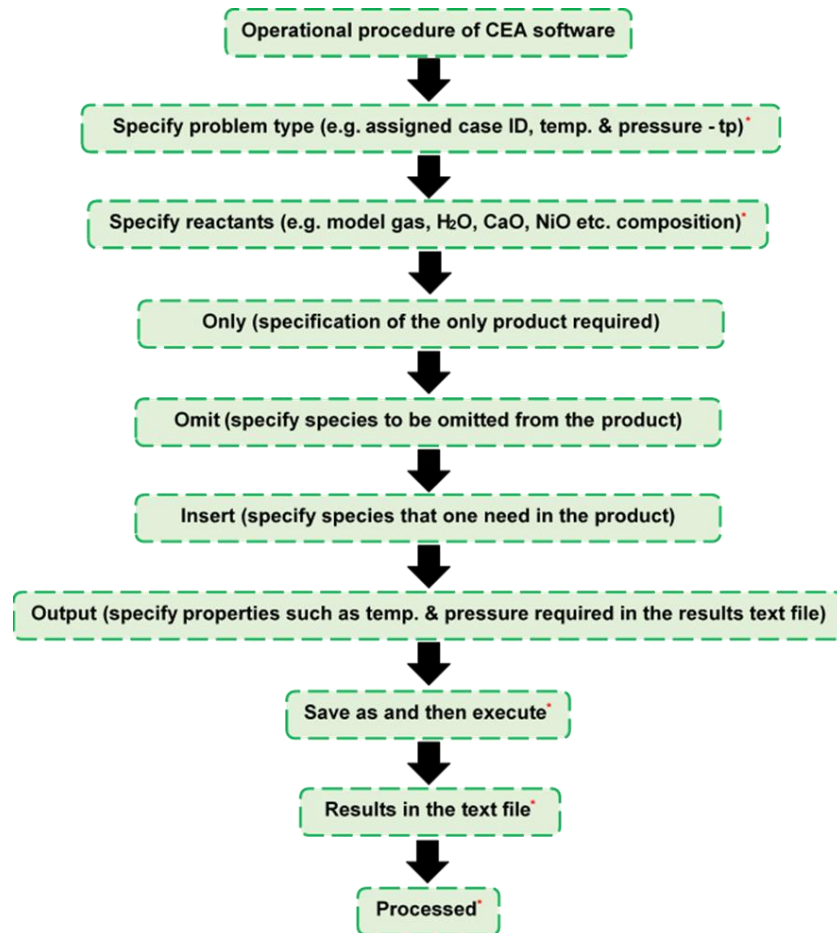


Figure 3.1 CEA operational procedure (Note: the red star signifies mandatory database. 'Only' and 'Omit' database are mutually exclusive).

## 3.2 Materials and methodology of laboratory experiments

The following methods, materials and equipment were used for the progress of the experimental research;

### 3.2.1 Materials

The following materials were used for the progress of this research;

### 3.2.1.1 Catalyst

Commercial nickel based catalyst on aluminium oxide support (NiO on Al<sub>2</sub>O<sub>3</sub> support) and nickel on calcium aluminium oxide support (NiO on CaO/Al<sub>2</sub>O<sub>3</sub> support) was provided by Twigg Scientific & Technical Ltd (UK) for the experimental study. Table 3.2 represents the characteristics of the fresh catalysts.

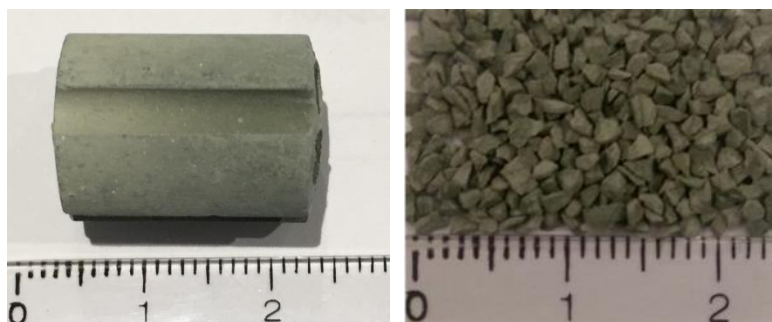


Figure 3.2 Left: Catalyst pellet Right: catalyst particles grain size 1.2 mm

Table 3.2 Characteristics of fresh catalyst

PROPERTY	NiO on Al <sub>2</sub> O <sub>3</sub> support	NiO on CaO/Al <sub>2</sub> O <sub>3</sub> support
Composition of NiO	18 wt. %	15 wt. %
Support	$\alpha$ alumina	CaO/alumina
Morphology	Crystal	Amorphous
BET surface area	3.456 m <sup>2</sup> /g	21.306 m <sup>2</sup> /g

### 3.2.1.2 Calcium oxide (CaO) sorbent

Calcium oxide (commonly known as quicklime or burned lime) is the most commonly used sorbent. It is one of the materials chosen for this study because of its low cost and high CO<sub>2</sub> sorption capacity, as well as well-documented behaviour in cyclic sorption desorption cycles. It is the most ideal sorbent from the thermodynamic point of view leading to a maximum H<sub>2</sub> yield (Ryden and Ramos, 2012).



**Figure 3.3 Left: Calcined calcium carbonate at 915 °C for 6 hours (CaO sorbent) particle grain size 1.2 mm Right: CaO sorbent and OTM/catalyst mixture particle grain size 1.2 mm**

### **3.2.2 Experimental rig**

The experimental rig schematic shown in 3.4 and Figure in 3.5, is located in laboratory 2.14 in Energy building of the School of Chemical and Process Engineering (SCAPE), at The University of Leeds, UK. The rig is integrated with a down flow quartz reactor (manufactured by York Glass Ltd), with an inner diameter of 12 mm and the length of 495 mm, held inside an electric tube furnace (Elite Thermal Systems Ltd. TSV12/50/300), where insulating K-wool of about 2-3 mm thick was placed between the quartz reactor and the furnace's bore. The quartz reactor was used in a packed bed configuration, i.e. it houses the steam reforming catalyst and CO<sub>2</sub> sorbent mixture as a fixed bed of particles. The temperature of the reactor was monitored in real time online using Picolog software by K-type thermocouple as shown in the schematic and image (Figure 3.4 and 3.5 respectively). A programmable syringe pump (New Era pump system) controls the flow rate of water to the reactor. The syringe pump is connected to the reactor through an injector system. The gas flows of H<sub>2</sub> (used for reduction of the catalyst), N<sub>2</sub> (inert gas), air (oxidant in chemical looping runs), and fuel feed (shale gas) were controlled by four separate MKS mass flow controllers. The latter regulates flow rates according to given set points via the control valves. A coolant (ethylene glycol and water in the volume of 1:1) at -6 °C was circulated between the condenser and a chiller (Fisher Scientific 3016S) to maintain the condenser at a low temperature (-6 °C). The condenser cools the hot product gases leaving the reactor and moisture was trapped by silica gel before going to the micro-gas chromatograph for analysis. The presence of Nitrogen gas in the feed aids calculation of parameters such as gas products yield and feedstock conversion using elemental balances as will be shown later.

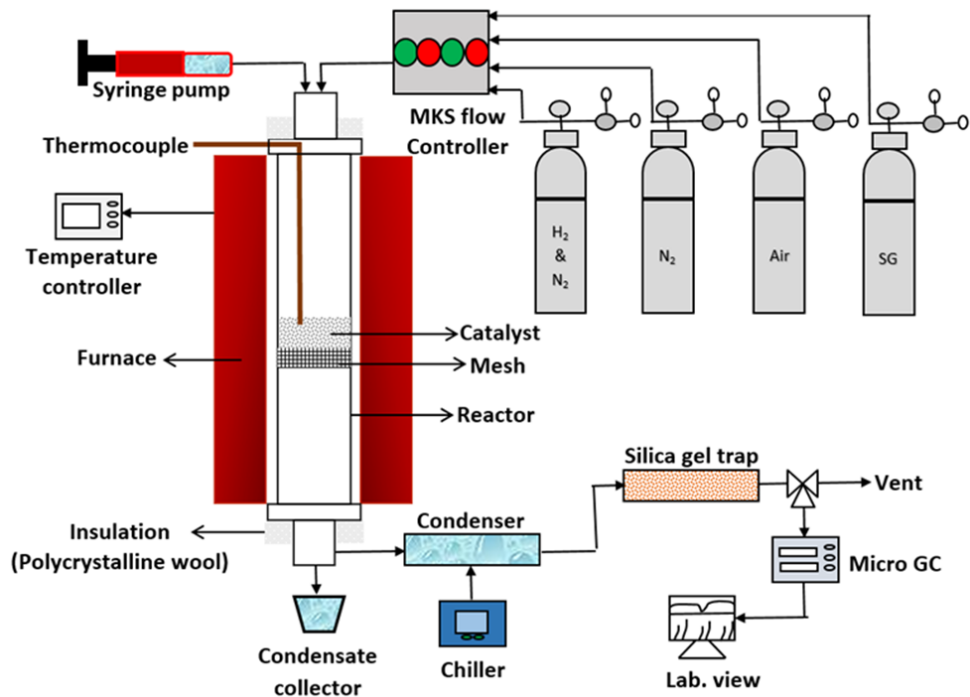


Figure 3.4 Schematic diagram of the rig

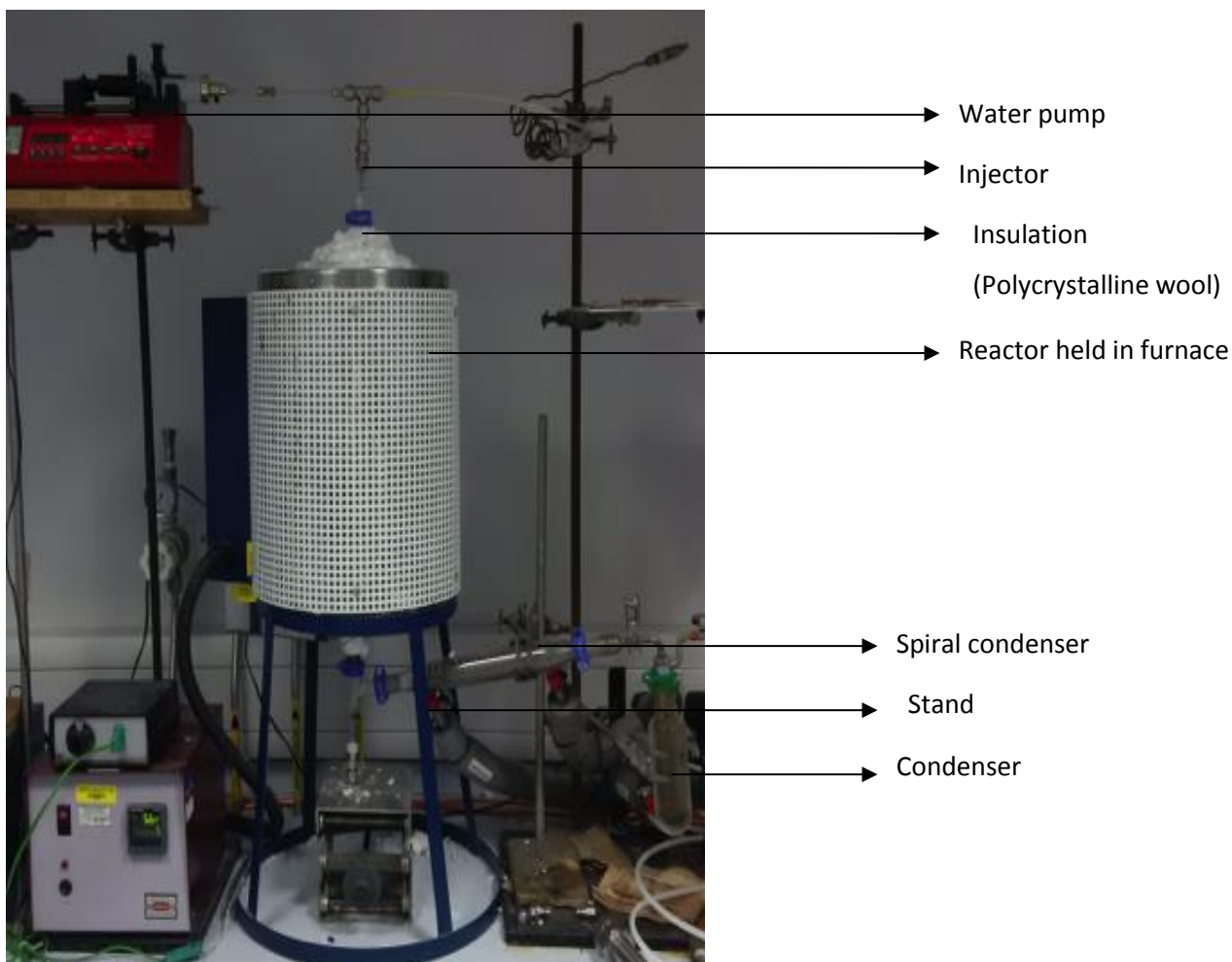


Figure 3.5 Picture of the experimental rig



Figure 3.6 Components of the experimental rig parts (a) Gas flow controller (b) water pump (c) condenser (d) spiral condenser (e) 1<sup>st</sup> silica gel trap (f) 2<sup>nd</sup> silica gel trap (g) chiller

### 3.2.3 Standard operational procedure of the rig

Figure 3.7 depicts the operational procedure schematic. After cleaning of the reactor with acetone, the chiller is turned on and water is loaded into the syringe. 3 g or any desired mass of crushed catalyst is loaded into the reactor, followed by assembling the rig as shown in its schematic (Figure 3.4).

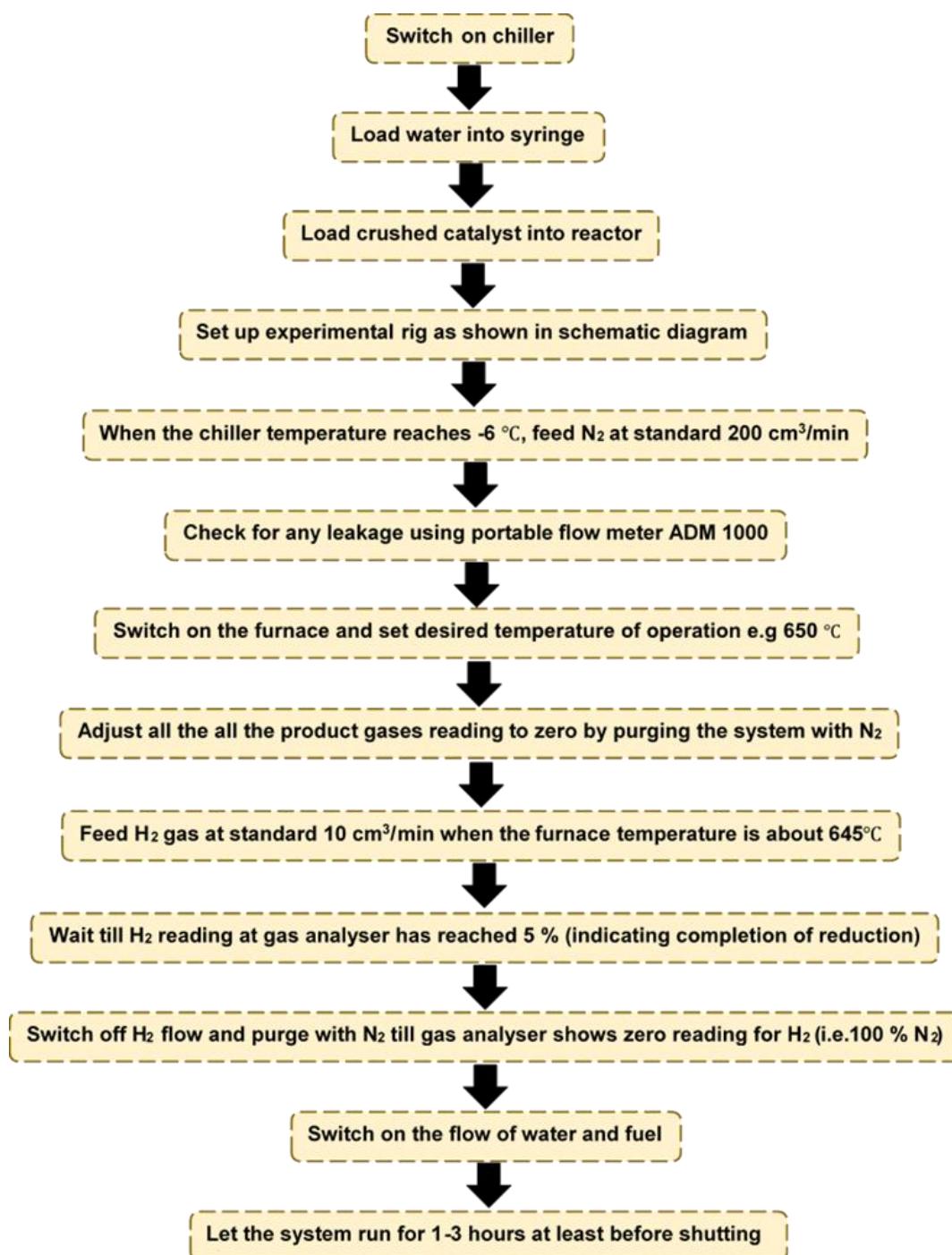


Figure 3.7 Schematic of operational procedure

Experimental were carried out at atmospheric pressure under a continuous N<sub>2</sub> flow of 200 sccm. Leakages are checked using a portable flow meter ADM 1000. Once there is no leakage and the chiller temperature has reaches -6 °C, the electrical tube furnace is turned on and set at the desired temperature for example 650 °C. The display reading of product gases (CH<sub>4</sub>, CO, CO<sub>2</sub> and H<sub>2</sub>) at the analyzer are then checked and adjusted to zero by purging the system with high flow of N<sub>2</sub> gas. Reduction of the catalyst (initially NiO on Al<sub>2</sub>O<sub>3</sub> or NiO on CaO/Al<sub>2</sub>O<sub>3</sub>) to active Ni on Al<sub>2</sub>O<sub>3</sub> or Ni on CaO/Al<sub>2</sub>O<sub>3</sub> using H<sub>2</sub> is required for all conventional steam reforming and sorption enhanced steam reforming process as well as first cycle of the chemical looping processes experiments. For the reduction, H<sub>2</sub> gas is fed at standard 10 cm<sup>3</sup>/min when the furnace temperature is at 650 °C or at desired set value. The system is left to reduce the catalyst until the H<sub>2</sub> reading at the gas analyzer that starts at zero reached 5 % (indicating the catalyst has completed its reduction step) after about 45 minutes. The H<sub>2</sub> flow is then stopped keeping just N<sub>2</sub> flowing until H<sub>2</sub> reading at the analyzer returned to zero. This is followed by turning on the flow of water (syringe pump) and fuel (mass flow controllers) to start the experiments, which last for a minimum of 1-3 hours (depending on the process) obtaining steady state values of all the exit gases before shutting down the system.

To shut down the rig, the furnace temperature is lowered to 298 K, the flow of the fuel gas and water are turned off, leaving only N<sub>2</sub> gas on to aid in cooling down of the system. Once the furnace and reactor temperature reached 298 K, an extra 10-20 minutes is given (to ensure the entire piping's are cool) before turning off the flow of N<sub>2</sub> gas.

### **3.2.4 Analysis Methods**

The following methods were used for analysis of outlet product gases, fresh and reacted catalyst, sorbent and sorbent and OTM/catalyst mixture:

#### **3.2.4.1 Micro GC analyzer**

Figure 3.8 depicts the micro gas chromatograph (CP 4900) supplied by Varian Instruments, UK. The gas chromatograph was equipped with two thermal conductivity (TCD) detectors and two columns; Molecular sieve 5A plot and Pora Plot U columns. The molecular sieve 5A (column 1) analyses H<sub>2</sub>, O<sub>2</sub>, N<sub>2</sub>, CO and CH<sub>4</sub>. While the Pora Plot U (column 2) analyse CH<sub>4</sub>, C<sub>2</sub>H<sub>6</sub>, C<sub>3</sub>H<sub>8</sub>, and CO<sub>2</sub>. Two pre columns were provided for each of the columns to prevent unwanted condensate or moisture from entering the columns. Column 1 was operated with a back flush of 22 Sec, preventing CO<sub>2</sub> from entering the column (The presence of CO<sub>2</sub> disrupts stable operation of the

column, affecting the column's performance). Even though the silica gel trap removed most of the moisture before the product gases enter the gas chromatograph, the columns were conditioned after every experiment by heating to 180°C to get rid of moisture that might enter the columns. The column temperatures were set to 100°C at 100 kpa pressure. It was equipped with a pump which sampled gas from the silica gel trap. The pump had a sampling time of 20 Sec. The inlet sample line to the gas chromatograph was maintained at 45°C.

The run time for the gas chromatograph was 3 min, which is much faster than conventional gas chromatographs, thus, offers ultra-fast analysis for process applications where the capability to obtain near real time measurements is required. The open Lab data acquisition software was provided by the manufacturers to set the column conditions and other important parameters for the instrument. An external standard method was used for the analysis of the products gases. The instrument was calibrated with various gas mixtures of different concentration to obtain a good calibration curve for all the gases (see appendix B1).



**Figure 3.8 Micro gas chromatography**

### **3.2.4.2 X-Ray powder diffraction**

The process in which crystal planes cause an incident beam of X-rays to constructively interfere with each other as they leave the crystal resulting in a diffracted beam detection is called X-ray diffraction (XRD). X-ray diffractometer (XPRT-PRO) was used to examine the crystallographic structure including phase and composition analysis of the fresh and used catalyst and sorbents samples. The sample was crushed to fine powder and a voltage of 40 kV and a current of 40 mA

were applied to the X-ray generator, where a stream of electrons were directed from cathode to anode and collided with anode material Cu to produce Cu K $\alpha$ 1 radiation (1.54060Å) and Cu K $\alpha$ 2 radiation (1.54443Å), which were the x-rays used. The scanning range (2 $\theta$ ) of X-rays was from 20 ° to 80 ° with an increment of 0.0332 ° per step and a speed of 0.7 second per step. Diffracted rays are produced by interference between the rays and the sample, which are then detected and processed.

The XRD patterns obtained were used in X'Pert HighScore Plus software from PANalytical for phase and composition analysis. The International Centre for Diffraction Data (ICDD) database was used for the phase analysis (by searching the best matched reference patterns from the database). Whereas the composition of a sample was calculated using Rietveld refinement method. The method calculate the entire XRD pattern using diverse refinable parameters. The least squares methods is used to improve the selection of these parameters by minimizing the differences between the measured data and the calculated data. Unlike other techniques (e.g. absorption-diffraction method, method of standard additions and internal standard method (Connolly, 2010)), the Rietveld refinement is able to deal reliably with strongly overlapping reflections (Bohre, 2014). Its result determines the mass percentage of each substance in a sample. Weighted residual value (Rwp) and goodness of fit (GOF) are used to evaluate the fit of the calculated pattern to the observed data [170]. In an ideal situation, the Rwp should be close to the statistically expected residual value (Rexp), reflecting the quality of the observed data. The GOF is defined as the square of the ratio between Rwp and Rexp. A fit with a GOF of less than 4 and a Rwp less than 10 is considered as satisfactory (Molinder et al., 2012).

The Scherrer equation (eq 3.26) was used to calculate the crystalline size of a substance. The formula relates the size of crystallites in a solid to the broadening of a peak in a diffraction pattern. The equation was developed by Paul Scherrer in 1918 to calculate the nano crystallite size ( $L$ ) by XRD radiation of wavelength  $\lambda$  (nm) from measuring full width at half maximum of peaks ( $\beta$ ) in radian located at any  $2\theta$  in the pattern. The dimensionless shape factor ( $K$ ) can vary from 0.62-2.08. The shape factor value is usually taken as 0.9, dependant on the actual shape of the crystallite (Monshi et al., 2012).

$$L = \frac{K\lambda}{\beta \cos\theta} \quad (3.26)$$

### 3.2.4.3 Specific surface area by BET analysis, pore characteristics by N<sub>2</sub> adsorption/desorption

Physical N<sub>2</sub> gas adsorption/desorption technique was used to examine the characteristics of the sample such as surface area, pore volume and pore size distribution via isotherm measurement through adsorption and desorption. The measurement was conducted based on the difference between input and output gas at a specified pressure. A Quantachrome Nova 2200 was used to de-gassed samples at 120 °C under vacuum for 3 hours to eliminate contaminants and moisture before the nitrogen adsorption step/analysis. The isothermal adsorption of nitrogen on the catalyst was performed at different pressure (high and low pressure). Thus, the quantity of absorbed gas was measured as a function of adsorbed relative pressure. The instrument was used to analyze the specific surface area of the catalyst, their micro pore volume and pore size distribution. Each sample was tested thrice to ensure reliable and precise results. Equation 3.27 presents the basic equation for the calculation of specific surface area from the adsorption data.  $X_m$  is the mass of adsorbate forming a monolayer on unit mass of adsorbent,  $M$  is the molecular weight of the adsorbate,  $A_m$  is the area occupied by one adsorbate molecule in the monolayer and  $N$  is the avogadro's number.

$$S = \frac{X_m}{M} N A_m \quad (3.27)$$



Figure 3.9 Left: XRD equipment Right: BET equipment

### 3.2.4.4 SEM-EDX

The surface structure of the fresh and used catalyst was checked using LEO-1530 Gemini FEGSEM scanning microscope (SEM), the unit is integrated with INCA 350 Energy Dispersive X-

ray (EDX) system. Images are formed by firing an electron beam that contains high energy electrons onto the sample, thus various signals are generated at the sample surface due to electron sample interactions. Transmitted signals include secondary electrons that were used for imaging (usually used for depicting the morphology and topography of sample), back-scattered electrons and characteristic X-rays etc. EDX detect the elements in the sample, it relies on the interaction of X-Ray excitation and sample after firing with high energy electron beam. The main aim of the analysis is to check carbon deposition on the surface of the catalyst and elemental in homogeneities caused by sintering after use of the solid bed materials.

Samples were prepared by mounting them on the sticky pad of SEM stem and then coated with a iridium (Ir) layer of 10 nm before the SEM-EDX test.



**Figure 3.10 Left: SEM-EDX equipment Right: CHNS equipment**

#### **3.2.4.5 CHNS elemental analysis**

CHNS elemental analysis is a common technique used for the determination of mass fractions of carbon, hydrogen, nitrogen and sulphur in a sample. A Flash EA 2000 by CE Instruments CHNS elemental analyser was used to determine the quantity of carbon and hydrogen, if any presence in the catalyst and catalyst/sorbent mixture sample. About 8-11 mg of powdered sample was weighed into a tin capsule; folded properly to remove any trapped air and then placed inside an auto-sampler. The sample was dropped into a combustion reactor and burned with excess oxygen gas at a high temperature (1000-1800 °C). Helium, a carrier gas, brought the combustion product CO<sub>2</sub> and H<sub>2</sub>O if presence to a chromatography column, in which the gases were separated. The amount of each gas (for example N<sub>2</sub>, H<sub>2</sub>, S) was measured using a highly sensitive thermal conductivity detector (TCD). Mass fractions of elements (carbon, hydrogen, nitrogen

and sulphur) present in the sample were generated by the CHNS analysis. Duplicate analysis was made on each sample to verify and certify precise result. Mean values were reported in results and discussion.

#### 3.2.4.6 Total organic carbon (TOC)

The total organic carbon (TOC) and total inorganic carbon (TIC) was determined using Hach Large IL550 TOC/TIC analyser. Two analytical methods are available on the IL550. The differential and the non-purgeable organic carbon (NPOC) method. The later (NPOC) is often used when the TIC is anticipated to be extremely high and/or not needed. The differential method (chosen for the present studies) is commonly used for samples containing volatile organic compound. In this method, an aliquot of sample 100-500  $\mu\text{l}$  roughly is measured by injecting it into the TIC reactor, where it is reacted with 10 % phosphoric acid. Inorganic carbon presents in the sample for example  $\text{CaCO}_3$  is released from the reaction with the acid as  $\text{CO}_2$ , which passes to two non-dispersive infra-red (NDIR) detectors. Additional aliquot of the sample is injected into the TOC reactor, where it completely combusts in a stream of high purity  $\text{O}_2$  carrier gas on a platinum-rhodium based catalyst at 800  $^\circ\text{C}$ . A condenser removes water and gases such as HCl generated and chemical are traps, prior to  $\text{CO}_2$  passing the NDIR detector. The total carbon includes the organic, inorganic and elemental carbon. The condensate sample was diluted with deionized water by 4 times prior to analysis. The analyser automatically calculated the total carbon considering the dilution.



Figure 3.11 Total organic carbon analyser

### **3.2.5 Experimental procedure**

#### **3.2.5.1 Conventional steam reforming (C-SR)**

All units of experimental rig were thoroughly cleaned with acetone before each experimental run. The catalyst was crushed using pestle and mortar and sieved to 1.2 mm mean sieve size using 1.4 and 1.00 mm mesh. The particle size of the catalyst was chosen to prevent diffusion limitation (caused by large particles) and high pressure drop (caused by very small particles). 3 g of catalyst was loaded into the reactor (random packing) before setting up the experimental rig as described previously (in section 3.2.3 Standard operational procedure of the rig). The furnace was set to desired experiment temperature e.g. 600°C. Each experiment consists of 2 major stages; reduction of catalyst and steam reforming process. Reduction of the catalyst from NiO to active Ni was preceded using 5 vol. % hydrogen in nitrogen carrier gas. The nitrogen and hydrogen flow rate were 200 and 10 cm<sup>3</sup> min<sup>-1</sup> (STP) respectively. Reading at the micro GC started at zero and when at 5 vol. % after about 45 minutes approximately, indicates that the catalyst had completed its reduction step.

Hydrogen flow is then stopped leaving only the nitrogen to keep flowing until hydrogen reading on the micro GC reached 0 % (flushing out all the H<sub>2</sub> in the reactor). This is followed by the steam reforming process, which started by feeding water and fuel (shale gas) to the reactor using the programmable syringe and MKS flow controller respectively. Steam and fuel was fed into the reactor at desired steam to carbon ratio. Experiments lasted for at least 1 to 2 hours (steady state conditions) and ended by turning off the water and fuel flows first, then the furnace. Thus, leaving only nitrogen flow on (remember all experiments are conducted at continuous N<sub>2</sub> flow of 200 sccm) to completely flush the reformate gases and aid in cooling down the reactor. Once the furnace temperature drops down to 25 °C the chiller is turned off and the rig is ready to be dismantled and set for the next experiment. Experimental results are collected online from laboratory computer.

#### **3.2.5.2 Sorption enhanced steam reforming process (SE-SR)**

Sorption enhanced steam-reforming process experimental procedure was the same as in C-SR process except that in addition to catalyst, 1 g of Ca based sorbent was also loaded into the reactor. The size of the sorbent was same as that of the catalyst to avoid altering the flow pattern of the reactor bed and for fairness when comparing conditions with and without Ca sorbent.

### 3.2.5.3 Chemical looping steam reforming (CL-SR) and Sorption enhanced chemical looping steam reforming process (SE-CLSR)

For chemical looping experiments, the experimental procedures for the first cycle was the same as those used for runs with and without Ca based sorbent. The second/next cycle begins when fuel and water are introduced to the system after re-oxidising the catalyst also burning off any carbon that might be deposited on the catalyst in air flow of  $500 \text{ cm}^3 \text{ min}^{-1}$  STP and  $750 \text{ }^\circ\text{C}$ . For the sorption enhanced chemical looping process with a Ca based sorbent, the higher oxidation temperature of  $850 \text{ }^\circ\text{C}$  was used to regenerate/calcined the sorbent as well. The online gas analyser monitored the release of carbon and oxygen species to complete the carbon and oxygen balances. The recorded temperature during air feed with and without Ca based sorbent increased by roughly  $10\text{-}15 \text{ }^\circ\text{C}$  owing to the oxidations reactions of the carbon residue and re-oxidation of the nickel-based catalyst. The major differences between the experimental procedures for chemical looping processes and those of the conventional steam reforming process was the oxidation step, which marks the end of each cycle.

### 3.2.6 Definition of process outputs (analysis of experimental data)

A nitrogen balance was used to facilitate the calculation of the total moles produced for the initial mixture chosen ( $\dot{n}_{out,dry}$ ) and derive products yields and reactants conversions ' $X_i$ ' and selectivity of carbon to either  $\text{CH}_4$  or other carbon containing species ' $S_{C \text{ to } \text{CH}_4 \text{ or } \text{CO} \text{ or } \text{CO}_2 \text{ etc.}$ ' as shown in Eqs. (3.28-3.34). Presentation and definition of process output was based on the following:

$$\dot{n}_{out,dry} = \frac{\dot{n}_{N_2,in}}{y_{N_2}} \quad (3.28)$$

Where  $\dot{n}_{N_2}$  stands for molar flow rate of nitrogen,  $y_{N_2}$  is mole fraction of  $\text{N}_2$  obtained from the gas chromatography, and 'in' for initial or input. Thus, the molar rate of any product gas ' $i$ ' can be calculated as follows;

$$\dot{n}_i = y_i \times \dot{n}_{out,dry} \quad (3.29)$$

Where ' $\dot{n}$ ' stand for molar flow rate and ' $y_i$ ' for mole fraction obtained from the gas chromatography. A carbon balance was used to calculate the fuel conversion  $X_{gas}$  to the main carbon containing products according to the following equation;

$$X_{gas}(\%) = \frac{T_{N_{C,in}} - (\dot{n}_{CH_4} + \dot{n}_{C_2H_6} + \dot{n}_{C_3H_8})_{out}}{T_{N_{C,in}}} \times 100 \quad (3.30)$$

$T_{N_{C,in}}$  is the total number of initial carbon moles in the fuel. It can also be written as;

$$X_{gas}(\%) = \frac{(2\dot{n}_{CH_4} + 3\dot{n}_{C_2H_6} + 4\dot{n}_{C_3H_8})_{in} - (\dot{n}_{CH_4} + \dot{n}_{C_2H_6} + \dot{n}_{C_3H_8})_{out}}{(2\dot{n}_{CH_4} + 3\dot{n}_{C_2H_6} + 4\dot{n}_{C_3H_8})_{in}} \times 100 \quad (3.31)$$

H<sub>2</sub> yield was defined as shown previously in equation 3.8 section 3.2.1 and H<sub>2</sub> purity was defined using Eqn. 3.32.

$$H_2 \text{ purity (dry basis \%)} = \frac{\dot{n}_{H_2}}{\sum \dot{n}_{\text{all dry gases, without } N_2}} \times 100 \quad (3.32)$$

$$S_{C \text{ to } CH_4 \text{ or } CO \text{ or } CO_2 \text{ etc. (\%)}} = \frac{\dot{n}_i (i = CH_4, CO \text{ or } CO_2)}{\sum \dot{n}_{\text{all C species}}} \times 100 \quad (3.33)$$

$$S_{H_2 \text{ to } CH_4 \text{ or } H_2 \text{ etc. (\%)}} = \frac{\dot{n}_i (i = CH_4 \text{ or } H_2)}{\sum \dot{n}_{\text{all H}_2 \text{ species}}} \times 100 \quad (3.34)$$

**Steam conversion fraction during the fuel/steam/N<sub>2</sub> feed;** when steam reforming is coupled with water gas shift, the production of hydrogen is the result of the contributions of the fuel-hydrogen and of the steam-hydrogen. Generally, for a 'C<sub>n</sub>H<sub>m</sub>' fuel reacting with (2n) H<sub>2</sub>O via steam reforming and the water gas shift reactions, the maximum production of H<sub>2</sub> is (2n + 0.5m), indicating clearly that in conditions of maximum H<sub>2</sub> production, the steam contribution fraction is (2n)/(2n + 0.5m) and that of the fuel, 0.5m/(2n + 0.5m). For the shale gas 1 used for experimental studies (containing CH<sub>4</sub>, C<sub>2</sub>H<sub>6</sub>, and C<sub>3</sub>H<sub>8</sub>), the steam contribution can therefore account for 52.6 % of the H<sub>2</sub> produced through SR and WGS, while that of the fuel is 47.4 %. Thus, steam conversions, which are hardly reported in literature, have great effect on steam reforming process. Factors limiting the steam conversion are not only equilibrium limitations, which the presence of the CO<sub>2</sub> sorbent aim to overcome, but also the catalyst's activity in both the steam reforming and the water gas shift reactions. Using hydrogen elemental balance, a minimum value for the steam conversion fraction can be estimated using Eq. (3.35) below:

$$X_{H_2O} = \frac{1}{\dot{n}_{H_2O,in}} \left[ (2\dot{n}_{CH_4} + 3\dot{n}_{C_2H_6} + 4\dot{n}_{C_3H_8} + \dot{n}_{H_2}) - 0.5m(\dot{n}_{gas,in}X_{gas}) \right] \quad (3.35)$$

Where m is the moles of atomic H in the fuel. The first, positive term in the Eq. (3.35) represents the formation of the hydrogen containing products and the second negative term accounts for the known contribution of the fuel to the hydrogen products, leaving only the contribution of water to the system.

**Fuel conversion on sorption enhanced processes;** Direct calculations of the fuel (shale gas) conversion during CO<sub>2</sub> sorption through the carbon balance was not possible because of the inability to measure the carbonation rate ' $\dot{n}_{CO_2} car$ ' on the solid sorbent at any given time (pre breakthrough and breakthrough period). However, a minimum fuel conversion fraction ' $X_{gas}$ ' during carbonation prior to and during the CO<sub>2</sub> breakthrough could be estimated by approximating it to the conversion reached at the CO<sub>2</sub> steady state (post CO<sub>2</sub> breakthrough). Thus, fuel conversion fraction was calculated as follows;

$$X_{gas,PB} = X_{gas,BT} = X_{gas,SS} = X_{gas} = \frac{(\dot{n}_{CH_4} + \dot{n}_{C_2H_6} + \dot{n}_{C_3H_8})_{ss}}{n \times \dot{n}_{gas,in}} \quad (3.36)$$

Where the suffix 'PB' stands for CO<sub>2</sub> pre breakthrough period, 'BT' means during CO<sub>2</sub> breakthrough period, 'SS' is at CO<sub>2</sub> steady state (post breakthrough period) and 'n' for atomic moles of carbon in the fuel.

**Sorbent carbonation rate and total carbonation efficiency during the fuel/steam/N<sub>2</sub> feed;** using the value of  $X_{gas,PB}$  derived Eq. (3.36), an estimate of the total moles of CO<sub>2</sub> produced and thus the carbonation rate ' $\dot{n}_{CO_2} car$ ' could be acquired through Eq. (3.37) below:

$$\dot{n}_{CO_2} car = X_{gas,PB,BT} \dot{n}_{gas,in} - (\dot{n}_{CH_4} + 2\dot{n}_{C_2H_6} + 3\dot{n}_{C_3H_8} + \dot{n}_{CO} + \dot{n}_{CO_2})_{PB,BT} \quad (3.37)$$

The positive term represents the molar rate of carbon converted from the fuel, and the second, negative term, the molar rate of gaseous carbon-containing products.

Prior to CO<sub>2</sub> breakthrough, since none of the carbon-containing products were detected, the negative term in Eq. (3.37) was negligible, and ' $\dot{n}_{CO_2} car$ ' was able to simplify to the first positive term only. During CO<sub>2</sub> breakthrough, the second negative term was significant and accounted for the simultaneous emergence of CH<sub>4</sub>, C<sub>2</sub>H<sub>6</sub>, C<sub>3</sub>H<sub>8</sub>, CO and CO<sub>2</sub> in the output gas stream. Eq. (3.38) gives the total carbonation efficiency as the sum of the carbonation efficiencies prior to and after CO<sub>2</sub> breakthrough, obtained by integration of the carbonation rates over the characteristic durations of pre-CO<sub>2</sub>-breakthrough and CO<sub>2</sub>-breakthrough period.

$$\alpha = \alpha_{PB} + \alpha_{BT} = \frac{(nX_{gas,PB} \dot{n}_{gas,in} \times (t_{BT} - t_0)) + \int_{t_{BT}}^{t_{SS}} \dot{n}_{CO_2,car,BT} dt}{n_{CO_2,max}} \times 100 \quad (3.38)$$

In Eq. (3.38),  $t_0$  is defined as the time at breakthrough of  $H_2$ , taken as evidence of onset of sorption enhanced steam reforming,  $t_{BT}$  was the time at breakthrough of  $CO_2$ , when the sorbent began to reach its capacity, and  $t_{SS}$ , was the time at reaching  $CO_2$ -steady state, evidencing the sorbent having reached its maximum capacity. It was of interest to split the total carbonation efficiency during fuel and steam feed into its pre-breakthrough and breakthrough contributions because for the former,  $H_2$  purity was close to 100%, while for the latter, the  $H_2$  purity slowly decreased to the steady state of the non-sorption enhanced process

## Chapter 4 Thermodynamic equilibrium studies

Detailed chemical equilibrium analysis based on minimisation of Gibbs Energy is conducted to illustrate the benefits of integrating sorption enhancement (SE) and chemical looping (CL) together with the conventional catalytic steam reforming (C-SR) process for hydrogen production from actual/typical shale gas feedstock composition.  $\text{CaO}_{(s)}$  was chosen as the  $\text{CO}_2$  sorbent and  $\text{Ni/NiO}$  is the oxygen transfer material (OTM) doubling as steam reforming catalyst. Results are presented and compared for the separate processes of C-SR, SE-SR, CL-SR and finally the coupled SE-CLSR. The effect of operational variables such as temperature, pressure and steam to carbon ratio were also discussed in detail. A comprehensive enthalpy balance for each of the studied process including the heating burden to bring inert bed materials in the reactor bed such as catalyst support or degraded  $\text{CO}_2$  sorbent from reforming temperature to sorbent regeneration temperature or to Ni oxidation temperature was also examined.

### 4.1 Introduction and chemical reactions involved in steam reforming

The precise gas composition selected for this study is given in Table 4.1. A comparison between C-SR of the shale gas with SE-SR followed by CL-SR and finally SE-CLSR was made to assess the effect on  $\text{H}_2$  yield, purity and energy efficiency of the processes, bearing in mind that C-SR of natural gas is at present the industrial standard of  $\text{H}_2$  generation. Figures and results at S:C ratio of 3 will be mainly used for illustrations unless otherwise needed.

**Table 4.1 Composition of shale gas used for stimulations (Bullin and Krouskop, 2008)**

Composition	Shale gas '1'
$\text{CH}_4$	79.4
$\text{C}_2\text{H}_6$	16.1
$\text{C}_3\text{H}_8$	4.0
$\text{CO}_2$	0.1
$\text{N}_2$	0.4
Total	100

The chemical reactions involved in C-SR, SE-SR, CL-SR- and SE-CLSR of shale gas are many and can be summarised by the global reactions R4.1-R4.17 in Table 4.2. Thermal decomposition of methane produces C and  $\text{H}_2$  via R4.1, so, despite producing  $\text{H}_2$ , R4.1 is undesirable as it

deactivates the catalyst by carbon deposition. Steam reforming of methane is defined by R4.2, which produces CO and H<sub>2</sub>, followed by the water gas shift reaction R4.7, which shifts CO to CO<sub>2</sub> with more H<sub>2</sub> production. Taken together, R4.2 and R4.7 result in R4.3, the complete steam methane reforming reaction. The desirable generation of H<sub>2</sub> from shale gas is via steam reforming of methane (R4.2 and R4.7 or R4.3) and that of the higher hydrocarbons, expressed by R4.4 (with ethane (R4.5) and propane (R4.6)), followed by R4.7. Methanation reactions R4.2<sub>b</sub> and R4.3<sub>b</sub>, (where subscript 'b' denotes reverse or 'backward' direction), are also possible reactions in steam reforming processes and are strongly temperature dependent. Calcium oxides CaO<sub>(s)</sub> undergoes carbonation (a.k.a in situ CO<sub>2</sub> capture) via R4.8 to produce calcium carbonate (CaCO<sub>3(s)</sub>). It is noteworthy that calcium oxide reacts readily with water to give calcium hydroxide (Ca(OH)<sub>2(s)</sub>) via R4.9 at low and moderate temperatures, and the calcium hydroxide can also capture CO<sub>2</sub> via R4.10 to form CaCO<sub>3</sub> (Fu et al., 2013, S G Adiya et al., 2017). The removal of CO<sub>2</sub> from the gas products may result in shifting to the right the reaction R4.7, with a knock effect on R4.2, and possibly R4.5 and R4.6 too, shifting to the right via the higher consumption of CO induced by the shift in R4.7, resulting in overall higher H<sub>2</sub> yield and purity.

The idea of CL-SR is to exothermally oxidise part of the fuel to heat up a bed material (Oxygen Transfer Material or 'OTM' and then to transfer the heat from the hot bed to enable the endothermic steam reforming of the rest of the fuel. This can be done using fixed bed reactors operated with alternating flows (air / fuel-steam), or moving beds fed with continuous, separate flows (air/ fuel-steam), with the beds interconnected to enable the bed materials to move from oxidiser to reformer reactors. This would result in potentially large temperature fluctuations for the bed materials. However, when the bed material contains a CO<sub>2</sub> sorbent, this promotes the exothermic sorption during steam reforming, and provides heat for the endothermic calcination during OTM oxidation, resulting in, in theory, smoothing out the temperature fluctuations when transitioning from oxidising feed to reducing feed conditions. In the presence of OTM in oxidised form, it is expected that part of the fuel may completely oxidise to CO<sub>2</sub> and H<sub>2</sub>O while reducing the OTM (R4.12), but some of it may partially oxidise to H<sub>2</sub> and CO according to NiO reduction reaction (R4.13) depending on the NiO:C in use. NiO reduction with generic shale gas fuel compound C<sub>n</sub>H<sub>m</sub> corresponds to (R4.12). When the fuel reacts according to reactions (R4.12 and R4.14) energy is released corresponding to the lower heating value of the fuel. In a similar manner, when the fuel reacts in accordance with reaction (R4.11) and (R4.14), energy corresponding to that of the partial oxidation of the fuel is released.

**Table 4.2 Main reactions identified in the gas-water-Ni-Ca equilibrium system (S G Adiya et al, 2017)**

No.	Reaction	Reaction type
R4.1	$CH_4 \xrightarrow{Heat} C + 2H_2$	thermal decomposition
R4.2	$CH_4 + H_2O \rightleftharpoons CO + 3H_2$	Steam methane reforming →/ Methanation (hydrogenation) of CO ←
R4.3	$CH_4 + 2H_2O \rightleftharpoons CO_2 + 4H_2$	Steam methane reforming →/ Methanation (hydrogenation) of CO <sub>2</sub> ←
R4.4	$C_nH_m + nH_2O \rightarrow nCO + (n + 0.5m)H_2$	Hydrocarbon steam reforming
e.g. R4.5	$C_2H_6 + 2H_2O \rightarrow 2CO + (2 + 3)H_2$	Ethane steam reforming
e.g. R4.6	$C_3H_8 + 3H_2O \rightarrow 3CO + (3 + 4)H_2$	Propane steam reforming
R4.7	$CO + H_2O \rightleftharpoons CO_2 + H_2$	Water gas shift (CO-shift) →/ Reverse water gas shift ←
R4.8	$CaO_{(s)} + CO_2 \rightleftharpoons CaCO_{3(s)}$	Carbonation of CaO <sub>(s)</sub> →/ decarbonation or calcination of CaCO <sub>3(s)</sub> ←
R4.9	$CaO_{(s)} + H_2O \rightleftharpoons Ca(OH)_2$	Hydration of CaO <sub>(s)</sub> →/dehydration of Ca(OH) <sub>2(s)</sub> ←
R4.10	$Ca(OH)_{2(s)} + CO_2 \rightarrow CaCO_{3(s)} + H_2O$	carbonation of Ca(OH) <sub>2(s)</sub>
R4.11	$C_nH_m + (n)NiO \rightarrow (n)CO + (n)Ni + (0.5m)H_2$	NiO reduction by the fuel, producing CO & H <sub>2</sub>
R4.12	$C_nH_m + (2n + 0.5m)NiO \rightarrow nCO_2 + (2n + 0.5m)Ni + (0.5m)H_2O$ E.g. n=1 and m=4 for methane	NiO reduction by the fuel, producing CO <sub>2</sub> & H <sub>2</sub> O
R4.13	$C_nH_m + (n + 0.25m)NiO + (n - 0.25m)H_2O \rightarrow (n + 0.25m)Ni + nCO_2 + (n + 0.25m)H_2$	Combined NiO reduction and global steam reforming reaction of the gas
R4.14	$Ni + 0.5O_2 \rightarrow NiO$	Ni oxidation to NiO
R4.15	$C_{(s)} + 2H_2 \rightarrow CH_4$	Carbon hydrogenation
R4.16	$2CO \rightleftharpoons C_{(s)} + CO_2$	Boudouard reaction (CO disproportionation) →/ reverse Boudouard reaction ←
R4.17	$C_{(s)} + H_2O \rightleftharpoons CO + H_2$	Steam gasification of carbon →

Based on the molar inputs of Table 1 for the shale gas/water equilibrium system, the maximum theoretical outputs can be determined according to stoichiometry of the H<sub>2</sub> producing reactions listed in Table 4.2. Accordingly, the maximum H<sub>2</sub> yield is obtained via the complete reactions R4.3, R4.5, 4.R6 (steam reforming of CH<sub>4</sub>, C<sub>2</sub>H<sub>6</sub> and C<sub>3</sub>H<sub>8</sub> respectively) followed by complete R4.7 (water gas shift). This would correspond to a H<sub>2</sub> yield of 49.0 wt % for shale gas '1' feedstock using R4.4. Therefore chemical equilibrium calculations of H<sub>2</sub> yield cannot exceed those values. In the case of H<sub>2</sub> purity, the maximum could be obtained in two ways, the first of which by complete thermal decomposition of CH<sub>4</sub>, C<sub>2</sub>H<sub>6</sub> and C<sub>3</sub>H<sub>8</sub> (e.g. R4.1), which would achieve a nearly pure H<sub>2</sub> product. This however would be to the detriment of the amount of H<sub>2</sub> produced (yield).

The second, more desirable way of obtaining a nearly pure gas product would be via complete reactions R4.3-R4.7 followed by complete carbonation via R4.8 or R4.10, after condensation of water product. The desirable outcomes of the equilibrium calculations are therefore first, a H<sub>2</sub> yield close to the maximum theoretical (stoichiometric) yield, followed by low energy cost, followed last by high H<sub>2</sub> purity. This is because due to stringent purity requirements of some commercial applications, such as in chemicals, pharmaceuticals and petroleum industries, food and beverages industries (Ramachandran and Menon, 1998) as well as fuel cell technologies (Ramachandran and Menon, 1998, Kumar et al., 2002) a last purification stage may always be needed.

## **4.2 Effect of temperature and presence of C<sub>2</sub>-C<sub>3</sub> feedstock in both C-SR and SE-SR processes**

H<sub>2</sub> yield and purity plots between 500 and 1200 K at S:C ratios of 1, 2, 3, 4, 5 and 6 are displayed in Figure. 4.1 (a and b), respectively. These profiles illustrate a comparative analysis of C-SR and SE-SR of shale gas. In the absence of water (S:C = 0, not shown in Figure. 4.1), the gas required in excess of 900 K to undergo thermal decomposition and to begin converting significantly to H<sub>2</sub>. For S:C of 1, 2, and 3, H<sub>2</sub> yield and purity increased steeply as temperature increased for both the processes. For C-SR, this was caused by conditions shifting from being favourable to methanation (main products CH<sub>4</sub> and CO<sub>2</sub> below 900 K) and other solid carbon forming reactions at a low temperature, to promoting steam methane reforming (main products H<sub>2</sub> and CO<sub>2</sub>). This occurred up to roughly 1100 K, where H<sub>2</sub> yield and purity declined and a gentle dwindling in both hydrogen yield and purity was seen with further temperature increase, independent of the S:C ratio, and caused by reverse water gas shift. In the case featuring in situ CO<sub>2</sub> sorption (SE-SR), the H<sub>2</sub> yield and purity profiles with temperature showed a much sharper rise with a wider range of plateau of maximum H<sub>2</sub> yield and purity with temperature, exhibiting the sorption enhancement effects; this is discussed in more detail in Section 4.4.

In the low temperature range (<720 K), the presence of C<sub>2</sub> and C<sub>3</sub> species in the reactant gas increases CH<sub>4</sub> yield significantly resulting from the cracking of those species and methanation as further confirmed by the negative CH<sub>4</sub> conversion from 500 to 720 K for C-SR process and from 500 to 540 K for SE-SR process (not shown). The latter resulted from the exothermicity of methanation, favoured at low temperature. Sorption enhancement results in reducing the equilibrium concentration of CH<sub>4</sub> in favour of the process at a higher temperature, thus the higher yield and purity than the conventional processes.

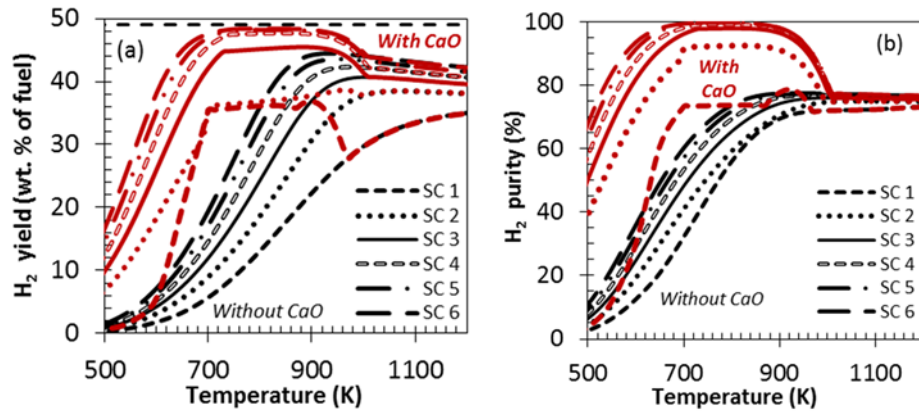


**Figure 4.1 (a) H<sub>2</sub> yield vs temperature at 1 bar, Ca:C 1 and varied S:C ratio 0-6, Table 1 inputs (b) H<sub>2</sub> purity vs temperature at 1 bar, Ca:C 1 and varied S:C ratio 0-6, Table 1 inputs (Note: the straight line in H<sub>2</sub> yield represent the theoretical maximum)**

Modelling the conditions S:C=3 with Aspen Plus V8.8 (reactor option RGibbs, properties method Peng Robinson) resulted in an excellent agreement with the results derived from CEA. However, for the SE-SR process a slight difference (decreased in H<sub>2</sub> purity and selectivity of carbon to calcium carbonate) was observed at 1000 K, which might result from the difference in thermodynamic properties of the programmes (ideal in CEA, non-ideal in Aspen Plus). Nonetheless this is relatively insignificant since Ca-sorption enhancement wanes at such high temperature. Similar thermodynamic studies were also conducted with or without Ca sorbent (C-SR and SE-SR process) using several fuels including methane (Anderson et al., 2014), propane (Wang et al., 2011), hydroxyacetone (Fu et al., 2013), acetic acid (Zin et al., 2012), and urea (Dupont et al., 2013). These results showed a similar trend to those of shale gas (this thesis) with regards to H<sub>2</sub> yield and purity and the effect of S:C ratio to be discussed later. Table 4.3 present C-SR maximum equilibrium output.

**Table 4.3 C-SR process maximum equilibrium output (H<sub>2</sub> yield, H<sub>2</sub> purity in the dry gas, and water conversion at 1 bar and S:C 0-3, Table 1 inputs)**

S:C ratio	H <sub>2</sub> yield (wt. % of fuel)	H <sub>2</sub> purity (%)	Water conversion (%)
0	22.4 @ 1200 K	64.0 @ 1200 K	N/A
1	35.0 @ 1200 k	73.1 @ 1200 K	97.7 @ 1200 K
2	38.5 @ 1070 K	75.0 @ 1070 K	61.1 @ 1010 K
3	41.0 @ 1010 K	76.0 @ 1010 K	46.9 @ 960 K

### 4.3 Effect of steam to carbon ratio in steam reforming processes

For the C-SR process, H<sub>2</sub> yield and purity behaviour with respect to S:C ratio follows Le Chatelier's principle, whereby an increase in the water reactant concentration in the system moves the equilibrium towards higher water conversion, thus causing higher H<sub>2</sub> yield and purity (Figure 4.1). However, operating at a large S:C ratio requires higher reactor volume, as well as high operational expenditure for raising steam (Wang et al., 2011, Zin et al., 2012, Dupont et al., 2013). The effect of S:C ratio levels off at higher values (above S:C 4 and 700-1200 K approximately) as depicted by Figure 4.1. Previous studies have also shown that S:C ratios higher than 4 do not have any significant beneficial effects (Antzara et al., 2014). The slight increase in the temperature range of 500-700 K in both H<sub>2</sub> yield and purity (above S:C 4) is reasonably insignificant, as industrial steam reforming plants operate around 1073-1273 K roughly (Adris et al., 1996, Fernández et al., 2012). Furthermore, using higher S:C ratio is known to cause catalyst and sorbent deactivation because of pore blocking (Martunus et al., 2012, Silva et al., 2015). Thus, S:C ratio of 3 typically used in industrial steam methane reforming will be focus on in the present studies (Dupont et al., 2013). The curves of H<sub>2</sub> yield and purity against temperature for the varied S:C ratio demonstrate the benefits of operating with high S:C ratio. For example, at 800 K, with the C-SR process case at S:C ratio of 1, the equilibrium H<sub>2</sub> yield is 13.2 wt. % of fuel with 56.0 % purity, but it becomes 24.3 wt. % of fuel with 65.4% purity at S:C ratio of 3. This is equivalent to 84 % and 17 % rises in H<sub>2</sub> yield and H<sub>2</sub> purity, respectively. The higher the S:C ratio, the closer the H<sub>2</sub> yield gets to the theoretical (stoichiometric) maximum e.g. 49.0 wt. % of fuel, as well as increasing H<sub>2</sub> purity. The use of high S:C ratio also prevents carbon product (potential deposition on the catalyst) through reaction (R4.17), however equilibrium carbon is discussed separately in section 4.7.

Figure 4.2(a) depicts the impact of S:C ratio through the value of the  $\Delta H$  ratio for the C-SR process (2<sup>nd</sup> y axis). Recall that the furthest  $\Delta H$  ratio below 1, the more thermally efficient the process is. The profiles in Figure 4.2(a) indicate that the  $\Delta H$  ratio of C-SR penetrated the <1 viability area at similar temperatures of 670 K for S:C ratio of 1, 2, and 3. For S:C ratio of 0 the process was viable at roughly 600 K, representing a process where H<sub>2</sub> is only a minor product, this is confirmed by the growing energy costs of operating at increasing S:C ratio, e.g. minimum  $\Delta H$  ratio of 0.41 was obtained at stoichiometric S:C ratio of 1 and 800 K, but minimum  $\Delta H$  ratio became 0.51 at the same temperature at S:C ratio of 3.

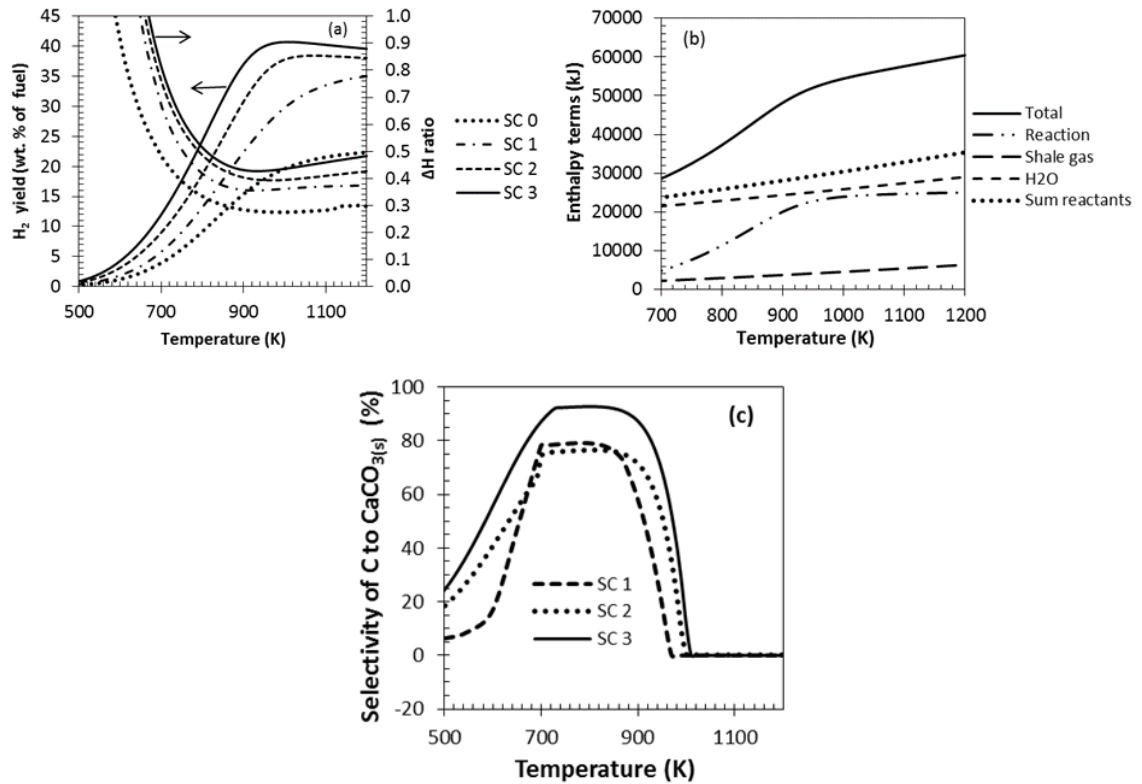


**Figure 4.2 (a) Effect of S:C ratio on H<sub>2</sub> yield and ΔH ratio vs reaction temperature at 1 bar and S:C 3, without Ca in the system, Table 1 inputs, (b) Enthalpy terms vs. temperature at 1 bar and S:C 3, without Ca in the system, Table 1 inputs (c) Selectivity of carbon to calcium carbonate vs temperature at 1 bar, Ca:C 1, and S:C 0-3, Table 1 inputs**

The energy balance for molar inputs of shale gas composition in Table 1 is further analysed with the help of figure 4.2(b) which depicts individual enthalpy terms profiles against temperature. The scales shown on the y axis of figure 4.2(b) in kJ are not particularly significant because they depend on the molar inputs chosen for the system, however what is significant is the relative positions of each enthalpy term profiles in the figure. The total enthalpy change of the process, and consequently the ΔH ratio, is seen to be dominated by the enthalpy change terms of bringing the gas and water reactants to reaction temperature, and in particular that of the water reactant, as opposed to the change in reaction enthalpy. At S:C 1 the total enthalpy change of the process at 800 K and 1070 K were 129 and 118 kJ per mol of H<sub>2</sub> produced, respectively, which further increased to 150 and 130 kJ/mol H<sub>2</sub> at S:C 2, and 159 and 145 kJ/mol H<sub>2</sub> at S:C 3, indicating the increased energy penalty of operating at higher S:C ratios.

#### 4.4 Sorption enhancement with CaO sorbent (SE-SR process)

Several benefits of in situ CO<sub>2</sub> sorption are identifiable (in all the studied gas compositions) in the temperature zone of the highest CaCO<sub>3(s)</sub> yield (500-990 K) on the gas water system at equilibrium. Firstly, H<sub>2</sub> yield increased, bringing it closer to theoretical maximum as depicted by figure 4.1(a). The effects of the CaO<sub>(s)</sub> sorbent on the H<sub>2</sub> yield in the low temperature range was brought about by the shift in equilibrium favoring the two H<sub>2</sub> generating reactions (water gas shift and steam reforming), caused by removal of the CO<sub>2</sub> from the syngas product. This would have increased both H<sub>2</sub> yield and purity simultaneously as seen in Figure 4.1. For instance, the H<sub>2</sub> purity increased from 65.4 % without Ca sorbent in the system to 98.0 % with CaO<sub>(s)</sub> sorbent, at S:C ratio of 3 and temperature of 800 K. This is equivalent to 50.0 % rise in purity between the two processes at a steam reforming temperature on the low side, ie. mild for the solid materials, thus preventing sintering. The latter was accompanied by significant CO and CO<sub>2</sub> reductions with dry mole fractions below 0.01 at 800 K and 0.1 at 1070 K. H<sub>2</sub> yield and efficiency of CO<sub>2</sub> capture is favoured in the low temperature range not only due to thermal decomposition of the sorbent at higher temperatures but also because the equilibrium vapour pressure of CO<sub>2</sub> over CaO<sub>(s)</sub> is low at low temperatures (Ryden and Ramos, 2012, Antzara et al., 2015). Effectively the SE-SR process extends by roughly 110-200 K (depending on S:C ratio in use) the conditions resulting in higher H<sub>2</sub> yield, shifted towards lower temperature, as depicted by Figure 4.1(a).

Two regions of temperature were observed in the trends of the process, that result from the sudden drops of Ca(OH)<sub>2(s)</sub> and CaCO<sub>3(s)</sub> product yield to zero. This was expected because at temperatures higher than 700 K, thermal decomposition of Ca(OH)<sub>2(s)</sub> occurs, while that of CaCO<sub>3(s)</sub> happens at temperatures higher than 1000 K (Figure 4.2(c)).

In addition, the presence of CaO<sub>(s)</sub> lowered the energy demand of H<sub>2</sub> generation from the gas-water system. This can be seen in the ΔH ratio farther from 1 for the system with CaO compared to the system without CaO, as shown in Figure 4.3(a), due to the lower total change in enthalpy obtained with CaO (Figure. 4.3b).

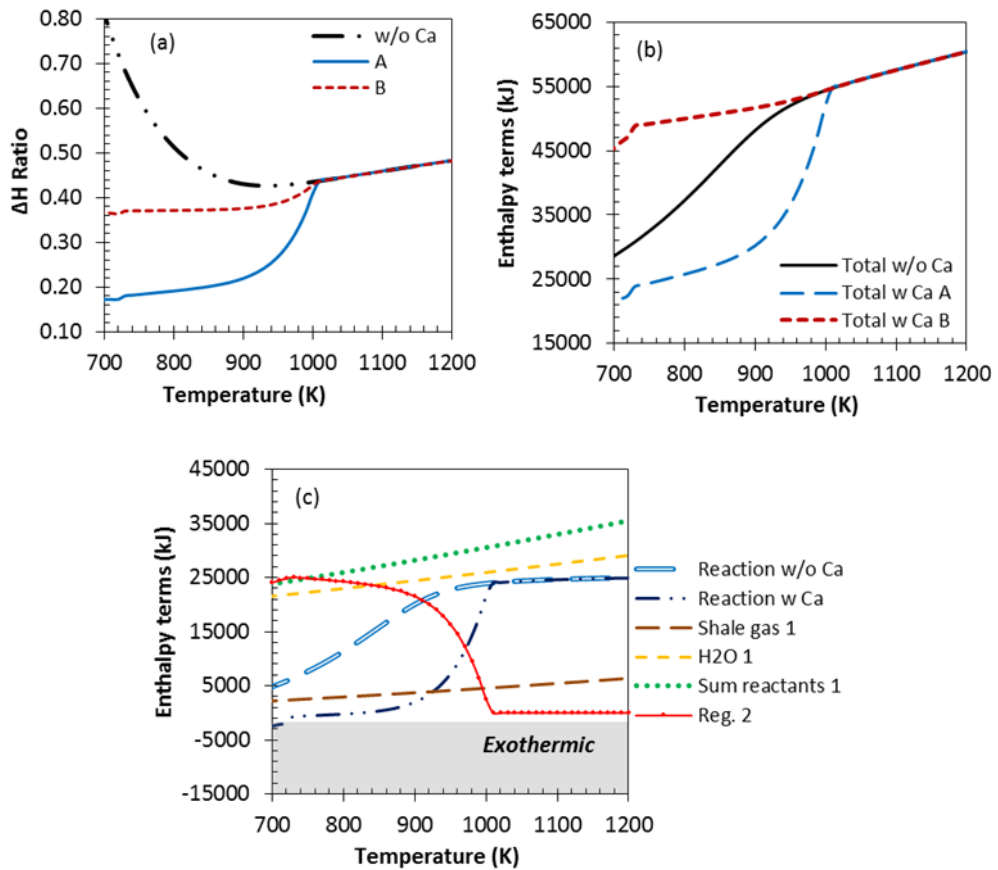


**Figure 4.3 (a)  $\Delta H$  ratio vs temperature at 1 bar, Ca:C 1, and S:C 3, Table 1 inputs (b) Total enthalpy terms vs. temperature at 1 bar, Ca:C 1, and S:C 3, Table 1 inputs (c) Enthalpy terms vs. temperature at 1 bar, Ca:C 1, and S:C 3, Table 1 inputs (Note: A and B mean without and with sorbent regeneration respectively while the number 1 and 2 denotes reaction process relevant to step 1 and step 2 respectively)**

Another benefit is reduced energy demand, as shown by the  $\Delta H$  ratio notably below that of the sorbent-free system, even when accounting for regeneration of the  $\text{CaCO}_{3(s)}$  back to  $\text{CaO}_{(s)}$  through a decarbonation step conducted at 1170 K, as represented by case 'B' (Figure. 4.3). Sorbent carbonation was reduced at S:C ratio of 0 and 1 due to low carbonate produced. Thus, the effect of sorption enhancement is not properly active at those conditions. For S:C of 2 and 3 the SE-SR process was overall moderately endothermic without sorbent regeneration (case A), but became overall significantly endothermic when accounting for the regeneration step of the sorbent (case B). Regeneration enthalpy change dropped to zero above 1000 K for all the S:C ratios considered due to thermal decomposition of  $\text{CaCO}_{3(s)}$ , and as a result, the  $\Delta H$  ratio vs. temperature profiles of the C-SR and SE-SR processes (with and without regeneration) merged with each other, making the later equivalent to the typical C-SR process. The heating cost of the gas was the same for the four S:C ratios (0, 1, 2, and 3) as their molar input remained unchanged.

The enthalpy change of raising steam increased with S:C ratio as expected. The energy of heating up the water further confirms the growing cost of operating at a high S:C ratio. The enthalpies of evaporating water and superheating steam at the reaction temperature still dominated the energy balance of the process with sorption enhancement as well. The reaction enthalpy is the backbone of the major difference seen between the two processes (C-SR and SE-SR), illustrated in the  $\Delta H$  ratios as depicted by Figure 4.3(c). This no doubt can be accredited to the carbonation process which is strongly exothermic.

To illustrate the energy savings brought about by in situ  $\text{CO}_2$  sorption using  $\text{CaO}_{(s)}$  sorbent, the case of S:C ratio of 3 is used. The minimum energy required to bring the system at equilibrium, starting from feed materials of the gas and liquid water at 298 K, was 159 kJ per mol of produced  $\text{H}_2$  at 800 K without  $\text{CaO}_{(s)}$  in the system. This decreased to 59 kJ/mol  $\text{H}_2$  with  $\text{CaO}_{(s)}$  without regeneration of the  $\text{CaCO}_{3(s)}$  (i.e. almost isenthalpic). When including the enthalpy of  $\text{CaCO}_{3(s)}$  regeneration back to  $\text{CaO}_{(s)}$  performed at 1170 K, the total enthalpy change rose to 114 kJ per mol of produced  $\text{H}_2$  at 800 K respectively, i.e. significantly lower than the sorbent-free system. It is noteworthy that the  $\text{H}_2$  producing step (step 1) would be physically separate from the sorbent regeneration step (step 2), and thus during the  $\text{H}_2$  production, near autothermal conditions would be reached in step 1 of the SE-SR process. Table 4.4 present SE-SR maximum equilibrium output.

**Table 4.4 SE-SR process maximum equilibrium outputs ( $\text{H}_2$  yield,  $\text{H}_2$  purity in the dry gas, selectivity of C to  $\text{CaCO}_{3(s)}$  and water conversion at 1 bar, Ca:C 1 and S:C 0-3, Table 1 inputs)**

Conditions	$\text{H}_2$ yield (wt. % of fuel)	$\text{H}_2$ purity (%)	Selectivity of C to $\text{CaCO}_{3(s)}$ (%)	Water conversion (%)
S:C 0 With CaO	22.4 @ 1200 K	63.5 @ 1200 K		0.01 @ 450 K
S:C 1 With CaO	37.0 @ 900 k	79.0 @ 920 K	97.7 @ 1200 K	79.0 @ 990 K
S:C 2 With CaO	38.6 @ 960 K	92.3 @ 820 K	76.9 @ 870 K	76.4 @ 810 K
S:C 3 With CaO	45.5 @ 880 K	98.0 @ 800 K	63.6 @ 720 K	93.0 @ 800 K

Accounting for  $\text{Ca(OH)}_{2(s)}$  and  $\text{CaCO}_{3(s)}$  as possible products of  $\text{CaO}_{(s)}$  conversion had different effects on process outputs depending on the S:C ratio and temperature. In situ  $\text{CO}_2$  capture by  $\text{CaO}_{(s)}$  (R4.8) and hydration reaction of CaO to produce  $\text{Ca(OH)}_{2(s)}$  (R4.9) are active at low to intermediate temperatures (< 700 K) and the latter competes with both steam reforming and water gas shift reactions for water usage. At temperature of maximum  $\text{H}_2$  yield, 800 K approximately, removal of water by CaO was insignificant because thermal decomposition of

$\text{Ca(OH)}_{2(s)}$  occurred at around the same temperature. Hence  $\text{CaO}_{(s)}$  was permitted to transform to  $\text{CaCO}_{3(s)}$  producing the desired sorption enhancement.

#### 4.5 Chemical looping with NiO coupled with steam reforming (CL-SR) of shale gas

Figure 4.4 summarises the outputs of steam reforming of shale gas when coupled with chemical looping (CL-SR) using NiO as the oxygen transfer material. For the purpose of comparison of processes, the outputs of C-SR are also included in the Figure. The process was investigated by first varying the NiO:C ratio while maintaining S:C of 3 in Figure 4.4 (a and b), then followed by changing the S:C between 0 and 3 while maintaining NiO:C 1.0 constant, as depicted in Figure 4.4 (c and d).

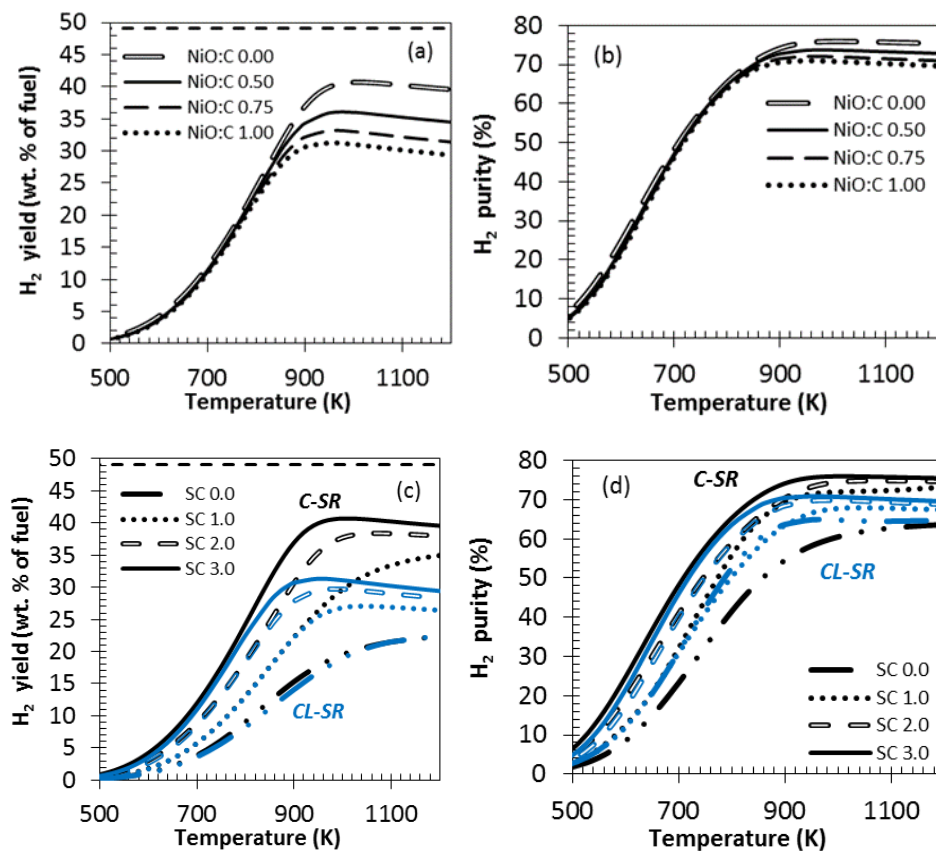


Figure 4.4 (a) H<sub>2</sub> yield vs temperature at 1 bar, S:C 3 and varied NiO:C 0.5-1.0, Table 1 inputs (b) H<sub>2</sub> purity vs temperature at 1 bar, S:C 3 and varied NiO:C 0.5-1.0, Table 1 inputs (c) H<sub>2</sub> yield vs temperature at 1 bar, NiO:C of 1.0 and varied S:C 0- 3, Table 1 inputs (d) H<sub>2</sub> purity vs temperature at 1 bar, NiO:C of 1.0 and varied S:C 0-3, Table 1 inputs (Note: NiO:C 0.0 denote C-SR process and the straight line in H<sub>2</sub> yield represents the theoretical maximum)

In the CL-SR process, complete conversion of the gas and good selectivity towards the desired products was achieved. NiO reduction with the fuel is thermodynamically possible at temperatures as low as 400 K, as indicated by negative water conversion below 400 K. Increasing the NiO:C ratio decreases monotonically the H<sub>2</sub> yield and purity (Figure 4.4a). The decrease in H<sub>2</sub> yield can be attributed to CL-processes using part of the fuel according to either R4.11 (co-products CO and H<sub>2</sub>) or R4.12 (co-products CO<sub>2</sub> and H<sub>2</sub>O) to meet the energy demand of steam reforming, a role that is normally played by the gas fired furnace in the C-SR process. H<sub>2</sub> purity also decreases with growing NiO:C ratio. This can be explained by concurrent CO<sub>2</sub> generation via the NiO reduction reaction (R4.12).

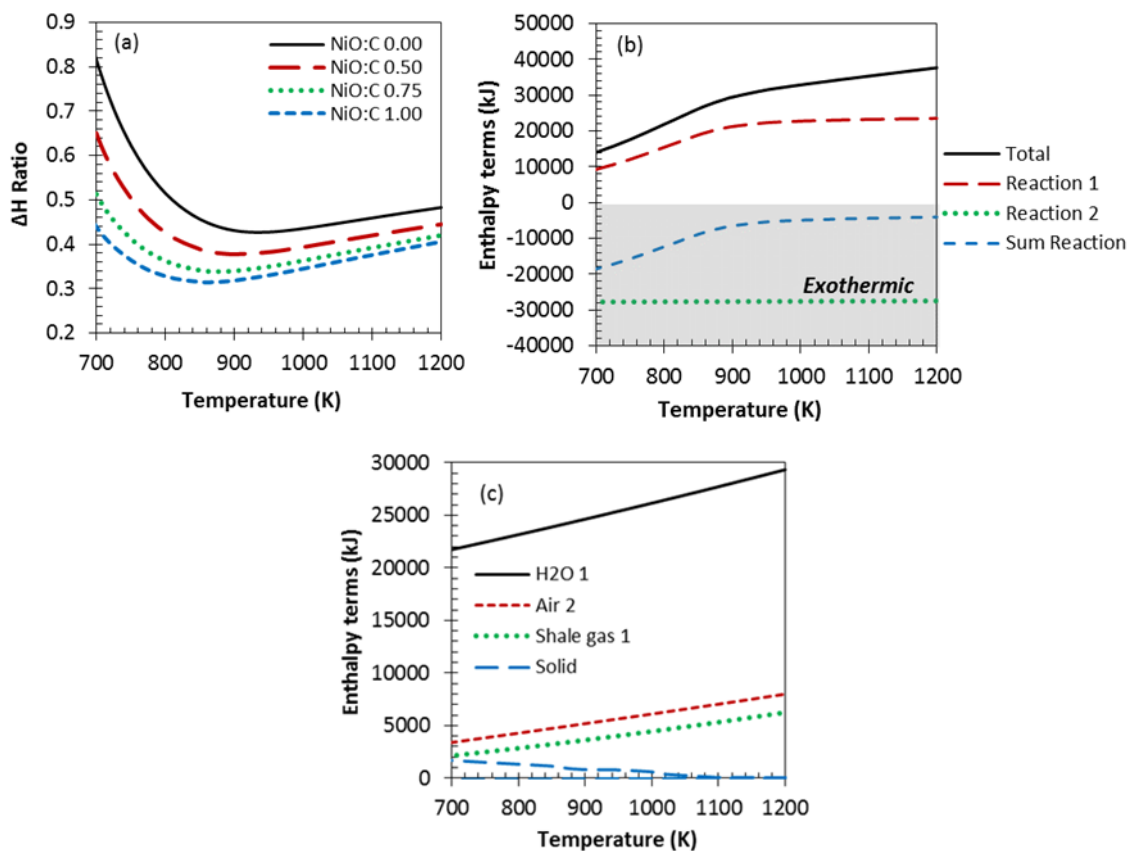


Figure 4.5 (a)  $\Delta H$  ratio of CL-SR vs. temperature at 1 bar, S:C 3 and NiO:C 0.0-1.0, Table 1 inputs (b) Reaction enthalpy terms and (c) Sensible enthalpy terms (gases: 298 K  $\rightarrow$  T(K) under stage 1, solid: T(K)  $\rightarrow$  1100 K under stage 2) vs. temperature at 1 bar, S:C 3 and NiO:C 1.0, Table 1 inputs (Note: the numbers 1 and 2 denote reaction processes stages 1 (reductive & reforming under fuel and steam feed) and 2 (oxidative under air feed) respectively). Temperature T(K) refers to reforming temperature. (Oxidation temperature is assumed to be 1100 K in all CL-SR cases)

One significant benefit of coupling C-SR with chemical looping is the reduced energy demand of the overall H<sub>2</sub> production. This is evidenced by the  $\Delta H$  ratio notably below that of the NiO-free system (Figure 4.5). The reduced energy demand can be attributed to the strongly exothermic nickel oxidation process (one of the major difference between the CL-SR and C-SR process) as shown in figure 4.5(b). The  $\Delta H$  ratio of the CL-SR process (steps 1&2) was fairly endothermic at low/medium temperature (700-850 K) but slightly decreases at higher temperatures (850-1200 K) with increase in operating temperature. The overall energy demand of the process decrease with increase in NiO:C ratio, making the process almost autothermal at the highest NiO:C ratio (1.0). However, even at the lowest NiO:C ratio energy demand of the CL-SR proces was still significantly lower than that of the conventional process (see appendix A1, table 3 for  $\Delta H$  total and  $\Delta H$  ratio values with varying NiO:C ratios). As expected, the  $\Delta H$  ratio increased with increasing S:C (0-3) due to the accrued cost of raising the excess steam, as explained earlier (figure not shown). This confirmed that the CL-SR process was also dominated by the cost of raising excess steam (S:C ratio in use). The energy demand of the whole process was dominated in the order of contributions of the following enthalpy terms: sum heating up reactants > sum reactions 1 & 2 as depicted in Figure 4.5(b and c). The energy demand of heating up the reactants was in the order H<sub>2</sub>O > air > shale gas. The cost of heating up the gas was relatively insignificant compared to those of raising steam from liquid water feed and preheating air. Table 4.5 present CL-SR maximum equilibrium output.

**Table 4.5 Maximum equilibrium outputs of CL-SR (H<sub>2</sub> yield, H<sub>2</sub> purity in the dry gas and H<sub>2</sub>O conversion at 1 bar, NiO:C 0.5-1.0 and S:C 0-3, Table 1 inputs)**

S:C ratio	Conditions	H <sub>2</sub> yield (wt. % of fuel)	H <sub>2</sub> purity (%)	Water conversion (%)
0	With NiO, NiO:C 1.00	22.5 @ 1200 K	65.0 @ 1010 K	n/a
1	With NiO, NiO:C 1.00	27.1 @ 1040 K	68.0 @ 1040 K	33.0 @ 1000 K
2	With NiO, NiO:C 1.00	30.0 @ 1000 K	70.0 @ 1000 K	27.0 @ 950 K
3	With NiO, NiO:C 0.50	36.0 @ 1000 k	74.0 @ 1000 K	34.6 @ 950 K
3	With NiO, NiO:C 0.75	33.2 @ 950 K	72.1 @ 950 K	27.1 @ 950 K
3	With NiO & NiO 1.00	31.3 @ 950 K	71.0 @ 950 K	22.3 @ 900 K

## **4.6 Effect of steam to carbon ration with given Ca:C and NiO:C ratio in sorption enhanced chemical looping steam reforming (SE-CLSR)**

### **4.6.1 H<sub>2</sub> yield, H<sub>2</sub> purity and selectivity to carbonate**

The effect of temperature on H<sub>2</sub> yield and purity is illustrated in Figure 4.6 for the three processes (C-SR, SE-SR and SE-CLSR) in the particular case of Ni:C 1.0 and the two S:C of 2 and 3.

Note that in the chemical looping processes CL-SR and SE-CLSR, some feedstock is consumed for NiO reduction according to R4.11 and R4.12, whilst for C-SR and SE-SR the fuel is fully available for the steam reforming process. The figure clearly portrays the significance of coupling sorption enhancement and chemical looping in steam reforming with both the superior H<sub>2</sub> yield ca. 700-850 K and H<sub>2</sub> purity ca. 700-1000 K obtained for SE-CLSR compared to the C-SR process (i.e. region of maximum CO<sub>2</sub> capture/efficient carbonation reaction). The presence of the CO<sub>2</sub> sorbent shifts the thermodynamic equilibria of both the steam reforming and the water gas shift reaction (R4.2 and R4.7) towards higher conversion to CO, then to CO<sub>2</sub>, followed by capture of the CO<sub>2</sub> on the sorbent, with the carbon product becoming almost exclusively solid calcium carbonate. Subsequently, the presence of the nickel based OTM in SE-CLSR led to even greater H<sub>2</sub> yield (in region of effective carbonation) than C-SR, although part of the fuel was used for reduction. This is because the reduction of fuel by NiO (R4.12) produces total oxidation products CO<sub>2</sub> and H<sub>2</sub>O, with the former being captured by the sorbent, and the latter increasing the water concentration of the system, effectively achieving a double or synergetic enhancement effect. The effect of coupling between C-SR and SE-SR on the H<sub>2</sub> purity in the low/medium temperature zone is explained by the efficiency of CO<sub>2</sub> capture by the Ca sorbent. At high temperatures (roughly above 1000 K), the efficiency of CO<sub>2</sub> capture declined rapidly and dropped to zero, hence the SE-SR process reverted back to C-SR, as conditions favoured CaCO<sub>3</sub> decomposition (Ryden and Ramos, 2012, Antzara et al., 2015). Regarding H<sub>2</sub> purity in the high temperature zone (above 1000 K), the inferiority of SE-CLSR process compared to C-SR and SE-SR was due to the additional CO<sub>2</sub> present at equilibrium resulting from the NiO reduction, whilst C-SR and SE-SR performed equally due to decomposition of the CaCO<sub>3(s)</sub>. On the other hand, the inferiority of the process (SE-CLSR) compared to SE-SR with regards to H<sub>2</sub> yield was due to the fact that part of fuel was used for NiO reduction while the fuel was completely available for steam reforming in the case of SE-SR process (Silvester et al., 2015).

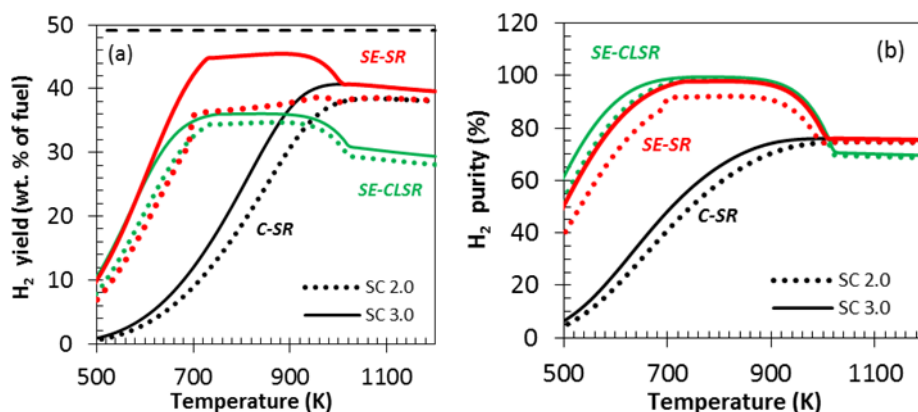


**Figure 4.6 (a) H<sub>2</sub> yield vs temperature with CaO<sub>(s)</sub> sorbent at 1 bar, Ca:C 1, NiO:C 1.0 and S:C 2 and 3, Table 1 inputs (b) H<sub>2</sub> purity vs temperature with CaO<sub>(s)</sub> sorbent at 1 bar, Ca:C 1, NiO:C 1.0 and S:C 2 and 3, Table 1 inputs (Note: the straight line in H<sub>2</sub> yield represent the theoretical maximum)**

Therefore the optimal operating temperatures for both SE-SR and SE-CLSR at atmospheric pressure were around 700-850 K approximately, as illustrated in Figure 4.6.

In practice, when using packed bed configuration used with alternating feed flows, it is envisaged that at least two packed bed reactors would be used in parallel, one undergoing the reductive stage with in situ CO<sub>2</sub> capture while the other is in oxidative stage with sorbent regeneration (and potentially carbon burn off). Table 4.6 and 4.7 presents the maximum equilibrium outputs of SE-CLSR process and comparison of the equilibrium outputs of C-SR and SE-CLSR process using CaO as the CO<sub>2</sub> sorbents at 800 K respectively.

**Table 4.6 Maximum equilibrium outputs of SE-CLSR (H<sub>2</sub> yield, H<sub>2</sub> purity in the dry gas, water conversion and selectivity of C to CaCO<sub>3(s)</sub>) at 1 bar, Ca:C 1, NiO:C 1.0 and S:C of 2 and 3, Table 1'inputs)**

S:C ratio	H <sub>2</sub> yield (wt. % of fuel)	H <sub>2</sub> purity (%)	Water conversion (%)	Selectivity of C to CaCO <sub>3(s)</sub> (%)
2	35.0 @ 870 K	98.5 @ 800 K	50.0 @ 720 K	96.1 @ 800 K
3	36.0 @ 850	99.5 @ 770 K	34.5 @ 740 K	99.0 @ 760 K

Figure 4.7 depicts the selectivity of carbon products to CaCO<sub>3(s)</sub> as a function of temperature for the SE-SR and the SE-CLSR processes. SE-CLSR offers higher selectivity to the carbonate product for a wider range of temperature over SE-SR with CaO. This is because the reduction process increased the water concentration in the system, in favour of CO<sub>2</sub> formation, hence allowing the maximum sorption. At temperatures above 1000 K the efficiency of the CO<sub>2</sub> capture declined

because of the favoured carbonate decomposition (Antzara et al., 2015, Ryden and Ramos, 2012).

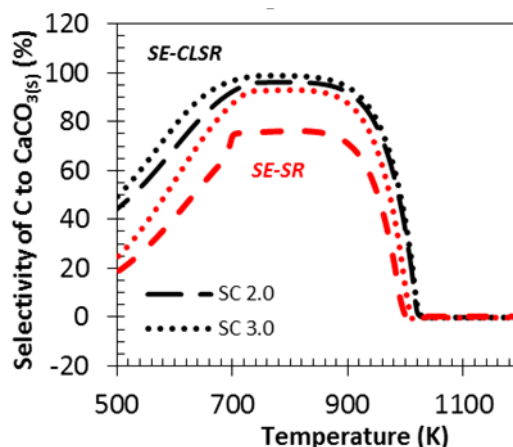


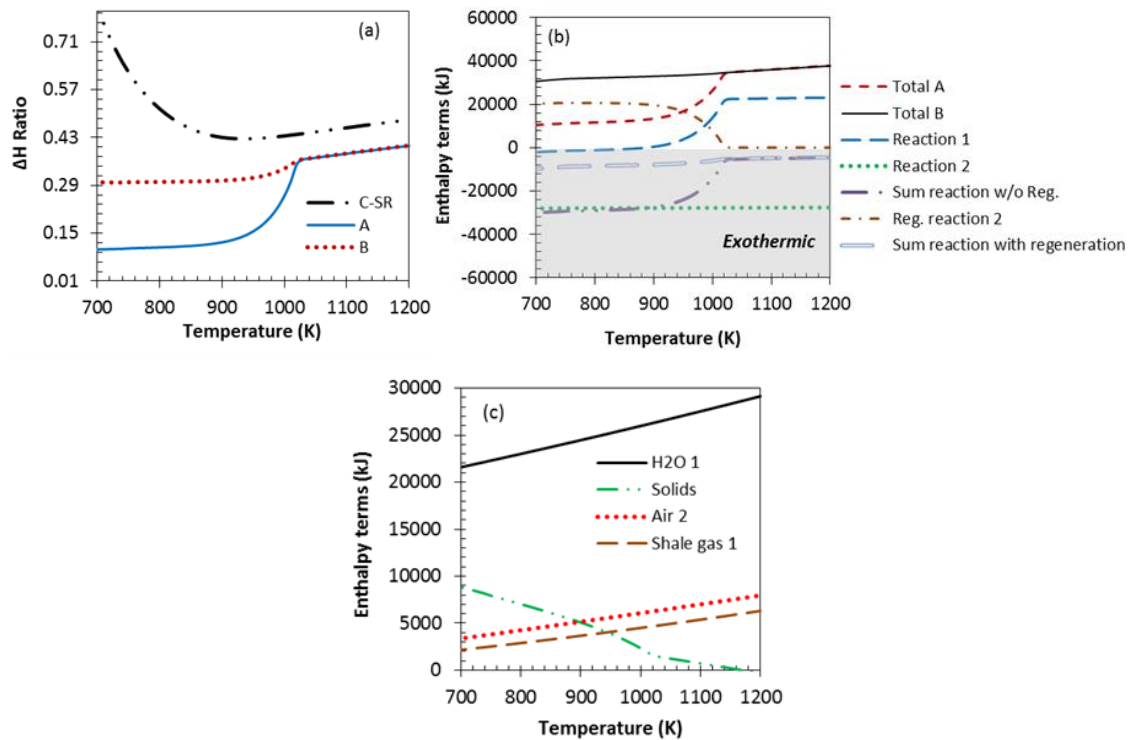
Figure 4.7 Selectivity of carbon to calcium carbonate vs temperature at 1 bar, Ca:C 1, NiO:C 1.0 and S:C 2 and 3 with  $\text{CaO}_{(s)}$  sorbent, Table 1 inputs

Table 4.7 Equilibrium outputs comparing C-SR and SE-CLSR ( $\text{H}_2$  yield,  $\text{H}_2$  purity in the dry gas, water conversion and selectivity of C to  $\text{CaCO}_{3(s)}$  at 1 bar, 800 K, Ca:C 1, NiO:C 1.0 and S:C of 2 and 3, Table 1 inputs)

S:C ratio	Conditions	$\text{H}_2$ yield (wt. % of fuel)	$\text{H}_2$ purity (%)	Water conversion (%)	Selectivity of C to $\text{CaCO}_{3(s)}$ (%)
2	Without Ca	19.0	59.2	39.0	n/a
2	With CaO & NiO	35.0	98.5	49.0	96.1
3	Without Ca	24.3	65.4	33.2	n/a
3	With CaO & NiO	36.1	99.5	34.3	99.0

#### 4.6.2 Enthalpy balance of SE-CLSR

Significantly reduced energy demand was seen in the SE-CLSR process as depicted in Figure 4.8, notably below those of both the C-SR and SE-SR process, even when accounting for complete regeneration of the  $\text{CaCO}_{3(s)}$  back to  $\text{CaO}_{(s)}$  via a decarbonation step conducted at 1170 K. The  $\Delta H$  ratio without regeneration was slightly endothermic (overall autothermal process) at low/medium temperature range (700-900 K) for S:C 2 but moderately endothermic (almost autothermal process) at S:C 3 with  $\text{CaO}_{(s)}$  sorbent. When the enthalpy of regenerating the  $\text{CaO}_{(s)}$  sorbent at 1170 K was included, the  $\Delta H$  ratios became significantly endothermic (positive) but remained significantly lower than the C-SR process, thus more energetically favourable.



**Figure 4.8**  $\Delta H$  ratio and enthalpy terms vs. reforming temperature for SE-CLSR at 1 bar, Ca:C 1, NiO:C 1.0 and S:C 3, Table 1 inputs (a)  $\Delta H$  ratio vs reforming temperature (b) Total enthalpy terms vs. reforming temperature (c) Sensible enthalpy terms vs. reforming temperature (Note: A and B mean without and with  $\text{CaCO}_{3(s)}$  regeneration to  $\text{CaO}_{(s)}$  at 1170 K, respectively, while the numbers 1 and 2 denote reaction process stages 1 (reductive/reforming) and 2 (oxidative/regenerating) respectively at 1170 K)

The heating demand of the gas and air was the same for the S:C 2 and 3 as their molar input remained unchanged. On the other hand, the heating demand of water increased with increase in S:C ratio (discussed earlier) i.e. S:C 2 < S:C 3. Although steam reforming and NiO reduction are endothermic processes, the total reaction enthalpy of the two-step cyclic process (stage 1 + stage 2) was overall exothermic, with the exothermicity decreasing with increase in stage 1 reaction temperature. We chose to show how this excess energy could be used by including a combustor/gas turbine/generator system in Figure 1.4(b), as it is the most flexible way to utilise the enthalpy of combustible as well as non-combustible streams via by-passing the combustor. The overall exothermicity resulted from the strongly exothermic Ni oxidation process, as shown in Figure 4.8. Both Ni oxidation and carbonation reactions have significantly lowered the energy demand of the hydrogen production. The  $\Delta H$  ratio of the two processes (C-SR and SE-CLSR) did not merge when decarbonation process stopped (at roughly 1000 K) like the SE-SR process, this effect can be explained by the activity of chemical looping and no doubt can be accredited to

the strongly exothermic nickel oxidation. The total energy cost of the process was, again, dominated by water enthalpy change followed by the reaction enthalpy (Figure 4.8(c)).

The results of the chemical looping processes (CL-SR and SE-CLSR) were further verified by the authors with Aspen plus 'RGibbs' reactor modelling and were in good agreement to those of CEA. Previous studies were conducted on CL-SR process by (Kathe et al., 2016) and SE-CLSR process by (Ryden and Ramos, 2012, Antzara et al., 2015, Antzara et al., 2014, Zhu and Fan, 2015). The results are in good agreement to those of the present study with regards to H<sub>2</sub> yield and purity, selectivity of carbon to calcium carbonates (SE-CLSR process only) as well as reduced energy requirement of the processes when compared to the conventional process. Optimum operating conditions for SE-CLSR also happen to be in the same range to those reported in the present study (700– 850 K, 1-4 bar pressure, S:C 3 and Ca:C 0.8-1 (Antzara et al., 2015)). Zhu and Fan, 2015 (Zhu and Fan, 2015) analysed the influence of Ca:M ratio, M(fuel):M ratio and Ni:M ratio on SE-CLSR process using equilibrium calculations, they found Ca:M = 1, M(fuel):M of 0.2 and Ni:M of 0.8 were optimum operating condition. Their conclusion (production of high purity hydrogen in the lower operating temperature range compared to CL-SR process) is in good agreement with the present study. Fan and Zhu, 2015 (Fan and Zhu, 2015) investigated the performance of a novel polygeneration system driven by methane aimed at producing high-purity H<sub>2</sub> through chemical looping combustion thermally coupled with CaO sorption enhanced methane steam reforming (they termed it CLC-SEMSR) combined with power generation through combined cycle. They simulated the process using Aspen Plus exiting functions and build in functions. They found that the novel polygeneration system can achieve higher exergy efficiency of 83.1% compared to 68.7 % in the C-SR process. Their conclusion that polygeneration systems for H<sub>2</sub> production and power generation simplifies the overall process with a more reasonable utilization of fuel, in addition to CLC-SEMSR process potential to produce higher H<sub>2</sub> yield and purity with reduced energy consumption for CO<sub>2</sub> separation is in good agreement with the present study. However, all of the thermodynamic studies (on SE-CLSR process) focussed pure methane as fuel in previous literature and most of the previous studies such as (Zhu and Fan, 2015, Fan and Zhu, 2015) used fluidised bed reactor (Air and fuel reactor separate). Researchers also investigated the performance of Ca-supported sorbent on the SE-CLSR process. For example, Fernandez et al., 2012 (Fernandez et al., 2012a), modelled the SE-CLSR process using a Ni based (9 % on Al<sub>2</sub>O<sub>3</sub> support) OTM/catalyst and a Ca/Cu sorbent with pure methane feedstock. They investigated the effect of catalyst/sorbent ratio, space velocity, S:C ratio, temperature and pressure. They found the optimum operating condition in the temperature range of 923-1023 K, at low-medium pressures (5-15 bar) and high S:C ratio of 3-6. The

differences in the optimum operating condition with the present study could be attributed to differences in operating conditions, model used for stimulation and most likely differences in CO<sub>2</sub> sorbent used in addition to the fact that temperatures lower than 873 K were not investigated. Martínez et al., 2014 (Martínez et al., 2014) performed a detailed and complete process design of a H<sub>2</sub> generation plant using natural gas as feedstock, Ni based OTM/catalyst and a novel Ca/Cu CO<sub>2</sub> sorbent as well. Their findings, compact design and the use of cheaper materials compared to C-SR process is in good agreement with the present study. Table 4.8 presents a comparison between C-SR and SE-CLSR process  $\Delta H$  total and ratio.

**Table 4.8 Equilibrium outputs comparing C-SR and SE-CLSR at 800 K, Table 1 inputs ( $\Delta H$  total and  $\Delta H$  ratio at 1 bar, Ca:C 1, NiO:C 1.0, and S:C 2 and 3. A and B mean without sorbent regeneration and with sorbent regeneration respectively)**

Conditions	$\Delta H$ total (kJ/mol H <sub>2</sub> )	$\Delta H$ ratio
C-SR S:C 2	150	0.49
SE-CLSR S:C 2 With CaO A	12	0.04
SE-CLSR S:C 2 With CaO B	71	0.23
C-SR S:C 3	159	0.51
SE-CLSR S:C 3 With CaO A	34	0.11
SE-CLSR S:C 3 With CaO B	92	0.30

#### 4.6.3 Effect of inert materials on enthalpy balance of the cyclic processes

The presence of inert solid materials in the reactor bed does not affect the equilibrium materials balances (i.e. H<sub>2</sub> yield and purity are the same with inert materials compared to without inert materials), as they do not affect the gas phase equilibrium reactions. However, inert materials would require heating or cooling as required during the cycles of the CL processes. There are two types of inert materials that may be present at any time in the reactor: the oxygen transfer catalyst support, and the degraded CO<sub>2</sub> sorbent material. During cyclic operation, the bed materials require heating from reaction temperature to regeneration temperature (SE-SR with regeneration, and SE-CLSR) or to oxidation temperature (CL-SR), and the active part of the sorbent undergoes decarbonation during regeneration. In the SE-CLSR process, Ni oxidation and decarbonation reactions occur together at sorbent regeneration temperature, 1170 K. In the following section, the individual effects of catalyst support and of degraded sorbent on the total enthalpy change of the cyclic processes are discussed.

#### 4.6.3.1 Oxygen transfer catalyst support

In practice, oxygen transfer materials as well as solid phase catalysts are structured so that a significant part of the material does not participate in the reactions (or it does in a minimal way), but imparts desirable properties to the reactor bed, e.g. morphological (high surface area), mechanical (strength) and thermal (phase stability), so they act as ‘support’ to the chemically active component (Adanez et al., 2012). Thus NiO is not used on its own in the reactor, but as part of NiO on a support. To represent this effect on the enthalpy balance, a 18 wt. % NiO on  $\alpha$ -Al<sub>2</sub>O<sub>3</sub> support (typical commercial steam reforming catalyst) (El-Bousiffi and Gunn, 2007) was simulated for the CL-SR and the SE-CLSR processes (Figure 4.9).

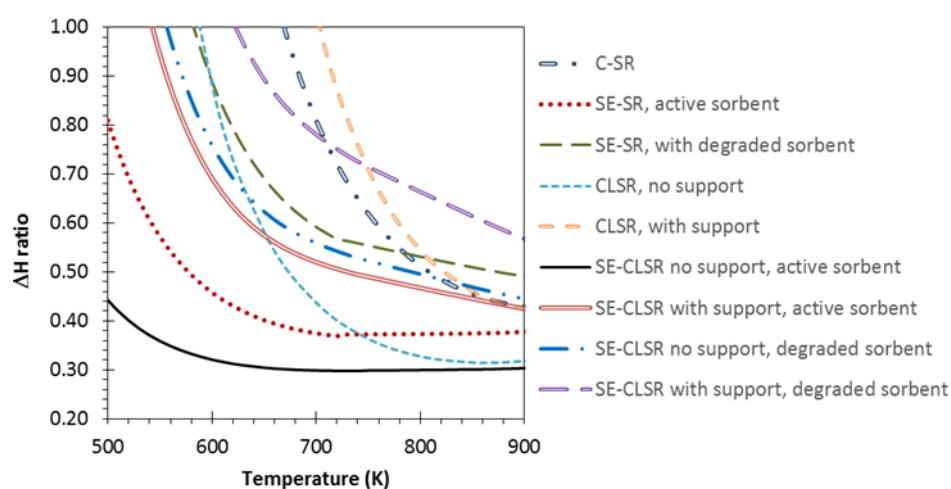


**Figure 4.9 SE-CLSR: process 2 at 1170 K, active Ca:C = 1, CL-SR: process 2 at 1100 K, S:C=3, NiO:C=1, no support: NiO 100 wt%, with support: 18 wt% NiO/Al<sub>2</sub>O<sub>3</sub>, active sorbent 100% CaO, degraded sorbent: 10% CaO active, 90% inert CaO.**

This introduced  $\alpha$ -Al<sub>2</sub>O<sub>3</sub> (corundum) as an additional ‘inert reactant’ in the molar ratio of Al<sub>2</sub>O<sub>3</sub>: NiO of 3.34, and the cases are described as either ‘with support’ or ‘without support’. Typically it was found that a cyclic process with support in proportions of Al<sub>2</sub>O<sub>3</sub>: NiO of 3.34 saw its  $\Delta H$  ratio increase by about 0.2 compared to the same process without support, although the gap between the two reduced as reforming temperature increased. For instance, at reforming temperature of 800 K, CL-SR without support had a  $\Delta H$  ratio of 0.33 compared to 0.54 with support. For the SE-CLSR, at 800 K,  $\Delta H$  ratio was 0.30 without support but 0.45 with support. By comparison C-SR at 800 K had a  $\Delta H$  ratio of 0.51. Here the CL-SR appears at disadvantage compared to the conventional process for reforming temperatures below 840 K, which was caused by the assumption that the oxidation step was carried out at 1100 K. When reducing the

oxidation temperature to 1050 K, which is sufficient to completely oxidise carbon black deposits on a 18 wt. % NiO/ $\alpha$ -Al<sub>2</sub>O<sub>3</sub> catalyst (Cheng et al., 2016), the  $\Delta H$  ratios of the CL-SR with support and the C-SR processes were the same at a reforming temperature of 800 K.

This illustrates that heat recuperation from the solids and gases from the regeneration step, not represented here, could play a crucial role in making the CL-SR viable when using a highly supported catalyst. The incentive is to minimise the amount of support required for the bed materials to maintain the right properties.

#### **4.6.3.2 Degraded CO<sub>2</sub> sorbent**

Similarly, another potential additional energy cost can be brought about by the deactivation of the CO<sub>2</sub> sorbent. Over many cycles, natural Ca-based sorbents typically stabilise to ca. 8-10 % of their 'fresh' CO<sub>2</sub> capacity (Fennell and Anthony, 2015). Sorbent materials such as limestone would then contain 90-92 wt. % of inert sorbent. The latter would also present a sensible enthalpy burden when bringing the bed materials to regeneration temperature (here assumed 1170 K). The effect of degraded sorbent in the bed was represented by introducing in the reactants mix the equivalent of 90 wt. % of the total molar calcium in the feed as inert CaO. The Ca:C ratio of 1 quoted in the figures refers to the active CaO.

The  $\Delta H$  ratios of the SE processes (SE-SR and SE-CLSR with and w/o support) were seen to also increase by around 0.2 at 800 K for the cases with degraded sorbent compared to the active sorbent, with a narrowing gap as the reforming temperature approached the regeneration temperature of 1170 K. Note that above 880 K, the sorption enhancement gradually disappeared as a result of decarbonation of the sorbent. This meant that, typically for reforming temperatures of above 800 K, the SE-SR with 90 % degraded sorbent and the SE-CLSR with support and 90 % degraded sorbent both became less energetically viable than the C-SR process. For the SE-CLSR process with support and 90 % degraded sorbent to become more energetically viable than the C-SR process, reforming temperatures would have to reach 720 K, which is the equilibrium lower limit for sorption enhancement as per Figures 4.6 and 4.7. This would imply the use of a very active steam reforming catalyst. At lower temperatures, energetics would be favourable but selectivity to hydrogen product would drop (lower yield and lower purity).

With regards to environmental aspects; SE-CLSR process could be an effective and eco-friendly way of generating  $H_2$  if the challenges associated with the energy costs of heating the bed materials to regeneration/oxidation temperature were to be addressed. The overall GWP of a C-SR plant is 11, 888 g  $CO_2$  equivalent/kg of  $H_2$  from which Hydrogen plant operation only account for 78.8 % (8,895 g  $CO_2$  equivalent/kg of  $H_2$ ) (Spath and Mann, 2001). SE-CLSR would have to address also the issues of life cycle analysis brought about by the use, operation lifetime and recyclability of the OTM catalyst and sorbent materials. As the majority of the world's hydrogen is generated through steam reforming of fossil fuels, there will be no elimination of greenhouse gases till  $CO_2$  is sequestered at the source (Goodman, 1996).

#### **4.7 Carbon product**

Generally, operating at a high S:C ratio inhibits solid carbon formation, as gasification reactions are promoted. This is one of the reasons steam reforming plants aim to operate with some excess of steam. Solid carbon in the equilibrium products not only deactivates catalyst by covering its active sites but also reduces  $H_2$  yield and purity because it represents carbon that does not react with steam to generate  $H_2$ . Solid carbon product is completely prevented at equilibrium conditions of S:C 2 and 3 in all the processes and varied gas composition via steam gasification of carbon (R17) (Goodman, 1996). As shown in Figure 4.10, solid carbon product mainly occurs at S:C between 0 and 1, with the quantity of carbon product depending on the process in use. As expected, enormous carbon was generated at S:C ratio of 0 in both the Ca free and  $CaO_{(s)}$  sorbent system. No doubt this resulted from the absence of steam reactant in the system which lowered the amount of  $CO_2$  product to be generated and thus to be adsorbed. Hence, the process behaves like C-SR, consequently the outputs of the SE-SR and C-SR processes at S:C 0 merge with each other. For S:C 1 in the Ca-free and  $CaO_{(s)}$  sorbent system, solid carbon equilibrium product was significantly low (nearly zero) in the low temperature range (500-650 K) but rose in the region of maximum  $H_2$  yield before exhibiting a gentle dwindling that approaches zero at higher temperatures (1000-1200 K). The sub stoichiometric conditions (limited water in the system) again are the reason behind this observation. As depicted in figure 4.10(b), solid carbon product is significantly low in the CL-SR system compared to C-SR system at same operating conditions. This stems from the fact that water can be a product in the NiO reduction process (R4.12), thus, favours suppression of equilibrium solid carbon. At S:C 1 in the CL-SR system, solid carbon formation declines gradually and approaches 0 significantly owing to the increase in water concentration in the system as mentioned previously. This further portrayed the positive impacts of operating at super-stoichiometric S:C ratio. In the SE-CLSR

process, formation of solid carbon was completely eliminated not only at S:C ratio of 2 and 3 but also at S:C ratio 0 and 1 as well. This no doubt is attributed to effectively achieving sorption enhancement of the NiO reduction reaction, which is identified here for the first time, and the sorption enhanced steam reforming reaction.

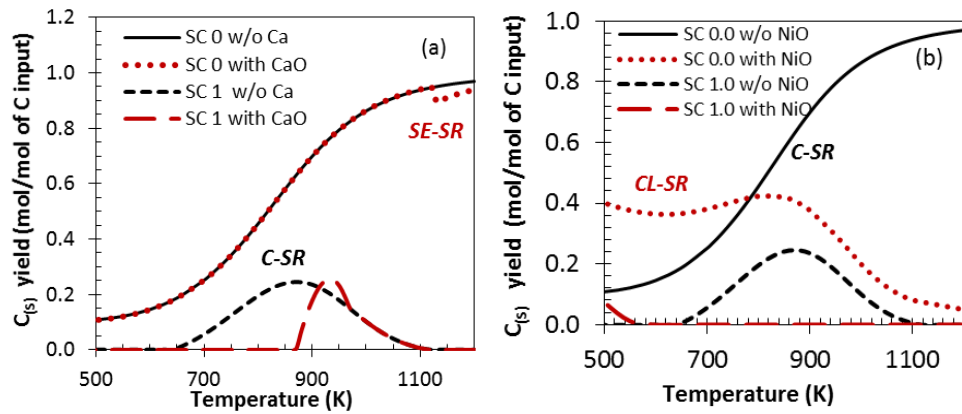
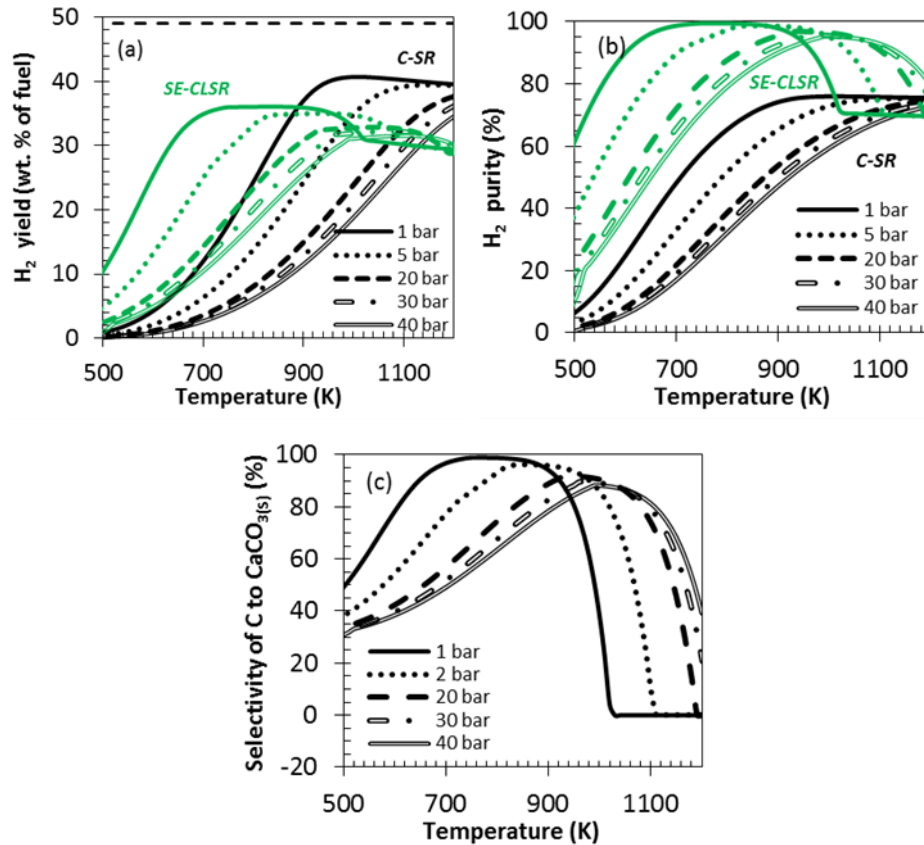


Figure 4.10 Carbon yield at 1 bar and S:C 0-1, Table 1 inputs (a) Ca free and Ca sorbent system at Ca:C 1.0, (b) Ca free and CL-SR system at NiO:C 1.0

#### 4.8 Effect of pressure on C-SR and SE-CLSR

Although steam reforming is affected by pressure negatively in accordance with Le Chatelier's principle due to volumetric increase, it is highly desirable to operate under elevated pressures in industrial plants, which enables higher throughputs, flows over large piping distances, sorption processes, and reduces Ca reactors and gas storage volumes. The effect of pressure on steam reforming is investigated at S:C ratio of 3 because it is the condition of excess steam typically used in industrial steam reforming (Dupont et al., 2013) aimed at hydrogen generation rather than syngas generation. Equilibrium conditions of 1 bar, 5 bars, 20 bars, 30 bars and 40 bars were calculated. Their choice was justified as follow: 1 bar represents atmospheric pressure and typically used for the lab-scale experimental work and derivation of kinetic rates, and a pressure range between 20-40 bar represents typical pressure values used in commercial steam reforming operations (Nielsen et al., 2002).



**Figure 4.11** Effect of pressure at Ca:C 1.0, NiO:C 1.0 and S:C 3, Table 1 inputs (a) H<sub>2</sub> yield vs temperature with CaO sorbent (b) H<sub>2</sub> purity vs temperature with CaO sorbent (c) selectivity of carbon to calcium carbonate vs temperature with CaO sorbent

The effect of pressure on both the Ca-free system and that with a Ca sorbent in the system follows Le Chatelier's principle. When the pressure was increased to above atmospheric pressure, the H<sub>2</sub> reactions equilibrium shifted to H<sub>2</sub> consumption to a very large extent to counteract product volume expansion, resulting in low H<sub>2</sub> yield and purity as depicted in Figure 4.11. H<sub>2</sub> yields of the C-SR and SE-CLSR processes decreased with increase in operating pressure. However, above 900 K, H<sub>2</sub> purity of the SE-CLSR process slightly increased with pressure. This occurred as partial pressure of CO<sub>2</sub> favoured the carbonation reaction leading to higher H<sub>2</sub> purity (Harrison, 2008).

In order to increase the partial pressure of CO<sub>2</sub> in the stripping gas the temperature of the adsorption step will always be lower than that of the desorption step. Furthermore, low/medium temperatures limit the maximum partial pressure of CO<sub>2</sub> that can be recuperated from the sorbent. Similarly, it is desirable that regeneration of sorbent (CO<sub>2</sub> desorption) be conducted at as lower total pressure as possible, to increase the quantity of CO<sub>2</sub> desorbed.

(Cobden et al., 2009, Hufton et al., 1999, Antzara et al., 2014). Thus, thermal swing is suggested for desorption of the sorbent, as per our assumption of regenerating at 1170 K. Steam is a good carrier gas for CO<sub>2</sub> since it can be easily condensed out of the CO<sub>2</sub> stream before being prepared for sequestration, with potential to minimise the steam usage. Thus, advantageous to the whole system performance (Cobden et al., 2009).

## 4.9 Conclusion

Using ideal materials properties, represented by an oxygen transfer material little diluted by inert support, and by fully active CO<sub>2</sub> sorbent, sorption enhanced chemical looping steam reforming can have considerable advantages compared to conventional steam reforming for H<sub>2</sub> production because of the substantial increase in H<sub>2</sub> yield and purity, as well as significant drop in temperature of the maximum H<sub>2</sub> yield with effective capture of CO<sub>2</sub> under well-chosen operational conditions. The opportunity of operating the Ca sorbent system at a low temperature could in turn decrease the need to operate at the higher pressure end, thus thermodynamically favouring the H<sub>2</sub> producing reactions. In the ideal bed materials conditions, near full sorption enhancement (over 95% efficiency of CO<sub>2</sub> capture) was observed about 700–900 K and atmospheric pressure, this nearly eliminated the need for further purification steps (CO shift, PSA) as well as expected to minimise the energy cost of operating the system. The energetic cost of shale gas reforming with and without Ca in the system is dominated by the enthalpy change of heating up the liquid water at 298 K and phase transformation to superheated steam at the reaction temperature, depending on S:C ratio in use. The choice of S:C ratio in conditions of excess steam represents a compromise between the higher H<sub>2</sub> yield and purity and low risk of solid carbon formation balanced by the increased energy demand of raising excess steam. The greater the S:C ratio of choice, the greater the enthalpy change of raising the steam will be, and vice versa. Addition of NiO to steam reforming system will decrease the thermal energy requirement of the process. Synergetic enhancement effects (favourable equilibrium shifts) are observed by the generation of steam from the NiO reduction step, which in turn promotes the steam consuming H<sub>2</sub> production and CO<sub>2</sub> generating reactions while CO<sub>2</sub> is captured, allowing for safe operation (non-carbon generating, high H<sub>2</sub> yield) at lower temperatures and lower S:C ratios than the conventional process with excess heat.

Atmospheric pressure and S:C ratio of 3 are found to be optimum for each of the studied processes. Temperature range between 1000 and 1010 K is best for the C-SR process, while 870 to 1000 K temperatures are optimum for CL-SR process. On the other hand the range 700 to 850

K are most beneficial for the SE-SR and SE-CLSR processes. Up to 49% and 52% rise in H<sub>2</sub> yield and purity respectively were achieved with SE-CLSR compared to C-SR at S:C 3 and 800 K. The enthalpy of bringing the system to equilibrium also decreased significantly in the system. A minimum energy of 159 kJ is required to produce 1 mol of H<sub>2</sub> at S:C 3 and 800 K in C-SR process, this significantly drops to 34 kJ/mol of produced H<sub>2</sub> in the CaO<sub>(s)</sub>/NiO system at same operating condition without regeneration of the sorbent, but when the energy of regenerating the sorbent at 1170 K was included, the enthalpy rose to 92 kJ/mol H<sub>2</sub>. This is still significantly lower than the Ca-free system.

Presence of inert bed materials in the reactor bed such as catalyst support or degraded CO<sub>2</sub> sorbent introduce a very substantial heating burden to bring these materials from reforming temperature to sorbent regeneration temperature or to Ni oxidation temperature, if different. Motivation for future research in the SE-CLSR process ought to focus on these two issues in order to maintain the theoretical advantages of SE-CLSR over the conventional steam reforming process.

## Chapter 5 Experimental studies

*An experimental programme aimed at proving feasibility of achieving the outcomes of thermodynamic equilibrium studies carried out earlier (Chapter 4) was conducted. Experimental illustration of the benefits of coupling sorption enhancement (SE) and chemical looping (CL) together with the conventional steam reforming (C-SR) process for hydrogen production from actual/typical shale gas feedstock at 650 °C using CaO sorbent and NiO on Al<sub>2</sub>O<sub>3</sub> support as the oxygen transfer material (OTM)/steam reforming catalyst was performed. Results are presented and compared for the separate processes of C-SR, SE-SR, CL-SR and finally the coupled SE-CLSR.*

### 5.1 Introduction to steam reforming experiments

In this chapter, bench scale experimental analysis in a fixed bed reactor for H<sub>2</sub> production from a synthesised Marcellus shale gas (see composition in Table 5.1) using SE-CLSR with CaO<sub>(s)</sub> sorbent and NiO as both catalyst and oxygen transfer material (OTM) was conducted. The model shale gas mixture was reproduced from cylinders of different hydrocarbons. Pure CH<sub>4</sub> gas used for the experiments was obtained through the laboratory piping (cylinder of CP grade 100 % for shared use throughout the building), while a mixture of 50 % C<sub>2</sub>H<sub>6</sub> and C<sub>3</sub>H<sub>8</sub> (in 40.1 and 9.9 % C<sub>2</sub>H<sub>6</sub> and C<sub>3</sub>H<sub>8</sub> proportion respectively) in an AZ size cylinder (1.2 L water capacity) containing 50 % inert N<sub>2</sub> gas (for safety reasons) was synthesised and obtained from BOC. The desired molar composition (Table 5.1) was calculated based on the mole fraction of the species and a given total volumetric flow rate, selected according to desired Gas hourly space velocity (GHSV), see 5.2.1. In addition to the 0.4 moles of N<sub>2</sub> gas in the synthesised shale gas, a nitrogen to carbon ratio (N:C) of 9.2 (N<sub>2</sub> obtained through the laboratory piping) was maintained in all the experiments to aide in the calculation of process outputs. The model shale gas presented in Table 1 represents a typical composition of natural gas, containing roughly up to 80 % of methane with roughly 20 % higher hydrocarbons (>C<sub>3</sub>), and inert gas (Mokhatab and Poe, 2012), representing a mixture rich in ethane and propane. This composition can also be representative of typical composition of natural gases from Nigeria (Sonibare and Akeredolu, 2004) and the North Sea UK (Peebles, 1992) , by containing up to 80 % methane (Peebles, 1992).

The experimental studies begin with conventional steam methane reforming (C-SR) first, investigating the effect of operating variables such as temperature, gas hourly space velocity (GHSV) and the effect of catalyst support on NiO based catalyst/OTM.

**Table 5.1 Composition of shale gas used for experiments (Bullin and Krouskop, 2008)**

Species	Shale gas (moles)
CH <sub>4</sub>	79.4
C <sub>2</sub> H <sub>6</sub>	16.1
C <sub>3</sub> H <sub>8</sub>	4.0
N <sub>2</sub>	0.4
Total	100

Sorption enhanced steam reforming (SE-SR) of the natural/shale gas feedstock was conducted as well. Here, the effect of Ca based CO<sub>2</sub> sorbent (CaO sorbent to be precise) in the C-SR process was examined. The effect of operating temperature on the sorption enhanced (SE) process using the optimum GHSV retrieved from the C-SR process as well as a comparison of the process (SE-SR) with the C-SR process was made to assess the feasibility of the process. This is followed by investigating the effect of integrating chemical looping (CL) in the C-SR process prior to studying the effect of coupling both SE and CL in the C-SR process. Cyclic behaviour and stability of the OTM and the CaO sorbent was studied and discussed in detail. The aim of the studies is to verify the feasibility of achieving the outcomes of the thermodynamic equilibrium studies investigated earlier (Chapter 4). Thus, steam to carbon ratio of 3 was used in all the experimental studies, as they were found to be optimum (Ryden and Ramos, 2012, Antzara et al., 2015, S G Adiya et al., 2017) and used in the industrial steam reforming plants (Dupont et al., 2013, S G Adiya et al., 2017).

PANalytical X'pert MPD instrument using Cu K $\alpha$  radiation was used to obtain the X-ray diffraction (XRD) pattern of unreacted and reacted catalysts, sorbent and catalyst-sorbents mixture. X'Pert HighScore Plus software was used for phase analysis of the XRD data. Quantification of the XRD data; catalyst, sorbent and catalyst-sorbents mixture (respective amounts of Ni, NiO, Al<sub>2</sub>O<sub>3</sub>, CaO and CaCO<sub>3</sub>) as well as crystalline size of the materials was calculated using the Rietveld refinement method and the Scherrer equation respectively. It is worth noting that the XRD analysis was only conducted on 18 wt. % NiO on Al<sub>2</sub>O<sub>3</sub> support. The 15 wt. % NiO on CaO/Al<sub>2</sub>O<sub>3</sub> support was not analyzed due to large amorphous content.

Field-emission scanning electron microscope (FESEM, LEO Gemini 1530) was used to study surface morphology of the unreacted and reacted catalyst, sorbent and the catalyst-sorbent mixture. The sample particles were coated with an Iridium layer of 10 nm and used for FESEM imaging. Energy dispersive X-rays (EDX) was used for further analyses such as phase identification of the fresh and used catalyst and/or sorbent.

CHNS Elemental Analyser (Flash EA2000 by CE Instruments) was used to measure the quantity of carbon deposited on the reacted catalyst and sorbent. The catalyst and catalyst-sorbent mixture were ground to fine powder before the CHNS measurements. An 8 g (approximately) of each sample was used for each analysis.

In order to know the actual carbon generated during experiments, Total organic carbon (TOC) content in the condensate (collected at the bottom of the reactor, see rig diagram in Chapter 3) was measured using a Hach-Lange IL550 analyser.

## **5.2 Conventional steam reforming (C-SR) of shale gas**

### **5.2.1 Effect of gas hourly space velocity (GHSV) on C-SR process**

The effect of gas hourly space velocity (GHSV) was investigated at 1 bar, S:C ratio of 3 and 650 °C using commercial steam reforming catalyst (18 wt. % NiO on Al<sub>2</sub>O<sub>3</sub> support). GHSV was defined here as the total volumetric flow rate of feedstock divided by the volume of catalyst. It was found that GHSV significantly affects fuel and water conversion and subsequently H<sub>2</sub> yield and purity as well. As the GHSV decreases (from 1.393, 1.094, 0.793 to 0.498), while all other parameters are kept constant, fuel (shale gas) conversion increases. This was expected because when the GHSV decreases, contact time between reactant gases and the catalyst is longer in the reactor and hence the conversion of fuel increases significantly.

Figure 5.1 depict plots of H<sub>2</sub> yield and purity, fuel and H<sub>2</sub>O conversion (average values) vs temperature. As shown in the figure all the process outputs decrease with increase in GHSV in succession i.e 0.498 > 0.793 > 1.094 > 1.393. Consequently, the lowest GHSV (0.498) with the highest contact time was chosen as optimum and used for all the subsequent experiments. Maximum fuel conversion i.e 100 % was not achieved even at the highest contact time (GHSV<sup>-1</sup> 0.498). Comparison of the experimental results with the equilibrium results showed that the experimental results are away from equilibrium which could be attributed to reaction kinetic limitations causing low fuel and water conversion and subsequently low H<sub>2</sub> yield and purity.

Table 5.2 presents a comparison between the experimental (average values) and equilibrium data. Previous studies on the effect of GHSV<sup>-1</sup> on steam reforming process such as Cavallaro et al (Cavallaro et al., 2003), Xu et al (Xu et al., 2009), Jiwanuruk et al (Jiwanuruk et al., 2016) and Abbas et al (Abbas et al., 2016) has also found that increasing the GHSV could result to decrease in fuel conversion, which in turn affects both the H<sub>2</sub> yield and purity negatively depending on the extent of increase as reported in the presence study.

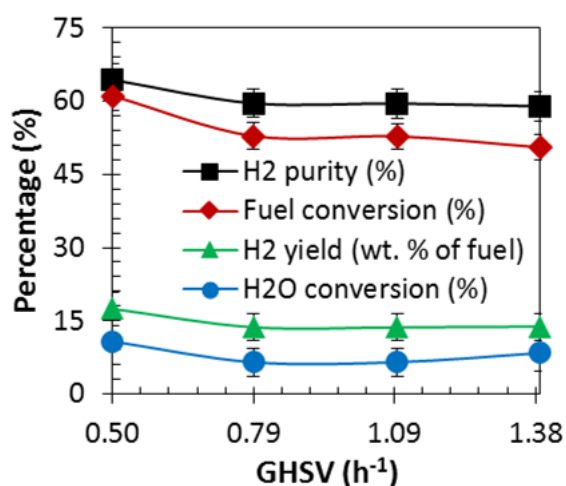


Figure 5.1 Effect of GHSV on H<sub>2</sub> yield and purity, fuel and H<sub>2</sub>O conversion using 18 wt. % NiO on Al<sub>2</sub>O<sub>3</sub> support at 1 bar, 650 °C and S:C 3 (average values)

Table 5.2 Comparison between the experimental (average values) and chemical equilibrium results at 1 bar, 650 °C and GHSV of 0.498-1.393, using 18 wt. % NiO on Al<sub>2</sub>O<sub>3</sub> support catalyst

GHSV	H <sub>2</sub> yield (wt. % of fuel)	H <sub>2</sub> purity (%)	Fuel conversion (%)	H <sub>2</sub> O conversion (%)
0.498	17.453	64.396	61.081	10.771
0.793	13.669	59.575	52.865	6.494
1.094	13.661	59.545	52.809	6.511
1.393	13.812	58.964	50.547	8.407
Chem. Eq.	41.76	76.36	98.35	51.18

### 5.2.2 Effect of temperature on C-SR process

C-SR process experiments were conducted isothermally using shale gas as feedstock (see table 1 for composition) in a packed/fixed bed reactor at atmospheric pressure. The effect of temperature was investigated at 1 bar, S:C ratio of 3 and the temperature range of 600 to 750 °C. The choice of condition S:C ratio of 3 for operation at 1 bar was due to the fact that they were found to be optimum from the thermodynamic studies conducted (See Chapter 4). Thus,

all experimental studies were conducted at these conditions for validation of processes outputs.

Fuel and H<sub>2</sub>O conversion, H<sub>2</sub> yield and purity increased as temperature increased. This was because high temperatures are in favour of the strong endothermic steam reforming reaction in accordance with Le Chatelier's principle (Figure 5.2). As the temperature of the reforming process increases, CH<sub>4</sub> outlet moles decreases indicating increase in fuel conversion consequently increasing the outlet moles of H<sub>2</sub>. C<sub>2</sub>H<sub>6</sub> and C<sub>3</sub>H<sub>8</sub> species in the fuel were completely reformed to syngas and/or cracked to CH<sub>4</sub> as confirmed by the absence of these species in the outlet product gases. The endothermic steam reforming of CH<sub>4</sub> was enhanced by an increased temperature to the detriment of methanation reaction that is favoured in the low/medium temperature range.

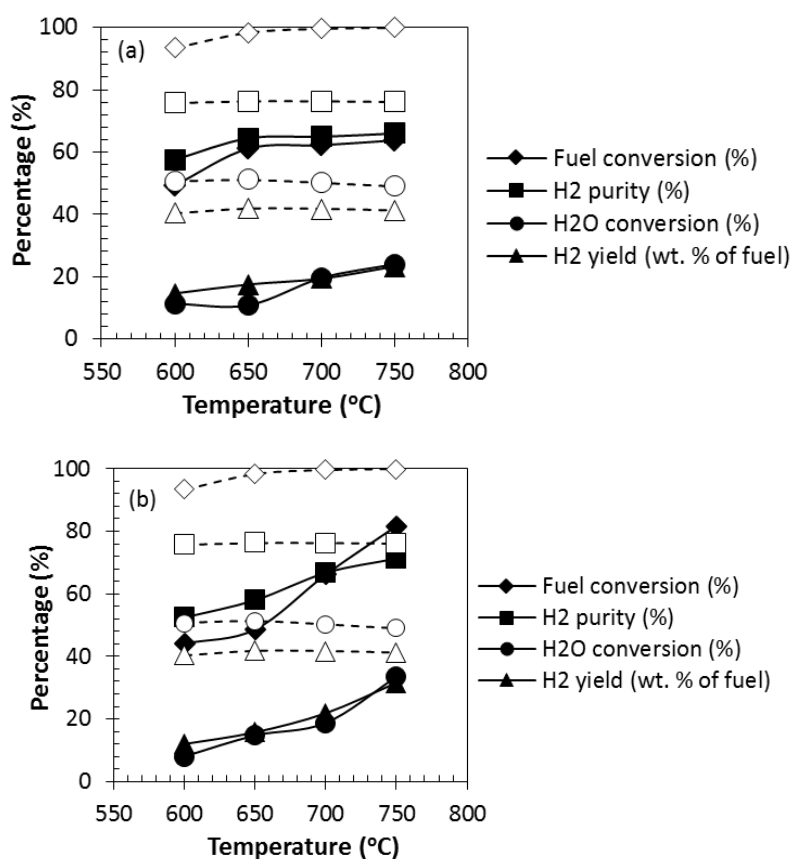


**Figure 5.2 Comparative analysis between experimental (average) process output and chemical equilibrium results at 1 bar, GHSV 0.498 and S:C 3 (a) using 18 wt. % NiO on Al<sub>2</sub>O<sub>3</sub> support catalyst (b) using 15 wt. % NiO on CaO/Al<sub>2</sub>O<sub>3</sub> support catalyst (Note: Solid lines are for experimental results and dashed lines for chemical equilibrium results)**

Comparison of the experimental results with the thermodynamic equilibrium results show the same trend with respect to temperature. However, the experimental process output was far away from the thermodynamic equilibrium results. Thus, the chemical equilibrium results demonstrated higher fuel and water conversion and consequently higher H<sub>2</sub> yield and purity. Reaction kinetics (reaction rate of methane on a conventional nickel on alumina support only depend on the partial pressure of methane (Van Beurden, 2004)) and thermodynamic equilibrium limitation (depicted in Figure 5.2) is the only explanation behind this observe phenomenon.

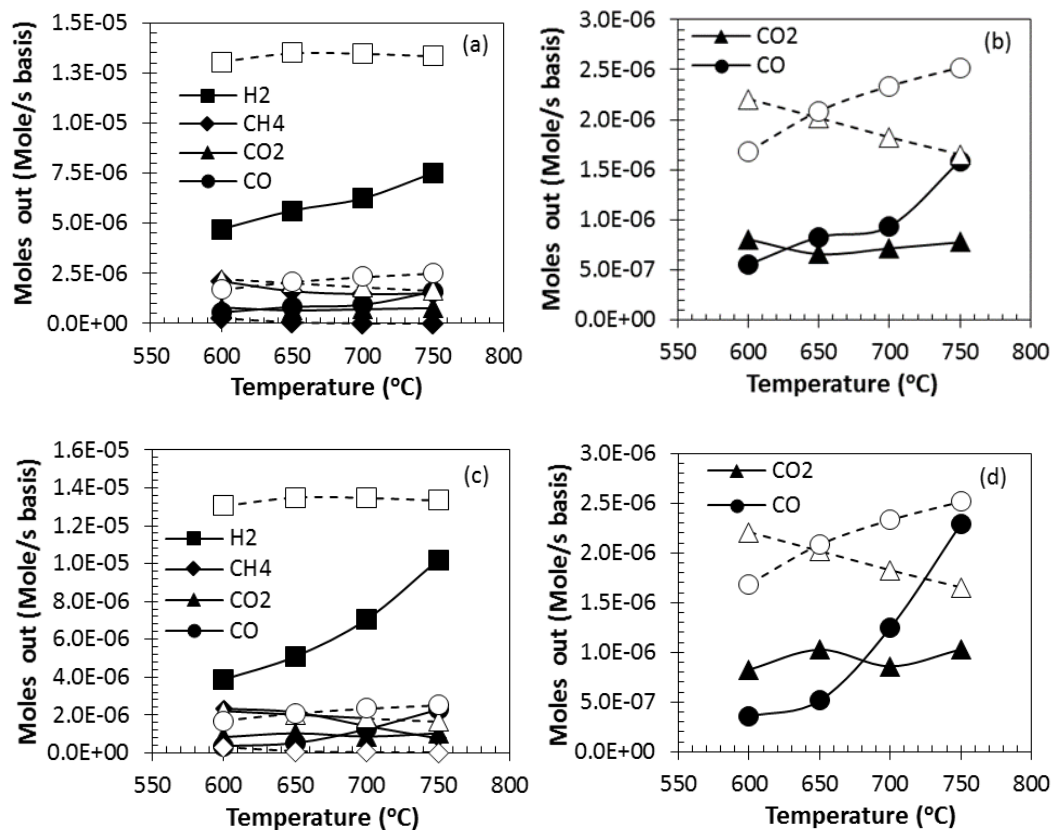


**Figure 5.3 Comparative analysis between experimental (average) process output and chemical equilibrium results at 1 bar, GHSV 0.498 and S:C 3 (a) outlet moles using 18 wt. % NiO on Al<sub>2</sub>O<sub>3</sub> support (b) Clearer graph of CO<sub>2</sub> and CO moles out using 18 wt. % NiO on Al<sub>2</sub>O<sub>3</sub> support (c) outlet moles using 15 wt. % NiO on CaO/Al<sub>2</sub>O<sub>3</sub> support (d) Clearer graph of CO<sub>2</sub> and CO moles out using 15 wt. % NiO on CaO/Al<sub>2</sub>O<sub>3</sub> support (Note: Solid lines are for experimental results and dashed lines for chemical equilibrium results)**

It can be concluded that Water gas shift reaction (WGS) was poorly active in all the temperature range investigated (during the experimental studies) particularly at 700 and 750 °C owing to the medium/high concentration of CO outlet moles (Figure 5.3) depending on the temperature.

Again, the outlet moles of the chemical equilibrium results showed exactly same trend as the experimental results except that the WGS reaction was more active in the chemical equilibrium system compared to the experimental.

The inhibition of the exothermic WGS reaction no doubt could be attributed to the unfavourably high temperature. However, At 600 °C (with 18 wt. % NiO on Al<sub>2</sub>O<sub>3</sub> support) and 600 and 650 °C (with 15 wt. % NiO on CaO/Al<sub>2</sub>O<sub>3</sub> support) the outlet moles of CO<sub>2</sub> were higher than those of CO (see figure 5.3(b) and (d) for clarity), this results from the fact that the low/medium temperature values favours the reaction even though it is not the optimum/desirable temperature for the WGS reaction. The catalyst support could also play a significant role in the observed phenomenon. However, the effect of catalyst support will be discussed in detail in the next section. The contribution of CH<sub>4</sub> (from the feedstock and that from the crack C2-C3 species) steam reforming to generate H<sub>2</sub> compensated the diminution in H<sub>2</sub> production caused by the inhibition of WGS reaction. Generally speaking, the suppression of two exothermic reactions (WGS and Boudouard reactions) by high temperatures causes the increase in the CO concentration and a decrease in the CO<sub>2</sub> concentration as shown in Figure 5.3.

Figure 5.4 shows the plots of process outputs with time on stream at 750 °C. Fuel and H<sub>2</sub>O conversion, H<sub>2</sub> yield and purity are fairly stable over the duration of (all) the experiments. Molar production rate of H<sub>2</sub>, CH<sub>4</sub> and CO were also stable. Conversely, CO<sub>2</sub> moles in the system with 18 wt. % NiO on Al<sub>2</sub>O<sub>3</sub> support increased gradually and stabilized at around 894 seconds approximately indicating dominance of the full steam reforming process. On the other hand the system with 15 wt. % NiO on CaO/ Al<sub>2</sub>O<sub>3</sub> shows a sharp increase in fuel and water conversion at approximately 3604 s, causing a rise in the H<sub>2</sub> yield and purity, H<sub>2</sub> and CO<sub>2</sub> moles out, and a decrease in the CH<sub>4</sub> and CO moles out at exactly same position.

At conditions of high temperature (700 and 750 °C), carbon deposition on the reactor wall was observed in a very large concentration compared to the low/medium temperatures (600 and 650 °C). Thermal decomposition reaction is the only explanation of the observe phenomenon. The reaction is endothermic, thus thermodynamically favoured at high temperature. Kinetically, it is expected to happen fast in the presence of a catalyst (Wang, 2014). Nonetheless , the carbon concentration on the wall of the reactor could be considered as negligible.

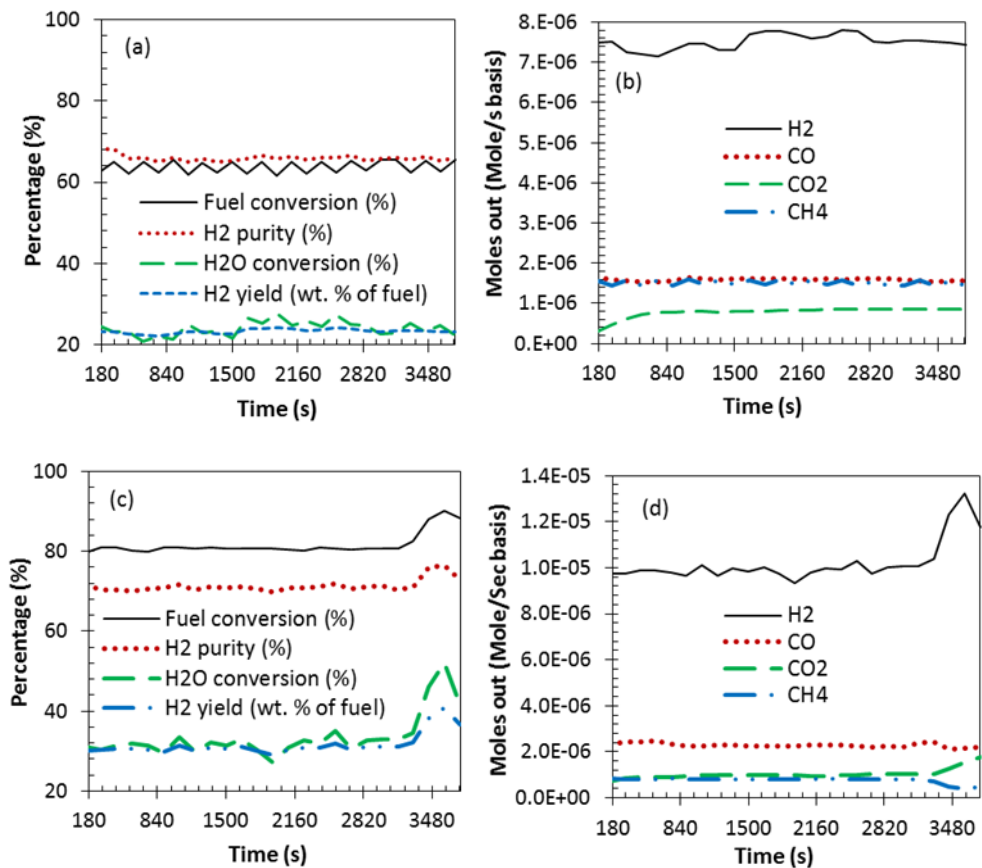


**Figure 5.4 Process output vs time at 750 °C, 1 bar, GHSV 0.498 and S:C 3 (a) H<sub>2</sub> yield and purity, fuel and H<sub>2</sub>O conversion vs time using 18 wt. % NiO on Al<sub>2</sub>O<sub>3</sub> support catalyst (b) moles out vs time using 18 wt. % NiO on Al<sub>2</sub>O<sub>3</sub> support catalyst (c) H<sub>2</sub> yield and purity, fuel and H<sub>2</sub>O conversion vs time using 15 wt. % NiO on CaO/Al<sub>2</sub>O<sub>3</sub> support catalyst (d) moles out vs time using 15 wt. % NiO on CaO/Al<sub>2</sub>O<sub>3</sub> support catalyst**

H<sub>2</sub> production using methane and natural gas steam reforming in a conventional and microreactor reaction systems was investigated by Izquierdo et al. (Izquierdo et al., 2012) with Ni based catalyst supported on MgO and Al<sub>2</sub>O<sub>3</sub> and Pd and Pt based catalyst supported on Al<sub>2</sub>O<sub>3</sub>. They investigated the influence of the catalytic activity of the above mentioned materials, temperature and S:C ratio at atmospheric pressure and constant GHSV and concluded that increasing the temperature improved fuel conversion but did not improve considerably at higher S:C ratios. The influence of temperature on C-SR they reported is in good agreement to that reported in the present study. Abbas et al. (Abbas et al., 2016) conducted a kinetics study and modelling of steam methane reforming process over a NiO/Al<sub>2</sub>O<sub>3</sub> catalyst in an adiabatic packed bed reactor. They found that higher temperature has a positive effect on H<sub>2</sub> yield and purity and concluded that high temperature, low pressure and high steam to carbon ratio are the optimal operating conditions with regards to fuel conversion and H<sub>2</sub> purity, which are in good agreement with the present study.

### 5.2.3 Effect of catalyst support on C-SR process

Two commercial NiO based catalyst were provided by Twigg Scientific and Technical Ltd, for the experimental studies. The performance of each of the catalyst (provided by the manufacturer as 18 wt. % NiO on  $\alpha$ -Al<sub>2</sub>O<sub>3</sub> support and 15 wt. % NiO on CaO/Al<sub>2</sub>O<sub>3</sub> support) were investigated over a range of temperature (600 to 750 °C). Both catalyst were reduced with 5 % H<sub>2</sub> (balance N<sub>2</sub>) at 700 °C for an hour to convert the NiO to active Ni. No significant difference was found between the two catalyst at low/medium temperature range (600 and 650 °C). However, at higher temperature (700 and 750 °C), the Ni on CaO/Al<sub>2</sub>O<sub>3</sub> support performed better/was more active than the Ni on Al<sub>2</sub>O<sub>3</sub> support with regards to product yield and feed conversion as depicted in Figure 5.5. Up to 36 % and 8 % rise in H<sub>2</sub> yield and purity respectively was seen between the two catalyst average outputs at 750 °C under same operating condition (1 bar, S:C 3 and GHSV 0.498).

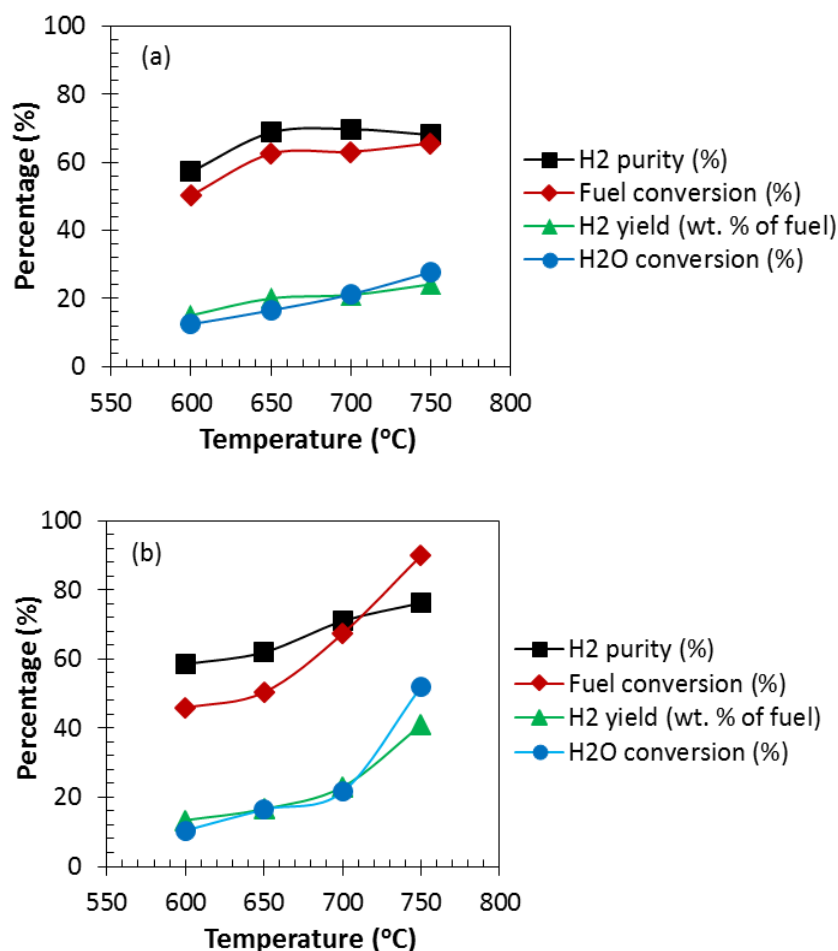
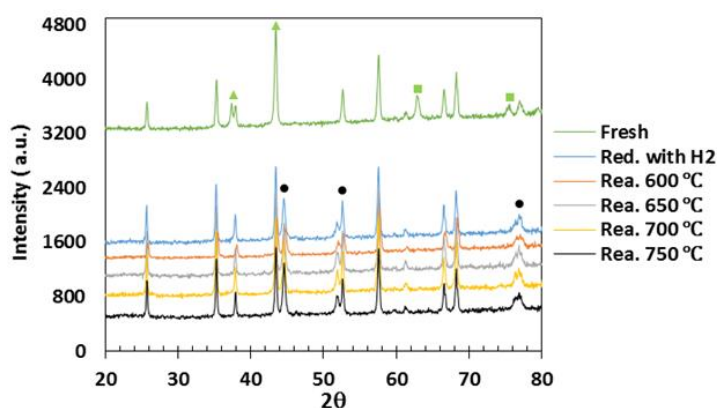


Figure 5.5 Maximum process output vs temperature at 1 bar, GHSV 0.498 and S:C 3 (a) Using 18 wt. % NiO on Al<sub>2</sub>O<sub>3</sub> support catalyst (b) Using 15 wt. % NiO on CaO/Al<sub>2</sub>O<sub>3</sub> support catalyst

This was expected because the presence of CaO in the catalyst will decrease its acidity (from Al<sub>2</sub>O<sub>3</sub> support) (Basagiannis and Verykios, 2006), consequently decreasing the chances of solid carbon deposition on the catalyst that tend to occur at higher temperatures. Thus, effectively increasing the feed conversion (fuel and H<sub>2</sub>O conversion), which in turn positively enhance the H<sub>2</sub> yield and purity. Previous studies by Basagiannis and Verykios (Basagiannis and Verykios, 2006) on steam reforming of acetic acid has proved that the acidity of alumina support favours solid carbon decomposition in a significant amount. Van Beurden (Van Beurden, 2004) also reported acidic support enhance cracking of CH<sub>4</sub>, therefore generating carbon. As a result, feed conversion and product yield are affected negatively to a large extent.

#### 5.2.4 Characterization of fresh and reacted catalyst

Parameters such as metal dispersion, crystallite size, etc. could greatly affect catalyst activity in steam reforming process (Cheng and Dupont, 2013). Thus NiO/Ni crystallite size and surface area of the fresh and reacted catalyst was studied using XRD (for 18 wt. % NiO on Al<sub>2</sub>O<sub>3</sub> support only) and BET (for 18 wt. % NiO on Al<sub>2</sub>O<sub>3</sub> support and 15 wt. % NiO on CaO/Al<sub>2</sub>O<sub>3</sub> support) analysis. CHNS and TOC analysis was used to found the quantity of carbon deposition on the surface of both used catalyst and their condensate respectively.



**Figure 5.6 XRD patterns of 18 wt. % NiO on Al<sub>2</sub>O<sub>3</sub> support catalyst; peaks with cycle on top represent Ni peaks, peaks with triangle on top represent superimposed NiO and Al<sub>2</sub>O<sub>3</sub> peaks, peaks with square on top represent NiO peaks while the unidentified peaks represents Al<sub>2</sub>O<sub>3</sub>**

Figure 5.6 depicts plot of XRD data. Peaks with black dot on top represents Ni peaks while the unidentified peaks are for Al<sub>2</sub>O<sub>3</sub> (ICDD reference code of Ni and Al<sub>2</sub>O<sub>3</sub> are 01-077-8341 and 04-006-9359 respectively at 750 °C, others given in appendix B2). No significant change/effect was seen in the peaks of both the H<sub>2</sub> reduced (only) and the reacted catalyst (used for experiments). As showed in Table 5.3, the Ni crystallite sizes of the reacted catalyst are in the range 30–35 nm.

The influence on Ni crystallite size after experiments is not evident. The textural property (BET surface area) of the fresh and reacted catalyst is also presented in Table 5.3. The surface area of the fresh and reacted Ni/Al<sub>2</sub>O<sub>3</sub> is in the range of 1-3 m<sup>2</sup>/g while that of Ni/CaO/Al<sub>2</sub>O<sub>3</sub> was in the range of 16-28 m<sup>2</sup>/g. From the values, it is obvious that the surface area of Ni/CaO/Al<sub>2</sub>O<sub>3</sub> catalyst is higher than that of Ni/Al<sub>2</sub>O<sub>3</sub> catalyst. This could be attributed to the presence of CaO in the catalyst; which has a high initial surface area (Beruto et al., 1984). For the case with Ni/Al<sub>2</sub>O<sub>3</sub> catalyst, no significant difference was found between the surface areas of both the H<sub>2</sub> reduced and reacted catalyst at varied temperatures. However, a slight reduction in the surface area of the reacted samples was observed when compared to fresh sample particularly when the reaction temperature is at 750 °C. Sintering and pore blockage at high temperatures could be the main reason behind this observation (Hafizi et al., 2016a). The results with the case of Ni/CaO/Al<sub>2</sub>O<sub>3</sub> catalyst shows a surprising trend. The BET surface area of the H<sub>2</sub> reduced and reacted catalyst slightly increased excluding at 750 °C. The decrease in the surface area at 750 °C might be caused by sintering and pore blockage at high temperatures explained earlier. The slight increase at the low/medium temperature range no doubt was caused by the presence of the CaO in the catalyst. Nonetheless, the increase is small and can be regarded as insignificant.

**Table 5.3 C-SR process characterisation results at 1 bar, GHSV 0.498, and S:C 3 (Table 5.1 inputs)**

Condition	NiO/Ni crystallite size (nm)	BET Surface area (m <sup>2</sup> /g)	C (wt. %) on catalyst	C (g/L) in condensate
Fresh NiO/Al <sub>2</sub> O <sub>3</sub>	45.05	3.456	N/A	N/A
Fresh NiO/CaO/Al <sub>2</sub> O <sub>3</sub>	N/A	21.306	N/A	N/A
Reduced with H <sub>2</sub> Ni/Al <sub>2</sub> O <sub>3</sub>	30.82	2.256	N/A	N/A
Reduced with H <sub>2</sub> Ni/CaO/Al <sub>2</sub> O <sub>3</sub>	N/A	36.751	N/A	N/A
600 °C with Ni/Al <sub>2</sub> O <sub>3</sub>	34.56	1.767	1.27	0.002
600 °C with Ni/CaO/Al <sub>2</sub> O <sub>3</sub>	N/A	25.245	1.14	0.026
650 °C with Ni/Al <sub>2</sub> O <sub>3</sub>	34.28	1.833	3.92	0.004
650 °C with Ni/CaO/Al <sub>2</sub> O <sub>3</sub>	N/A	28.320	1.10	0.032
700 °C with Ni/Al <sub>2</sub> O <sub>3</sub>	31.04	2.385	3.56	0.006
700 °C with Ni/CaO/Al <sub>2</sub> O <sub>3</sub>	N/A	24.657	1.63	0.039
750 °C with Ni/Al <sub>2</sub> O <sub>3</sub>	32.00	1.683	1.19	0.004
750 °C with Ni/CaO/Al <sub>2</sub> O <sub>3</sub>	N/A	16.175	0.40	0.040

Both fresh and used/reacted catalyst were again studied using FESEM. The images of fresh, H<sub>2</sub> reduced and reacted catalyst are clearly showed in Figure 5.7 and 5.8 for 18 wt. % NiO on Al<sub>2</sub>O<sub>3</sub> support and 15 wt. % NiO on CaO/Al<sub>2</sub>O<sub>3</sub> support respectively. Using EDX (mapping method;

images in appendix B3) it was found that carbon deposit were not uniformly distributed on the surface of the catalyst. Some parts of the catalyst surface had zero or were nearly free of carbon deposits. Carbon filaments growth were also observed in some of the reacted catalyst (such as Figure 5.7 (c) and Figure 5.8(d)). The low activity of both catalyst in the low/medium temperature might be the cause of the carbon filament growth covering surface of the catalyst (Izquierdo et al., 2012).

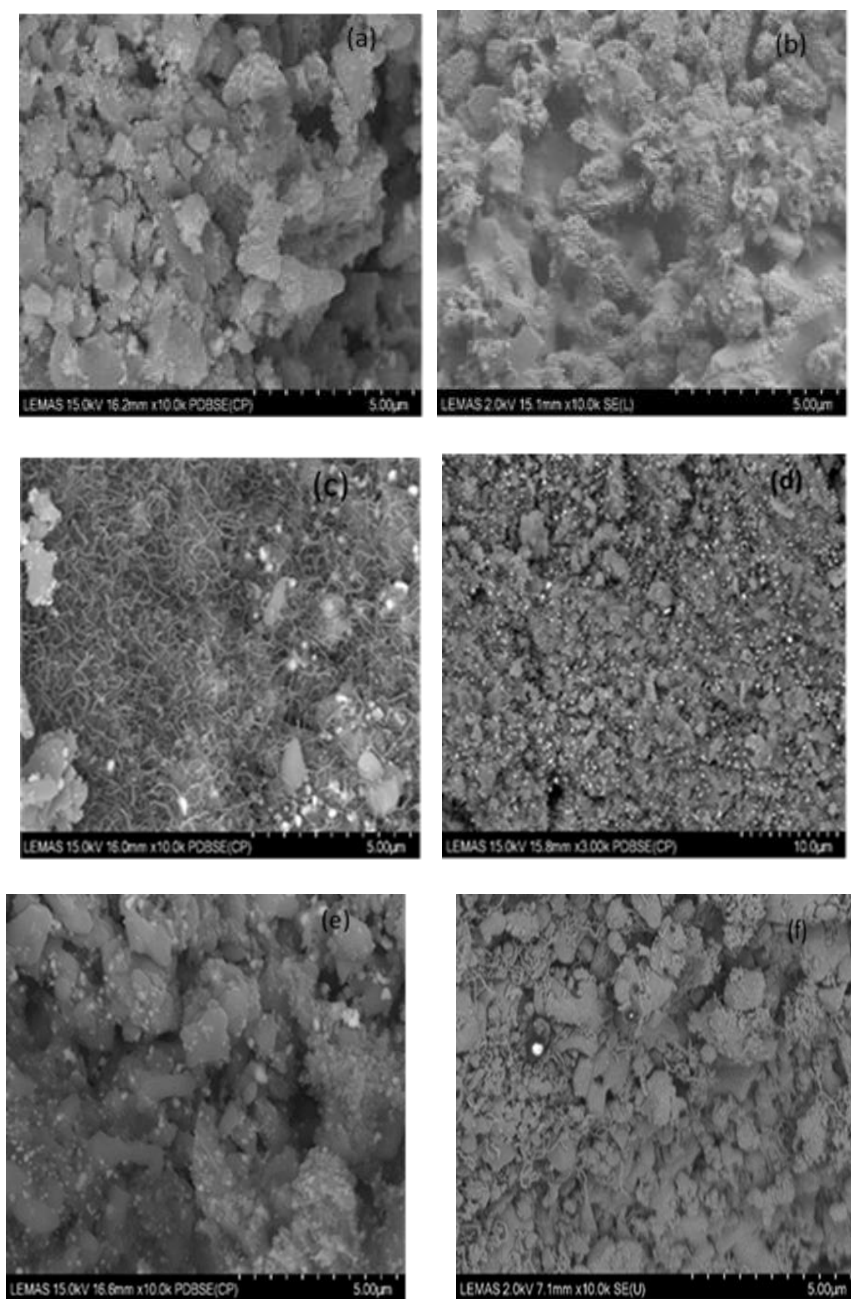


**Figure 5.7 FESEM images of 18 wt. % NiO on Al<sub>2</sub>O<sub>3</sub> support catalyst (a) Fresh catalyst (b) H<sub>2</sub> reduced catalyst at 700 °C (c) reacted at 600 °C (d) reacted at 650 °C (e) reacted at 700 °C (f) reacted at 750 °C**

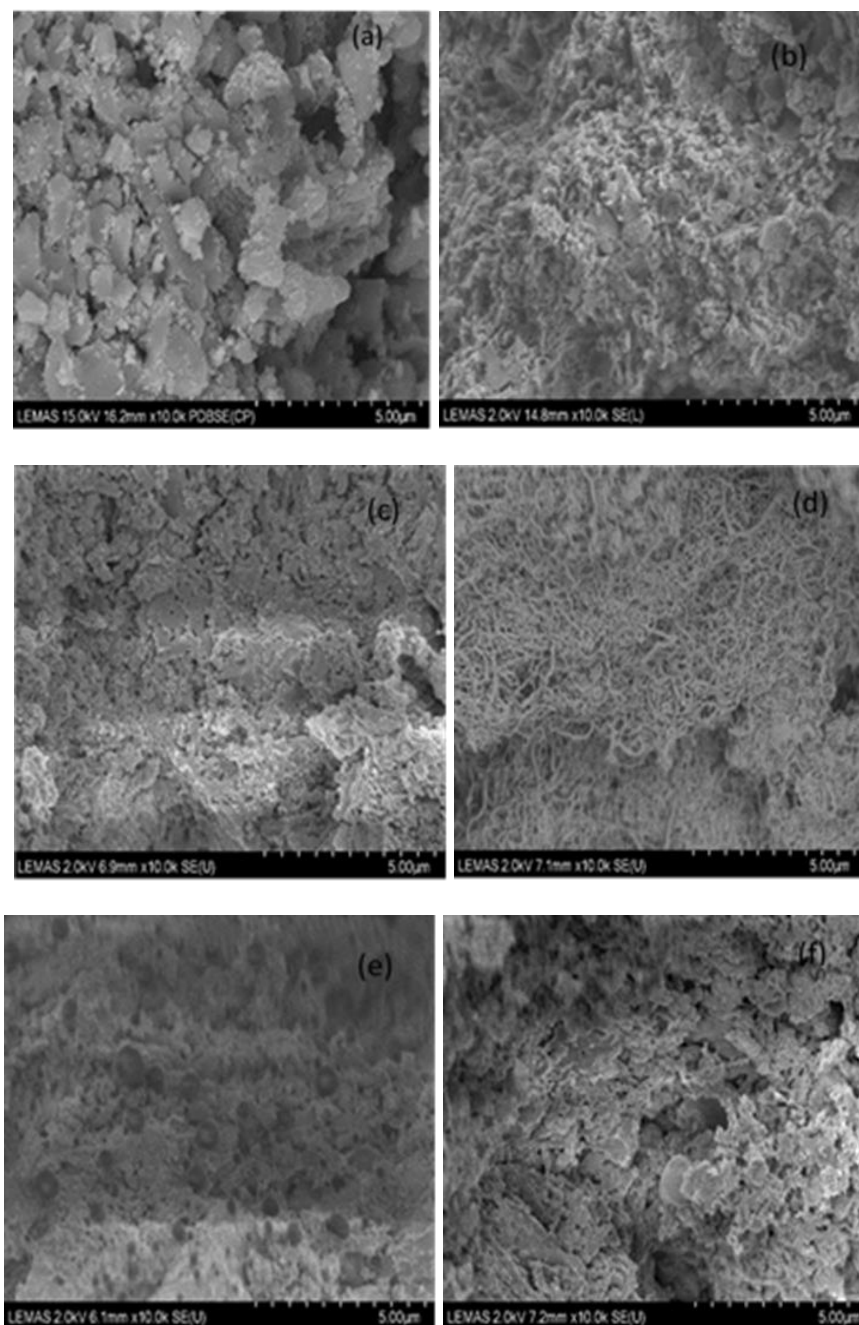


**Figure 5.8 FESEM images of 15 wt. % NiO on CaO/Al<sub>2</sub>O<sub>3</sub> catalyst (a) Fresh catalyst (b) H<sub>2</sub> reduced catalyst at 700 °C (c) reacted at 600 °C (d) reacted at 650 °C (e) reacted at 700 °C (f) reacted at 750 °C**

Solid carbon deposition on the surface of the catalyst varied according reaction temperature. Less carbon was observed in the Ni on CaO/Al<sub>2</sub>O<sub>3</sub> support catalyst compared to the Ni on Al<sub>2</sub>O<sub>3</sub> support. As explained earlier, this was not surprising because the presence of CaO in the catalyst will decrease the acidity of the catalyst, subsequently reducing the chances of solid carbon deposition on the catalyst (Basagiannis and Verykios, 2006). A significant decrease in the solid carbon deposition was also seen at 750 °C with Ni on CaO/Al<sub>2</sub>O<sub>3</sub> support catalyst. Again, this

was not surprising owing to the high fuel and water conversion and subsequently high H<sub>2</sub> yield and purity obtained in the condition. Moreover, solid carbon deposition on the surface of the catalyst represents carbon that does not react with steam to generate H<sub>2</sub>. A carbon balance was conducted and found to be off by 20 to 40 % approximately depending on the temperature, rendering the results unreliable. However, for 700 and 750 °C Ni on CaO/Al<sub>2</sub>O<sub>3</sub> support catalyst the carbon balance indicated that 23 % and 7 % solid carbon was deposited on the surface of the catalyst. The TOC analysis showed zero/no significant amount of carbon in the condensate sample. Table 5.3 present experimental condition and test results.

### **5.3 Sorption enhanced steam reforming (SE-SR) process of shale gas**

Prior to the SE-SR process experiments, calcium carbonate (CaCO<sub>3</sub>) was crushed to 1.2 mm grain size (same size as the catalyst to avoid altering the flow pattern of the reactor) and calcined at 915 °C for 6 hours to obtain pure CaO sorbent. 1 g of the CaO sorbent was randomly mixed with 2 g of 18 wt. % NiO on Al<sub>2</sub>O<sub>3</sub> support catalyst. The later was used as bed material for the SE-SR process.

#### **5.3.1 Effect of temperature on SE-SR process**

Temperature is one of the major variables on which the conversion of CaO and its carbonation capacity is determined. The effect of temperature on sorption enhanced steam reforming (SE-SR) process was investigated from 600 to 700°C at GHSV 0.498, 1 bar pressure and S:C 3 using CaO as CO<sub>2</sub> sorbent. Higher temperature were not investigated as they are reasonably insignificant in sorption enhanced (SE) process owing to the thermal decomposition of CaCO<sub>3(s)</sub> (strongly endothermic; thus favours at higher temperature) (Florin and Harris, 2007, Wei et al., 2004, Wang et al., 2011, S G Adiya et al., 2017). Moreover, the equilibrium vapour pressure of CO<sub>2</sub> over CaO<sub>(s)</sub> is low at low temperatures (Ryden and Ramos, 2012, Antzara et al., 2015, S G Adiya et al., 2017). Consequently, only the range of 600 to 700°C was investigated. Lower temperatures were not investigated because they suppressed catalyst activity.

Figure 5.9 presents the plots of average values of H<sub>2</sub> yield and purity over the temperature range. H<sub>2</sub> yield and purity decrease gradually as temperature increases. This was expected because SE process is favoured at low/medium temperature (Antzara et al., 2016a) for reasons explained earlier. The conversion of feedstocks (fuel and H<sub>2</sub>O conversion) were not reported during the carbonation period because they are not reliable. It is worth noting/remembers at this stage

that fuel and H<sub>2</sub>O conversion was based on carbon balance and inlet and outlet moles respectively (See Chapter 3). Direct calculations of the fuel (shale gas) conversion during CO<sub>2</sub> sorption through the carbon balance was not possible due to the inability to quantify the carbonation rate on the solid sorbent at any given time. Likewise, the outlet moles required for the calculation of H<sub>2</sub>O conversion were unreliable because the process is SE.

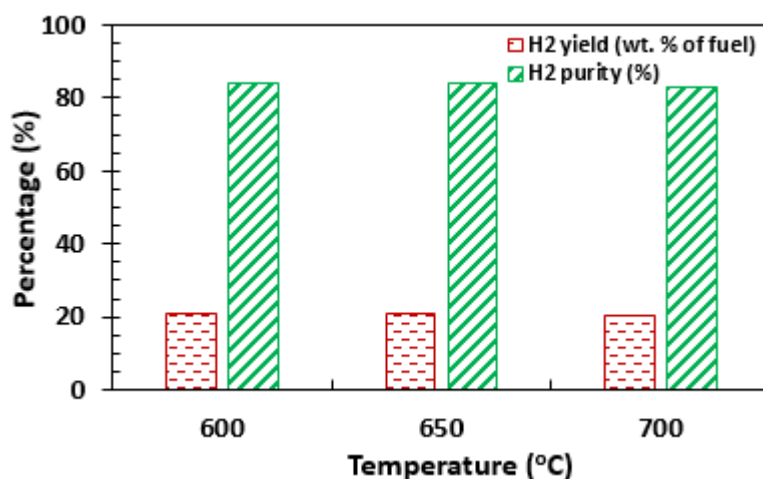


**Figure 5.9 H<sub>2</sub> yield and purity vs temperature in the pre breakthrough period at 1 bar, GHSV 0.498 and S:C 3 using 18 wt. % NiO on Al<sub>2</sub>O<sub>3</sub> support catalyst (average values)**

The effect of temperature (600-700 °C) on the outlet gas composition in the SE-SR during the pre-breakthrough period is depicted in Figure 5.10. In the pre-breakthrough period, the molar production rate of CO and CO<sub>2</sub> was completely zero (at all the investigated temperature) owing to the presence of the sorbent (carbonation reaction and enhancement of water gas shift). CH<sub>4</sub> yield increased with increase in operating temperature. The low CH<sub>4</sub> yield in the low/medium temperature range was due to the shift in equilibrium caused by the CO<sub>2</sub> capture favouring the H<sub>2</sub> generation reactions and subsequently higher fuel conversion. The increase in the CH<sub>4</sub> yield with increasing temperature is no doubt caused by limited carbonation reaction, thermal decomposition of CaCO<sub>3</sub> which occurs at higher temperatures (Florin and Harris, 2007, Wei et al., 2004, Wang et al., 2011).

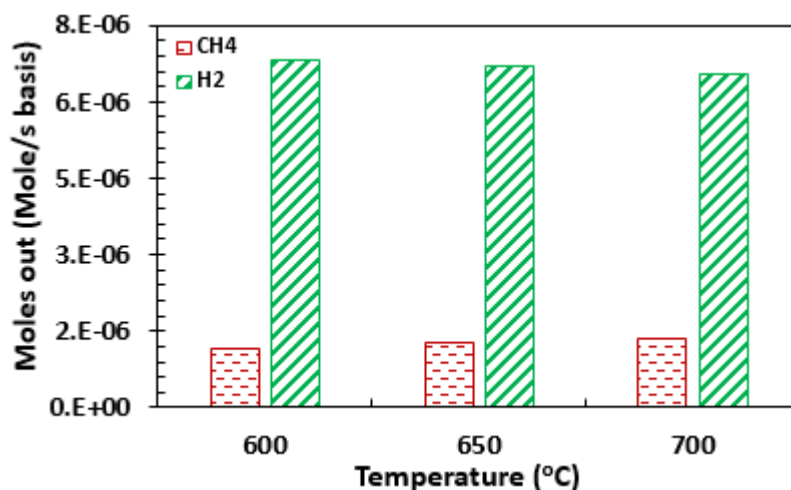


**Figure 5.10 Molar production rate of CH<sub>4</sub> and H<sub>2</sub> in the pre breakthrough period at 1 bar, GHSV 0.498 and S:C 3 using 18 wt. % NiO on Al<sub>2</sub>O<sub>3</sub> support catalyst (average values)**

In all the investigated temperatures, after the pre-breakthrough period, CO and CO<sub>2</sub> generation commence gently and stabilises at a certain point (roughly after about 3960 s of experiments) representing the emergence of the post breakthrough period as depicted in Figure 5.11(b and c). H<sub>2</sub> yield also decreases gently with move from the breakthrough period to the post breakthrough period as depicted in Figure 5.11 (a) almost degenerating the process back to the C-SR process. However, a comparison between the SE-SR and C-SR process will be made later.

The exothermic nature of the WGS reaction leads to a higher concentration of CO in both the breakthrough and post breakthrough period at higher temperatures. As for CO<sub>2</sub>, sorbent saturation inhibits its removal to a certain extent by the exothermic carbonation reaction, thus the gradual increase in the CO<sub>2</sub> content of the product gas as the process moves from the breakthrough period to the post breakthrough period. During the breakthrough period, the molar production rate of CO<sub>2</sub> is primarily determined by the WGS reaction. At this point, less CO<sub>2</sub> is generated with increasing temperature owing to the suppression of the WGS reaction.

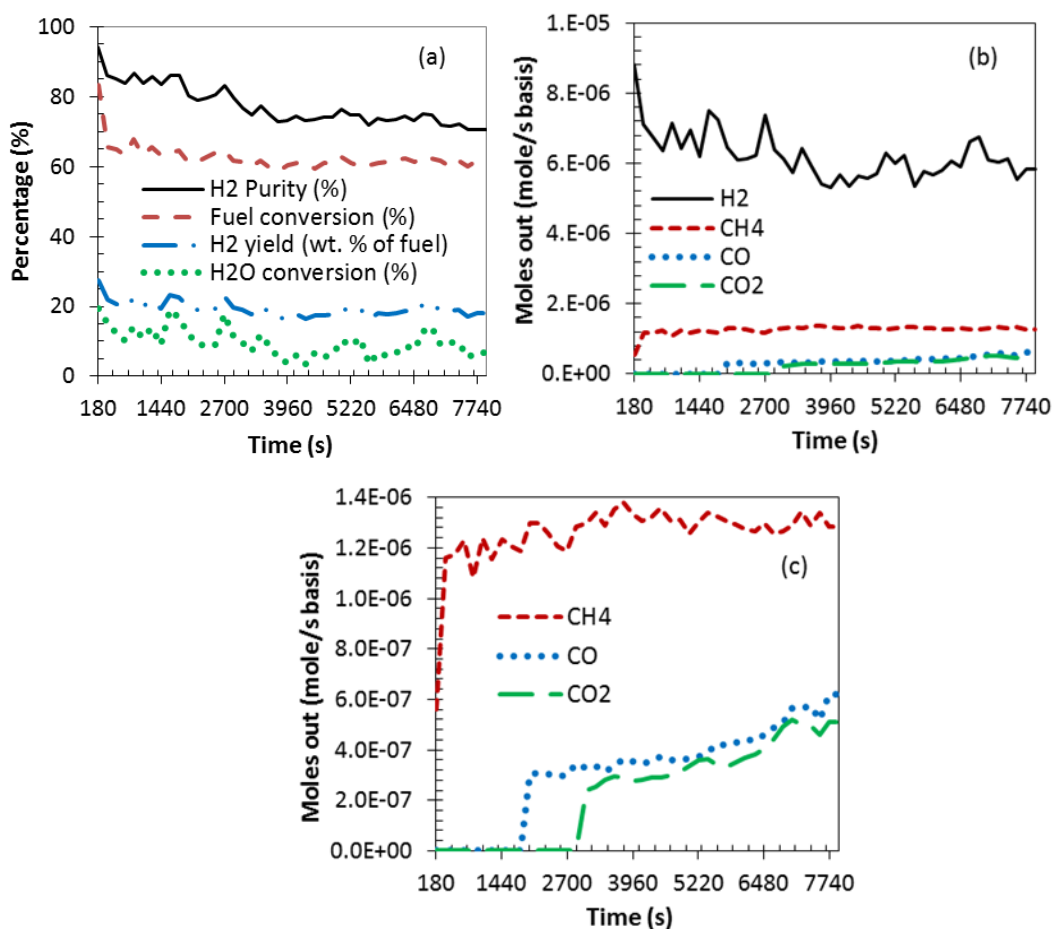


**Figure 5.11 Process output vs time at 600 °C , 1 bar, GHSV 0.498 and S:C 3 (a) H<sub>2</sub> yield and purity, fuel and H<sub>2</sub>O conversion vs time using 18 wt. % NiO on Al<sub>2</sub>O<sub>3</sub> support catalyst (b) moles out vs time using 18 wt. % NiO on Al<sub>2</sub>O<sub>3</sub> support catalyst (c) clearer graph of moles out vs time using 18 wt. % NiO on Al<sub>2</sub>O<sub>3</sub> support catalyst**

Numerous experimental research has been done on the SE-SR process with varied feedstocks and sorbent. For example, Ding et al (Ding and Alpay, 2000) examined the SE-SR process of CH<sub>4</sub> using hydrotalcite-based CO<sub>2</sub> adsorbent. Martavaltzi and Lemonidou (Martavaltzi and Lemonidou, 2010) also investigation the SE-SR process using CH<sub>4</sub> and a new hybrid material NiO–CaO–Ca<sub>12</sub>Al<sub>14</sub>O<sub>33</sub> performing the dual action of both steam reforming catalyst and CO<sub>2</sub> sorbent. A direct comparison of the present study with previous work is not possible owing to the difference in the feedstock and sorbent material use. Nonetheless, most of the previous studies on the SE-SR process such as Zin et al and Esteban-Díez et al. (Zin et al., 2012, Esteban-Díez et al., 2016) including those mention earlier Ding et al and Martavaltzi and Lemonidou (Ding and Alpay, 2000, Martavaltzi and Lemonidou, 2010) are in good agreement to those of the present studies with regards to substantial increased on H<sub>2</sub> yield and purity compared to the C-SR process.

### 5.3.2 Comparison of SE-SR with C-SR process and chemical equilibrium results

Figure 5.12 depicts a comparative analysis of the SE-SR and the C-SR process. As shown in the figures both H<sub>2</sub> yield and purity increase significantly in the presence of CaO sorbent compared to the Ca free system. Up to 45 % and 46 % rise in H<sub>2</sub> yield and purity was achieved when the average process output of SE-SR was compared with that of the C-SR process at 600 °C under same operational condition (GHSV 0.498, 1 bar pressure and S:C 3). This is significantly higher than the C-SR process.

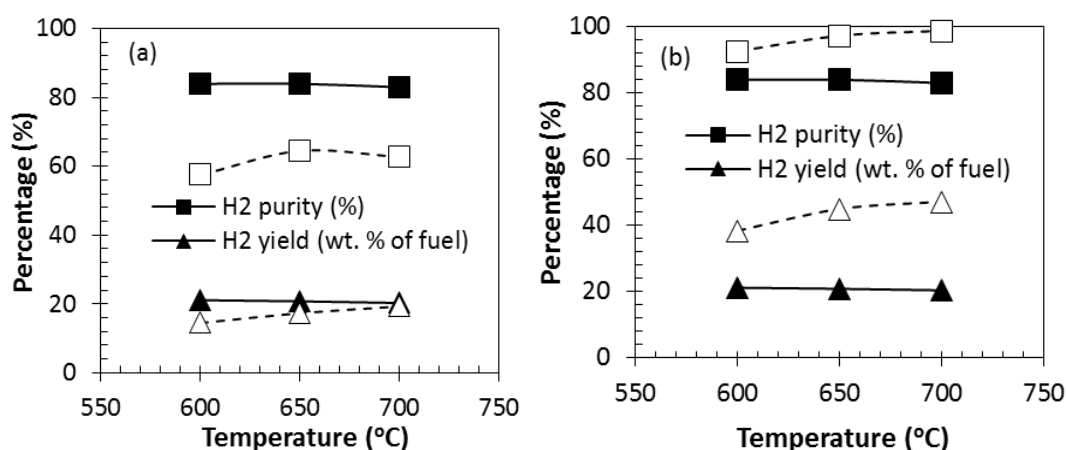


**Figure 5.12 Comparison of SE-SR during the pre-breakthrough period with C-SR and chemical equilibrium results at 1 bar, GHSV 0.498 and S:C 3 using 18 wt. % NiO on Al<sub>2</sub>O<sub>3</sub> support catalyst (a) comparison of SE-SR and C-SR process, H<sub>2</sub> yield and purity vs temperature (average values) (b) comparison of SE-SR and chemical equilibrium, H<sub>2</sub> yield and purity vs temperature (average values) (Note: Solid lines are for experimental results and dashed lines for C-SR process and chemical equilibrium results as applicable)**

The inability of the experimental results to reach the equilibrium results could be attributed to thermodynamic limitation as depicted in Figure 5.12 (b). Reaction kinetics could also be the limiting factor as explained earlier; the loss of sorbent capacity over time could also be one of the major reasons. The SE-SR process outputs (H<sub>2</sub> yield and purity and efficiency of CO<sub>2</sub> capture) is favored in the low/medium temperature range due to the thermal decomposition of the sorbent at higher temperatures in addition to the fact that the vapour pressure of CO<sub>2</sub> over CaO<sub>(s)</sub> is low at low temperature (Ryden and Ramos, 2012, Antzaraa et al., 2015, S G Adiya et al., 2017). The presence of sorbent in the system also lowered the temperature of maximum H<sub>2</sub> yield as depicted in Figure 5.12(a). To illustrate this, a comparison between the C-SR and SE-SR process optimum operating temperature can be used. The maximum H<sub>2</sub> yield and purity in the temperature range investigated (600-700 °C) was at 700 °C for the C-SR process, which

significantly drop to 600 °C for the SE-SR process. This equivalent to 14 % drop in operating temperature between the two processes (C-SR and SE-SR). The latter also significantly reduced the cost of operating the system and permits the use of low/medium reaction temperature due to the exothermic nature of the carbonation reaction and thus more materials-friendly temperature improving the economics of the process by the use of cheaper reactor materials afforded by the mild temperatures of the process unit.

Comparing the results of the SE-SR process during the post-breakthrough period with that of the conventional process leads to a surprising observation. It was expected that the SE-SR process will degenerate back to the C-SR process after the sorbent has become fully saturated (post breakthrough period). However, the opposite was observed. H<sub>2</sub> purity was higher in the SE-SR process even though the sorbent is believed to be fully saturated owing to a steady production of CO<sub>2</sub>. Previous studies by Albrecht et al and Xie et al (Albrecht et al., 2010, Xie et al., 2012) have reported a similar observation and attributed it to the fact that CO<sub>2</sub> is still absorbed by the sorbent during the post-breakthrough period but very slowly.

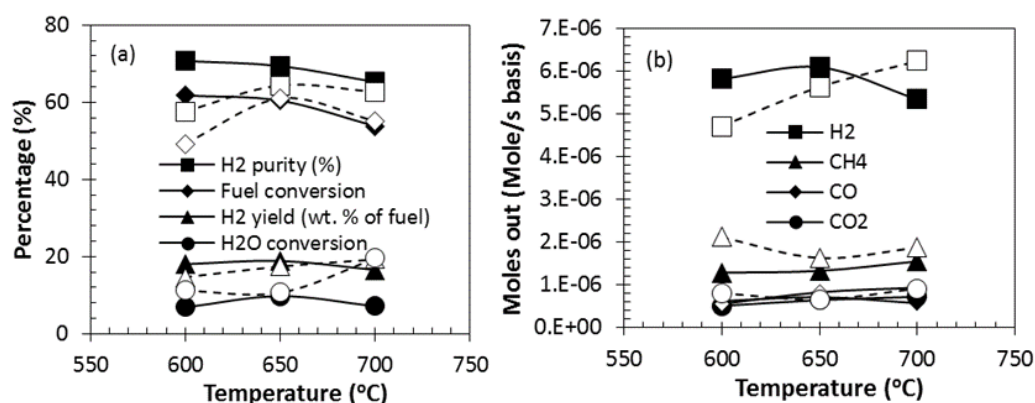


**Figure 5.13 Comparison of SE-SR process during the post breakthrough period with C-SR process at 1 bar, GHSV 0.498 and S:C 3 using 18 wt. % NiO on Al<sub>2</sub>O<sub>3</sub> support (a) average H<sub>2</sub> yield and purity, fuel and H<sub>2</sub>O conversion (b) average outlet moles vs temperature (Note: Solid lines are for experimental results and dashed lines for C-SR process)**

H<sub>2</sub> yield and fuel and water conversion were also higher at 600 °C in the SE-SR but merged (with insignificant difference) with the C-SR process at higher temperatures (650 and 700 °C) as depicted in Figure 5.13. The phenomenon observed at 600 °C results from the fact that the carbonation reaction is favoured at low/medium temperatures while that of high temperatures (650 and 700 °C) might result from the fact that the carbonation reaction is limited at higher

temperatures (S G Adiya et al., 2017) explained earlier. Table 5.4 presents percentage (%) enhancement of SE-SR process over the C-SR process (H<sub>2</sub> yield and purity)

**Table 5.4 Percentage (%) enhancement of SE-SR process over C-SR process (H<sub>2</sub> yield and purity)**

Condition	H <sub>2</sub> yield (%)	H <sub>2</sub> purity (%)
600 °C	45	46
650 °C	19	30
700 °C	5	32

### 5.3.3 Characterization of fresh and reacted catalyst 18 wt. % NiO on Al<sub>2</sub>O<sub>3</sub> support and sorbent during SE-SR process

Presently, CaO is the most well-known natural CO<sub>2</sub> sorbent that exist naturally in the forms of limestone (CaCO<sub>3</sub>) and dolomite (CaMg(CO<sub>3</sub>)<sub>2</sub>). Because of the sorbent low cost, high CO<sub>2</sub> sorption/desorption capacity after repeated cycles and sufficient reaction kinetics, the sorbent has attracted much attention. CO<sub>2</sub> capture capacity of CaO is as high as 0.786 g of CO<sub>2</sub>/g of sorbent theoretical (Shokrollahi Yancheshmeh et al., 2016). In this studies CaO sorbent originally from CaCO<sub>3</sub> was used.

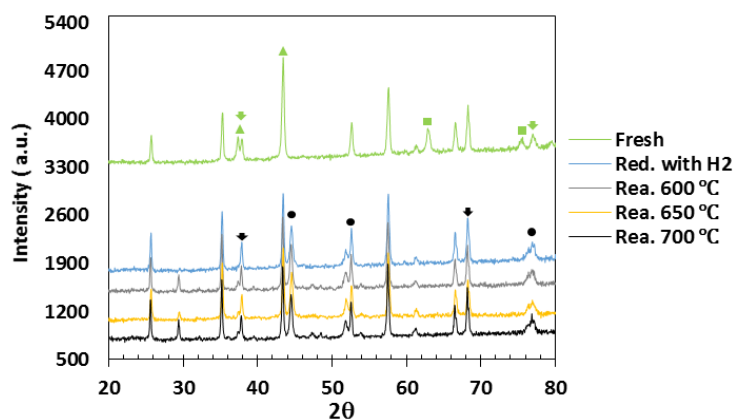


**Figure 5.14 XRD patterns of fresh, reduced and reacted catalyst (18 wt. % NiO on Al<sub>2</sub>O<sub>3</sub> support) and sorbent mixture; peaks with cycle on top represent Ni peaks, peaks with square on top represent NiO peaks, peaks with triangle on top represent superimposed NiO and Al<sub>2</sub>O<sub>3</sub> peaks, peaks with arrow on top represent superimposed CaO and Al<sub>2</sub>O<sub>3</sub> peaks, while the unidentified peaks represents Al<sub>2</sub>O<sub>3</sub>**

Analysis of XRD data of the fresh, H<sub>2</sub> reduced and reacted catalyst (18 wt. % NiO on Al<sub>2</sub>O<sub>3</sub> support) and sorbent mixture is showed in Figure 5.14. The Ni crystallite sizes of the reacted catalyst are in the range 29.69 – 30.82 nm with no significant difference to those of the C-SR process. Significant effect owing to the mixing of the catalyst and sorbent; with exposure to high temperature is not apparent. The effect of reacting temperature is also not apparent in the XRD

data. A very small peak of Al<sub>2</sub>O<sub>3</sub> around 30 2θ roughly appeared in the reacted catalyst but was absent in the fresh and H<sub>2</sub> reduced catalyst. This might be caused by crystallisation after long (1 hour 30 minutes roughly) exposure of the sorbent and catalyst mixture to reaction temperature (Peaks ICDD reference code given in appendix B2).

Table 5.5 showed the textural property (BET surface area). Here, carbon deposition on the surface of the 18 wt. % NiO on Al<sub>2</sub>O<sub>3</sub> support catalyst and sorbent mixture (conducted through CHNS analysis) and in the condensate (using TOC analysis) were analysed. An insignificant reduction in the surface area of the catalyst and sorbent mixture was seen. Sintering and pore blockage at high temperatures are the major reason that cause decrease on surface area (Hafizi et al., 2016a), as explained earlier. Overall, the effect of temperature on the surface area, carbon concentration on the surface of the catalyst and the condensate was not obvious. The absence of any major difference in the solid carbon concentration on the surface of the catalyst was not surprising because all the temperatures were investigated at S:C 3, which thermodynamically inhibits solid carbon deposition (Dupont et al., 2013, S G Adiya et al., 2017). A carbon balance indicated that the surface of the catalyst was covered with 0.02 moles carbon at 600 °C and 0.01 moles at 650 and 700 °C.

**Table 5.5 SE-SR process characterisation results at 1 bar, GHSV 0.498 and S:C 3 using Ni on Al<sub>2</sub>O<sub>3</sub> support catalyst (table 5.1 inputs)**

Condition	NiO/Ni crystallite size (nm)	BET Surface area (m <sup>2</sup> /g)	C (wt. %) on catalyst	C (g/L) in condensate
Pure CaO	48.23	7.121	N/A	N/A
Fresh catalyst	45.05	3.456	N/A	N/A
Reduced with H <sub>2</sub>	30.82	2.256	N/A	N/A
Fresh sorbent and catalyst mixture	N/A	5.131	N/A	N/A
Reduced sorbent and catalyst mixture	N/A	4.633	N/A	N/A
Reacted mixture at 600 °C	29.69	3.060	5.92	0.096
Reacted mixture at 650 °C	30.41	2.532	5.18	0.091
Reacted mixture at 700 °C	30.40	2.901	4.59	0.083

FESEM images are presented in Figure 5.15. With the help of EDX (mapping method) it was found that solid carbon deposition on the surface of the catalyst and sorbent mixture (mixed randomly) was not homogeneously distributed. The lack of homogeneity from carbon deposition could be

attributed to the level/position of the catalyst in the bed. It is expected that the topmost part of the catalyst will be more prone to solid carbon deposition than the depth.

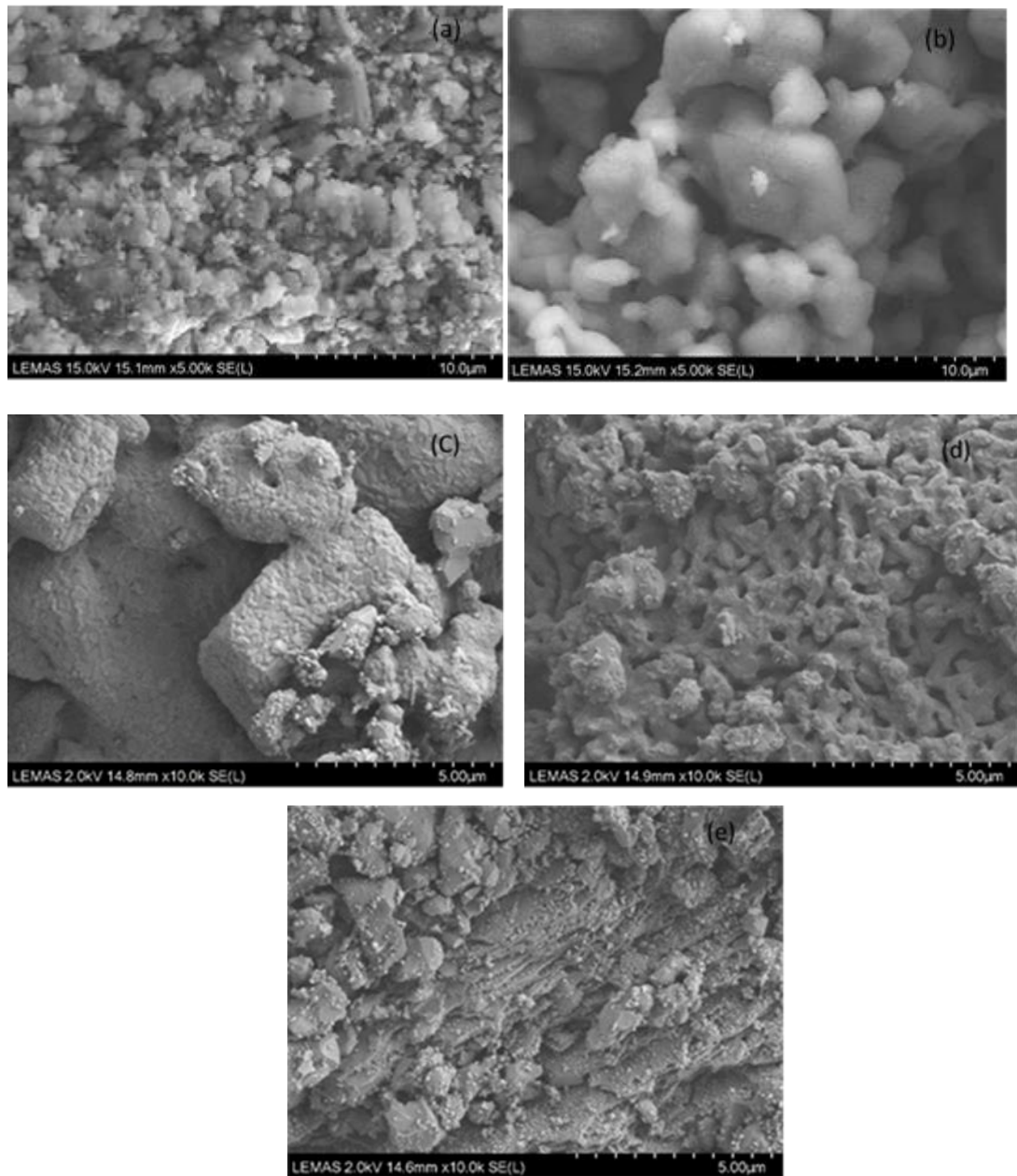


**Figure 5.15 FESEM images of Ni on Al<sub>2</sub>O<sub>3</sub> and CaO sorbent mixture (a) Fresh catalyst and sorbent mixture (b) H<sub>2</sub> reduced catalyst and sorbent mixture at 700 °C (c) reacted mixture at 600 °C (d) reacted mixture at 650 °C (e) reacted mixture at 700 °C**

## 5.4 Chemical looping steam reforming (CL-SR) process of shale gas

### 5.4.1 Effect of chemical looping on steam reforming process

Reduction-oxidation multicycles were conducted in a fixed bed reactor with NiO based oxygen transfer material (OTM) performing the dual action of both the OTM and reforming catalyst. 3 g of the OTM/catalyst was placed in a quartz reactor with diameter of 12 mm height. The fixed bed reactor was placed inside a vertical electrical furnace with temperature controlled using a K type thermocouple. The oxidation process using air marked the end of each cycle while the reduction/reforming process (feeding of steam and shale gas under constant flow of inert N<sub>2</sub>) marked the beginning of each cycle (remember the catalyst was reduced with H<sub>2</sub> in the first cycle). A details description of the CL-SR experimental procedure can be found in Chapter 3 of this thesis.

The CL-SR process experiments were conducted at 1 bar, S:C 3 and GHSV of 0.498 at 650 °C (with NiO on Al<sub>2</sub>O<sub>3</sub> support) and 750 °C (with NiO on CaO/Al<sub>2</sub>O<sub>3</sub> support). 20 redox-oxidation cycles were performed for each of the investigated temperature/OTM/catalyst. Simultaneous reforming and reduction of OTM/catalysts with the fuel was possible in all the studied OTM/catalyst at the reaction temperature, as further confirmed by good selectivity towards the desired products (H<sub>2</sub> and CO<sub>2</sub>). This shows that the use of shale gas or gas with higher composition of C<sub>2</sub> and C<sub>3</sub> species as a feedstock for the CL-SR process is feasible.

At both temperatures (650 °C with NiO on Al<sub>2</sub>O<sub>3</sub> support and 750 °C with NiO on CaO/Al<sub>2</sub>O<sub>3</sub> support) the molar production rate of H<sub>2</sub> was higher than that of the other gaseous products CO, CO<sub>2</sub>, and CH<sub>4</sub> as depicted in Figure 5.16. The molar production rates of CO and CO<sub>2</sub> were fairly stable in both cases and dependent on the water conversion rate. This is because steam is a reactant in the WGS reaction that produces CO<sub>2</sub>. The molar production of CH<sub>4</sub> was higher than those of CO and CO<sub>2</sub> for the case of NiO on Al<sub>2</sub>O<sub>3</sub> support at 650 °C. This could be attributed to the poor fuel conversion below 80 % approximately for all 20 cycles. For the case of NiO on CaO/Al<sub>2</sub>O<sub>3</sub> support at 750 °C, the molar production rate of CH<sub>4</sub> was lower than those of CO and CO<sub>2</sub> in the first 8 cycles. However, the production rate increase gradually from the 9<sup>th</sup> cycle, stabilizing and merging with the production rate of CO at approximately the 11<sup>th</sup> to the last cycle (20<sup>th</sup>). This observation could result from the fact that the activity of the OTM/catalyst was decreasing with increasing number of cycles. As further confirmed by the decrease in fuel

conversion in the cycles. Solid carbon deposition on the surface of the OTM/catalyst might also be the reason of the low activity and subsequently low fuel conversion (Wang et al., 2016).

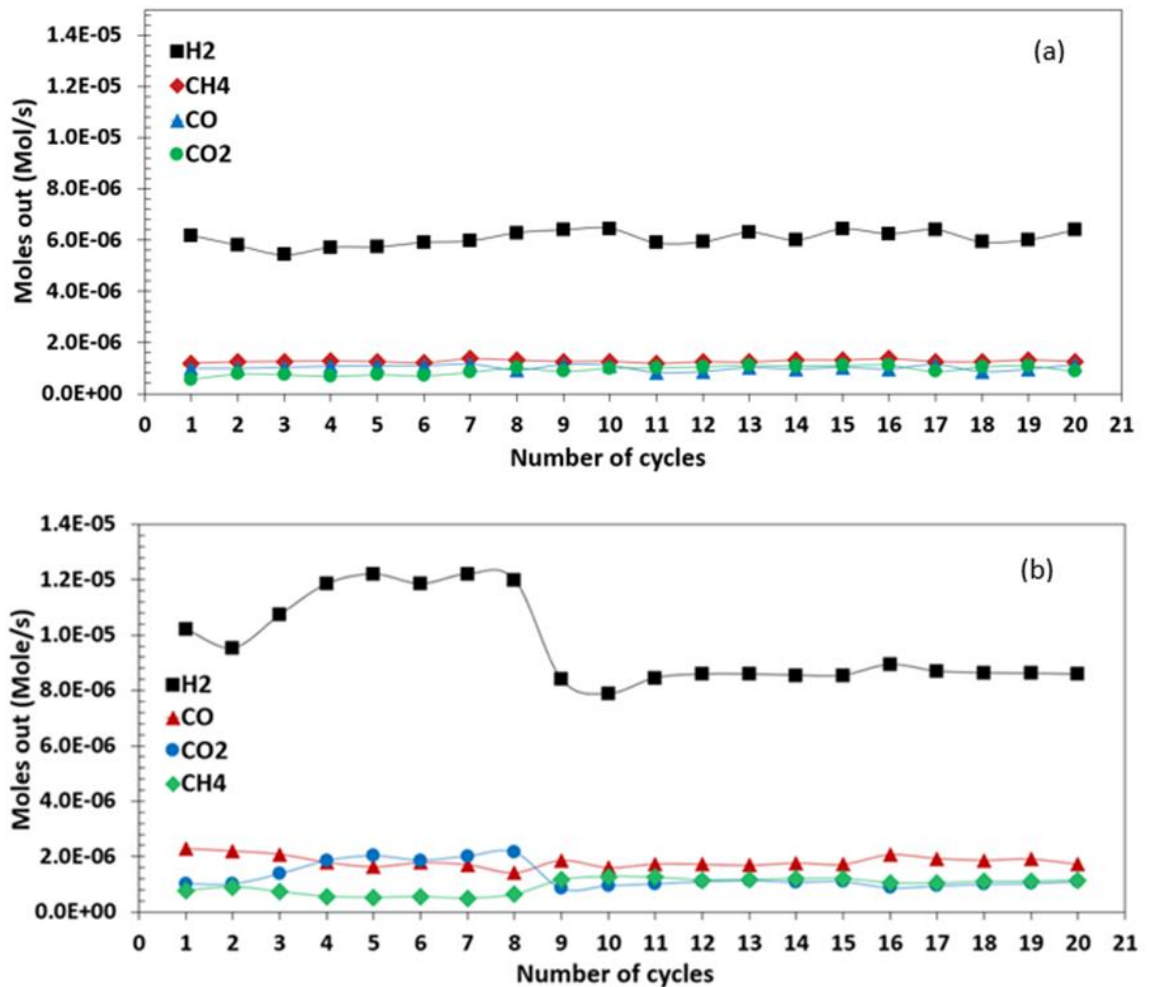


Figure 5.16 Moles out at 1 bar, GHSV 0.498 and S:C 3 (average values). (a) Reforming/reduction reaction at 650 °C and oxidation reaction at 750 °C with 18 wt. % NiO on Al<sub>2</sub>O<sub>3</sub> support as OTM/catalyst, (b) Reforming/reduction reaction at 750 °C and oxidation reaction at 750 °C with 15 wt. % NiO on CaO/Al<sub>2</sub>O<sub>3</sub> support as OTM/catalyst

Fuel and water conversion, H<sub>2</sub> yield and purity increased in the CL-SR process as shown in Figure 5.17 (prior to the OTM/catalyst deactivation for the case with 15 wt. % NiO on CaO/Al<sub>2</sub>O<sub>3</sub>) compared to the C-SR process; even though part of the fuel was used for reduction process (co products CO and H<sub>2</sub> or CO<sub>2</sub> and H<sub>2</sub>O). The phenomenon could be attributed to the fact that water is a product of the reduction reaction which in turn is a reactant in the reforming and WGS reaction. Thus, favouring the two H<sub>2</sub> producing reaction (SR and WGS reaction). Table 5.6 and 5.7 present the percentage enhancement of CL-SR process with C-SR process at 650 °C using 18 wt. % NiO on Al<sub>2</sub>O<sub>3</sub> support as OTM/catalyst and at 750 °C using 15 wt. % NiO on CaO/Al<sub>2</sub>O<sub>3</sub>

support as OTM/catalyst respectively. In the system with 18 wt. % NiO on Al<sub>2</sub>O<sub>3</sub> support as OTM/catalyst H<sub>2</sub> yield was lower than the C-SR process in the 3<sup>rd</sup> cycle with approximately 4 % and H<sub>2</sub> purity was slightly lower than 1 % in 3<sup>rd</sup>, 7<sup>th</sup>, 14<sup>th</sup> and 19<sup>th</sup> cycle. However, water conversion was higher in the C-SR process than the CL-SR process in almost all the 20 cycles. This phenomenon could be attributed to variation in reaction kinetics (over time) and thermodynamic equilibrium in the cycles, carbon deposition on the surface of the catalyst and Ni active sites blockage could also play a vital role. It is worth noting that fuel conversion was higher in the CL-SR process than the C-SR process in all the 20 cycles conducted, even though process outputs were slightly lower in a few cycles. This could be a sign that steam reforming and reduction reactions were taking place simultaneously. The process outputs (yield, purity and conversion) were moderately stable with a negligible variation depending on the fuel and water conversion (high or low) as presented in Figure 5.17.

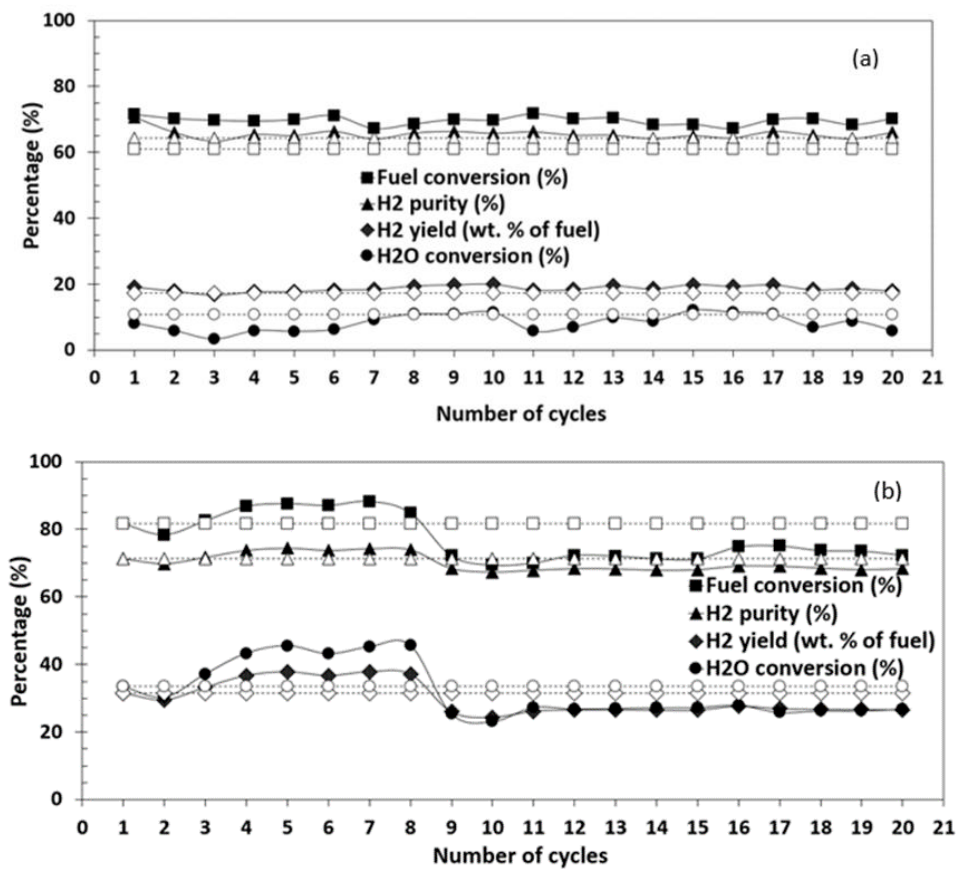


Figure 5.17 Comparison of CL-SR and C-SR process H<sub>2</sub> yield and purity, fuel and water conversion at 1 bar, GHSV 0.498, S:C 3 (average values) (a) Reforming/reduction reaction at 650 °C and oxidation reaction at 750 °C with 18 wt. % NiO on Al<sub>2</sub>O<sub>3</sub> support as OTM/catalyst, (b) Reforming/reduction reaction at 750 °C and oxidation reaction at 750 °C with 15 wt. % NiO on CaO/Al<sub>2</sub>O<sub>3</sub> support as OTM/catalyst (Note: Solid lines are for experimental results and dashed lines for C-SR process)

For the case with NiO on CaO/Al<sub>2</sub>O<sub>3</sub> support as OTM/catalyst at 750 °C, feedstock and water conversion, H<sub>2</sub> yield and purity increased gradually with increase in number of cycles to the 9<sup>th</sup> cycle, where a gentle dwindling with the cycles was seen that became steady at approximately the 11<sup>th</sup> cycle to the end. Surprisingly, the decrease in the process outputs was lower than the C-SR process. The decrease in process outputs might have resulted from the activity of the OTM/catalyst decreasing with time, partial oxidation of Ni to NiO (during the oxidation stage), solid carbon formation on the surface of the OTM/catalyst and Ni active site blockage mentioned earlier. The gradual increase in H<sub>2</sub> yield and purity and fuel and water conversion after the 2<sup>nd</sup> cycle might not only be attributed to the initial good performance of the OTM/catalyst but also to the fact that Ni activity increases after first contact with fuel (Ryden and Ramos, 2012). The first cycle process outputs were exactly the same as the C-SR process further validating the reproduction of the condition.

**Table 5.6 Percentage (%) enhancement of CL-SR process with C-SR process reforming/reduction reaction at 650 °C and oxidation reaction at 750 °C using 18 wt. % NiO on Al<sub>2</sub>O<sub>3</sub> support as OTM/catalyst (H<sub>2</sub> yield and purity, fuel and water conversion).**

Cycle number	H <sub>2</sub> yield (%)	H <sub>2</sub> purity (%)	Fuel conversion (%)	H <sub>2</sub> O conversion (%)
1 <sup>st</sup> cycle	9.81	9.85	17.11	-23.70
2 <sup>nd</sup> cycle	2.92	2.70	15.05	-44.69
3 <sup>rd</sup> cycle	<u>-3.63</u>	<u>-1.49</u>	14.21	-68.86
4 <sup>th</sup> cycle	1.53	1.68	13.72	-45.50
5 <sup>th</sup> cycle	1.83	1.18	14.45	-46.97
6 <sup>th</sup> cycle	4.89	3.22	16.57	-42.21
7 <sup>th</sup> cycle	5.92	<u>-0.36</u>	10.08	-13.36
8 <sup>th</sup> cycle	11.56	2.42	12.29	1.85
9 <sup>th</sup> cycle	13.56	3.18	14.52	1.99
10 <sup>th</sup> cycle	14.51	2.30	14.22	6.82
11 <sup>th</sup> cycle	4.67	2.99	17.45	-46.47
12 <sup>th</sup> cycle	5.25	1.41	15.03	-34.90
13 <sup>th</sup> cycle	11.79	1.38	15.39	-8.92
14 <sup>th</sup> cycle	6.66	<u>-0.26</u>	11.99	-17.47
15 <sup>th</sup> cycle	14.14	1.15	12.14	13.19
16 <sup>th</sup> cycle	10.86	0.10	10.04	7.39
17 <sup>th</sup> cycle	13.56	3.18	14.52	1.99
18 <sup>th</sup> cycle	5.25	1.41	15.03	-34.90
19 <sup>th</sup> cycle	6.66	<u>-0.26</u>	11.99	-17.47
20 <sup>th</sup> cycle	2.92	2.70	15.05	-44.69

**Table 5.7 Percentage (%) enhancement of CL-SR process with C-SR process reforming/reduction reaction at 750 °C and oxidation reaction at 750 °C using 15 wt. % NiO on CaO/Al<sub>2</sub>O<sub>3</sub> support as OTM/catalyst (H<sub>2</sub> yield and purity, fuel and water conversion).**

Cycle number	H <sub>2</sub> yield (%)	H <sub>2</sub> purity (%)	Fuel conversion (%)	H <sub>2</sub> O conversion (%)
1 <sup>st</sup> cycle	0.00	0.00	0.00	0.00
2 <sup>nd</sup> cycle	<u>-6.51</u>	<u>-2.15</u>	<u>-4.02</u>	<u>-9.30</u>
3 <sup>rd</sup> cycle	5.21	0.55	1.02	11.01
4 <sup>th</sup> cycle	16.19	3.47	6.24	29.23
5 <sup>th</sup> cycle	19.66	4.44	7.27	36.00
6 <sup>th</sup> cycle	16.25	3.54	6.56	28.85
7 <sup>th</sup> cycle	19.73	4.19	8.07	34.86
8 <sup>th</sup> cycle	17.60	3.81	3.93	36.40

Oxidation of the OTM/catalyst at 750 °C to return it back to its original form (NiO) as well as to burn off any carbon deposits on the surface of the OTM/catalyst with air was successful (in the system with 18 wt. % NiO on Al<sub>2</sub>O<sub>3</sub> support as OTM/catalyst to be precise), as confirmed by the carbon balance/analysis conducted on the OTM/catalyst samples after experiments. However, this would be discussed in detail in the characterisation section later. An increase in the oxidation temperature (10-15°C roughly) was observed during the oxidation process as expected owing to the exothermicity of the reaction. The burning off of the solid carbon (coke) deposition during the air feed was coincidental with CO<sub>2</sub> and CO generation. The reactor temperature also increased owing to the oxidation of the deposited carbon simultaneously. Full details and discussion of the reduction and oxidation reaction process are not available owing to the fact that the micro gas chromatography take readings every 3 minutes, thus the most significant part of these rapid processes are missed making the results unreliable.

The experimental results were found to be away from the chemical equilibrium results as depicted in Figure 5.18. Catalyst selectivity (Xiu et al., 2003), reaction kinetics and mass transfer limitation might also contribute to the observed phenomenon.

It is difficult to compare the results of the present studies with previous research work because most of the studies in CL-SR used low steam to carbon ratios (Rydén et al., 2006, de Diego et al., 2009, Gayán et al., 2008, Dupont et al., 2007) or focused on pure methane as a feedstock

(Antzara et al., 2016b). Antzara et al (Antzara et al., 2016b) investigated the performance of NiO based OTM/catalyst supported on ZrO<sub>2</sub>, TiO<sub>2</sub>, SiO<sub>2</sub>, Al<sub>2</sub>O<sub>3</sub> and NiAl<sub>2</sub>O<sub>4</sub> for CL-SR of CH<sub>4</sub>. Conditions for twenty redox cycles in a fixed bed flow unit at 650 °C, S:C 3, GHSV 100,000. They found that NiO/Al<sub>2</sub>O<sub>3</sub> support demonstrated a high initial activity, but also high deactivation, leading to methane conversion of 59 % at the end of the test. The high initial activity of OTM/catalyst (NiO/Al<sub>2</sub>O<sub>3</sub> support) and high deactivation towards the end of the test is in good agreement to those reported in the present study.

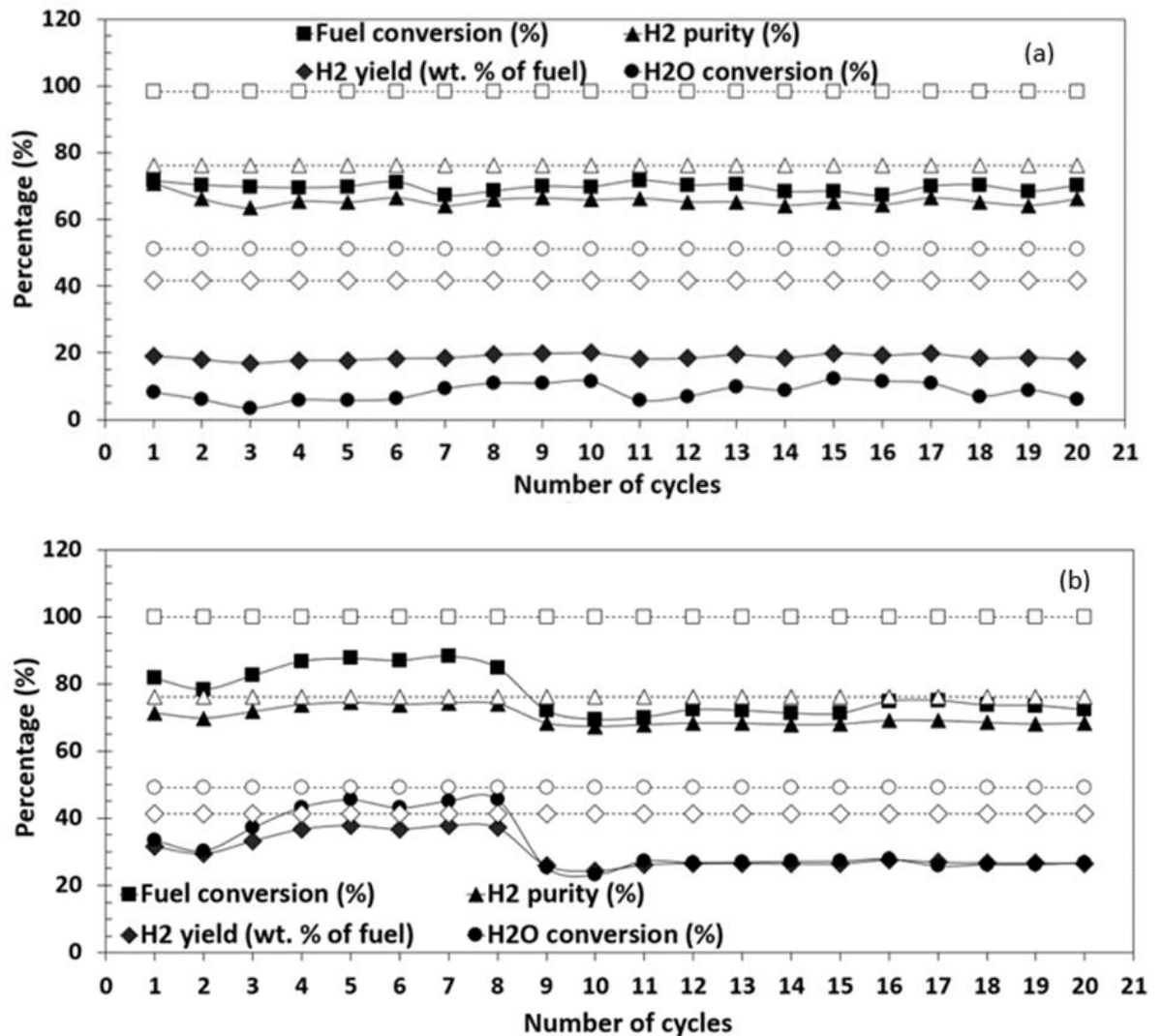


Figure 5.18 Comparison of CL-SR and chemical equilibrium results H<sub>2</sub> yield and purity, fuel and water conversion at 1 bar, GHSV 0.498, S:C 3 (average values) (a) Reforming/reduction reaction at 650 °C and oxidation reaction at 750 °C with 18 wt. % NiO on Al<sub>2</sub>O<sub>3</sub> support, (b) Reforming/reduction reaction at 750 °C and oxidation reaction at 750 °C with 15 wt. % NiO on CaO/Al<sub>2</sub>O<sub>3</sub> support (Note: Solid lines are for experimental results and dashed lines for chemical equilibrium results)

#### 5.4.2 Cyclic stability of output during CL-SR process

To investigate the OTM stability/lifetime, 20 redox cycles were conducted at 650 °C and 750 °C using NiO on Al<sub>2</sub>O<sub>3</sub> support and NiO on CaO/Al<sub>2</sub>O<sub>3</sub> support as OTM/catalyst, respectively. Figure 5.17 (upper graph) depicts the process outputs of 20 redox cycles at 650 °C with NiO on Al<sub>2</sub>O<sub>3</sub> support. Interestingly, the average process outputs for the system with NiO on Al<sub>2</sub>O<sub>3</sub> support at 650 °C were quite stable with almost negligible difference between the 20 redox-oxidation cycles. On the other hand, the case was different at 750 °C using NiO on CaO/Al<sub>2</sub>O<sub>3</sub> as OTM/catalyst. Even though the sudden decrease in the activity of the OTM/catalyst could be attributed to the high temperature used in favor of solid carbon deposition, the sudden drop of the OTM/catalyst at the 9 (ninth) cycle is seen as too early. This is because the air feed step (oxidation of the Ni to NiO) is accompanied by burning off of the solid carbon deposit on the surface of the OTM/catalyst. Nonetheless, the observed phenomenon could be attributed to partial re-oxidation of the metallic Ni phase to NiO, significant coke deposition accumulated over the range of the cycles (Rostrup-Nielsen and Trimm, 1977, Rostrup-Nielsen, 1973) or even extensive sintering of the Ni particles on the surface of the OTM/catalyst (Bartholomew, 2001, Antzara et al., 2016b). To evaluate the mentioned possibilities, characterization of the OTM/catalyst before and after the 20 redox-oxidation cycles was performed and discussed in the next section. Comparison between the activity and stability of the two OTM/catalysts investigated is not feasible as their experiments were conducted at different temperatures.

Figure 5.19 (a and b) shows the plots of process outputs with time on stream of the 7<sup>th</sup> cycle at 650 °C with 18 wt. % NiO on Al<sub>2</sub>O<sub>3</sub> support OTM/catalyst. The fuel conversion and H<sub>2</sub> purity decreased gradually and stabilised at around 810 s. Water conversion increased gradually and stabilised before 810 s. This observation could be attributed to the reduction process (occurring in the first 3 to 6 minutes of start-up), generating water as a product, thus increasing the steam concentration in the system enhancing the fuel conversion and H<sub>2</sub> purity. Although, the concurrent CO or CO<sub>2</sub> generation via the NiO reduction reaction could have counteracting effects on the system, the observed phenomenon indicates that the water product had a dominant effect on steam reforming compared to that of the adverse CO or CO<sub>2</sub> release in the system. The increase of Ni activity after first contact with fuel could also be the reason for the observed phenomenon (Ryden and Ramos, 2012). H<sub>2</sub> yield and molar production rate of H<sub>2</sub>, CH<sub>4</sub> and CO over time were also quite stable with a negligible difference over time. Figure 5.19 (c and d) depicts the process outputs against time of the 7<sup>th</sup> cycle at 750 °C using 15 wt. % NiO on

CaO/Al<sub>2</sub>O<sub>3</sub> support OTM/catalyst. Fuel and H<sub>2</sub>O conversion and H<sub>2</sub> yield and purity were stable over the duration of the experiments. Molar production rate of H<sub>2</sub>, CH<sub>4</sub> and CO were also stable with insignificant differences over time. The slight increase in the molar H<sub>2</sub> yield at 1944 s, 2070 s and 2574 s roughly resulting in a peak like section in Figure 5.19 (d) is no doubt attributed to the slight increase in fuel and water conversion at exactly the same time as further confirmed by same sections in Figure 5.19(a). The sudden appearance of the sections could be attributed to experimental uncertainty.

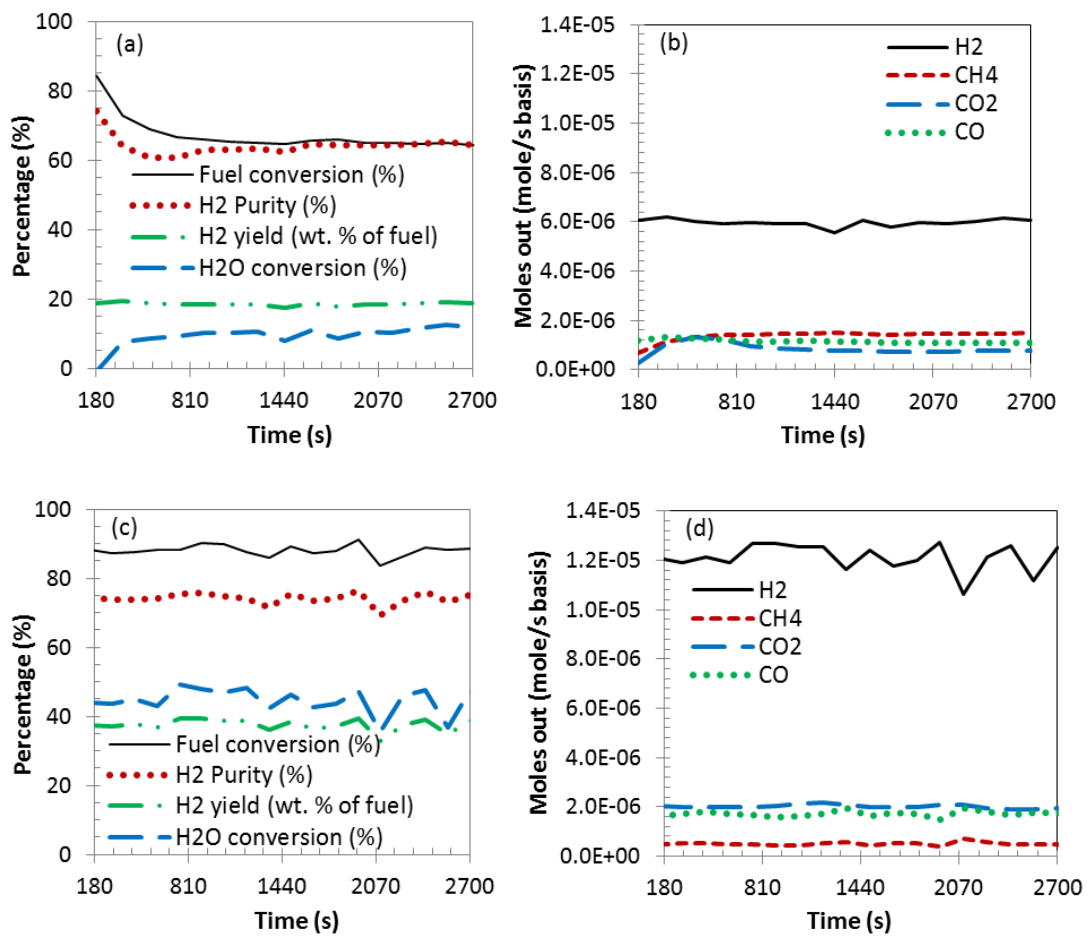


**Figure 5.19** 7<sup>th</sup> cycle process output vs time 1 bar, GHSV 0.498 and S:C 3 (a) H<sub>2</sub> yield and purity, fuel and H<sub>2</sub>O conversion vs time using 18 wt. % NiO on Al<sub>2</sub>O<sub>3</sub> support as OTM/catalyst reforming/reduction reaction at 650 °C and oxidation reaction at 750 °C (b) moles out vs time using 18 wt. % NiO on Al<sub>2</sub>O<sub>3</sub> support as OTM/catalyst reforming/reduction reaction at 650 °C and oxidation reaction at 750 °C (c) H<sub>2</sub> yield and purity, fuel and H<sub>2</sub>O conversion vs time using 15 wt. % NiO on CaO/Al<sub>2</sub>O<sub>3</sub> support as OTM/catalyst reforming/reduction reaction at 750 °C and oxidation reaction at 750 °C (d) moles out vs time using 15 wt. % NiO on CaO/Al<sub>2</sub>O<sub>3</sub> support as OTM/catalyst reforming/reduction reaction at 750 °C and oxidation reaction at 750 °C

### 5.4.3 Catalyst/Oxygen transfer material (OTM) characterization

To compare the fresh and reacted 18 wt. % NiO on Al<sub>2</sub>O<sub>3</sub> support OTM/catalyst, an X-ray diffractometer was used. The samples were analyzed using the step-scan method over the angular 2θ range of 10-90°. Figure 5.20 depicts the XRD data of the fresh and reacted OTM/catalyst. There was no chemical change(s) in the reacted catalyst/OTM compared to the fresh one. NiO and Al<sub>2</sub>O<sub>3</sub> were the main crystalline phases in the reacted material and were found to be exactly the same with the fresh sample as shown in Figure 5.20.

Thus, it can be concluded that the NiO-Al<sub>2</sub>O<sub>3</sub> OTM catalyst was fully oxidized from Ni to NiO during the oxidation reaction process. The most intense peak of NiO is around 2θ = 64° approximately while that of Al<sub>2</sub>O<sub>3</sub> is roughly around 44°. The spectral/peaks of both the fresh and reacted OTM/catalyst were completely unchangeable after 20 redox-oxidation cycles. ICDD reference code of NiO and Al<sub>2</sub>O<sub>3</sub> are 01-078-4374 and 04-015-8609 respectively. XRD analysis was performed on NiO/CaO/Al<sub>2</sub>O<sub>3</sub> but spectra obtained were not crystalline enough to provide output analysis likely due to large amorphous content.

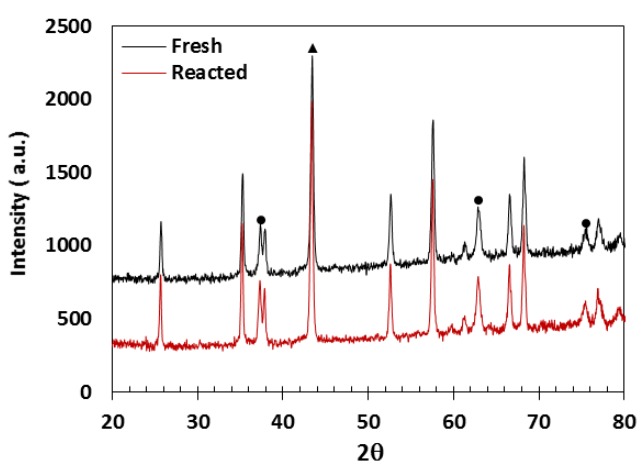


**Figure 5.20** 18 wt. % NiO on Al<sub>2</sub>O<sub>3</sub> support XRD patterns; peaks with circle on top represent NiO peaks, peak with triangle on top represent a superimposed NiO and Al<sub>2</sub>O<sub>3</sub> peak while the unidentified peaks represents Al<sub>2</sub>O<sub>3</sub> peaks. Reforming/reduction reaction at 650 °C and oxidation reaction at 750 °C

To check on significant chemical changes and reactivity deterioration of the catalysts/OTM, BET surface area of both the fresh and reacted sample was checked using Quantachrome Nova 2200. A significant change was seen in the BET surface area of the NiO/Al<sub>2</sub>O<sub>3</sub> OTM/ catalyst. The BET surface area of reacted OTM/catalyst, decreased to approximately half of that of the fresh OTM/catalyst (see Table 5.8). The notable decreased in the BET surface area might be caused

by agglomeration of the OTM/catalyst after sintering in reasonably long period of the 20 redox-oxidation cycles (Shen et al., 2009). Conversely, for the case with NiO/CaO/Al<sub>2</sub>O<sub>3</sub> catalyst/OTM, a slight negligible increase in the BET surface area was observed, which effect on the OTM/catalyst was not evident

**Table 5.8 CL-SR process characterisation results at 1 bar, GHSV 0.498 and S:C 3. Reforming/reduction reaction at 650 °C and oxidation reaction at 750 °C (Table 5.1 inputs)**

Condition	NiO crystallite size (nm)	BET Surface area (m <sup>2</sup> /g)	C (wt. %) on catalyst	C (g/L) in condensate
Fresh NiO/Al <sub>2</sub> O <sub>3</sub> catalyst/OTM	45.05	3.45	N/A	N/A
Reacted at 600 °C (NiO/Al <sub>2</sub> O <sub>3</sub> )	24.00	1.59	0.08	0.063
Fresh NiO/CaO/Al <sub>2</sub> O <sub>3</sub> catalyst/OTM	N/A	21.31	N/A	N/A
Reacted at 750 °C (NiO/CaO/Al <sub>2</sub> O <sub>3</sub> )	N/A	23.82	7.59	0.069

There was virtually almost zero/insignificant solid carbon deposition on the surface of the Ni/Al<sub>2</sub>O<sub>3</sub> catalyst/OTM investigated using CHNS analysis after 20 redox-oxidation cycles at 650 °C (Table 5.8). This shows that burning off of the solid carbon during the oxidation reaction process at 750 °C with Ni on Al<sub>2</sub>O<sub>3</sub> support OTM/catalyst was possible as well as further explained the stability of the process at outputs. Solid carbon deposition on the surface of the Ni on CaO/Al<sub>2</sub>O<sub>3</sub> support catalyst was found to be as high as 7.58 wt % in an 8 g sample of the OTM/catalyst analyses thrice with CHNS analyzer for precision and credibility. Thus, it can be concluded that, the oxidation reaction process did not successfully burn off the solid carbon deposit on the surface of the Ni on CaO/Al<sub>2</sub>O<sub>3</sub> support OTM/ catalyst at 750 °C. The observe phenomenon could probably be evaded by the use of higher oxidation temperature. The higher concentration of solid carbon deposit on the Ni/CaO/Al<sub>2</sub>O<sub>3</sub> OTM/catalyst compared to the Ni/Al<sub>2</sub>O<sub>3</sub> OTM/ catalyst might also result from the high reaction temperature (750 °C) used. Because high reaction temperature are well known to enhance solid carbon deposition on the surface of the catalyst. The partial burning off of the solid carbon deposition on the surface of the Ni on CaO/Al<sub>2</sub>O<sub>3</sub> support OTM/catalyst explained the decrease in the activity of the material discussed earlier. Using EDX (mapping method; images in appendix B3) it was found that carbon deposit were not regularly distributed on the surface of the catalyst.

The magnification of the reacted 18 wt.% NiO on Al<sub>2</sub>O<sub>3</sub> support OTM/catalyst at 5 µm shows clearly in Figure 5.21(a and b) that the reacted OTM/catalyst was compacted, rougher with small

and big grain size compared to the fresh OTM/catalyst. Depicting significant chemical changes in the external surface of the OTM/catalyst; this could be attributed to agglomeration and sintering mentioned earlier. These large grains might result from agglomeration while the small ones could be caused by sintering of the OTM/catalyst. The FESEM of 15 wt. % NiO on CaO/Al<sub>2</sub>O<sub>3</sub> support fresh OTM/catalyst (Figure 5.21 (c)) on the other hand appears to be rougher compared to the reacted OTM/catalyst (Figure 5.21 (d)) at exactly same magnification of 5 μm. The uniformity on the surface of the porous reacted OTM/catalyst might be due to high accumulative influence of long term alternations reactions of the redox-oxidation cycles at high temperature (750 °C). Diffusion was aided by the porous external surface of the OTM/catalyst, hence enhancing the reactions between the gas feed and the OTM/catalyst. The morphological characteristics of the reacted OTM/catalyst further confirmed the high reactivity of the OTM/catalyst and subsequently the high fuel and water conversion discussed previously and the slight increase in the BET surface area of OTM/catalyst.

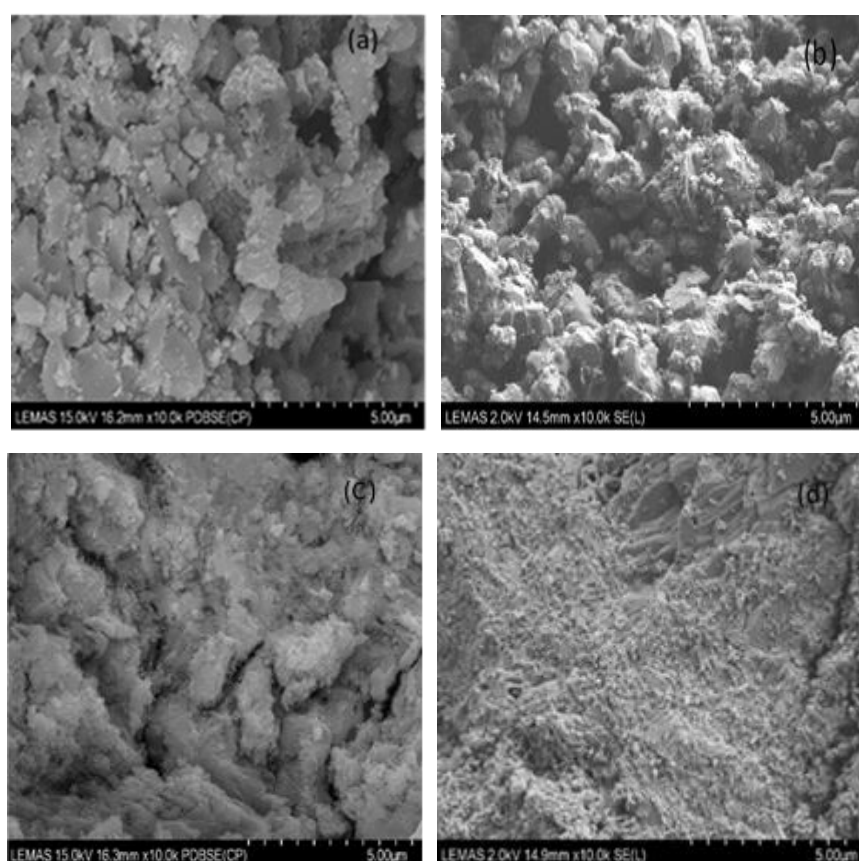


**Figure 5.21** FESEM images (a) Fresh 18 wt. % NiO on Al<sub>2</sub>O<sub>3</sub> support OTM/catalyst (b) Reacted 18 wt. % NiO on Al<sub>2</sub>O<sub>3</sub> support OTM/catalyst at 650 °C (c) Fresh 15 wt. % NiO on CaO/Al<sub>2</sub>O<sub>3</sub> support OTM/catalyst (d) Reacted 15 wt. % NiO on CaO/Al<sub>2</sub>O<sub>3</sub> support OTM/catalyst at 750 °C

## 5.5 Sorption Enhanced Chemical looping steam reforming (SE-CLSR)

The combination of sorption enhancement and chemical looping in a C-SR process as one single process is called sorption enhanced chemical looping steam reforming (SE-CLSR) (S G Adiya et al., 2017). In a packed bed configuration, the material bed then consists of a mixture of particles comprising of solid oxygen carrier and catalyst, as well as CO<sub>2</sub> sorbent.

### 5.5.1 Effect of sorbent and chemical looping on steam reforming process

Reduction-oxidation-calcination cycles were conducted in the quartz fixed bed reactor already discussed previously (See chapter 3 and Effect of chemical looping on steam reforming process in the current chapter). 2 g (1.2 mm grain size) of the OTM/catalyst was randomly mixed with 1 g (1.2 mm grain size) of pure CaO sorbent and loaded in the reactor. The cycling experiments were conducted in exactly the same way as in the CL-SR process described in section 5.4 except that the oxidation process (transformation of the active Ni back to its original NiO state and burning of any carbon deposit on the surface of the OTM/catalysts) using air was simultaneously accompanied with regeneration of CaCO<sub>3</sub> (form during the reforming and carbonation stage) to active solid CaO sorbent at 850 °C.

For the purpose of studying the effect of sorption enhancement coupled with chemical looping in the C-SR process; the SE-CLSR experiments were performed at atmospheric pressure, GHSV 0.498, S:C ratio of 3 and a temperature of 650 °C under constant flow of inert N<sub>2</sub> gas. The choice of GHSV 0.498 was based on our previous experiments in section 5.2 that proved it to be optimum while the choice of S:C 3 and a temperature of 650 °C was based on our thermodynamic studies (chapter 4) and previous thermodynamic work by Antara et al and S G Adiya et al (Antzaraa et al., 2015, S G Adiya et al., 2017) that showed the conditions to be optimum. 20 redox-oxidation-calcination cycles were conducted to investigate the cyclic behaviour and stability of the Ca based CaO sorbent and the 18 wt. % NiO on Al<sub>2</sub>O<sub>3</sub> support OTM/catalyst.

Figure 5.22 depicts the average process outputs (H<sub>2</sub> yield and purity) achieved in the 20 redox oxidation-calcination cycles. Fuel and water conversion during the pre-breakthrough period was excluded owing to the inability to accurately measure the carbonation rate on the solid sorbent at any given time explained earlier in section 5.4.

NiO reduction, steam reforming of shale gas and WGS reactions happen concurrently with in-situ CO<sub>2</sub> capture, causing substantial increase in H<sub>2</sub> yield and purity (compared to the C-SR process as depicted in Figure 5.22) as expected in the pre breakthrough (active carbonation stage). The observed phenomenon results from the presence of the CO<sub>2</sub> sorbent shifting the equilibria of both the steam reforming and the WGS reaction to the right towards higher conversion to CO, then to CO<sub>2</sub>, followed by capture of the CO<sub>2</sub> on the sorbent, with the carbon product becoming entirely solid calcium carbonate (during pre-breakthrough).

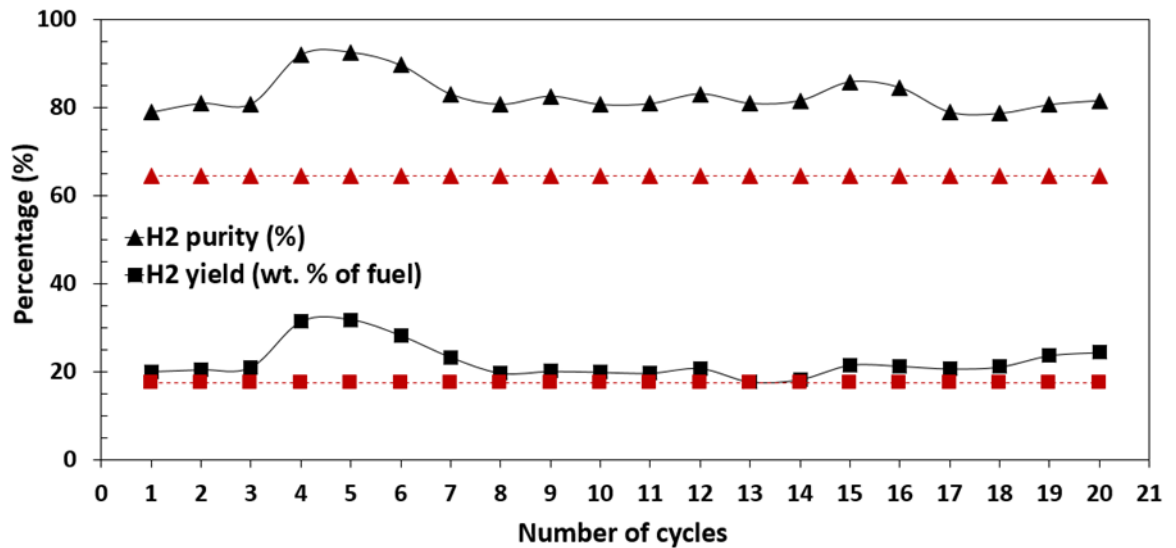


**Figure 5.22 Comparison of SE-CLSR process outputs with C-SR at 1 bar, GHSV 0.498, S:C 3, reforming/reduction temperature at 650 °C and oxidation at 850 °C with CaO and NiO on Al<sub>2</sub>O<sub>3</sub> support as sorbent and OTM/catalyst respectively (average process outputs) (Note: Solid lines are for experimental results and dashed lines for C-SR process)**

Additionally, the presence of the nickel based OTM/catalyst in the SE-CLSR system also causes further positive effect on H<sub>2</sub> yield and purity, even though part of the fuel was initially used for reduction of the OTM/catalyst. This is because the reduction of fuel by NiO produces total oxidation products CO<sub>2</sub> and H<sub>2</sub>O, with the former being captured by the sorbent, and the latter increasing the water concentration of the system, effectively achieving a dual effect or enhancement in accordance with the Le Chatelier's principle. Comparison of the SE-CLSR process outputs with chemical equilibrium results is presented in Figure 5.23, the comparison shows that the SE-CLSR process experimental results are away from equilibrium. This could be attributed to at least two factors. First, thermodynamic equilibrium limitation as shown in Figure 5.23 and secondly chemical reaction kinetics. Limitation occurring from both phenomena has been reported to negatively influence the performance of steam reforming process.

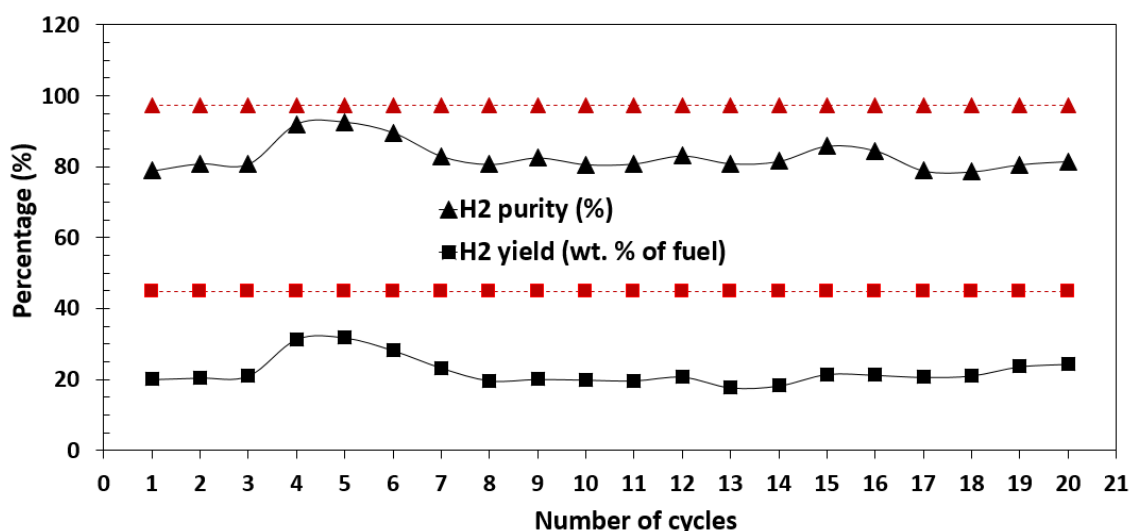


**Figure 5.23 Comparison of SE-CLSR process outputs with chemical equilibrium results at 1 bar, GHSV 0.498, S:C 3, reforming/reduction temperature at 650 °C and oxidation at 850 °C with CaO and NiO on Al<sub>2</sub>O<sub>3</sub> support as sorbent and OTM/catalyst respectively (average process outputs) (Note: Solid lines are for experimental results and dashed lines for chemical equilibrium results)**

Approximately after 24 minutes; the pre breakthrough period gently declined and a gentle emergence of the breakthrough period (unsteady formation of CO<sub>2</sub>) began. This no doubt indicated the Ca based CO<sub>2</sub> sorbent has begun/fully saturated. Figure 5.24 present the 4<sup>th</sup> cycle outputs against time stream chosen as representative of all the 20 reduction-oxidation-calcination cycles. The breakthrough period is followed by the post breakthrough period (CO<sub>2</sub> steady state production). At this stage the process is expected degenerate back completely to the C-SR process owing to the full saturation of the Ca based CO<sub>2</sub> sorbent. The plots of H<sub>2</sub> yield and purity, fuel and water conversion (Figure 5.24 (a)) against time stream shows same trend as the CO and CO<sub>2</sub> molar production rate. i.e. Both H<sub>2</sub> yield and purity were higher during the pre-break through period with a gentle decline at the breakthrough period that approaches stability towards the post pre-through period. However, it is worth remembering that, fuel and water conversion during the pre-breakthrough periods are not reliable for reasons explained earlier.

During the oxidation stage conducted at 850 °C, three major reactions were expected to happen. The regeneration of the sorbent, carbon oxidation reactions and nickel oxidation reaction. Both sorbent generation and carbon oxidation reactions have the potential to generate CO<sub>2</sub>. The later (carbon oxidation reactions) and nickel oxidation reaction consumed oxygen from the air feed. Thus, carbon and oxygen elemental balances are not enough to define the three unknown rates

of Ni oxidation, carbon oxidation, and sorbent calcination. Moreover, the most vital part of the oxidation reaction process is in the first 3 minutes, as the process is quite fast in the reactor. The micro gas chromatography analyses the results after every 3 minutes, rendering monitoring of the oxidation reaction process with time on stream impossible or unreliable. However, an increase in the oxidation temperature was observed during the oxidation process due to the exothermic nature of the reaction. Just like the CL-SR process, the burning off of the solid carbon (coke) deposition during the air feed was coincidence with CO<sub>2</sub> and CO generation. As the oxidation reaction approached its end, a gradual decrease in the reactor temperature was observed. Table 5.9 presents a percentage enhancement of SECL-SR process with C-SR process (H<sub>2</sub> yield and purity percentage increase in SE-CLSR process) reforming/reduction stage at 650 °C and oxidation stage at 750 °C using CaO and 18 wt. % NiO on Al<sub>2</sub>O<sub>3</sub> support as sorbent and OTM/catalyst respectively.

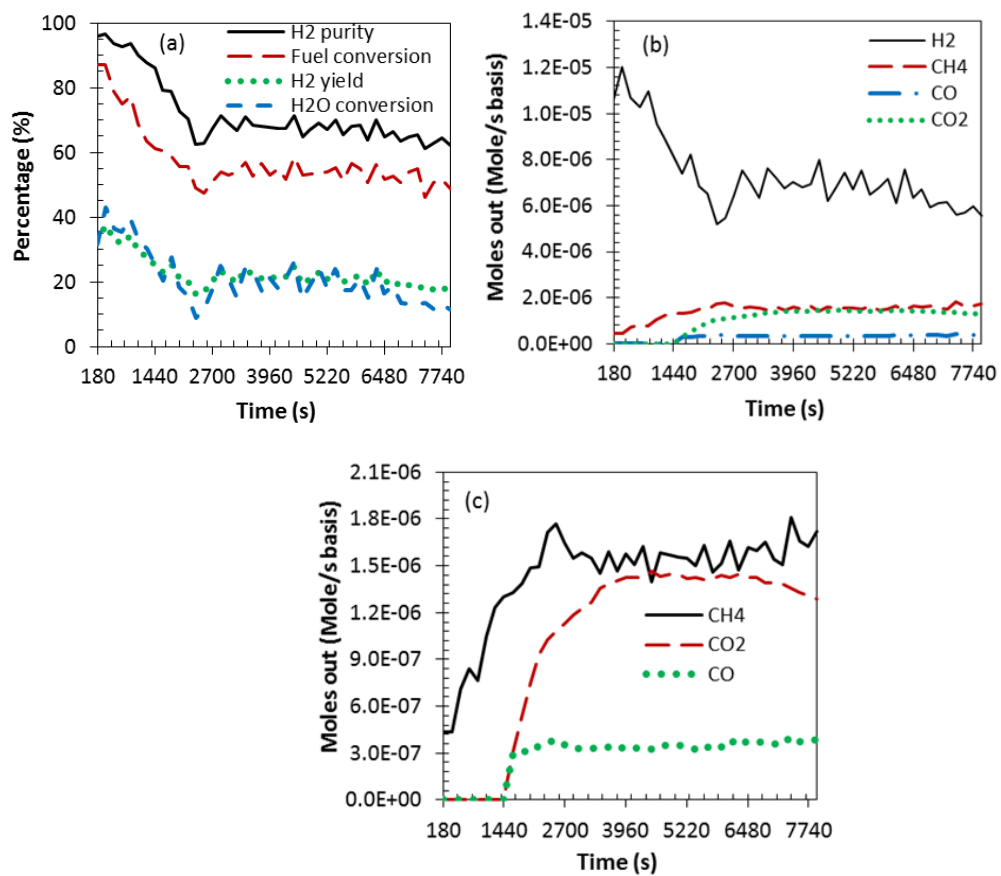


**Figure 5.24** Process outputs for the 4<sup>th</sup> cycle at 1 bar, GHSV 0.498, S:C 3, reforming/reduction temperature at 650 °C and oxidation at 850 °C with CaO and NiO on Al<sub>2</sub>O<sub>3</sub> support as sorbent and OTM/catalyst respectively (a) H<sub>2</sub> yield and purity, fuel and H<sub>2</sub>O conversion vs time using 18 wt. % NiO on Al<sub>2</sub>O<sub>3</sub> support catalyst (b) moles out vs time using 18 wt. % NiO on Al<sub>2</sub>O<sub>3</sub> support catalyst (c) clearer graph of moles out vs time using 18 wt. % NiO on Al<sub>2</sub>O<sub>3</sub> support catalyst

**Table 5.9 Percentage (%) enhancement of SECL-SR process over C-SR process reforming/reduction at 650 °C and oxidation at 850 °C using CaO and 18 wt. % NiO on Al<sub>2</sub>O<sub>3</sub> support as sorbent and OTM/catalyst respectively (H<sub>2</sub> yield and purity).**

Cycle number	H <sub>2</sub> yield (%)	H <sub>2</sub> purity (%)
1 <sup>st</sup> cycle	14.85	22.48
2 <sup>nd</sup> cycle	17.35	25.60
3 <sup>rd</sup> cycle	20.59	25.45
4 <sup>th</sup> cycle	79.93	42.93
5 <sup>th</sup> cycle	82.18	43.72
6 <sup>th</sup> cycle	61.54	39.13
7 <sup>th</sup> cycle	33.26	28.84
8 <sup>th</sup> cycle	12.84	25.30
9 <sup>th</sup> cycle	15.20	28.14
10 <sup>th</sup> cycle	14.01	25.22
11 <sup>th</sup> cycle	12.83	25.55
12 <sup>th</sup> cycle	18.83	29.00
13 <sup>th</sup> cycle	1.42	25.62
14 <sup>th</sup> cycle	4.57	26.63
15 <sup>th</sup> cycle	23.16	33.27
16 <sup>th</sup> cycle	21.77	31.23
17 <sup>th</sup> cycle	18.39	22.52
18 <sup>th</sup> cycle	20.83	22.08
19 <sup>th</sup> cycle	35.56	25.17
20 <sup>th</sup> cycle	39.48	26.61

Comparison of our results with previous research is difficult mainly because researchers focused on pure methane as feedstock, promoted Ca based CaO sorbent and a different OTM/catalyst. For example, similar studies coupling sorption enhancement and chemical looping has been conducted by (Hafizi et al., 2016a) showing the application of 2Fe<sub>2</sub>O<sub>3</sub>/MgAl<sub>2</sub>O<sub>4</sub> and 22Fe<sub>2</sub>O<sub>3</sub>/Al<sub>2</sub>O<sub>3</sub> as OTM/catalyst and cerium promoted CaO as CO<sub>2</sub> sorbent using pure methane as feedstock. Their characterisation findings and the SE-CLSR process experimental outputs

shows the better performance of cerium promoted CaO sorbent for CO<sub>2</sub> removal. They also found that 2Fe<sub>2</sub>O<sub>3</sub>/MgAl<sub>2</sub>O<sub>4</sub> OTM/ catalyst has better performance compared to 22Fe<sub>2</sub>O<sub>3</sub>/Al<sub>2</sub>O<sub>3</sub>. The OTM(s)/catalyst(s) and sorbent demonstrated stable performance at 600 °C in good nine reduction and calcination cycles. Antzara et al. (Antzara et al., 2016a) also investigated the performance of SE-CLSR process using a mixture of a bifunctional NiO-based OTM/catalyst supported on ZrO<sub>2</sub>, and a ZrO<sub>2</sub>-promoted CaO-based CO<sub>2</sub> sorbent with pure methane as feedstock. The materials shows excellent stability without deterioration in their performance for 20 continues reforming and regeneration cycles. They reported high H<sub>2</sub> concentration throughout the pre-breakthrough period with low concentration of CO and CO<sub>2</sub> which is in good agreement with the present study. Their conclusion that SE-CLSR process has significant advantages compared to the C-SR process is also in good agreement to that of the present study.

### 5.5.2 Comparison of SE-CLSR at post CO<sub>2</sub> breakthrough period with C-SR process

Comparison of the post breakthrough period of the SE-CLSR process and the C-SR process is shown in Figure 5.25; this presents a significant decrease in fuel and water conversion, consequently H<sub>2</sub> yield and purity in the SE-CLSR process at steady state of post CO<sub>2</sub> breakthrough in most of the cycles. This could be attributed to a number of factors.

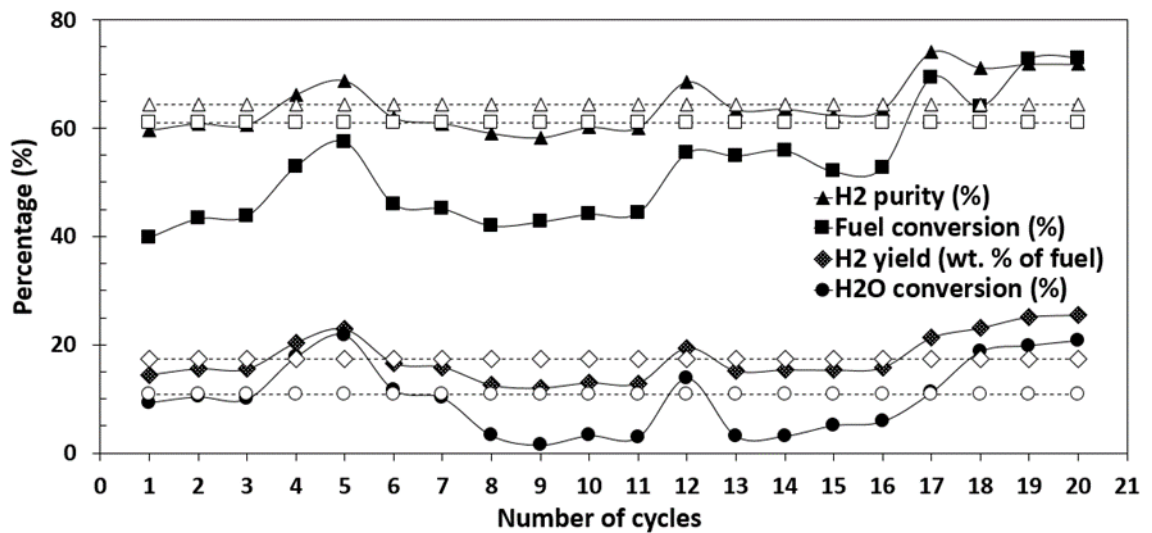


Figure 5.25 Comparison of post breakthrough period of SE-CLSR with the C-SR process at 1 bar, GHSV 0.498, S:C 3, reforming/reduction temperature at 650 °C and oxidation at 850 °C with CaO and NiO on Al<sub>2</sub>O<sub>3</sub> support as sorbent and OTM/catalyst respectively (Note: Solid lines are for experimental results and dashed lines for C-SR process)

First, our catalyst bed is diluted with calcium carbonate, affecting the activity of the catalyst. Another possible reason is the fact that there is potential deposit of carbon in both the catalyst

and calcium carbonate after approximately 1 hour 30 minutes of use. This will significantly affect both the fuel and water conversion, and subsequently the H<sub>2</sub> yield and purity. On the other hand the higher conversion on the fuel and water causing (better H<sub>2</sub> yield and purity) in the C-SR process might result from the un-dilution of the catalyst and probably the absent of significant solid carbon deposits on the surface of the catalyst. Moreover, the C-SR process experiments were conducted for a period of 1 hour 30 minutes while those of SE-CLSR process were conducted for a period of 3 hours. No doubt the presence of 3 g of catalyst in the C-SR process as opposed to the 2 g used in SE-CLSR process played a significant role in the process outputs.

### **5.5.3 Cyclic stability and behavior of sorbent and OTM/catalyst during SE-CLSR process**

The stability of the CaO sorbent (from pure limestone) couple with 18 wt. % Ni on Al<sub>2</sub>O<sub>3</sub> support as OTM/catalyst was determined by the increasing number of cycles and the carbonation efficiency of the sorbent. Using the mass of the CaO sorbent and the molecular weight of the sorbent, the maximum molar CO<sub>2</sub> capacity (0.02) was calculated. As seen in Figure 5.22; H<sub>2</sub> yield and purity increase steadily with increase in the number of cycles first. At exactly the 4<sup>th</sup> cycle a significant rise in both the H<sub>2</sub> yield and purity was seen which is followed with a gentle decrease in both the yield and purity till approximately the 9<sup>th</sup> cycle; where the process output almost stabilizes (with insignificant difference). The later no doubt can be attributed to decrease in the sorbent capacity and loss of activity of the OTM/catalyst with increasing usage. Even though CaO sorbents has many advantages as a CO<sub>2</sub> sorbent, the sorbent industrial application has faced some serious concerns including the loss of sorption capacity in long-term operation, after repeated absorption-desorption cycles and the formation of CaSO<sub>4</sub> owing to loss of reactivity with sulphur containing gases (Silaban et al., 1996, Sun et al., 2008, Shokrollahi Yancheshmeh et al., 2016, Fennell and Anthony, 2015). Sintering of the sorbent, including agglomeration of particles, pore shape and shrinkage change are major cause of decrease/loss of CaO Sorbents capacity (Shokrollahi Yancheshmeh et al., 2016). The gradually increased in the 1st cycle, might results from the fact that the reactivity NiO particles (OTM/catalyst in the process) is known to increased slightly after their first contact with fuel (Rydén et al., 2009, Ryden and Ramos, 2012).

Others researchers have studied the CO<sub>2</sub> sorption behavior of limestone sorbents in repeated cyclic absorption desorption cycles (Shokrollahi Yancheshmeh et al., 2016), for example, over 500 carbonation/calcination cycles were conducted by Grasa and Abanades (Grasa and

Abanades, 2006), there results are in good agreement to those of the present study in the sense that sorbent capture capacity significantly decreased during the first 20 cycles and then stabilized at a certain point limit.

#### 5.5.4 SE-CLSR process materials characterization

Field emission- scanning electron microscopy (FESEM) was used to study morphological characteristics of the sorbent before and after calcination and after the 20 redox-calcination-oxidation cycles. Figure 5.26 clearly depict the structural transformation of pure  $\text{CaCO}_3$  before and after calcination to pure  $\text{CaO}$  sorbent. The pure  $\text{CaCO}_3$  undergoes massive structural transformation after calcination to pure  $\text{CaO}$  sorbent at  $915^\circ\text{C}$  for 4 hours. The surface of the  $\text{CaCO}_3$  completely change after calcination to  $\text{CaO}$  sorbent with significant pores developed owing to release of  $\text{CO}_2$  (from  $\text{CaCO}_3$ ) as shown in Figure 5.26.

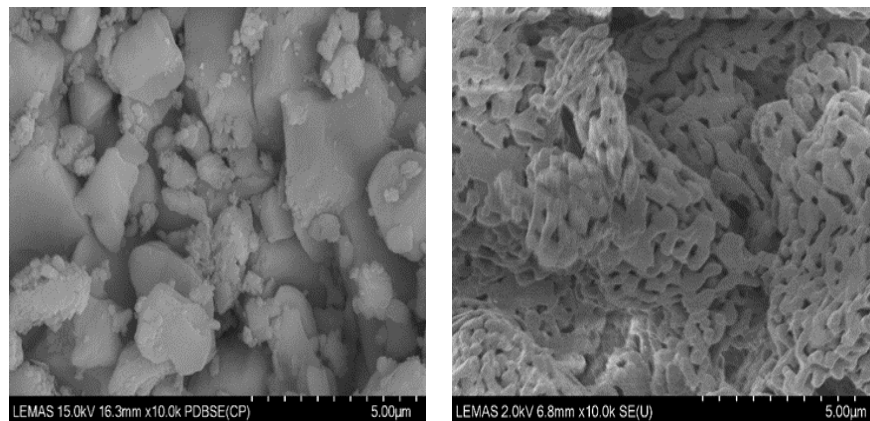


**Figure 5.26 Left: Pure  $\text{CaCO}_3$  Right: pure  $\text{CaO}$  sorbent (calcined at  $915^\circ\text{C}$  for 4 hours)**

Comparison of the Fresh and the reacted  $\text{CaO}$  sorbent and OTM/catalyst mixture after 20 redox-calcination-oxidation cycles shows sintering and excessive agglomeration of the mixture as depicted in Figure 5.27. Expansion of the  $\text{CaO}$  sorbent particles during  $\text{CO}_2$  adsorption causes sintering of the particles (Zhang et al., 2012, Shokrollahi Yancheshmeh et al., 2016).

The expansion that causes sintering is extremely influenced by temperature and particle separation distance. A high adsorption temperature and shorter distance between two sorbent particles increases the sintering rate during the adsorption process (Shokrollahi Yancheshmeh et al., 2016). The latter, shorter distance between two sorbent particles might be the major cause of sintering in the present studies, since the adsorption temperature is moderately low.

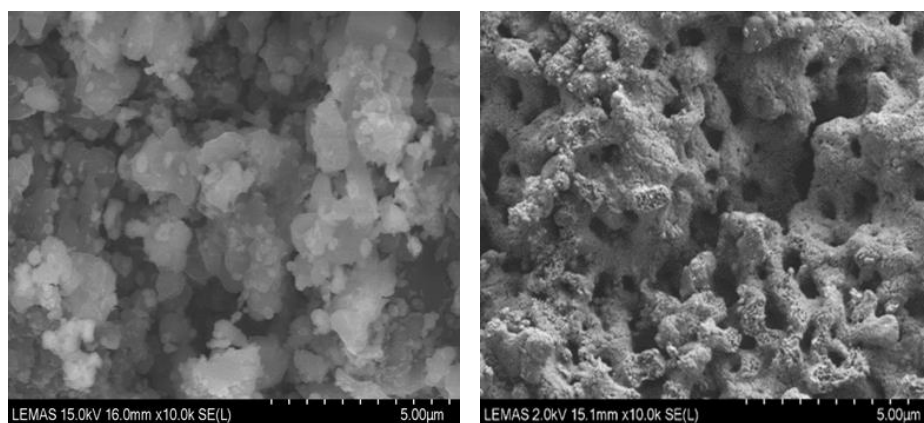


**Figure 5.27 CaO sorbent and NiO on Al<sub>2</sub>O<sub>3</sub> support OTM/catalyst mixture Left: Fresh mixture Right: mixture after 20 redox-calcination-oxidation cycles at 1 bar, GHSV 0.498, S:C 3 reforming/reduction temperature at 650 °C and oxidation at 850 °C.**

The textural properties of the sorbent; BET surface area of the fresh and reacted mixture samples are given in Table 5.10. The BET surface area of the pure CaCO<sub>3</sub> was found to be 0.349 m<sup>2</sup>/g, while after calcination to CaO is 7.121 m<sup>2</sup>/g. The BET surface area of pure CaCO<sub>3</sub> increased significantly compared to that of pure CaO sorbent due release of CO<sub>2</sub> present in the CaCO<sub>3</sub> explained earlier; causing formation of a highly porous layer with small particles on the surface of CaO sorbent. In addition, the surface area of the reacted mixture after 20 redox-calcination-oxidation cycles shows a slight decrease compared fresh mixture of the sorbent and OTM/catalyst which could be owed to sintering and pore blockage after repeated cyclic absorption and desorption cycles (Hafizi et al., 2016a).

**Table 5.10 SE-CLSR process characterisation results at 1 bar, GHSV 0.498, S:C 3, reforming/reduction temperature at 650 °C and oxidation at °C 850 using CaO and Ni on Al<sub>2</sub>O<sub>3</sub> support as sorbent and OTM/catalyst respectively (Table 5.1 inputs)**

Condition	NiO/Ni crystallite size (nm)	BET Surface area (m <sup>2</sup> /g)	C (wt. %) on catalyst	C (g/L) in condensate
Pure CaCO <sub>3</sub>	N/A	0.349	N/A	N/A
Pure CaO	48.23	7.121	N/A	N/A
Fresh catalyst	45.05	3.45	N/A	N/A
Fresh sorbent and OTM/catalyst mixture	44.89	5.131	N/A	N/A
Reduced sorbent and OTM/catalyst mixture	46.03	4.633	N/A	N/A
Reacted at 650 °C	49.08	4.605	0.26	0.16

The X-ray diffraction patterns of the fresh and reacted mixture of the sorbent and OTM/catalyst after 20 redox-oxidation-calcination cycles of SE-CLSR are presented in Figure 5.28. The patterns were identified by the usual peaks of nickel oxide, alumina and CaO by X'Pert HighScore Plus software for phase analysis of the XRD data (ICDD reference code 04-004-5528, 04-012-6349 and 01-071-1683 for CaO, NiO and Al<sub>2</sub>O<sub>3</sub> respectively). The Scherrer equation was used to find the crystalline size of the NiO. A slight increase in the crystalline size of the reacted mixture was observe. The slight increased depict sintering of the Ni cubic crystal size during stability test of the OTM/catalyst (Wang et al., 2016). The great characteristics peaks of NiO exactly like the fresh sorbent and OTM/catalyst mixture suggested sufficient oxidation of the Ni to NiO.

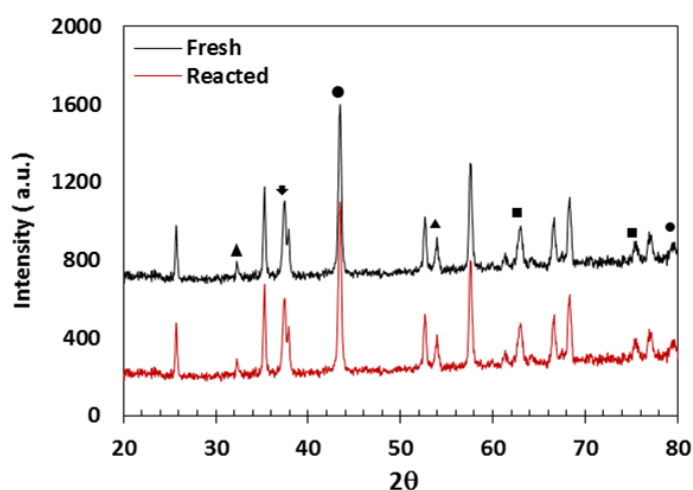


**Figure 5.28** 18 wt. % NiO on Al<sub>2</sub>O<sub>3</sub> support XRD patterns; peaks with triangle on top represent CaO peaks, peak with square on top represent NiO peaks, peak with arrow represent superimposed NiO, CaO and Al<sub>2</sub>O<sub>3</sub> peaks, peaks with cycle on top represent superimposed NiO and Al<sub>2</sub>O<sub>3</sub> peaks, while the unidentified peaks are Al<sub>2</sub>O<sub>3</sub> peaks

The concentration of solid carbon found on the surface of the sorbent and OTM/catalyst mixture is completely negligible/insignificant. Thus, it can be concluded that burning off of the solid carbon during the oxidation reaction process at 850 °C was successful. 157 ppm of solid carbon was found in the condensate sample of 20 redox-oxidation-calcination cycles collectively. The collective small concentration of the solid carbon also made us consider it insignificant.

## 5.6 Conclusion

Increasing the GHSV decreases the contact time of the reactant in the reactor, thus operating at the lowest possible GHSV is more suitable in a steam reforming process. High operating temperatures are in favour of the strong endothermic steam reforming reaction but to the

detriment of the water gas shift reaction. The influence of catalyst support and NiO loading was not evident at low/medium operating temperature (600 and 650 °C). However, at higher temperature (700 and 750 °C), Ni on CaO/Al<sub>2</sub>O<sub>3</sub> support catalyst showed better performance than the Ni on Al<sub>2</sub>O<sub>3</sub> support with regards to feed conversion and product yield caused by the alkalinity of CaO, suppressing solid carbon formation on the surface of the catalyst.

In order to define the optimum operating conditions for the SE-CLSR process, an investigation of the sorption enhanced process termed SE-SR process and chemical looped process termed CL-SR was conducted at S:C of 3 and GHSV of 0.498 retrieved to be optimum from the thermodynamics studies and the C-SR process experiment respectively. The effect of Ca based CaO sorbent and operating temperature in the range of 600-700 °C was studied. It was found that low/medium operating temperature is more suitable for a SE-SR process owing to the thermal decomposition of CaO sorbent at high temperatures, in addition to that, carbonation process is favoured thermodynamically in low/medium temperature range. It was also discovered that the presence of a Ca based CaO sorbent has the potential to significantly increase H<sub>2</sub> yield and purity as well decreased the cost of operating the system because of the mild operating condition the process permits. The influence of chemical looping on steam reforming (CL-SR process) was investigated at 650 °C and 750 °C using Ni on Al<sub>2</sub>O<sub>3</sub> support and Ni on CaO/Al<sub>2</sub>O<sub>3</sub> support as OTM/catalyst respectively. Both materials demonstrated good performance as OTM/catalyst with better process outputs compared to the C-SR process. The case with Ni on Al<sub>2</sub>O<sub>3</sub> support at 650 °C showed excellent stability without significant deterioration in the performance for 20 successive redox-oxidation cycles, corresponding to 80 h of testing. Nonetheless, fuel conversion was low, below 70 %, caused by the low operating temperature use. Ni on CaO/Al<sub>2</sub>O<sub>3</sub> support tested at 750 °C showed a significant deterioration after about 9 successive redox-oxidation cycles approximately, corresponding to 80 h of testing as well. However, Fuel conversion was high (over 80 % approximately prior to deterioration of the OTM/catalyst), that can be strongly attributed to the high temperature in favoured of steam reforming process. The deterioration in the activity of the OTM/catalyst was caused by the partial burning off of the solid carbon deposition on the surface of the OTM/catalyst confirmed during the CHNS analysis.

High purity H<sub>2</sub> was generated using a novel low energy consumption process termed SE-CLSR process using actual shale gas as feedstock. The feasibility of the intensified C-SR process

(coupled with sorption enhancement and chemical looping) was demonstrated experimentally over a mixture of a bifunctional NiO-based OTM/catalyst supported on Al<sub>2</sub>O<sub>3</sub> and a Ca-based CaO sorbent. 20 redox-oxidation-calcination cycles of experiments were performed in a bench-scale fixed bed reactor at 1 bar, GHSV 0.498, S:C 3 and 650 °C. High hydrogen yield of 31 wt. % and purity of 92 % was obtained (in the 4<sup>th</sup> cycle) during the pre-breakthrough period of the SE-CLSR process (prior to cycles with low sorbent capacity). The post breakthrough period do not degenerated fully to the C-SR process due to OTM/catalyst bed dilution and decreased in the quantity of catalyst compared to the C-SR process. The surface area of the sorbent and OTM/catalyst mixture after 20 redox-calcination-oxidation cycles underwent a slight decrease compared fresh mixture of the sorbent and OTM/catalyst caused by sintering and pore blockage after repeated cyclic absorption-desorption cycles. The FESEM images of the mixture also showed sintering and agglomeration on the reacted sorbent and OTM/catalyst mixture. Sorbent regeneration and Ni oxidation to NiO at 850 °C using pure air feed successfully burn off the solid carbon deposition on the surface of the sorbent and OTM/catalyst mixture. Regeneration and oxidation of the CaO sorbent and OTM/catalyst was also accomplished at the same temperature.

The results of the experimental analysis shown that there are important benefits of coupling C-SR with sorption enhancement and chemical looping compared to the typical C-SR process in packed bed configuration. The SE-CLSR process is an advanced integrated technology for high purity H<sub>2</sub> generation with in-situ CO<sub>2</sub> capture. The process can be operated with very low overall CO<sub>2</sub> released from the system as opposed to the C-SR process, since the steam reforming reaction is accompanied with CO<sub>2</sub> capture. The re-oxidation of the reduced OTM/catalyst can cover a large part of the heat required for the endothermic sorbent regeneration, further decreasing the overall heat demands of the process. However, for the process to be commercially applicable, a more advanced analysis of the SE-CLSR process is necessary, together with detailed technological and economic analysis and whole process design for scaling purposes. Yet, it is obvious that the combination of sorption enhancement and chemical looping on C-SR process has great prospective for high H<sub>2</sub> yield and purity generation at reasonable lower cost and high energy efficiency.

## Chapter 6 Effect of hydrocarbon fractions, N<sub>2</sub> and CO<sub>2</sub> in feed gas on hydrogen production

Chapter 6 provides a detailed thermodynamic equilibrium studies on the influence of hydrocarbon fractions, N<sub>2</sub> and CO<sub>2</sub> in feed gas on hydrogen production using sorption enhanced steam (SE-SR). Detailed discussion on the effect of gas composition on H<sub>2</sub> yield, purity and selectivity of carbon to calcium carbonate product, including magnitude of sorption enhancement effects due to hydrocarbon content, N<sub>2</sub> and CO<sub>2</sub> content in the feed gas and enhancements variation with N<sub>2</sub> and CO<sub>2</sub> content in feedstock were also discussed in detail. The effect of inert bed materials, hydrocarbon fractions, N<sub>2</sub> and CO<sub>2</sub> content on energy balance was also analysed.

### 6.1 Introduction

Outputs of the materials balances were given in terms of H<sub>2</sub> yield as mass percentage of the fuel gas, as well as H<sub>2</sub> purity and selectivity of carbon containing products to calcium carbonate. With shale gases consisting in X, Y and Z mol% of the alkanes CH<sub>4</sub>, C<sub>2</sub>H<sub>6</sub> and C<sub>3</sub>H<sub>8</sub> respectively, T mol% of CO<sub>2</sub> and I mol % of N<sub>2</sub>, the absolute maxima of H<sub>2</sub> yield, H<sub>2</sub> and CO<sub>2</sub> or CaCO<sub>3</sub> products could be expressed as:

$$\text{Max H}_2 \text{ yield wt\%} = 100 \times \frac{2.02(2n_{SG} + 0.5m_{SG})}{12.01n_{SG} + 1.01m_{SG} + (44.01T/100) + (28.02I/100)} \quad (\text{Eq.1})$$

Where the hydrocarbon content in the shale gas is defined by the molar formula  $C_{n_{SG}}H_{m_{SG}}$  with

$$n_{SG} = \frac{X + 2Y + 3Z}{100} \quad (\text{Eq.2}) \quad \text{and} \quad m_{SG} = \frac{4X + 6Y + 8Z}{100} \quad (\text{Eq.3})$$

Substituting Eqs 2 & 3 into Eq. 1 and simplifying, we obtain Eq. 4 as function of X, Y, Z, T and I:

$$\text{Max H}_2 \text{ yield wt\%} = 100 \times \frac{2.02(4X + 7Y + 10Z)}{16.05X + 30.08Y + 44.11Z + 44.01T + 28.02I} \quad (\text{Eq. 4})$$

H<sub>2</sub> purity in the reformat gas for the SG mixtures was defined according to Eq. 5:

$$H_2 \text{ purity} = 100 \times \frac{\text{moles H}_2}{\text{moles all dry gases}} \quad (\text{Eq. 5})$$

Enhancement effects of SE-SR overs C-SR are measured by using equations 6-8:

Percent increase in H<sub>2</sub> yield =  $100 \times (\text{H}_2 \text{ yield SE-SR} - \text{H}_2 \text{ yield C-SR}) / \text{H}_2 \text{ yield C-SR}$  (Eq. 6)

Percent increase in H<sub>2</sub> purity =  $100 \times (\text{H}_2 \text{ purity SE-SR} - \text{H}_2 \text{ purity C-SR}) / \text{H}_2 \text{ purity C-SR}$  (Eq. 7)

Percent drop in CH<sub>4</sub> yield =  $100 \times (\text{CH}_4 \text{ yield C-SR} - \text{CH}_4 \text{ yield SE-SR}) / \text{H}_2 \text{ yield C-SR}$  (Eq. 8)

In the presence of sufficient CaO<sub>(s)</sub> sorbent and steam, maximum H<sub>2</sub> purity for SG1, which contains negligible N<sub>2</sub> (Eq.5), could reach 100% as all the hydrocarbon feed content converts to CO<sub>2</sub> and H<sub>2</sub> via steam reforming, with all CO<sub>2</sub> product and feed becoming carbonate (CaCO<sub>3(s)</sub>). The latter would be concurrent with maximum H<sub>2</sub> yield. However, 100% H<sub>2</sub> purity for SG1 could potentially also be attained via 100% conversion through the thermal decomposition reaction, which generates C<sub>(s)</sub> and H<sub>2</sub>, whilst the sorbent would capture the little CO<sub>2</sub> originally present in the SG feed. In this case the H<sub>2</sub> yield would be half the maximum corresponding to just H<sub>2</sub> and CaCO<sub>3(s)</sub> products, because the hydrogen content from the water co-reactant would not have been used. For this reason, H<sub>2</sub> purity is considered a secondary output behind H<sub>2</sub> yield. Table 1 displays both the maximum theoretical (stoichiometric) H<sub>2</sub> yields for each shale gas and the H<sub>2</sub> purity values associated with these maxima, assuming the C-SR process and the SE-SR process. In the results section, equilibrium outputs can then be compared with these maxima to assess which conditions were optimum for highest H<sub>2</sub> yield, purity, and energy demand.

**Table 6.1 Composition in mol % for shale gases SG1-4 used in the simulation (Bullin and Krouskop, 2008), maximum H<sub>2</sub> yield (Eq.4) and corresponding H<sub>2</sub> purity (Eq.5) in conditions of max. H<sub>2</sub> yield (Eq.4), assuming C-SR and SE-SR.**

Composition	SG1	SG2	SG3	SG4
X (CH <sub>4</sub> )	79.4	77.5	57.3	27.5
Y (C <sub>2</sub> H <sub>6</sub> )	16.1	4.0	4.9	3.5
Z (C <sub>3</sub> H <sub>8</sub> )	4.0	0.9	1.9	1.0
T (CO <sub>2</sub> )	0.1	3.3	0.0	3.0
I (N <sub>2</sub> )	0.4	14.3	35.9	65.0
Total (mol %)	100	100	100	100
Max H <sub>2</sub> yield (wt% of SG), Eq.4	48.7	35.9	26.5	11.5
H <sub>2</sub> purity (Eq.5) at max H <sub>2</sub> yield (%) C-SR (Eq.4)	79.1	77.2	72.2	58.5
H <sub>2</sub> purity (Eq.5) at max H <sub>2</sub> yield (%) SE-SR (Eq.4)	99.9	96.0	88.7	69.0

As in Chapter 4, the thermal efficiency of the process is assessed here via the 'ΔH ratio'. Remember, the 'ΔH ratio' is the enthalpy of generating 1 mol of H<sub>2</sub> via the equilibrium process

considered (e.g. C-SR or SE-SR), divided by that gained from reacting this H<sub>2</sub> with oxygen, representing its final use in a fuel cell or combustion process (Dupont et al., 2013, S G Adiya et al., 2017).  $\Delta H$  ratio greater than one (>1) corresponds to a non-efficient process while  $\Delta H$  ratio <1 is a proficient process and potentially economic from energy perspective. The farther  $\Delta H$  ratio is from one, the more proficient and feasible the process should be considered. As a measure of theoretical thermal efficiency,  $\Delta H$  ratio allows comparing between feedstocks for a same process, or between different processes with the same feedstock, based on the same outcome of 1 mol of H<sub>2</sub> produced. For each process, generally two terms were calculated, the change in physical transformations (sensible and latent enthalpy changes for all the species) due to heating and cooling, and the change in reaction enthalpy (isothermal). Regeneration of the Ca-sorbent was assumed to take place at 1170 K, otherwise reforming reactions had given temperatures within a wide range investigated.

For the individual reactants enthalpy change terms, the subscript '1' denoted 'reaction process 1', i.e., the first time step of the cyclic reforming process under consideration (steam reforming and carbonation), and the subscript '2' was used when there is a second step in the cyclic process, i.e., (regeneration of CO<sub>2</sub> sorbent). It is worth noting that the enthalpy of a typical commercial steam reforming catalyst i.e. 18 wt.% NiO on  $\alpha$ -Al<sub>2</sub>O<sub>3</sub> support was included in the energy balance, representing a packed bed reactor operation as opposed to a fluidised bed operation in Chapter 4.

## **6.2 Effect of varying composition in feedstock on SE-SR process outputs**

### **6.2.1 H<sub>2</sub> yield, H<sub>2</sub> purity and selectivity to calcium carbonate product**

H<sub>2</sub> yield and purity plots over temperature range of 500-1200 K, atmospheric pressure and S:C ratio of 3 are displayed in Figure 6.1 and 6.2(a) for the different shale gas compositions using CaO<sub>(s)</sub> sorbent. H<sub>2</sub> yield and purity was not only dependent on temperature and S:C ratio (to be discussed later) but also on the content of hydrocarbons in the gases (i.e. SG 1 > SG 2 > SG 3 > SG 4) as well. The figures show that gases with low hydrocarbons composition had the lowest H<sub>2</sub> yield. This was expected because of the combined effects of decreasing numerator (less moles of H<sub>2</sub> produced from lower C and H content) and increasing denominator (increasing molar mass of fuel due to heavier inert CO<sub>2</sub> and N<sub>2</sub> content) in Eq. 4, as SG mixtures varied from SG1 to SG4. To further illustrate the effect of gas composition on H<sub>2</sub> yield and purity a common case of S:C 3 with CaO<sub>(s)</sub> sorbent can be used. The highest equilibrium H<sub>2</sub> yield for SG1 was 45.5 wt.% of fuel at 880 K, i.e. 93% of the maximum corresponding to complete reactions, as per Eq. 4 (Table 1).

This became 34.0 wt.% of fuel at 890 K for SG2 (or 95% of max.), 25.0 wt.% of fuel at 880 K for SG3 (95% of max.), and 11.0 wt.% of fuel at 860 K for SG4 (96% of max.). Highest equilibrium H<sub>2</sub> yields for SG2-SG4 represented 25%, 45%, and 76% decreases compared to SG1, i.e. the same relative decreases can be calculated between the maximum H<sub>2</sub> yield according to Eq.4 for SG1 and the rest of the shale gases (SG2-SG4) using values shown in Table 1.

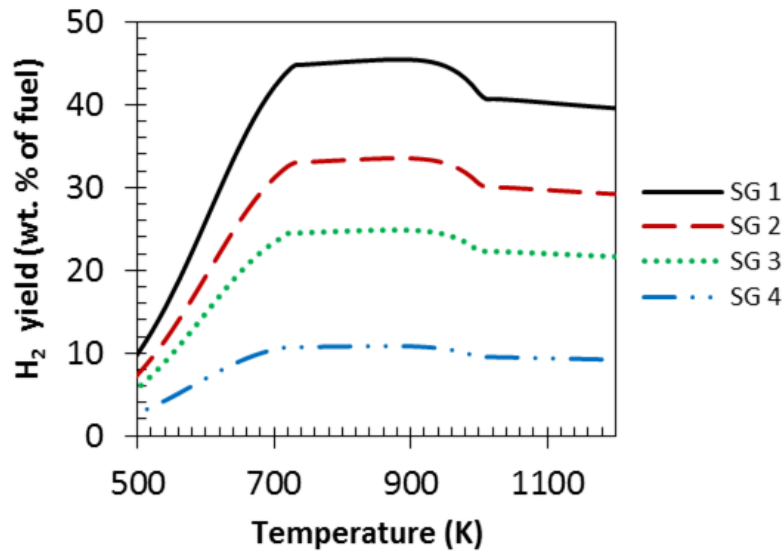


**Figure 6.1 Equilibrium H<sub>2</sub> yield vs temperature at 1 bar, Ca:C 1 and S:C 3 for SG1-4 using CaO<sub>(s)</sub> sorbent. Maximum H<sub>2</sub> yield by complete reaction to CaCO<sub>3(s)</sub> given in Table 1.**

This is because carbon selectivity to CaCO<sub>3(s)</sub> was in excess of 90% for all the shale gases as can be seen in Figure 6.2b. Highest H<sub>2</sub> purity at equilibrium was found between 720 K and 950 K followed the trend of decreasing from close to 100% for SG1, to 66% for SG4, in agreement with values calculated in Table 1, corroborating equilibrium conditions close to complete reaction to H<sub>2</sub> and CaCO<sub>3(s)</sub>. As selectivity to CaCO<sub>3(s)</sub> dropped for temperatures above 950K, the H<sub>2</sub> purity could be seen to revert to below those given in Table 1 for C-SR values (75% vs. 79% for SG1, 50% vs. 58% for SG4), as the CO co-product from reverse water gas shift prevented the maximum purity to be reached at these higher temperatures.

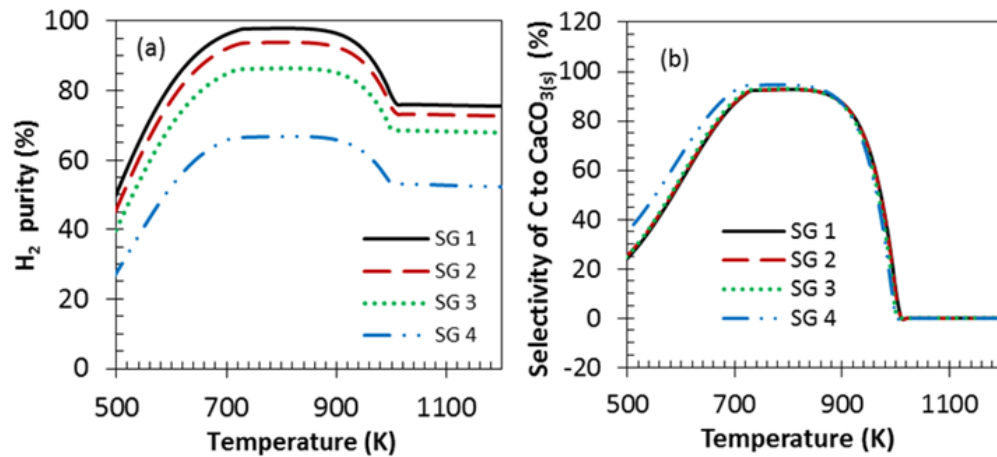


**Figure 6.2 (a) H<sub>2</sub> purity vs temperature at 1 bar, Ca:C 1 and S:C 3 for shale gases 1-4, using CaO<sub>(s)</sub> sorbent (b) selectivity of carbon to CaCO<sub>3(s)</sub> vs temperature at 1 bar, Ca:C 1 and S:C 3 for shale gases 1-4, using CaO<sub>(s)</sub> sorbent. Maximum H<sub>2</sub> purity by complete reaction to CaCO<sub>3(s)</sub> given in Table 1.**

One of the most significant uses of Ca sorbent in a reforming process, if not the best, is the fact that it effectively captures CO<sub>2</sub> as depicted in Figure 6.2(b). This process (carbonation reaction) is the backbone of all the benefits observed in the process from substantial increase in H<sub>2</sub> yield and purity to significant energy savings brought about by the SE-SR process. Examples and a discussion of such energy savings can be found for SG1 in Chapter 4. In Chapter 4, it is shown that the equilibrium moles of CaCO<sub>3(s)</sub> decrease gradually reaching zero with increase in temperature from approximately 960 or 990 K depending on S:C ratio for SG 1 considered. This was expected because of the high reaction temperature in favour of the strong endothermic decomposition of CaCO<sub>3(s)</sub> (Florin and Harris, 2007, Wei et al., 2004, Wang et al., 2011). Formation of CaCO<sub>3(s)</sub> above 1000 K is not possible owing to its decomposition. In the absence of steam in the system and stoichiometric S:C ratio i.e. S:C 1, the generation of CO<sub>2</sub> is limited by steam available for steam reforming, thus, the production of CaCO<sub>3(s)</sub> is significantly low or not possible. Previous studies on SE-SR process such as Silva et al (Lima da Silva and Müller, 2011), Chen et al (Chen et al., 2009b) and Dupont et al (Dupont et al., 2013) were in good agreement with the results of present studies with regards to H<sub>2</sub> yield and purity and efficiency of CO<sub>2</sub> capture.

### **6.2.2 Magnitude of sorption enhancement effects due to hydrocarbon content in feed gas**

SG1-4 contain varying ratios of C<sub>2</sub>H<sub>6</sub> and C<sub>3</sub>H<sub>8</sub> species with respect to CH<sub>4</sub>. In this section we explore whether sorption enhancement effects on H<sub>2</sub> yield and purity at medium high

temperatures are affected by the nature of the hydrocarbon gases present in the shale gas. Figure 6.3(a-b), which correspond to feedstocks composed in turn of 99.5 vol% of either CH<sub>4</sub>, C<sub>2</sub>H<sub>6</sub> or C<sub>3</sub>H<sub>8</sub>, (with 0.1 vol% CO<sub>2</sub> and 0.4 vol.% of N<sub>2</sub>, like SG1), shows the profile of sorption enhancement in H<sub>2</sub> yield (Eq. 6) is not affected by the nature of the alkane gases present in the feedstock. The sorption enhancement effect in H<sub>2</sub> purity (Eq 7) is seen to be minimally affected by the nature of the alkanes in the feedstock.

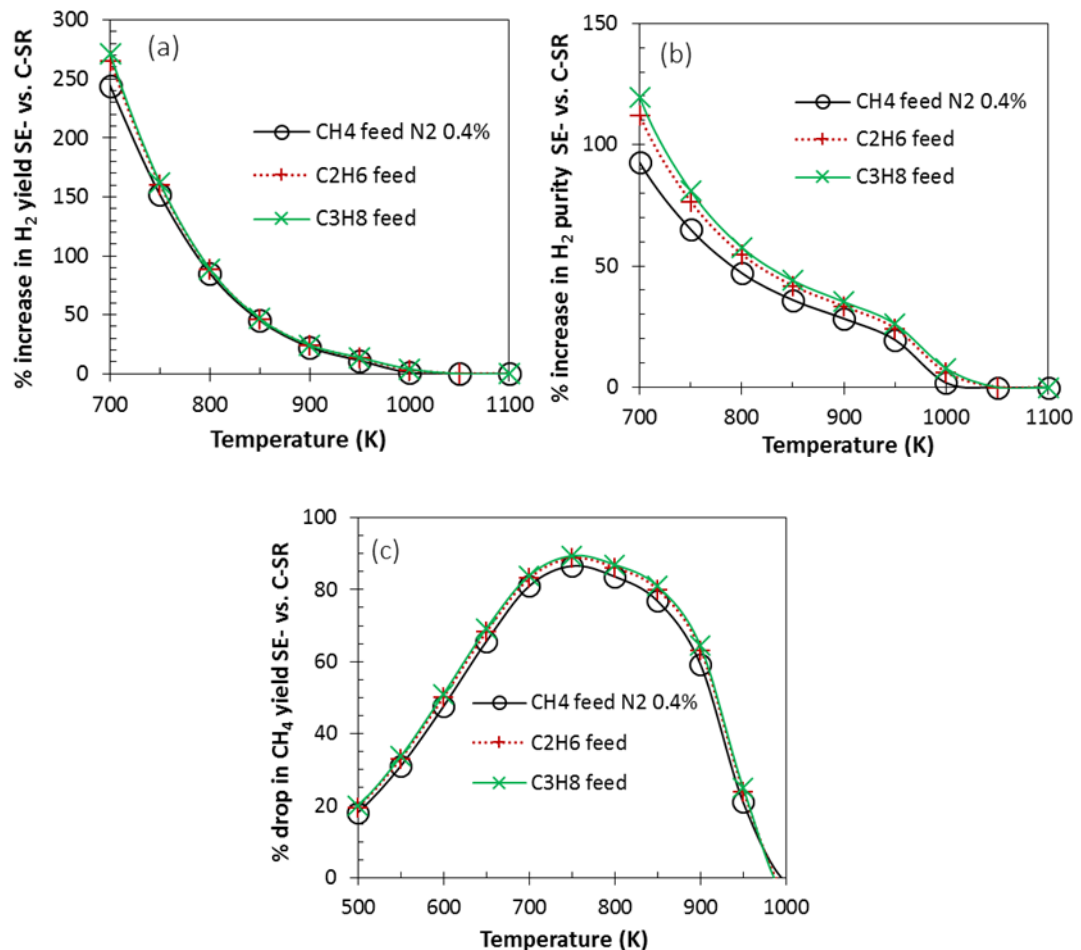


**Figure 6.3 Enhancement effects at 1 bar, S:C 3 and Ca:C 1 compared to C-SR when using feedstocks of single alkane content (CH<sub>4</sub> / C<sub>2</sub>H<sub>6</sub> / C<sub>3</sub>H<sub>8</sub>) at 99.5 vol.%, with 0.1 vol.% CO<sub>2</sub> and 0.4 vol.% N<sub>2</sub> (same inerts as in SG1). (a) % increase in H<sub>2</sub> yield (b) % increase in H<sub>2</sub> purity, (c) % drop in CH<sub>4</sub> yield.**

Similarly, sorption enhancement has a beneficial effect on the undesirable CH<sub>4</sub> yield. Figure 6.3c plots the decrease in % CH<sub>4</sub> yield introduced by the presence of CaO sorbent in ratio Ca:C = 1 compared to that of the C-SR (Eq. 8). It can be seen that, again, the % drop in CH<sub>4</sub> yield is not affected by the nature of the alkane present in the feedstock. Thus it is expected that varying the ratio of C<sub>2</sub>H<sub>6</sub> and C<sub>3</sub>H<sub>8</sub> to CH<sub>4</sub> will not affect the extent of the sorption enhancement effects for a given set of Ca:C ratio, S:C and temperature. The maximum combined enhancement effects

by introducing the CaO sorbent in the system with Ca:C of 1 in the conditions tested are observed at 750 K, which sees the CH<sub>4</sub> yield decrease by 85-90%, concurrent with 150-160 % increase in H<sub>2</sub> yield and 65-81 % increase in H<sub>2</sub> purity.

### **6.2.3 Magnitude of sorption enhancement effects due to N<sub>2</sub> and CO<sub>2</sub> content in the feed gas**

Another characteristic of the shale gases and conventional natural gases is their varying content in non-hydrocarbon gases, represented by the CO<sub>2</sub> and N<sub>2</sub>. CO<sub>2</sub> and N<sub>2</sub> content in the feed gas may not perform the same role in the predicted equilibrium sorption enhancement effects. N<sub>2</sub> has little participation in the main reactions, except for the little ammonia that may be predicted, its presence changes the partial pressures of the other gas species in the equilibrium system. In contrast CO<sub>2</sub> is the product of steam reforming, water gas shift and calcium carbonate decomposition, its presence in the feed would affect not only the partial pressures of other gases but would also shift the equilibrium of these reactions.

#### **6.2.3.1 Sorption enhancements variation with N<sub>2</sub> content**

Figure 6.4(a and b) plots the percent relative increases brought about by CaO in the steam reforming process (SE-SR at Ca:C of 1) to both H<sub>2</sub> yield and H<sub>2</sub> purity compared to the sorbent free system (C-SR) for varying temperatures and S:C. The feedstock chosen for the study was a composition of SG consisting of just CH<sub>4</sub>, CO<sub>2</sub> (0.1 vol%, like SG1) and N<sub>2</sub>, where N<sub>2</sub> was varied between 0.4 vol.% and 70 vol.%, with increments of 10 vol.%. For the purpose of clarity, Figure 6.4 only shows the results for N<sub>2</sub> in the feed gas of 0.4, 40 and 70 vol %.

Figure 6.4c shows the percent relative drop in CH<sub>4</sub> yield caused by a Ca:C of 1 in the steam reforming process (SE-SR) compared to the Ca-free process (C-SR). It can be seen that increasing the inert gas N<sub>2</sub> in the feed has small but non negligible effects on the enhancement effects as measured by increases in H<sub>2</sub> yield and purity as well as drop in CH<sub>4</sub> yield (i.e, increase in CH<sub>4</sub> conversion). For a given reforming temperature, as N<sub>2</sub> vol.% increases in the feed, the enhancement on H<sub>2</sub> yield decreases, that on H<sub>2</sub> purity increases, while the inhibition of CH<sub>4</sub> yield increases. For the whole range of N<sub>2</sub> vol.%, the inhibition of CH<sub>4</sub> yield peaked at 750 K, beyond which the differences in inhibition of CH<sub>4</sub> yield disappeared, and all inhibition effect was negligible at 1000 K. Given that sorption enhanced steam reforming at 1 atm and S:C of 3 would be conducted at temperatures above 700 K and below 900 K to maximise H<sub>2</sub> yield and purity

(Figure 6.1 and 6.2a), then highest enhancement effects would be achieved for feed gas with little N<sub>2</sub> dilution.

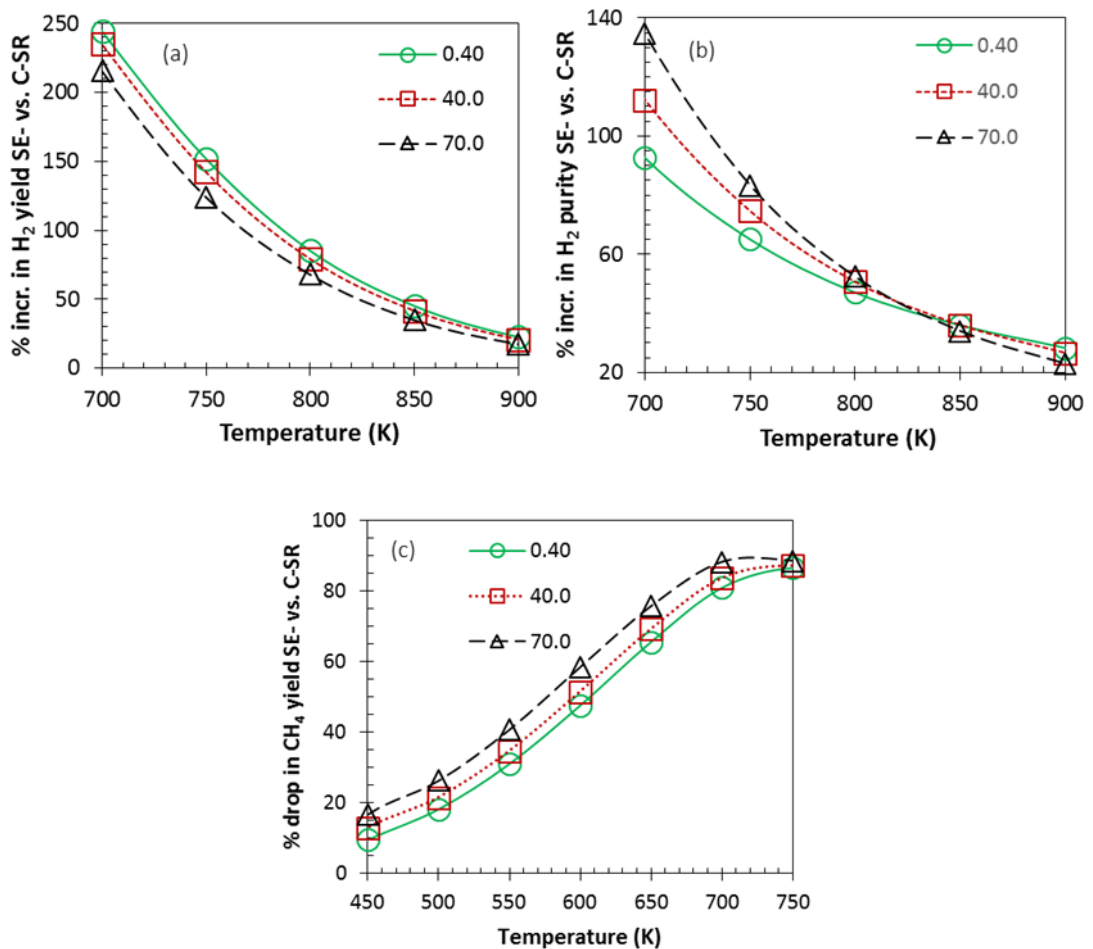


Figure 6.4 Enhancement effects at 1 bar, S:C 3 and Ca:C 1 compared to C-SR when using feedstocks of single alkane content CH<sub>4</sub>, with 0.1 vol.% CO<sub>2</sub> and varying N<sub>2</sub> content between 0.4 and 70 vol.% (a) % increase in H<sub>2</sub> yield (b) % increase in H<sub>2</sub> purity, (c) % drop in CH<sub>4</sub> yield

### 6.2.3.2 Sorption enhancements variation with CO<sub>2</sub> content in the feed

The range of CO<sub>2</sub> content in the feed gas investigated here is 0.1-40 vol.%, as CO<sub>2</sub> content is unlikely to exceed 40 vol.% (typical of biogas composition). Enhancements effects were considered for feed gases with only CH<sub>4</sub> as the hydrocarbon content, with a Ca:C of 1 which included the carbon from the CO<sub>2</sub> in the feed, and a N<sub>2</sub> vol.% of 0.4 (as in SG1). Figure 6.5(a-c) shows the increases in H<sub>2</sub> yield and H<sub>2</sub> purity and the drop in CH<sub>4</sub> yield of SE-SR vs. the C-SR.

For the range of CO<sub>2</sub> content investigated (0.1-40 vol.%) , increases in H<sub>2</sub> yield between SE-SR and C-SR were more significant for the larger CO<sub>2</sub> content and for lower temperatures. The difference in enhancement between the different CO<sub>2</sub> contents dropped steadily with increasing temperature. A similar effect was found for H<sub>2</sub> purity. This can be explained by the presence of the CO<sub>2</sub> sorbent in Ca to feed Carbon molar ratio of 1 acting in two ways, as capture of the inert feed CO<sub>2</sub> and as equilibrium shift agent by removing a gas reaction product of steam reforming and water gas shift, unlike the inert N<sub>2</sub>. In contrast, the drop in CH<sub>4</sub> yield in the temperature region favourable to methanation was found to be insensitive to CO<sub>2</sub> content, and peaked at 750 K.

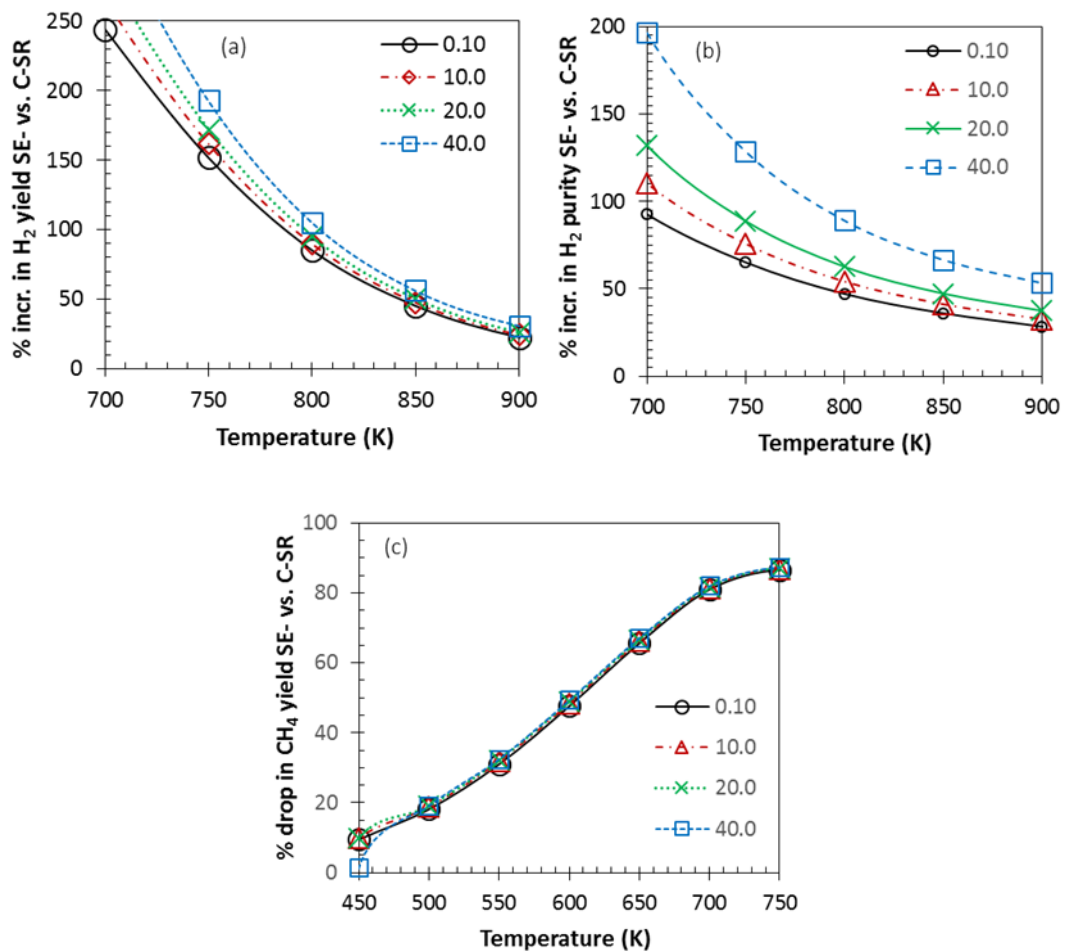


Figure 6.5 Enhancement effects at 1 bar, S:C 3 and Ca:C 1 compared to C-SR when using feedstocks of single alkane content CH<sub>4</sub>, with 0.4 vol.% N<sub>2</sub> and varying CO<sub>2</sub> content between 0.1 and 40 vol.% (a) % increase in H<sub>2</sub> yield (b) % increase in H<sub>2</sub> purity, (c) % drop in CH<sub>4</sub> yield

Performing tests at higher vol.% of CO<sub>2</sub> than 40 vol.% yielded contrasting results with those obtained below 40 vol.% and were attributed to a CO<sub>2</sub>: hydrocarbon C ratio larger than 1,

resulting in significant solid carbon product predicted for the C-SR equilibrium and non-monotonic enhancement effects for SE-SR compared to C-SR (not shown).

#### 6.2.4 Enhancement effects of SE-SR vs. C-SR for SG1-4

Differences in SG1, SG2, SG3 and SG4's compositions, which represent real shale gases, are characterised by their varying C1+ alkane content, ie. 4.5-20.1 vol.% of (C<sub>2</sub>H<sub>6</sub> +C<sub>3</sub>H<sub>8</sub>), almost constant CO<sub>2</sub> content (0-3%), and significantly changing N<sub>2</sub> content (0.4-65.0 vol.%), with several species compositions altering simultaneously from one SG to the next. It was determined in 6.2.3 that for a given reforming temperature and S:C ratio, percent increases in H<sub>2</sub> yield and percent drops in CH<sub>4</sub> yield (SE-SR vs. C-SR) were not sensitive individually to either presence of C1+ content (CH<sub>4</sub>/C<sub>2</sub>H<sub>6</sub>/C<sub>3</sub>H<sub>8</sub>) in the feed, nor to CO<sub>2</sub> content in the 0.1-10.0 vol.% range, but were slightly affected by varying N<sub>2</sub> content in the 0.4-70.0 vol.% range. This explains that the percent increases in H<sub>2</sub> yield and purity, and percent drops in CH<sub>4</sub> yield when considering in turn SG1-4, exhibited also a small quasi linear dependence on the N<sub>2</sub> content in the shale gas, but not on their other compounds. This is illustrated in Figure 6.6 below.

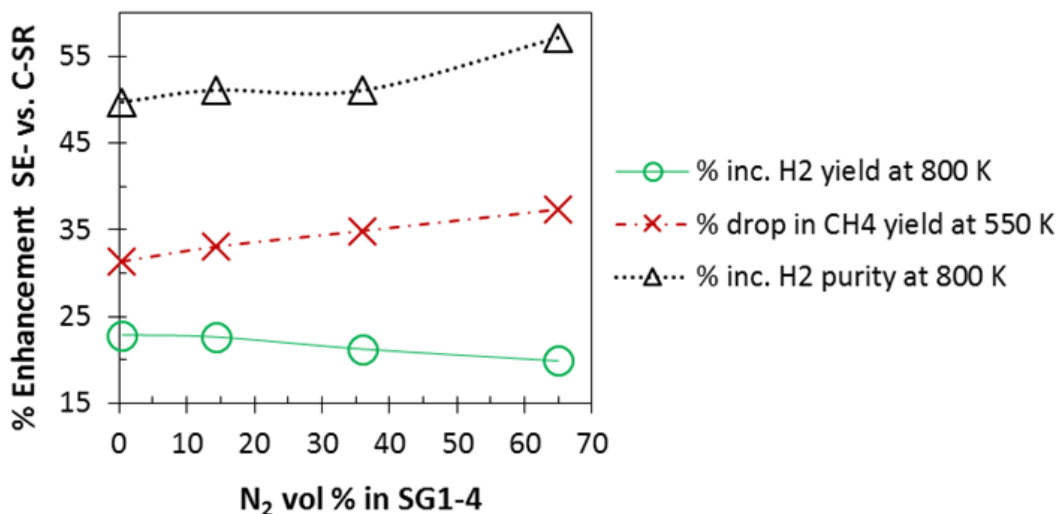


Figure 6.6 Magnitude of enhancement effects between SE-SR and C-SR as function of N<sub>2</sub> content in the shale gases SG1-4, represented by percent increases in H<sub>2</sub> yield and purity at 800 K and % drop in CH<sub>4</sub> yield at 550 K.

#### 6.2.5 Effect of temperature on SE-SR process output

Maximum water and minimum CO<sub>2</sub> yield in the equilibrium products was seen in the low temperature zone in agreement with methanation reactions. The methane conversion was particularly negative (output higher than the input) in the low temperature range (298-540 K).

As temperature rose the yield of methane dropped gradually, and CO<sub>2</sub> dominated. Nearly complete conversion of fuel (shale gas) was observed for all the temperatures investigated. Both shale gases required temperature in the range of 900-1000 K to undergo thermal decomposition and begin converting significantly to H<sub>2</sub> at S:C 0. For S:C of 1, 2, and 3, H<sub>2</sub> yield and purity increased steeply as temperature increased (Figure not shown). This was caused by shift from the strongly exothermic methanation reaction favoured at low temperature to endothermic steam methane reforming favoured at high temperatures. As soon as a certain point limit is reached, at about 700 K approximately, H<sub>2</sub> yield and purity stabilised and then declined at a point, where a gentle dwindling in H<sub>2</sub> yield and purity is seen, independent of the S:C ratio. This is caused by the reverse water gas shift reaction which tends to dominate at higher temperatures. The main equilibrium products from the gas-water system at S:C ratio of 1, 2, and 3 are; CH<sub>4</sub>, CO, CO<sub>2</sub>, and H<sub>2</sub>, with the later (H<sub>2</sub>) dominating in the medium/high temperature range. Steam reforming took place significantly, dominating methanation reaction at roughly 700 K (427 °C ), as described by a sharp increase in H<sub>2</sub> yield in Figure 6.1. The condition of S:C 3, Ca:C 1 and 1 bar indicated maximum equilibrium H<sub>2</sub> yield and purity. It is interesting to note that the optimum temperature for SE-SR is in the range of 800-900 K approximately based on the maximum equilibrium output (see Table 6.2). The temperature range also corresponds to the range of maximum CO<sub>2</sub> sorption to CaCO<sub>3(s)</sub> as depicted in Figure 6.2(b).

### **6.2.6 Effect of steam to carbon ratio on process outputs**

Nearly complete water conversion (e.g. 99.9 % at 500 K maximum for shale gas '2') was seen at S:C 1 with CaO<sub>(s)</sub> sorbent in the system, no doubt this is because stoichiometric amount of water (reactant) was provided to the system. At S:C ratio of 2 and 3 incomplete water conversion was seen because water was provided in excess to the system (see Table 6.2 for maximum conversion). It was found that the effect of S:C ratio for the four SG was also dependent on the gas composition. The term 'S:C ratio' defined here as the total moles of water inputted divided by the total moles of carbon species in the feed. Consequently, the higher the moles of carbon species in the feedstock, the higher the moles of water to be used as reactant. Thus, contributing to the high H<sub>2</sub> yield, decreasing with decreasing number of carbon species in the feedstock which corresponds to decreasing concentration of water in the system. Although the maximum steam conversion (at the varied S:C ratio) was in the same range for all the varied gases, for example at S:C ratio of 3, steam conversion was in the range of 63-64 % for all the four shale gases, with almost no or negligible difference.

**Table 6.2 Maximum equilibrium outputs**

<b>H<sub>2</sub> yield (wt. % of fuel and % of stoichiometric maximum)</b>				
<b>Conditions</b>	<b>Shale gas 1</b>	<b>Shale gas 2</b>	<b>Shale gas 3</b>	<b>Shale gas 4</b>
S:C 0 With CaO	22.4 @ 1200 K 46%	17.2 @ 1200 K 48%	13.0 @ 1200 K 49%	5.4 @ 1200 K 47%
S:C 1 With CaO	37.0 @ 900 K 76%	26.3 @ 1200 K 73%	19.3 @ 1200 K 73%	8.3 @ 1200 K 72%
S:C 2 With CaO	38.6 @ 960 K 79%	29.0 @ 960 K 81%	21.2 @ 960 K 80%	9.3 @ 940 K 81%
S:C 3 With CaO	45.5 @ 880 K 93%	34.0 @ 890 K 95%	25.0 @ 880 K 94%	11.0 @ 860 K 96%
Stoich. Maximum	48.7	35.9	26.5	11.5
<b>H<sub>2</sub> purity (%)</b>				
<b>Conditions</b>	<b>Shale gas 1</b>	<b>Shale gas 2</b>	<b>Shale gas 3</b>	<b>Shale gas 4</b>
S:C 0 With CaO	63.5 @ 1200 K	61.0 @ 1200 K	55.1 @ 1200 K	39.3 @ 1200 K
S:C 1 With CaO	79.0 @ 920 K	68.0 @ 1200 K	67.0 @ 920 K	49.0 @ 1200 K
S:C 2 With CaO	92.3 @ 820 K	88.1 @ 820 K	80.4 @ 830 K	61.0 @ 840 K
S:C 3 With CaO	98.0 @ 800 K	94.0 @ 810 K	86.0 @ 810 K	67.0 @ 820 K
<b>Selectivity of C to CaCO<sub>3(s)</sub> (%)</b>				
<b>Conditions</b>	<b>Shale gas 1</b>	<b>Shale gas 2</b>	<b>Shale gas 3</b>	<b>Shale gas 4</b>
S:C 0 With CaO	0.01 @ 450 K	0.0	0.0	0.0
S:C 1 With CaO	79.0 @ 990 K	46.0 @ 780 K	45.0 @ 780 K	20.4 @ 760 K
S:C 2 With CaO	76.4 @ 810 K	77.0 @ 810 K	77.0 @ 800 K	80.2 @ 800 K
S:C 3 With CaO	93.0 @ 800 K	93.0 @ 800 K	93.1 @ 800 K	95.0 @ 780 K
<b>Water conversion (%)</b>				
<b>Conditions</b>	<b>Shale gas 1</b>	<b>Shale gas 2</b>	<b>Shale gas 3</b>	<b>Shale gas 3</b>
S:C 0 With CaO	n/a	n/a	n/a	n/a
S:C 1 With CaO	97.7 @ 1200 K	99.9 @ 500 K	99.9 @ 500 K	91.0 @ 1080 K
S:C 2 With CaO	76.9 @ 870 K	81.9 @ 690 K	82.0 @ 680 K	83.2 @ 670 K
S:C 3 With CaO	63.6 @ 720 K	63.5 @ 720 K	63.0 @ 710 K	63.1 @ 700 K

Generally speaking, steam variation (a reactant in both reforming and the water gas shift reaction process) can significantly affect the equilibrium of both reactions. S:C ratio was varied in the range of 0-3, higher values were not considered as previous study by S G Adiya et al (S G Adiya et al., 2017) and Antzara et al (Antzara et al., 2014) has showed that higher S:C ratios do not have any significant further effect on H<sub>2</sub> yield and purity. The variation of S:C ratio in SE-SR process is in agreement with Le Chatelier's principle in all the four varied gas composition,

whereby an increase in the water concentration in the system favours the equilibrium of the  $H_2$  producing reactions towards conversion of the excess water into  $H_2$ , thus triggering higher  $H_2$  yield and purity.

### **6.3 Effect of inert bed materials, hydrocarbon fractions, inert $N_2$ and $CO_2$ and on enthalpy balance**

#### **6.3.1 Effect of inert bed materials on energy balance**

Reduced energy demand was caused by the carbonation reaction in the SE-SR process even though a complete regeneration of the  $CaCO_{3(s)}$  back to  $CaO_{(s)}$  via a decarbonation step was conducted at 1170 K in the presence of a typical commercial steam reforming catalyst (18 wt.% NiO on  $\alpha-Al_2O_3$  support). The equilibrium materials balances were not affected by the presence of non-reacting solid materials in the reactor bed (catalyst and its support, and the fresh and degraded sorbent). In other words,  $H_2$  yield and purity are the same with non-reacting solid materials compared to without, as they do not have any influence on them. However, non-reacting bed materials significantly affect the energy of operating the system. This is because they would require heating or cooling as required during the operation.

This is further demonstrated in Figure 6.7(a) depicting the  $\Delta H$  ratio of shale gas 3 (used for demonstration) with degraded sorbent been higher than the system without degraded sorbent at exactly same operating condition. The effect of degraded sorbent in the bed was represented by introducing in the reactants mix the equivalent of 90 wt.% of the total molar calcium in the feed as inert CaO. The Ca:C ratio of 1 quoted in the figures refers to the active CaO. The  $\Delta H$  ratios of the system with degraded sorbent were seen to increase compared to the system with active sorbent only by 0.118 at 880 K (region of maximum  $H_2$  yield and purity), with a narrowing gap as the reforming temperature approached the regeneration temperature of 1170 K. This no doubt can be attributed to the enthalpy cost of heating the degraded sorbent as shown in Figure 6.7(c), increasing the total enthalpy of the entire process as depicted by Figure 6.7(b).

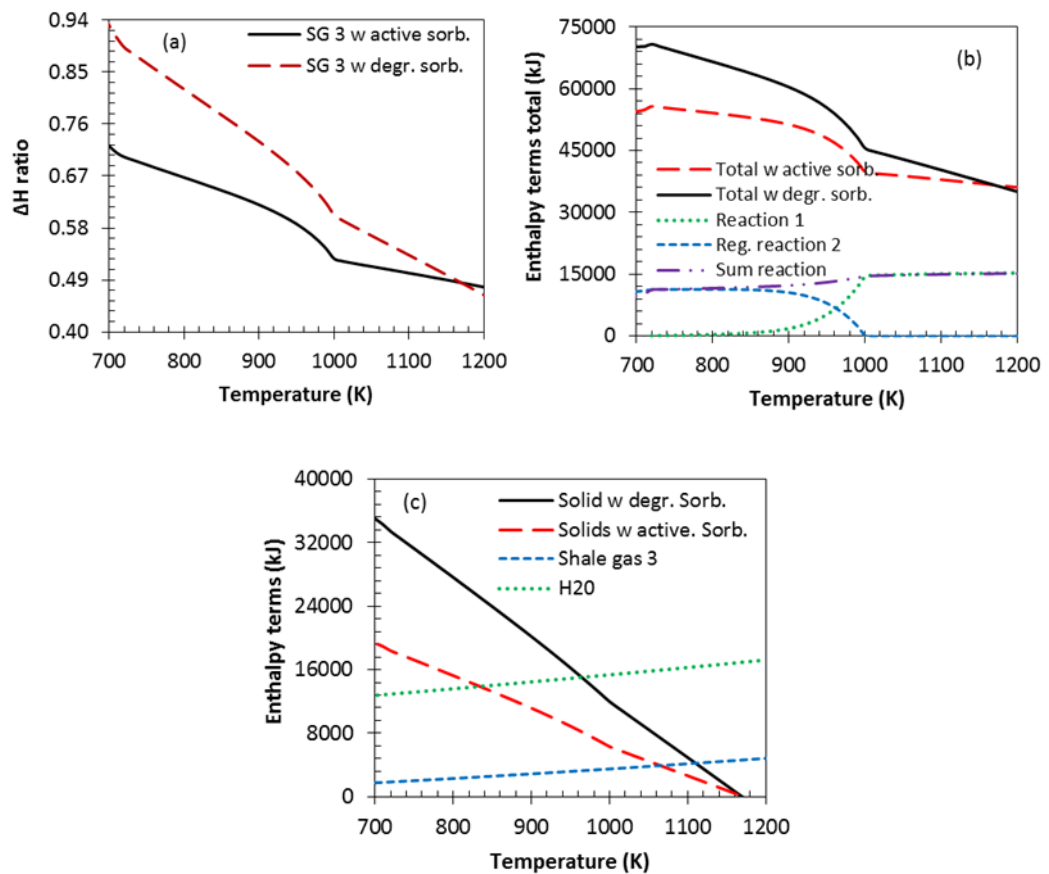
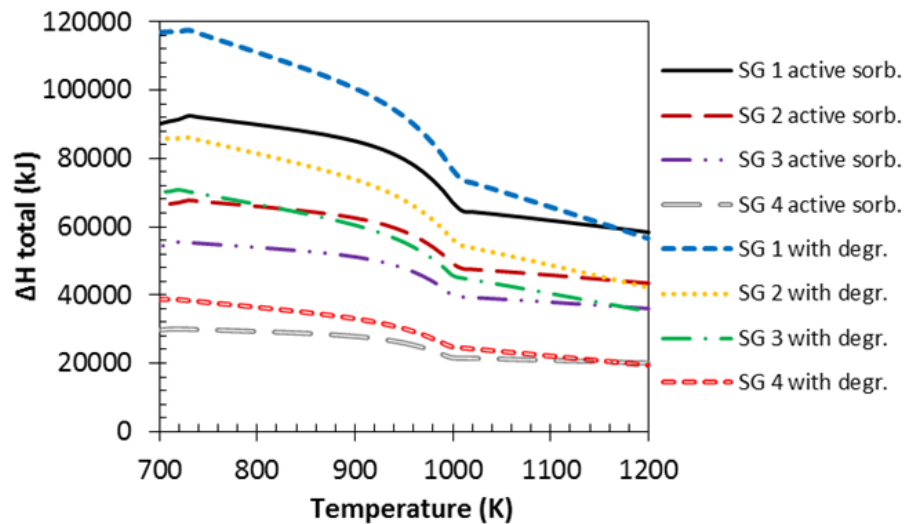


Figure 6.7 Enthalpy terms for SG3, catalyst 18 wt.% NiO/Al<sub>2</sub>O<sub>3</sub>, active Ca:C 1, S:C 3 (a) ΔH ratio vs temperature, (b) and (c) enthalpy terms vs temperature: process 2 at 1170 K, “active Sorb.”: 100 % CaO, “degr. Sorb.”: 10 % active CaO and 90 % inert CaO.

### 6.3.2 Effect of hydrocarbon fractions on enthalpy balance

The cost of heating up the gas was relatively insignificant compared to those of raising steam from liquid water feed. The total energy cost of the process was dominated by water enthalpy change accounting for over 70 % approximately of the total energy required to heat the cold reactants. Using shale gas termed ‘1’ for example at 880 K (region of maximum H<sub>2</sub> yield and purity) 88 % of the total energy required to heat the cold reactants was dominated by water. However, this decreased to 86 %, 84 % and 77 % for shale gas termed 2, 3 and 4 respectively at same conditions. This was expected since the concentration of water in each of the system was based on number of carbon concentration explained earlier. This compromise the choice of gas feedstock with high hydrocarbon content; between high cost of raising excess steam (cause by the use of high S:C ratio) balance by higher H<sub>2</sub> yield and purity (cause by the high hydrocarbon content in the feedstock). Figure 6.8 further help in analysing the energetic cost of operating

with each of the SGs. Although not particularly significant because they depend on the molar inputs chosen for the system, what matters is the relative positions of each enthalpy term profiles in the figure. The figure clearly depicts that it is more energetically costly to operate with shale gas termed 1 compared 2, 3 and 4. This energetic cost is found to be dominated by enthalpy of raising steam which is dependent on the carbon specie concentration in each of the gas.



**Figure 6.8  $\Delta H$  total vs. temperature for 18 wt.% NiO/Al<sub>2</sub>O<sub>3</sub> catalyst, active Ca:C 1, S:C 3 and SG1-4: process 2 at 1170 K, “active Sorb.”: 100 % CaO, “degr. Sorb”’: 10 % active CaO and 90 % inert CaO.**

No significant difference was found between the  $\Delta H$  ratio and total enthalpy terms in kJ/mol of H<sub>2</sub> produced of SG1-3. However, significant difference was observed between SG1 and SG4 as shown in Figure 6.9 caused by the significant concentration of N<sub>2</sub> in SG4 costing 12.00 % at 880 K of the total energy required in heating the cold reactants as opposed to 0.03 % for SG1, 1.25 % and 4.00 % for SG2 and SG3 respectively at same operating condition. The effect of N<sub>2</sub> and CO<sub>2</sub> gas fractions on steam reforming process will be discussed in more detail in the next section.

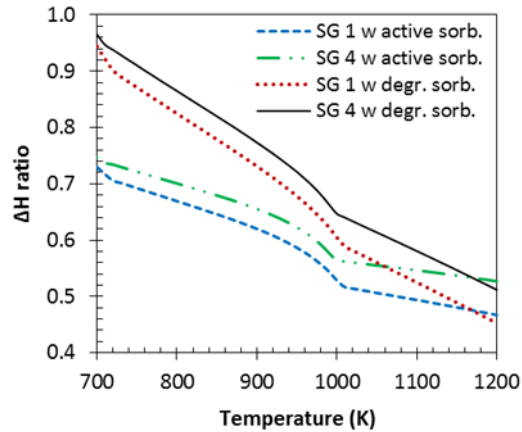


**Figure 6.9 ΔH ratio vs temperature comparing SG1-4: for 18 wt.% NiO/Al<sub>2</sub>O<sub>3</sub> catalyst, active Ca:C 1, S:C 3 and process 2 at 1170 K; “active sorbent”: 100 % CaO, “degraded sorbent”: 10 % active CaO and 90 % inert CaO.**

### 6.3.3 Effect of N<sub>2</sub> and CO<sub>2</sub> content in the feed gas on enthalpy balance

Although most gases contain inert species with varied concentrations according to their source (from 1 to over 40 %) (Laosiripojana et al., 2004) as reflected in the N<sub>2</sub> contents listed in Table 1, a gas with high hydrocarbon content and reasonable inert composition is more suitable for steam reforming from almost all perspective especially the economic part. A gas with significantly high inerts contents, as reflected by N<sub>2</sub> concentration in SG3 and SG4 particularly affects the cost of reforming plants significantly in a very negative way. This is because the energy of heating up the inert gas flow adds to the total energy of the whole process, thus increasing the cost of operating the plant. Moreover, inert gases do not directly generate H<sub>2</sub>, hence, their presence in the system has relatively no significance to H<sub>2</sub> generation. Nonetheless, a positive effect of inert gas content in the shale gas is that the partial pressure of the N<sub>2</sub> reduces that of the reactants (e.g CH<sub>4</sub> and steam) in the system, thus favouring the equilibrium of the steam reforming process in accordance with Le Chatelier’s principle and as proved by several laboratory scale studies (Zhu et al., 2001).

The effect of CO<sub>2</sub> in the shale gas feedstock, has, by comparison a more negative effect on the SR due to CO<sub>2</sub> being one of the desirable products of the shale gas conversion and the equilibrium shift towards methanation and reverse water gas shift at medium temperatures. However, gases with significant amount of CO<sub>2</sub> can generate H<sub>2</sub> through dry reforming of CH<sub>4</sub> at

higher temperatures (R5) (Olsbye et al., 1997, Barroso Quiroga and Castro Luna, 2007), but studies on the rate of the reaction while occurring simultaneously with steam reforming are limited/not available. For the SE-SR process, significant concentration or flow of CO<sub>2</sub> can lead to fast saturation of the sorbent, which in turn will increase the cost of operation either by frequent regeneration of the sorbent or require over-sizing of the sorbent bed. The increased frequency of regeneration may also result in faster loss of sorbent capacity owing to deactivation over repeated use. According to an experiment represented by Laosiripojana et al (Laosiripojana et al., 2004), both CO<sub>2</sub> and H<sub>2</sub>S inhibit methane steam reforming rate over both catalysts (Ni/CeO<sub>2</sub> and Ni/Al<sub>2</sub>O<sub>3</sub>) investigated and subsequently caused a decreased on H<sub>2</sub> production yield.

## 6.4 Conclusion and final remarks

A detailed thermodynamic equilibrium analysis of four varied shale gas composition (as represented by content in higher hydrocarbon, inert N<sub>2</sub> and CO<sub>2</sub> gas in the various gases, with methane always being the main hydrocarbon component) in the presence of CaO sorbent for H<sub>2</sub> production has been conducted. The influence of hydrocarbon fractions, temperature, S:C ratio, inert N<sub>2</sub>, CO<sub>2</sub> gas and inert bed materials on equilibrium yield and enthalpy balance has been investigated. The analysis yielded the following fundamental insights and recommendations:

H<sub>2</sub> yield and purity was not only dependent on temperature and S:C ratio but also on the content of hydrocarbons in the gases. H<sub>2</sub> yield and purity decrease in succession of the hydrocarbon content (i.e. SG 1 > SG 2 > SG 3 > SG 4). Up to 25 %, 45 % and 76 % decrease in maximum H<sub>2</sub> yield was seen in SG2-4 respectively compared to SG1 with the highest hydrocarbon content. The magnitude of enhancement effects brought on by sorption enhanced steam reforming compared to conventional steam reforming at given temperature and steam to carbon ratio are not dependent on the alkane mix, nor the CO<sub>2</sub> content in the feed (0.1-10 vol. %), but slightly dependent on the nitrogen content in the feed (0.4-70 vol%), with larger H<sub>2</sub> purity enhancement but lower H<sub>2</sub> yield enhancement for larger N<sub>2</sub> content, inhibition of methanation is also larger for larger N<sub>2</sub> content at temperatures below 750 K. The conditions of S:C 3, 1 bar, and temperature range of 800-900 K are optimal conditions of SE-SR process.

SE-SR could have considerable advantages for H<sub>2</sub> production because of the substantial increase in H<sub>2</sub> yield and purity, as well as significant drop in temperature of the maximum H<sub>2</sub> yield with effective capture of CO<sub>2</sub> under well-chosen operational conditions. Near full sorption

enhancement (over 90 % efficiency of CO<sub>2</sub> capture) was seen in the temperature range of about 880-900 K, this will reduce, if not eliminate, the need for further purification steps required in C-SR as well as minimise the cost of operating the system, depending on the purity requirement and end use of the H<sub>2</sub> produced. The opportunity of operating the system at low temperature (due to the presence of Ca sorbent) could in turn decrease the need to operate at high pressure, thus, favouring the H<sub>2</sub> producing reactions. The presence of degraded CO<sub>2</sub> sorbent in the reactor bed introduces a heating burden associated with heating the material from reforming temperature to sorbent regeneration temperature.

## Chapter 7 Conclusion and future work

*The work carried out in this thesis has shown the importance of coupling sorption enhancement (SE) and chemical looping (CL) in conventional steam reforming (C-SR) process. A conclusion and final remarks on the thermodynamic equilibrium and experimental studies are given in this chapter, including the major findings of the studies. Recommendations for future work that could not be investigated owing to time limitation are also given in the chapter.*

### 7.1 Conclusion and final remarks

Using ideal materials properties, represented by an oxygen transfer material little diluted by inert support, and by fully active Ca-based CO<sub>2</sub> sorbent, sorption enhanced chemical looping steam reforming at equilibrium, as predicted by minimisation of Gibbs energy can have considerable advantages compared to conventional steam reforming for H<sub>2</sub> production because of the substantial increase in H<sub>2</sub> yield and purity, as well as significant drop in temperature of the maximum H<sub>2</sub> yield with effective capture of CO<sub>2</sub> under well-chosen operational conditions. The opportunity of operating the Ca sorbent system at a low temperature could in turn decrease the need to operate at the higher pressure end, thus thermodynamically favouring the H<sub>2</sub> producing reactions. In the ideal bed materials conditions, near full sorption enhancement (over 95% efficiency of CO<sub>2</sub> capture) is predicted for 700–900 K and atmospheric pressure, this would have nearly eliminated the need for further purification steps (CO shift, PSA) as well as minimising the energy cost of operating the system. The energetic cost of shale gas reforming with and without Ca in the system is dominated by the enthalpy change of heating up the liquid water at 298 K and phase transformation to superheated steam at the reaction temperature, depending on S:C ratio in use. The choice of S:C ratio in conditions of excess steam represents a compromise between the higher H<sub>2</sub> yield and purity and low risk of solid carbon formation balanced by the increased energy demand of raising excess steam. The greater the S:C ratio of choice, the greater the enthalpy change of raising the steam will be, and vice versa. Addition of NiO to steam reforming system will decrease the thermal energy requirement of the process. Synergetic enhancement effects (favourable equilibrium shifts) are observed by the generation of steam from the NiO reduction step, which in turn promotes the steam consuming H<sub>2</sub> production and CO<sub>2</sub> generating reactions while CO<sub>2</sub> is captured, allowing for safe operation (non carbon generating, high H<sub>2</sub> yield) at lower temperatures and lower S:C ratios than the conventional process with excess heat.

Atmospheric pressure and S:C ratio of 3 are found to be optimum for each of the studied processes. Temperature range between 1000 and 1010 K is best for the C-SR process, while 870 to 1000 K temperatures are optimum for CL-SR process. On the other hand the range 700 to 850 K are most beneficial for the SE-SR and SE-CLSR processes. Up to 49% and 52% rise in H<sub>2</sub> yield and purity respectively were predicted with SE-CLSR at equilibrium compared to C-SR at S:C 3 and 800 K. The enthalpy of bringing the system to equilibrium also decreased significantly in the system. A minimum energy of 159 kJ is required to produce 1 mol of H<sub>2</sub> at S:C 3 and 800 K in C-SR process, this significantly drops to 34 kJ/mol of produced H<sub>2</sub> in the CaO<sub>(s)</sub>/NiO system at same operating condition without regeneration of the sorbent, but when the energy of regenerating the sorbent at 1170 K was included, the enthalpy rose to 92 kJ/mol H<sub>2</sub>. This is still significantly lower than the Ca-free system.

Presence of inert bed materials in the reactor bed such as catalyst support or degraded CO<sub>2</sub> sorbent introduce a very substantial heating burden to bring these materials from reforming temperature to sorbent regeneration temperature or to Ni oxidation temperature, if different. Motivation for future research in the SE-CLSR process ought to focus on these two issues in order to maintain the theoretical advantages of SE-CLSR over the conventional steam reforming process.

Investigating the influence of gas composition on steam reforming, it was found that predicted H<sub>2</sub> yield and purity at equilibrium was not only dependent on temperature and S:C ratio but also on the content of hydrocarbons in the gases. H<sub>2</sub> yield and purity decrease in succession of the hydrocarbon content (i.e. SG 1 > SG 2 > SG 3 > SG 4). Up to 25 %, 45 % and 76 % decrease in maximum H<sub>2</sub> yield was seen in SG2-4 respectively compared to SG1 with the highest hydrocarbon content. The magnitude of enhancement effects brought on by SE-SR compared to C-SR at given temperature and steam to carbon ratio is not dependent on the alkane mix, nor the CO<sub>2</sub> content in the feed (0.1-10 vol. %), but slightly dependent on the nitrogen content in the feed (0.4-70 vol%), with larger H<sub>2</sub> purity enhancement but lower H<sub>2</sub> yield enhancement for larger N<sub>2</sub> content, inhibition of methanation is also larger for larger N<sub>2</sub> content at temperatures below 750 K.

The experimental studies on a bench scale packed bed reactor on the other hand yielded the following conclusions; increasing the GHSV decreases the contact time of the reactant in the reactor, thus operating at the lowest possible GHSV is more suitable in a steam reforming

process. High operating temperatures are in favour of the strong endothermic steam reforming reaction but to the detriment of the water gas shift reaction. The influence of catalyst support and NiO loading was not evident at low/medium operating temperature (600 and 650 °C). However, at higher temperature (700 and 750 °C), Ni on CaO/Al<sub>2</sub>O<sub>3</sub> support catalyst showed better performance than the Ni on Al<sub>2</sub>O<sub>3</sub> support with regards to feed conversion and product yield caused by the alkalinity of CaO, suppressing solid carbon formation on the surface of the catalyst.

In order to define the optimum experimental operating conditions for the SE-CLSR process, an investigation of the sorption enhanced process termed SE-SR process and chemical looped process termed CL-SR was conducted at S:C of 3 and GHSV of 0.498. The effect of Ca based CaO sorbent and operating temperature in the range of 600-700 °C was studied experimentally in a bench scale packed bed reactor with Nickel catalysts. It was found that low/medium operating temperature is more suitable for a SE-SR process owing to the thermal decomposition of CaO sorbent at high temperatures, in addition to that, the carbonation process is favoured thermodynamically in low/medium temperature range. It was also discovered that the presence of a Ca based CO<sub>2</sub> sorbent has the potential to significantly increase H<sub>2</sub> yield and purity as well decreased the cost of operating the system because of the mild operating condition the process permits. The influence of chemical looping on steam reforming (CL-SR process) was investigated at 650 °C and 750 °C using Ni on Al<sub>2</sub>O<sub>3</sub> support and Ni on CaO/Al<sub>2</sub>O<sub>3</sub> support as OTM/catalyst respectively. Both materials demonstrated good performance as bi-functional OTM/catalyst with better process outputs compared to the C-SR process. The case with Ni on Al<sub>2</sub>O<sub>3</sub> support at 650 °C showed excellent stability without significant deterioration in the performance for 20 successive redox-oxidation cycles, corresponding to 80 h of testing. Nonetheless, fuel conversion was low, below 70 %, caused by the low operating temperature use. Ni on CaO/Al<sub>2</sub>O<sub>3</sub> support tested at 750 °C showed a significant deterioration after about 9 successive redox-oxidation cycles approximately, corresponding to 80 h of testing as well. However, fuel conversion was high (over 80 % approximately prior to deterioration of the OTM/catalyst), that can be strongly attributed to the high temperature in favoured of steam reforming process. The deterioration

in the activity of the OTM/catalyst was caused by the partial burning off of the solid carbon deposition on the surface of the OTM/catalyst confirmed during the CHNS analysis.

High purity H<sub>2</sub> was generated using a novel low energy consumption process termed SE-CLSR process using a model gas mixture representing actual shale gas as feedstock (Marcellus). The feasibility of the intensified C-SR process (coupled with sorption enhancement and chemical looping) was demonstrated experimentally over a mixture of a bifunctional NiO-based OTM/catalyst supported on Al<sub>2</sub>O<sub>3</sub> and a Ca-based CaO sorbent. 20 redox-oxidation-calcination cycles of experiments were performed in a bench-scale fixed bed reactor at 1 bar, GHSV 0.498, S:C 3 and 650 °C. High hydrogen yield of 31 wt. % and purity of 92 % was obtained (in the 4<sup>th</sup> cycle) during the pre-breakthrough period of the SE-CLSR process (prior to cycles with low sorbent capacity). The H<sub>2</sub> yield of the post breakthrough period did not degenerate fully to that of the C-SR process due to OTM/catalyst bed dilution with the CaO sorbent material and decreased in the quantity of catalyst compared to the C-SR process. The surface area of the sorbent and OTM/catalyst mixture after 20 redox-calcination-oxidation cycles underwent a slight decrease compared fresh mixture of the sorbent and OTM/catalyst caused by sintering and pore blockage after repeated cyclic absorption-desorption cycles. The FESEM images of the mixture also showed sintering and agglomeration on the reacted sorbent and OTM/catalyst mixture. Sorbent regeneration and Ni oxidation to NiO at 850 °C using pure air feed successfully burned off the solid carbon deposited on the surface of the sorbent and OTM/catalyst mixture. Regeneration and oxidation of the CaO sorbent and OTM/catalyst was also accomplished at the same temperature.

The results of the experimental analysis have confirmed that there are important potential benefits of coupling C-SR with sorption enhancement and chemical looping compared to the typical C-SR process in packed bed configuration. The SE-CLSR process is an advanced integrated technology for high purity H<sub>2</sub> generation with in-situ CO<sub>2</sub> capture. The process can be operated with very low overall CO<sub>2</sub> released from the system as opposed to the C-SR process, since the steam reforming reaction is accompanied with CO<sub>2</sub> capture. The re-oxidation of the reduced OTM/catalyst can cover a large part of the heat required for the endothermic sorbent regeneration, further decreasing the overall heat demands of the process. However, for the process to be commercially applicable, a more advanced analysis of the SE-CLSR process is

necessary, together with detailed technological and economic analysis and whole process design for scaling purposes. Yet, it is obvious that the combination of sorption enhancement and chemical looping on C-SR process has great prospects for high H<sub>2</sub> yield and purity generation at reasonable lower cost and high energy efficiency.

## **7.2 Recommendation and Future work**

SE-CLSR is a complicated process in development, there is always areas requiring further study. From the present study (including literature review), some areas that could not be investigated owing to time limitation, thus, suggested for future investigations, include:

- Detailed investigation on the effect of sorbent degradation on the performance of sorption enhanced processes and how it can be overcome
- Analysis on the performance of different support materials to improve the stability of CaO sorbent
- Experimental studies addressing the influence of pressure on sorbent regeneration during the cyclic reforming and regeneration steps
- Investigation on the performance of different catalyst with dual actions (catalyst and OTM) via SE-CLSR
- Simple flow sheet and numerical model validation using Aspen Plus, gPROMS or other software(s)
- Stimulation of refinery hydrogen plant by replacing the C-SR process used presently with SE-CLSR process
- Detailed technological and economic analysis and whole process design for scaling purposes.

## References

- AASBERG-PETERSEN, K., CHRISTENSEN, T. S., DYBKJAER, I., OSTBERG, M., COERTZEN, R. M., SEHESTED, J., KEYSER, M. J. & STEYNBERG, A. P. 2004. *Synthesis gas production for FTsynthesis*, Amsterdam: Elsevier, Fischer-Tropsch technology.
- ABAD, A., ADÁNEZ-RUBIO, I., GAYÁN, P., GARCÍA-LABIANO, F., DIEGO, L. F. D. & ADÁNEZ, J. 2012. Demonstration of chemical-looping with oxygen uncoupling (CLOU) process in a 1.5 kWth continuously operating unit using a Cu-based oxygen-carrier. *International Journal of Greenhouse Gas Control*, 6, 189–200.
- ABADA, A., MATTISSON, T., LYNGBELT, A. & JOHANSSON, M. 2007. The use of iron oxide as oxygen carrier in a chemical-looping reactor. *Fuel*, 86, 1021–1035.
- ABBAS, S. Z., DUPONT, V. & MAHMUD, T. 2016. Kinetics study and modelling of steam methane reforming process over a NiO/Al<sub>2</sub>O<sub>3</sub> catalyst in an adiabatic packed bed reactor. *International Journal of Hydrogen Energy*, 42, 2889–2903.
- ABRARDO, J. M., KHURANA, V. & 1995. Hydrogen technologies to meet refiner's future need. *Hydrocarbon Processing*, 74, 43-49.
- ADANEZ, J., ABAD, A., GARCIA-LABIANO, F., GAYAN, P. & DIEGO, L. F. D. 2012. Progress in Chemical-Looping Combustion and Reforming technologies. *Progress in Energy and Combustion Science*, 38, 215-282.
- ADÁNEZ, J., DIEGO, L. F. D., GARCÍA-LABIANO, F., GAYÁN, P. & ABAD, A. 2004. Selection of oxygen carriers for chemical-looping combustion. *Energy & Fuels*, 18, 371-377.
- ADRIS, A. M., PRUDEN, B. B., LIM, C. J. & GRACE, J. R. 1996. On the reported attempts to radically improve the performance of the steam methane reforming reactor. *The Canadian Journal of Chemical Engineering*, 74, 177-186.
- AHMADA, H., KAMARUDINA, S. K., MINGGUA, L. J. & KASSIMA, M. 2015. Hydrogen from photo-catalytic water splitting process: A review. *Renewable and Sustainable Energy Reviews*, 43, 599-610.
- AHMED, S., KRUMPELT, M., KUMAR, R., LEE, S., CARTER, J., WILKENHOENER, R. & MARSHALL, C. 1998. Catalytic Partial Oxidation Reforming of Hydrocarbon Fuels. *Fuel cell seminar, Palm Springs, CA*.
- AITANI, A. M. 1995. Catalytic Naphtha Reforming. In: ANTOS, G. J., AITANI, A. M. & PARERA, J. M. (eds.). New York: Mercel Dekker.
- AITANI, A. M. 1996. Processes to enhance refinery-hydrogen production. *International Journal of Hydrogen Energy*, 21, 267-271.
- AKERS, W. & CAMP, D. 1955. Kinetics of the methane steam reaction. *AIChE Journal*, 1, 471-475.
- ALBRECHT, K. O., SATRIO, J. A., SHANKS, B. H. & WHEELLOCK, T. D. 2010. Application of a combined catalyst and sorbent for steam reforming of methane. *Industrial & Engineering Chemistry Research*, 49, 4091-4098.
- ALLAM, R. J., CHIANG, R., HUFTON, R., MIDDLETON, P., WEIST, E. L. & WHITE, V. 2005. *Development of the sorption enhanced water gas shift process. Carbon dioxide capture for storage in deep geologic formations*, Oxford, Elsevier.
- ALVES, J. J. & TOWLER, G. P. 2002. Analysis of Refinery Hydrogen Distribution Systems. *Industrial & Engineering Chemistry Research*, 41, 5759-5769.
- ANCHEYTA, J. & SPEIGHT, J. G. 2007. *Hydroprocessing of Heavy Oils and Residua*, London, Taylor & Francis.
- ANDERSON, D. M., KOTTKE, P. A. & FEDOROV, A. G. 2014. Thermodynamic analysis of hydrogen production via sorption-enhanced steam methane reforming in a new class of variable volume batch-membrane reactor. *International Journal of Hydrogen Energy*, 39, 17985–17997.

- ANON. 2008a. *Hydrogen (H<sub>2</sub>) Properties, Uses, Applications Hydrogen Gas and Liquid Hydrogen* [Online]. Easton, PA. : Universal Industrial Gases. Available: <http://www.uigi.com/hydrogen.html> [Accessed 4 February 2015].
- ANON. 2008c. *Hydrogen production: Proposed rule for mandatory reporting of greenhouse gases* [Online]. Office of Air and Radiation, U.S. Environmental Protection Agency. Available: <http://nepis.epa.gov/Exe/ZyNET.exe/P10054D9.TXT?ZyActionD=ZyDocument&Client=EPA&Index=2006+Thru+2010&Docs=&Query=&Time=&EndTime=&SearchMethod=1&TocRestrict=n&Toc=&TocEntry=&QField=&QFieldYear=&QFieldMonth=&QFieldDay=&IntQFieldOp=0&ExtQFieldOp=0&XmlQuery=&File=D%3A%5Czyfiles%5CIndex%20Data%5C06thru10%5Ctxt%5C00000011%5CP10054D9.txt&User=ANONYMOUS&Password=anonymous&SortMethod=h%7C-&MaximumDocuments=1&FuzzyDegree=0&ImageQuality=r75g8/r75g8/x150y150g16/i425&Display=p%7Cf&DefSeekPage=x&SearchBack=ZyActionL&Back=ZyActionS&BackDesc=Results%20page&MaximumPages=1&ZyEntry=1&SeekPage=x&ZyPURL> [Accessed 4 February 2015].
- ANON 2008f. *The Impact of Increased Use of Hydrogen on Petroleum Consumption and Carbon Dioxide Emissions*. Washington: U.S. Department of Energy.
- ANON. 2013. *The effects of shale gas production on natural gas prices*. PPI Energy and Chemicals Team. U.S. Bureau of Labor Statistics [Online]. Available: <http://www.bls.gov/opub/btn/volume-2/the-effects-of-shale-gas-production-on-natural-gas-prices.htm> [Accessed 29 November 2013].
- ANON. 2014. *Ammonia global market to 2020 - Food security concerns driving demand for ammonia-based fertilizers* [Online]. Research and Markets. Available: <http://www.prnewswire.com/news-releases/ammonia-global-market-to-2020---food-security-concerns-driving-demand-for-ammonia-based-fertilizers-216913621.html> [Accessed 9 March 2015].
- ANON. 2015. *Shale gas production in the United States from 1999 to 2015 (in trillion cubic feet)* [Online]. Statista. Available: <http://www.statista.com/statistics/183740/shale-gas-production-in-the-united-states-since-1999/> [Accessed 23 May 2015].
- ANON. c2000. *Refining overview - Petroleum, Process and Products* [Online]. New York: The Fuels and Petrochemical Divisions of AIChE. Available: [www.aiche-fpd.org/listing/Refinery\\_overview.pdf](http://www.aiche-fpd.org/listing/Refinery_overview.pdf) [Accessed 20 November 2013].
- ANON c2005. *Catalysis in petroleum and petrochemical industries* In: BHATTACHARYYA, K. G. & TALUKDAR, A. K. (eds.). New Delhi: Narosa Publishing House Pvt. Ltd.
- ANON. c2015. *CO<sub>2</sub> capture from hydrogen production* [Online]. Union Engineering. Available: <http://www.union.dk/reference-cases/oil-gas/co2-capture-from-hydrogen-production/> [Accessed 4 February 2015].
- ANTZARA, A., HERACLEOUS, E., BUKUR, D. B. & LEMONIDOU, A. A. 2014. Thermodynamic Analysis of Hydrogen Production via Chemical Looping Steam Methane Reforming Coupled with in Situ CO<sub>2</sub> Capture. *Energy Procedia*, 63, 6576-6589.
- ANTZARA, A., HERACLEOUS, E., BUKUR, D. B. & LEMONIDOU, A. A. 2015. Thermodynamic analysis of hydrogen production via chemical looping steam methane reforming coupled with in situ CO<sub>2</sub> capture. *International Journal of Greenhouse Gas Control*, 32, 115-128.
- ANTZARA, A., HERACLEOUS, E. & LEMONIDOU, A. A. 2016a. Energy efficient sorption enhanced-chemical looping methane reforming process for high-purity H<sub>2</sub> production: Experimental proof-of-concept. *Applied Energy*, 180, 457-471.
- ANTZARA, A., HERACLEOUS, E., SILVESTER, L., BUKUR, D. B. & LEMONIDOU, A. A. 2016b. Activity study of NiO-based oxygen carriers in chemical looping steam methane reforming. *Catalysis Today*, 272, 32-41.

- ANTZARAA, A., HERACLEOUSA, E., BUKURC, D. B. & LEMONIDOUA, A. A. 2015. Thermodynamic analysis of hydrogen production via chemical looping steam methane reforming coupled with in situ CO<sub>2</sub> capture. *International Journal of Greenhouse Gas Control*, 32, 115-128.
- AUER, W. 1971. A new catalyst for the Co shift conversion of sulfur containing gases. *68th National Meeting of American Institute of Chemical Engineers*. Houston, Texas: American Institute of Chemical Engineers.
- BALASUBRAMANIAN, B., ORTIZ, A. L., KAYTAKOGLU, S. & HARRISON, D. 1999. Hydrogen from methane in a single-step process. *Chemical Engineering Science*, 54, 3543-3552.
- BARELLI, L., BIDINI, G., GALLORINI, F. & SERVILI, S. 2008. Hydrogen production through sorption-enhanced steam methane reforming and membrane technology: a review. *Energy*, 33, 554-570.
- BARROSO QUIROGA, M. M. & CASTRO LUNA, A. E. 2007. Kinetic Analysis of Rate Data for Dry Reforming of Methane. *Industrial & Engineering Chemistry Research*, 46, 5265-5270.
- BARTHOLOMEW, C. H. 2001. Mechanisms of catalyst deactivation. *Applied Catalysis A: General*, 212, 17-60.
- BASAGIANNIS, A. C. & VERYKIOS, X. E. 2006. Reforming reactions of acetic acid on nickel catalysts over a wide temperature range. *Applied Catalysis A: General*, 308, 182-193.
- BERUTO, D., BARCO, L. & SEARCY, A. W. 1984. CO<sub>2</sub> - Catalyzed Surface Area and Porosity Changes in High - Surface - Area CaO Aggregates. *Journal of the american ceramic society*, 67, 512-516.
- BEYER, F., BRIGHTLING, J., FERNELL, P. & FOSTER, C. 2005. *Steam Reforming-50 years of developments and the challenges for the next 50 years* [Online]. Toronto, Canada: Uhde GmbH. 18.06.16].
- BIRJANDIA, M. R. S., SHAHRAKIA, F., BIRJANDIB, M. S. & NOBANDEGANIC, M. S. 2014. Application of global optimization strategies to refinery hydrogen network. *international journal of hydrogen energy*, 39, 14503-14511.
- BOHRE, A. 2014. *Immobilization of radioactive waste in ceramic based hosts: Radioactive waste Immobilization*, Anchor Academic Publishing.
- BORGES, J. L., PESSOA, F. L. P. & QUEIROZ, E. M. 2012. Hydrogen Source Diagram: A Procedure for Minimization of Hydrogen Demand in Petroleum Refineries. *Industrial & Engineering Chemistry Research*, 51, 12877-12885.
- BOYANO, A., BLANCO-MARIGORTA, A.-M., MOROSUK, T. & TSATSARONIS, G. 2012. Steam Methane Reforming System for Hydrogen Production: Advanced Exergetic Analysis. *International Journal of Thermodynamics*, 15, 1-9.
- BRODA, M., MANOVIC, V., IMTIAZ, Q., KIERZKOWSKA, A. M., ANTHONY, E. J. & MÜLLER, C. R. 2013. High-Purity Hydrogen via the Sorption-Enhanced Steam Methane Reforming Reaction over a Synthetic CaO-Based Sorbent and a Ni Catalyst. *Environmental Science & Technology*, 47, 6007-6014.
- BRUN-TSEKHOVOI, A., ZADORIN, A., KATSOBASHVILI, Y. R. & KOURDYUMOV, S. The process of catalytic steam-reforming of hydrocarbons in the presence of carbon dioxide acceptor. Hydrogen Energy Progress VII, Proceedings of the 7th World Hydrogen Energy Conference, 1988. 25-29.
- BULLIN, K. & KROUSKOP, P. 2008. *Composition variety complicates processing plans for US shale gas* [Online]. USA: Bryan Research & Engineering, Inc. Available: [www.digitalrefining.com/article/1000568](http://www.digitalrefining.com/article/1000568) [Accessed 5 May 2014].
- CASTAÑEDA, L. C., MUÑOZ, J. A. D. & ANCHEYTA, J. 2011. Comparison of approaches to determine hydrogen consumption during catalytic hydrotreating of oil fractions. *Fuel*, 90, 3593-3601.

- CAVALLARO, S., CHIODO, V., FRENI, S., MONDELLO, N. & FRUSTERI, F. 2003. Performance of Rh/Al<sub>2</sub>O<sub>3</sub> catalyst in the steam reforming of ethanol: H<sub>2</sub> production for MCFC. *Applied Catalysis A: General*, 249, 119-128.
- CECERE, D., GIACOMAZZI, E. & INGENITO, A. 2014. A review on hydrogen industrial aerospace applications. *International Journal of Hydrogen Energy*, 39, 1-17.
- CHAUBEY, R., SATANANDESAHU, OLUSOLAO.JAMES & SUDIPMAITY 2013. A review on development of industrial processes and emerging techniques for production of hydrogen from renewable and sustainable sources. *Renewable and Sustainable Energy Reviews*, 23, 443-462.
- CHEN, H., YU, H., TANG, Y., PAN, M., YANG, G., PENG, F., WANG, H. & YANG, J. 2009a. Hydrogen production via autothermal reforming of ethanol over noble metal catalysts supported on oxides. *Journal of Natural Gas Chemistry*, 18, 191-198.
- CHEN, H., ZHANG, T., DOU, B., DUPONT, V., WILLIAMS, P., GHADIRI, M. & DING, Y. 2009b. Thermodynamic analyses of adsorption-enhanced steam reforming of glycerol for hydrogen production. *International Journal of Hydrogen Energy*, 34, 7208-7222.
- CHENG, F. & DUPONT, V. 2013. Nickel catalyst auto-reduction during steam reforming of bio-oil model compound acetic acid. *International Journal of Hydrogen Energy*, 38, 15160-15172.
- CHENG, F., DUPONT, V. & TWIGG, M. V. 2016. Temperature-programmed reduction of nickel steam reforming catalyst with glucose. *Applied Catalysis A: General*, 527, 1-8.
- CHIRON, F.-X., PATIENCE, G. S. & RIFFLART, S. 2011. Hydrogen production through chemical looping using NiO/NiAl<sub>2</sub>O<sub>4</sub> as oxygen carrier. *Chemical Engineering Science*, 66, 6324-6330.
- CHRISTENSEN, K. O., CHEN, D., LØDENG, R. & HOLMEN, A. 2006. Effect of supports and Ni crystal size on carbon formation and sintering during steam methane reforming. *Applied Catalysis A: General*, 314, 9-22.
- COBDEN, P. D., BEURDEN, P. V., REIJERS, H. T. J., ELZINGA, G. D., KLUITERS, S. C. A., DIJKSTRA, J. W., JANSEN, D. & BRINK, R. W. V. D. 2007. Sorption-enhanced hydrogen production for pre-combustion CO<sub>2</sub> capture: thermodynamic analysis and experimental results. *International Journal of Greenhouse Gas Control* 1, 170-179.
- COBDEN, P. D., ELZINGAA, G. D., BOONEVELD, S., DIJKSTRA, J. W., JANSEN, D. & VAN DEN BRINK, R. W. 2009. Sorption-enhanced steam-methane reforming: CaO-CaCO<sub>3</sub> capture technology. *Energy Procedia*, 1, 733-739.
- COLLODI, G. & WHEELER, F. 2009. Hydrogen Production via Steam Reforming with CO<sub>2</sub> Capture. *Corsico – Milan - Italy*.
- CONNOLLY, J. R. 2010. Introduction quantitative X-ray diffraction methods. *EPS400-001, Introduction to X-ray Powder Diffraction*.
- CORTRIGHT, R. D., DAVDA, R. R. & DUMESIC, J. A. 2002. Hydrogen from catalytic reforming of biomass-derived hydrocarbons in liquid water. *Nature*, 418, 964-967.
- D'ORAZIO, A., ORECCHINI, F. & VALITUTTI, V. 2015. Preface to the special section on Young Scientists Symposium (YSS). *International Journal of Hydrogen Energy*, 40, 11771-11772.
- DAUENHAUER, P. J., DREYER, B. J., DEGENSTEIN, N. J. & SCHMIDT, L. D. 2007. Millisecond Reforming of Solid Biomass for Sustainable Fuels. *Gesellschaft Deutscher Chemiker*, 46, 5864-5867.
- DAVDA, R. R., SHABAKER, J. W., HUBER, G. W., CORTRIGHT, R. D. & DUMESIC, J. A. 2005. A review of catalytic issues and process conditions for renewable hydrogen and alkanes by aqueous-phase reforming of oxygenated hydrocarbons over supported metal catalysts. *Applied Catalysis B: Environmental*, 56, 171-186.

- DE DIEGO, L. F., ORTIZ, M., GARCÍA-LABIANO, F., ADÁNEZ, J., ABAD, A. & GAYÁN, P. 2009. Hydrogen production by chemical-looping reforming in a circulating fluidized bed reactor using Ni-based oxygen carriers. *Journal of Power Sources*, 192, 27-34.
- DELUGA, G. A., SALGE, J. R., SCHMIDT, L. D. & VERYKIOS, X. E. 2004. Renewable Hydrogen from Ethanol by Autothermal Reforming. *Science*, 303, 993-997
- DENG, C., PAN, H., LI, Y., ZHOU, Y. & FENG, X. 2014. Comparative analysis of different scenarios for the synthesis of refinery hydrogen network. *Applied Thermal Engineering*, 70, 1162–1179.
- DIEGO, L. F. D., ORTIZ, M., ADÁNEZ, J., GARCÍA-LABIANO, F., ABAD, A. & GAYÁN, P. 2008. Synthesis gas generation by chemical-looping reforming in a batch fluidized bed reactor using Ni-based oxygen carrier. *Chemical Engineering Journal*, 144, 289-298.
- DING, Y. & ALPAY, E. 2000. Adsorption enhanced steam-methane reforming. *Chemical Engineering Science*, 55, 3929-3940.
- DOU, B., RICKETT, G. L., DUPONT, V., WILLIAMS, P. T., CHEN, H., DING, Y. & GHADIRI, M. 2010. Steam reforming of crude glycerol with in situ CO<sub>2</sub> sorption. *Bioresource Technology*, 101, 2436-2442.
- DOU, B., SONG, Y., WANG, C., CHEN, H., YANG, M. & XU, Y. 2014. Hydrogen production by enhanced-sorption chemical looping steam reforming of glycerol in moving-bed reactors. *Applied Energy*, 130, 342-349.
- DUBEY, P. K., SINHA, A. S. K., TALAPATRA, S., KORATKAR, N., AJAYAN, P. M. & SRIVASTAVA, O. N. 2010. Hydrogen generation by water electrolysis using carbon nanotube anode. *International Journal of Hydrogen Energy* 35, 3945 – 3950.
- DUPONT, V., ROSS, A. B., HANLEY, I. & TWIGG, M. V. 2007. Unmixed steam reforming of methane and sunflower oil: A single-reactor process for -rich gas. *International Journal of Hydrogen Energy*, 32, 67-79.
- DUPONT, V., ROSS, A. B., KNIGHT, E., HANLEY, I. & TWIGG, M. V. 2008. Production of hydrogen by unmixed steam reforming of methane. *Chemical Engineering Science*, 63, 2966-2979.
- DUPONT, V., TWIGG, M. V., ROLLINSON, A. N. & JONES, J. M. 2013. Thermodynamics of hydrogen production from urea by steam reforming with and without in situ carbon dioxide sorption. *International Journal of Hydrogen Energy*, 38, 10260-10269.
- EDWARDS, P. P., KUZNETSOV, V. L., DAVID, W. I. & BRANDON, N. P. 2008. Hydrogen and fuel cells: towards a sustainable energy future. *Energy Policy*, 36, 4356-4362.
- EL-BOUSIFFI, M. A. & GUNN, D. J. 2007. A dynamic study of steam-methane reforming. *International Journal of Heat and Mass Transfer*, 50, 723-733.
- EL DOUKKALI, M., IRIONDO, A., ARIAS, P. L., REQUIES, J., GANDARÍAS, I., JALOWIECKI-DUHAMEL, L. & DUMEIGNIL, F. 2012. A comparison of sol-gel and impregnated Pt or/and Ni based  $\gamma$ -alumina catalysts for bioglycerol aqueous phase reforming. *Applied Catalysis B: Environmental*, 125, 516-529.
- ENGERA, B. C., LØDENG, R. & ANDERS HOLMENA 2008. A review of catalytic partial oxidation of methane to synthesis gas with emphasis on reaction mechanisms over transition metal catalysts. *Applied Catalysis A, General*, 346, 1-27.
- ESTEBAN-DÍEZ, G., GIL, M. V., PEVIDA, C., CHEN, D. & RUBIERA, F. 2016. Effect of operating conditions on the sorption enhanced steam reforming of blends of acetic acid and acetone as bio-oil model compounds. *Applied Energy*, 177, 579-590.
- EWAN, B. C. R. & ALLEN, R. W. K. 2005. A figure of merit assessment of the routes to hydrogen. *International Journal of Hydrogen Energy*, 30, 809-819.
- EZIROGLU, T. N. & BARBIR, F. 1998. *Hydrogen energy technologies*, Vienna, United Nations Industrial Development Organization.

- FAN, J. & ZHU, L. 2015. Performance analysis of a feasible technology for power and high-purity hydrogen production driven by methane fuel. *Applied Thermal Engineering*, 75, 103-114.
- FAN, L. S. 2014. *Chemical Looping Technology* [Online]. Department of Chemical and Biomolecular Engineering The Ohio State University Columbus, Ohio 43210. Available: <http://energy.columbia.edu/files/2014/02/1-Fan-Columbia-U-workshop-2014.pdf> [Accessed 21 June 2016].
- FENNELL, P. & ANTHONY, B. 2015. *Calcium and Chemical Looping Technology for Power Generation and Carbon Dioxide (CO<sub>2</sub>) Capture*, Elsevier.
- FERNANDEZ, J. R., ABANADES, J. C. & GRASA, G. 2012a. Modeling of sorption enhanced steam methane reforming—Part II: Simulation within a novel Ca/Cu chemical loop process for hydrogen production. *Chemical Engineering Science*, 84, 12-20.
- FERNÁNDEZ, J. R., ABANADES, J. C., MURILLO, R. & GRASA, G. 2012. Conceptual design of a hydrogen production process from natural gas with CO<sub>2</sub> capture using a Ca–Cu chemical loop. *International Journal of Greenhouse Gas Control*, 6, 126–141.
- FERNANDEZ, J. R., J.C.ABANADES & R.MURILLO 2012b. Modeling of sorption enhanced steam methane reforming in an adiabatic fixed bed reactor. *Chemical Engineering Science*, 84, 1-11.
- FIERROA, V., AKDIMB, O., PROVENDIERB, H. & MIRODATOSB, C. 2005. Ethanol oxidative steam reforming over Ni-based catalysts. *Journal of Power Sources*, 145, 659–666.
- FIGEN, H. E. & BAYKARA, S. Z. 2015. Hydrogen production by partial oxidation of methane over Co based, Ni and Ru monolithic catalysts. *International Journal of Hydrogen Energy*, 40, 7439–7451.
- FLORIN, N. H. & HARRIS, A. T. 2007. Hydrogen production from biomass coupled with carbon dioxide capture: The implications of thermodynamic equilibrium. *International Journal of Hydrogen Energy*, 32, 4119-4134.
- FREEDONIA 2014. World hydrogen The Freedonia Group, Inc.
- FU, P., YI, W., LI, Z., LI, Y., WANG, J. & BAI, X. 2013. Comparative analysis on sorption enhanced steam reforming and conventional steam reforming of hydroxyacetone for hydrogen production: Thermodynamic modeling. *International Journal of Hydrogen Energy*, 38, 11893-11901.
- GARCÍA-LARIO, A. L., GRASA, G. S. & MURILLO, R. 2015. Performance of a combined CaO-based sorbent and catalyst on H<sub>2</sub> production, via sorption enhanced methane steam reforming. *Chemical Engineering Journal* 264 697–705.
- GAUDERNACK, B. & LYNUM, S. 1998. Hydrogen from natural gas without release of CO<sub>2</sub> to the atmosphere. *International Journal of Hydrogen Energy*, 23, 1087-1093.
- GAYÁN, P., DE DIEGO, L. F., GARCÍA-LABIANO, F., ADÁNEZ, J., ABAD, A. & DUESO, C. 2008. Effect of support on reactivity and selectivity of Ni-based oxygen carriers for chemical-looping combustion. *Fuel*, 87, 2641-2650.
- GAZZANI, M. & MANZOLINI, E. M. G. 2013. CO<sub>2</sub> capture in integrated gasification combined cycle with SEWGS – Part A: Thermodynamic performances. *Fuel*, 105, 206-219.
- GEHRING, M. & PHILLIPS, F.-K. 2016. *Intersections of the Paris agreement and carbon offsetting; legal and functional considerations* [Online]. Available: [https://www.cigionline.org/sites/default/files/pb\\_no.88web.pdf](https://www.cigionline.org/sites/default/files/pb_no.88web.pdf) [Accessed 25 December 2016].
- GIL, M. V., FERMOSO, J., PEVIDA, C., CHEN, D. & RUBIERA, F. 2016. Production of fuel-cell grade H<sub>2</sub> by sorption enhanced steam reforming of acetic acid as a model compound of biomass-derived bio-oil. *Applied Catalysis B: Environmental*, 184, 64-76.
- GILASSI, S. & RAHMANIAN, N. 2015a. CFD modelling of a hollow fibre system for CO<sub>2</sub> capture by aqueous amine solutions of MEA, DEA and MDEA. *International Journal of Chemical Reactor Engineering*, 14, 53-61.

- GILASSI, S. & RAHMANIAN, N. 2015b. Mathematical modelling and numerical simulation of CO<sub>2</sub>/CH<sub>4</sub> separation in a polymeric membrane. *Applied Mathematical Modelling*, 39, 6599-6611.
- GOODMAN, D. R. (ed.) 1996. *Catalyst handbook*, London: Manson publishing limited.
- GRASA, G. S. & ABANADES, J. C. 2006. CO<sub>2</sub> capture capacity of CaO in long series of carbonation/calcination cycles. *Industrial & Engineering Chemistry Research*, 45, 8846-8851.
- HAFIZI, A., RAHIMPOUR, M. R. & HASSANAJILI, S. 2016a. High purity hydrogen production via sorption enhanced chemical looping reforming: Application of 22Fe<sub>2</sub>O<sub>3</sub>/MgAl<sub>2</sub>O<sub>4</sub> and 22Fe<sub>2</sub>O<sub>3</sub>/Al<sub>2</sub>O<sub>3</sub> as oxygen carriers and cerium promoted CaO as CO<sub>2</sub> sorbent. *Applied Energy*, 169, 629-641.
- HAFIZI, A., RAHIMPOUR, M. R. & HASSANAJILI, S. 2016b. Hydrogen production via chemical looping steam methane reforming process: Effect of cerium and calcium promoters on the performance of Fe<sub>2</sub>O<sub>3</sub>/Al<sub>2</sub>O<sub>3</sub> oxygen carrier. *Applied Energy*, 165, 685-694.
- HALLALE, N. & LIU, F. 2001. Refinery Hydrogen Management for Clean Fuels Production. *Advances in Environmental Research*, 6, 81-98.
- HAMAD, T. A., AGLL, A. A., HAMAD, Y. M., BAPAT, S., THOMAS, M., MARTIN, K. B. & SHEFFIELD, J. W. 2014. Hydrogen recovery, cleaning, compression, storage, dispensing, distribution system and End-Uses on the university campus from combined heat, hydrogen and power system. *International Journal of Hydrogen Energy*, 39, 647-653.
- HAN, C. & HARRISON, D. P. 1994. Simultaneous shift reaction and carbon dioxide separation for the direct production of hydrogen. *Chemical Engineering Science*, 49, 5875-5883.
- HAO, S. R. 1996. Hydrocarbon steam reforming process, feedstock and catalysts for hydrogen production in China. In: VEZIROGLU, T. N., WINTER, C. J., BASELT, J. P. & KREYSA, G. (eds.) *HYDROGEN ENERGY PROGRESS XI*.
- HARRISON, D. P. 2008. Sorption-Enhanced Hydrogen Production: A Review. *Industrial & Engineering Chemistry Research*, 47, 6486-6501.
- HARRISON, D. P. & PENG, Z. 2003. Low-carbon monoxide hydrogen by sorption enhanced reaction. *International Journal of Chemical and Reactor Engineering*, 1, 1542-6580.
- HEFFER, P. & PRUD'HOMME, M. 2014. *Fertiliser outlook 2013-2018*. International Fertilizer Industry Association (IFA) [Online]. Available: <http://www.fertilizer.org> [Accessed 17 June 2016].
- HOLLADAY, J. D., HU, J., KING, D. L. & WANG, Y. 2009. An overview of hydrogen production technologies. *Catalysis Today*, 139, 244-260.
- HOLLOWAY, S. 1997. An overview of the underground disposal of carbon dioxide. *Energy Conversion and Management*, 38, 193-198.
- HOSSAIN, M. M. & DE LASA, H. I. 2008. Chemical-looping combustion (CLC) for inherent separations—a review. *Chemical Engineering Science*, 63, 4433-4451.
- HOTEIT, A., FORRET, A., PELLETANT, W., ROESLER, J. & GAUTHIER, T. 2011. Chemical Looping Combustion with Different Types of Liquid Fuels Combustion en boucle chimique avec différentes charges liquides. *Oil Gas Sci. Technol. – Rev. IFP Energies nouvelles* 66, 193 - 199.
- HUFTON, J. R., MAYORGA, S. & SIRICAR, S. 1999. Sorption enhanced reaction process for hydrogen production. *AIChE Journal*, 45, 248-256.
- IULIANELLI, A., LIGUORI, S., WILCOX, J. & BASILE, A. 2016. Advances on methane steam reforming to produce hydrogen through membrane reactors technology: A review. *Catalysis Reviews*, 58, 1-35.
- IZQUIERDO, U., BARRIO, V. L., CAMBRA, J. F., REQUIES, J., GUÑEMEZ, M. B., P.L. ARIAS A, KOLB, G., ZAPF, R., GUTIE'RREZ, A. M. & C, J. R. A. 2012. Hydrogen production from methane and natural gas steam reforming in conventional and microreactor reaction systems. *International Journal of Hydrogen Energy*, 37, 7026-7033.

- JAMES, L. K. c1993. *Nobel laureates in chemistry* United States of America, American chemical society and Chemical Heritage Foundation.
- JANG, H. M., KANG, W. R. & LEE, K. B. 2013. Sorption-enhanced water gas shift reaction using multi-section column for high-purity hydrogen production. *International journal of hydrogen energy* 38, 6065-6071.
- JIANG, B., DOU, B., SONG, Y., ZHANG, C., DU, B., CHEN, H., WANG, C. & XU, Y. 2015. Hydrogen production from chemical looping steam reforming of glycerol by Ni-based oxygen carrier in a fixed-bed reactor. *Chemical Engineering Journal*, 280, 459-467.
- JIANG, B., DOU, B., WANG, K., SONG, Y., CHEN, H., ZHANG, C., XU, Y. & LI, M. 2016. Hydrogen production from chemical looping steam reforming of glycerol by Ni based Al-MCM-41 oxygen carriers in a fixed-bed reactor. *Fuel*, 183, 170-176.
- JIWANURUK, T., PUTIVISUTISAK, S., PONPESH, P., BUMROONGSAKULSAWAT, P., TAGAWA, T., YAMADA, H. & ASSABUMRUNGRAT, S. 2016. Effect of flow arrangement on micro membrane reforming for H<sub>2</sub> production from methane. *Chemical Engineering Journal*, 293, 319-326.
- JOHANSSON, M., MATTISSON, T., LYNGFELT, A. & ABAD, A. 2008. Using continuous and pulse experiments to compare two promising nickel-based oxygen carriers for use in chemical-looping technologies. *Fuel*, 87, 988-1001.
- JOHNSEN, F. & ROSTRUP-NIELSEN, J. R. 2002. Conversion of hydrocarbons and alcohols for fuel cells. *Journal of Power Sources*, 105, 195-201.
- JOHNSEN, K., RYU, H. J., GRACE, J. R. & LIM, C. J. 2006. Sorption-enhanced steam reforming of methane in a fluidized bed reactor with dolomite as CO<sub>2</sub>-acceptor. *Chemical Engineering Science* 61, 1195-1202.
- JONES, D. S. J. c1995. *Elements of petroleum processing*. Chichester: John Wiley & Sons Ltd.
- KÄLLÉN, M., RYDÉN, M., LYNGFELT, A. & MATTISSON, T. 2015. Chemical-looping combustion using combined iron/manganese/silicon oxygen carriers. *Applied Energy*, 157, 330–337.
- KARGBO, D. M., WILHELM, R. G. & CAMPBELL, D. J. 2010. Natural Gas Plays in the Marcellus Shale: Challenges and Potential Opportunities. *Environmental Science & Technology*, 15, 5679–5684.
- KATHE, M. V., EMPFIELD, A., NA, J., BLAIR, E. & FAN, L.-S. 2016. Hydrogen production from natural gas using an iron-based chemical looping technology: Thermodynamic simulations and process system analysis. *Applied Energy*, 165, 183-201.
- KEEM, J. & HONIG, J. 1978. Selected electrical and thermal properties of undoped nickel oxide. DTIC Document.
- KELLEY, K. K. 1960. Contributions to the data on theoretical metallurgy. *Bulletin 584 United States burea of mines*.
- KOH, A. C. W., CHEN, L., LEONG, W. K., JOHNSON, B. F. G., KHIMYAK, T. & LIN, J. 2007. Hydrogen or syngas production via the partial oxidation of methane over supported nickel-cobalt catalysts. *International Journal of Hydrogen Energy*, 32, 725-730.
- KUMAR, R. V., LYON, R. K. & COLE, J. A. 2002. *Unmixed Reforming: A Novel Autothermal Cyclic Steam Reforming Process*, US, Springer.
- LAMBERT, G. J., SCHOEBER, W. J. & HELDEN, H. J. A. V. 1994. The hydrogen balance in refineries *Foster Wheeler Conference on Heavy Oil and Hydrogen*. Noordwijk, Netherlands.
- LAN, R., IRVINE, J. T. S. & TAO, S. 2012. Ammonia and related chemicals as potential indirect hydrogen storage materials. *International Journal of Hydrogen Energy*, 37, 1482-1494.
- LAOSIROPOJANA, N., RAJESH, S. K., SINGHTO, W., PALIKANON, T. & PENGYONG, S. 2004. Effects of H<sub>2</sub>S, CO<sub>2</sub>, and O<sub>2</sub> on Catalytic Methane Steam Reforming over Ni Catalyst on CeO<sub>2</sub> and Al<sub>2</sub>O<sub>3</sub> Supports. *The Joint International Conference on "Sustainable Energy and Environment (SEE)"*. Hua Hin, Thailand.

- LEA-LANGTON, A., ZIN, R. M., DUPONT, V. & TWIGG, M. V. 2012. Biomass pyrolysis oils for hydrogen production using chemical looping reforming. *International Journal of Hydrogen Energy*, 37, 2037-2043.
- LEACH, B. 1983. *Applied Industrial Catalysis*, Oxford, Elsevier Science.
- LEE, C. H. & LEE, K. B. 2014. Application of one-body hybrid solid pellets to sorption-enhanced water gas shift reaction for high-purity hydrogen production. *International Journal of Hydrogen Energy*, 39, 18128 -18134.
- LEE, G., YU, J., GOLIKERI, S. V. & KLEIN, B. 2013. *Market conditions encourage refiners to recover by-product gases* [Online]. Available: <http://www.ogj.com/articles/print/volume-111/issue-10/processing/market-conditions-encourage-refiners-to-recover.html> [Accessed 10 December 2013].
- LEE, K. B., BEAVER, M. G., CARAM, H. S. & SIRCAR, S. 2007. Reversible chemisorption of carbon dioxide: simultaneous production of fuel-cell grade H<sub>2</sub> and compressed CO<sub>2</sub> from synthesis gas. *Adsorption*, 13, 385-397.
- LEE, K. B., BEAVER, M. G., CARAM, H. S. & SIRCAR, S. 2008. Performance of Na<sub>2</sub>O promoted alumina as CO<sub>2</sub> chemisorbent in sorptionenhanced reaction process for simultaneous production of fuel-cell grade H<sub>2</sub> and compressed CO<sub>2</sub> from synthesis gas. *Journal of Power Sources* 176, 312-319.
- LEVALLEY, T. L., RICHARD, A. R. & FAN, M. 2014. The progress in water gas shift and steam reforming hydrogen production technologies – A review. *International Journal of Hydrogen Energy*, 39, 16983-17000.
- LI, K., WANG, H. & WEI, Y. 2013. Syngas Generation from Methane Using a Chemical-Looping Concept: A Review of Oxygen Carriers. *Journal of Chemistry*.
- LI, Z., LIU, Y. & CAI, N. 2012. Effect of CaO hydration and carbonation on the hydrogen production from sorption enhanced water gas shift reaction *International journal of hydrogen energy* 37, 11227-11236.
- LIGURAS, D. K., KONDARIDES, D. I. & VERYKIOS, E. 2003. Production of hydrogen for fuel cells by steam reforming of ethanol over supported noble metal catalysts. *Applied Catalysis B: Environmental*, 43, 345-354.
- LIMA DA SILVA, A. & MÜLLER, I. L. 2011. Hydrogen production by sorption enhanced steam reforming of oxygenated hydrocarbons (ethanol, glycerol, n-butanol and methanol): Thermodynamic modelling. *International Journal of Hydrogen Energy*, 36, 2057-2075.
- LINDERHOLM, C., MATTISSON, T. & LYNGFELT, A. 2009. Long-term integrity testing of spraydried particles in a 10-kW chemical-looping combustor using natural gas as fuel. *Fuel*, 88, 2083–2096.
- LONG, R., PICIOCCIO, K. & ZAGORIA, A. 2011. *Optimising hydrogen production and use* [Online]. UOP LLC, A Honeywell Company. Available: <https://www.uop.com/?document=uop-optimizing-hydrogen-production-and-use-white-paper&download=1> [Accessed 3 December 2013].
- LYNGFELT, A., LECKNER, B. & MATTISSON, T. 2001. A fluidized-bed combustion process with inherent CO<sub>2</sub> separation; application of chemical-looping combustion. *Chemical Engineering Science*, 56, 3101-3113.
- LYON, R. K. 1996. *Methods and systems for heat transfer by unmixed combustion*. PCT/US1996/003694 [Online]. Available: <http://www.google.com/patents/WO1996033794A1?cl=ko> [Accessed 23 June 2016].
- LYON, R. K. & COLE, J. A. 2000. Unmixed combustion: an alternative to fire *Combustion and Flame*, 121, 249-261.
- LYSIKOV, A., DEREVSCHIKOV, V. & OKUNEV, A. 2015. Sorption-enhanced reforming of bioethanol in dual fixed bed reactor for continuous hydrogen production. *International Journal of Hydrogen Energy*, 40, 14436–14444.

- MACDOWELL, N., FLORIN, N., BUCHARD, A., HALLETT, J., GALINDO, A., JACKSON, G., ADJIMAN, C. S., WILLIAMS, C. K., SHAH, N. & FENNELL, P. 2010. An overview of CO<sub>2</sub> capture technologies. *Energy & Environmental Science*, 3, 1645-1669
- MANZOLINI, G., MACCHI, E., BINOTTI, M. & GAZZANI, M. 2011. Integration of SEWGS for carbon capture in Natural Gas Combined Cycle. Part B: Reference case comparison. *International Journal of Greenhouse Gas Control*, 5, 214-225.
- MANZOLINI, G., MACCHI, E., BINOTTI, M. & GAZZANI, M. 2012. CO<sub>2</sub> capture in integrated gasification combined cycle with of SEWGS. Part B: Economic assessments. *Fuel*, 105, 220-227.
- MARION, C. P. & SLATER, W. L. 1963. Manufacture of tonnage hydrogen by partial oxidation combustion, the Texaco process. *6th World Petroleum Congress*. Frankfurt, Germany: World Petroleum Congress.
- MARTAVALTZI, C. S. & LEMONIDOU, A. A. 2010. Hydrogen production via sorption enhanced reforming of methane: Development of a novel hybrid material—reforming catalyst and CO<sub>2</sub> sorbent. *Chemical Engineering Science*, 65, 4134-4140.
- MARTÍNEZ, I., ROMANO, M. C., CHIESA, P., GRASA, G. & MURILLO, R. 2013. Hydrogen production through sorption enhanced steam reforming of natural gas: Thermodynamic plant assessment. *International Journal of Hydrogen Energy* 38, 15180–15199.
- MARTÍNEZ, I., ROMANO, M. C., FERNÁNDEZ, J. R., CHIESA, P., MURILLO, R. & ABANADES, J. C. 2014. Process design of a hydrogen production plant from natural gas with CO<sub>2</sub> capture based on a novel Ca/Cu chemical loop. *Applied Energy*, 114, 192-208.
- MARTUNUS, HELWANI, Z., WIHEEB, A. D., KIM, J. & OTHMAN, M. R. 2012. Improved carbon dioxide capture using metal reinforced hydrotalcite under wet conditions. *International Journal of Greenhouse Gas Control*, 7, 127-136.
- MATTISSON, T., JÄRDNÄS, A. & LYNGFELT, A. 2003. Reactivity of Some Metal Oxides Supported on Alumina with Alternating Methane and Oxygens Application for Chemical-Looping Combustion. *Energy and Fuel*, 17, 643-651.
- MATTISSON, T. & LYNGFELT, A. 2001. Applications of chemical-looping combustion with capture of CO<sub>2</sub>. *Second Nordic Minisymposium on CO<sub>2</sub> Capture and Storage, Göteborg, Sweden*.
- MATTISSON, T., LYNGFELT, A. & LEION, H. 2009. Chemical-looping with oxygen uncoupling for combustion of solid fuels. *International Journal Greenhouse Gas Control*, 3, 11–19.
- MCBRIDE, B. J. & GORDON, S. 1996. Computer Program for Calculation of Complex Chemical Equilibrium Compositions and Applications II. User's Manual and Program Description. Cleveland, Ohio: Lewis Research Center.
- MCBRIDE, B. J., GORDON, S. & RENO, M. 1993. *Coefficients of calculating thermodynamics and transport properties of individual species* [Online]. NASA report TM-4513. Available: <http://ntrs.nasa.gov/archive/nasa/casi.ntrs.nasa.gov/19940013151.pdf> [Accessed 20 February 2014].
- METZ, B., DAVIDSON, O., CONINCK, H. D., LOOS, M. & MEYER, L. 2005. *IPCC Special Report on Carbon Dioxide Capture and Storage. Prepared by Working Group III of the Intergovernmental Panel on Climate Change* [Online]. Cambridge: Cambridge University Press. Available: [https://www.ipcc.ch/pdf/special-reports/srccs/srccs\\_wholereport.pdf](https://www.ipcc.ch/pdf/special-reports/srccs/srccs_wholereport.pdf) [Accessed 11 October 2014].
- MIN HYE YOUNA, SEOA, J. G., KIMB, P., KIMA, J. J., LEEA, H.-I. & SONG, I. K. 2006. Hydrogen production by auto-thermal reforming of ethanol over Ni/γ-Al<sub>2</sub>O<sub>3</sub> catalysts: effect of second metal addition. *Journal Power Sources*, 162, 1270–1274.
- MOKHATAB, S. & POE, W. A. 2012. *Handbook of Natural Gas Transmission and Processing*, USA, Gulf Professional Publishing

- MOLINDER, R., COMYN, T. P., HONDOW, N., PARKER, J. E. & DUPONT, V. 2012. In situ X-ray diffraction of CaO based CO<sub>2</sub> sorbents. *Energy & Environmental Science*, 5, 8958-8969.
- MOMIRLANA, M. & VEZIROGLU, T. 1999. Recent directions of world hydrogen production. *Renewable and Sustainable Energy Reviews*, 3, 219-231.
- MONSHI, A., FOROUGHI, M. R. & MONSHI, M. R. 2012. Modified Scherrer equation to estimate more accurately nano-crystallite size using XRD. *World Journal of Nano Science and Engineering*, 2, 154.
- N. JHAVERI, MOHANTY, B. & KHANAM, S. 2014. Mathematical modeling and optimization of hydrogen distribution network used in refinery. *International Journal of Hydrogen Energy*, 39, 339-348.
- NATERER, G. F., GABRIEL, K., WANG, Z. L., DAGGUPATI, V. N. & GRAVELSINS, R. 2008. Thermochemical hydrogen production with a copper–chlorine cycle. I: oxygen release from copper oxychloride decomposition. *International Journal of Hydrogen Energy*, 33, 5439-5450.
- NELSON, W. L. c1958. *Petroleum Refining Engineering*. 4 ed. London: McGRAW-HILL.
- NI, M., LEUNG, M. K. H., LEUNG, D. Y. C. & SUMATHY, K. 2007. A review and recent developments in photocatalytic water-splitting using for hydrogen production. *Renewable and Sustainable Energy Reviews*, 11, 401-425.
- NICHOLLS, T., GORST, I., LEWIS, L. & RUDDY, M. 2012. *Everything you wanted to know about gas... But were afraid to ask*, London, Silverstone communications Ltd (Energy Future).
- NIELSEN, J. R. R., SEHESTED, J. & NORSKOV, J. K. 2002. Advances in Catalysis. 47, 65-139.
- NIEVA, M. A., VILLAVARDE, M. M., MONZÓN, A., GARETTO, T. F. & MARCHI, A. J. 2014. Steam-methane reforming at low temperature on nickel-based catalysts. *Chemical Engineering Journal*, 235, 158-166.
- NOELKER, K. & JOHANNING, J. 2010. Autothermal reforming: a flexible syngas route with future potential. *Nitrogen & Syngas 2010 International Conference*. Bahrain.
- NUMAGUCHI, T. & KIKUCHI, K. 1988. Intrinsic kinetics and design simulation in a complex reaction network; steam-methane reforming. *Chemical Engineering Science*, 43, 2295-2301.
- OCHOA-FERNANDEZ, E., HAUGEN, G., ZHAO, T., RONNING, M., AARTUN, I., BORRESEN, B., RYTTER, E., RONNEKLEIV, M. & CHEN, D. 2007. Process design simulation of H<sub>2</sub> production by sorption enhanced steam methane reforming: evaluation of potential CO<sub>2</sub> acceptors. *Green Chemistry*, 9, 654-662.
- OCIC, O. 2005. Energy optimization in oil refinery - case study: catalytic reforming unit. *18th World Petroleum Congress, 25-29 September*. Johannesburg, South Africa: World Petroleum Congress.
- OCIC, O. J. & PERISIC, B. J. 2002. Methods of determining the catalytic reforming process energy and technological efficiency. *17th World Petroleum Congress*. Rio de Janeiro, Brazil: World Petroleum Congress.
- OGDEN, J., T. KREUTZ, KARTHA, S. & IWAN, L. 1996. *Assessment of technologies for producing hydrogen from natural gas at small scale*, Princeton, Princeton University Center for Energy and Environmental Studies
- OGDEN, J. M. 2001. *Review of small stationary reformers for hydrogen production. A report for the International Energy Agency Agreement on the Production and Utilization of Hydrogen. Task 16, Hydrogen from Carbon-Containing Materials*
- [Online]. Princeton: Center for Energy and Environmental Studies. Princeton University. Available: <http://www.afdc.energy.gov/pdfs/31948.pdf> [Accessed 23th June 2016].
- OLSBYE, U., WURZEL, T. & MLECZKO, L. 1997. Kinetic and Reaction Engineering Studies of Dry Reforming of Methane over a Ni/La/Al<sub>2</sub>O<sub>3</sub> Catalyst. *Industrial & Engineering Chemistry Research*, 36, 5180-5188.

- PALO, D. R., DAGLE, R. A. & HOLLADAY, J. D. 2007. Methanol steam reforming for hydrogen production. *Chemical Reviews*, 107, 3992-4021.
- PALTSEV, S., JACOBY, H. D., REILLY, J. M., EJAZ, Q. J., MORRIS, J., O'SULLIVAN, F., RAUSCH, S., WINCHESTER, N. & KRAGHA, O. 2011. The future of U.S. natural gas production, use, and trade. *Energy Policy*, 39, 5309-5321.
- PANS, M. A., GAYÁN, P., DIEGO, L. F. D., GARCÍA-LABIANO, F., ABAD, A. & ADÁNEZ, J. 2015. Performance of a low-cost iron ore as an oxygen carrier for Chemical Looping Combustion of gaseous fuels. *Chemical Engineering Research and Design*, 93, 736-746.
- PARKASH, S. c2003. *Refining Processes Handbook*, London Gulf Professional Pub.
- PASEL, J., SAMSUN, R. C., TSCHAUDER, A., PETERS, R. & STOLTEN, D. 2015. A novel reactor type for autothermal reforming of diesel fuel and kerosene. *Applied Energy* 150, 176-184.
- PATEL, N., BAADE, B., FONG, L. W. & KHURANA, V. 2006. Creating Value through Refinery Hydrogen Management. *Asian Refinery Technology Conference*. Singapore.
- PATH. 2011. *Annual Report on World Progress in Hydrogen* [Online]. Washington, D.C. Available: <http://www.hpath.org/ReportBook.pdf> [Accessed 5 May 2015].
- PEEBLES, M. W. H. 1992. *Natural gas fundamentals*, London, Shell International Gas Limited.
- PENG, S. L. 2014. *Banking on U.S. shale gas boom, Asia petrochemical firms switch to LPG* [Online]. Singapore [Accessed 1 October 2014].
- PÉREZ-MORENO, L., SOLER, J., HERGUIDO, J. & MENÉNDEZ, M. 2013. Stable hydrogen production by methane steam reforming in a two zone fluidized bed reactor: Experimental assessment. *Journal of Power Sources*, 243, 233-241.
- PERMANU, S., COX, S. G. & PRUDEN, B. B. 1999. Economics of hydrogen recovery processes for the purification of hydroprocessor purge and off-gases. *International Journal of Hydrogen Energy*, 24, 405-425.
- PHILCOX, J. & FENNER, G. W. A. 1997. Texas project illustrates the benefits of integrated gasification. *Oil Gas Journal*, 95.
- PIMENIDOU, P., RICKETT, G., DUPONT, V. & TWIGG, M. V. 2010. High purity H<sub>2</sub> by sorption-enhanced chemical looping reforming of waste cooking oil in a packed bed reactor. *Bioresource Technology*, 101, 9279-9286.
- PORGAR, S. & RAHMANIAN, N. 2015. Hydrodesulfurization of Crude Oil Over Co-Mo Catalysts in a Slurry Reactor. *Journal of Multidisciplinary Engineering Science and Technology*, 2, 1205-1211.
- PRÖLL, T. & HOFBAUER, H. Chemical Looping Combustion and Reforming. 9th European Conference on Industrial Furnaces and Boilers (INFUB-9), 26-29 April 2011 Estoril, Portugal.
- RABIEI, Z. 2012. Hydrogen management in refineries *Petroleum & Coal* 54(4) 357-368.
- RAHIMPOUR, M. R., JAFARI, M. & IRANSHAHI, D. 2013. Progress in catalytic naphtha reforming process: A review. *Applied Energy*, 109, 79-93.
- RAMACHANDRAN, R. & MENON, R. K. 1998. An overview of industrial uses of hydrogen. *International Journal of Hydrogen Energy*, 23, 593-598.
- RAMAGE, M. P. 2008. *Transitions to Alternative Transportation Technologies—A Focus on Hydrogen*, Washington, DC,, US National Research Council of National Academics Press.
- RATAN, S. & UFFELEN, R. V. 2008. Curtailing refinery CO<sub>2</sub> through H<sub>2</sub> plant. *PTQ*. London, UK.
- RAVI V. KUMAR, COLE, J. A. & LYON, R. K. 1999. Unmixed reforming: an advanced steam reforming process *Fuel Cell Reformer Conference*. South Coast Air Quality District, Diamond Bar, CA.
- RAY, A. K., SINHA, S. K., TIWARI, Y. N., SWAMINATHAN, J., DAS, G., CHAUDHURI, S. & SINGH, R. 2003. Analysis of failed reformer tubes. *Engineering Failure Analysis*, 10, 351-362.

- REINKINGH, J. 1998. Hot Spot Fuel Processor, Society of Automotive Engineers, Fuel Cells for Transportation TOPTC. Cambridge.
- ROGATISA, M. D., MONTINIA, T., COGNIGNIB, A., OLIVIB, L. & FORNASIEROA, P. 2009. Methane partial oxidation on NiCu-based catalysts. *Catalysis Today*, 145, 176–185.
- ROMANO, M. C., CASSOTTI, E. N., CHIESA, P., MEYER, J. & MASTIN, J. 2011. Application of the Sorption Enhanced-Steam Reforming process in combined cycle-based power plants. *Energy Procedia*, 4, 1125–1132.
- ROSEN, M. A. 1991. Thermodynamic investigation of hydrogen production by steam-methane reforming. *International Journal of Hydrogen Energy*, 16, 207-217.
- ROSEN, M. A. 2010. Advances in hydrogen production by thermochemical water decomposition: A review. *Energy*, 35, 1068-1076.
- ROSES, L., GALLUCCI, F., MANZOLINI, G. & VAN SINT ANNALAND, M. 2013. Experimental study of steam methane reforming in a Pd-based fluidized bed membrane reactor. *Chemical Engineering Journal*, 222, 307-320.
- ROSTRUP-NIELSEN, J. & TRIMM, D. L. 1977. Mechanisms of carbon formation on nickel-containing catalysts. *Journal of Catalysis*, 48, 155-165.
- ROSTRUP-NIELSEN, J. R. 1973. Activity of nickel catalysts for steam reforming of hydrocarbons. *Journal of Catalysis*, 31, 173-199.
- ROSTRUP-NIELSEN, J. R., SEHESTED, J. & NØRSKOV, J. K. 2000. Hydrogen and synthesis gas by steam- and CO<sub>2</sub> reforming. *Advances in Catalysis*, 47, 65-137.
- RUTKOWSKI, M. 2005. *Current (2005) hydrogen from SMR natural gas with CO<sub>2</sub> capture and sequestration* [Online]. Available: [https://www.hydrogen.energy.gov/H2A\\_PROD\\_STUDIES.HTML](https://www.hydrogen.energy.gov/H2A_PROD_STUDIES.HTML) [Accessed 25 September 2016].
- RYDÉN, M. 2008. *Hydrogen production from fossil fuels with carbon dioxide capture, using chemical-looping technologies*, Chalmers University of Technology.
- RYDÉN, M., JING, D., KÄLLÉN, M., LEION, H., LYNGFELT, A. & MATTISSON, T. 2014. CuO-based oxygen-carrier particles for chemical-looping with oxygen uncoupling – experiments in batch reactor and in continuous operation. *Industrial and Engineering Chemistry research*, 53, 6255–6267.
- RYDÉN, M., JOHANSSON, M., LYNGFELT, A. & MATTISSON, T. 2009. NiO supported on Mg–ZrO<sub>2</sub> as oxygen carrier for chemical-looping combustion and chemical-looping reforming. *Energy & Environmental Science*, 2, 970-981.
- RYDÉN, M., LEION, H., MATTISSON, T. & LYNGFELT, A. 2013. Combined oxides as oxygen-carrier material for chemical-looping with oxygen uncoupling. *Applied Energy*, 113, 1924–1932.
- RYDÉN, M. & LYNGFELT, A. 2006. Using steam reforming to produce hydrogen with carbon dioxide capture by chemical-looping combustion. *International Journal of Hydrogen Energy* 31, 1271-1283.
- RYDEN, M., LYNGFELT, A. & MATTISSON, T. 2008. Chemical-looping combustion and chemical-looping reforming in a circulating fluidized-bed reactor using Ni based oxygen carriers. *Energy & Fuels*, 22, 2585-2597.
- RYDÉN, M., LYNGFELT, A. & MATTISSON, T. 2006. Synthesis gas generation by chemical-looping reforming in a continuously operating laboratory reactor. *Fuel*, 85, 1631-1641.
- RYDEN, M. & RAMOS, P. 2012. H<sub>2</sub> production with CO<sub>2</sub> capture by sorption enhanced chemical-looping reforming using NiO as oxygen carrier and CaO as CO<sub>2</sub> sorbent. *Fuel Processing Technology*, 96, 27-36.
- S G ADIYA, Z. I., DUPONT, V. & MAHMUD, T. 2017. Chemical equilibrium analysis of hydrogen production from shale gas using sorption enhanced chemical looping steam reforming. *Fuel Processing Technology*, 159, 128-144.

- SÁ, S., SILVA, H., BRANDÃO, L., SOUSA, J. M. & MENDES, A. 2010. Catalysts for methanol steam reforming—A review. *Applied Catalysis B: Environmental*, 99, 43-57.
- SADEGHBEIGI, R. 1995. Fluid Catalytic Cracking Handbook. Houston, Texas: Gulf Publishing Company.
- SADOOGHI, P. & RAUCH, R. 2015. Experimental and modeling study of hydrogen production from catalytic steam reforming of methane mixture with hydrogen sulfide. *International Journal of Hydrogen Energy*, 40, 10418-10426.
- SCOTT, J. W. & BRIDGE, A. G. 1971. Origin and refining of petroleum. In: MCGRATH, H. G. & CHARLES, M. E. (eds.). Washinton, DC: Advances in Chemistry
- SEO, J. G., YOUN, M. H. & SONG, I. K. 2007. Hydrogen production by steam reforming of LNG over Ni/Al<sub>2</sub>O<sub>3</sub>-ZrO<sub>2</sub> catalysts: effect of Al<sub>2</sub>O<sub>3</sub>-ZrO<sub>2</sub> supports prepared by a grafting method. *Journal of Molecular Catalysis A: Chemistry*, 268, 9-14.
- SHALYGIN, M. G., ABRAMOV, S. M., NETRUSOV, A. I. & TEPLYAKOV, V. V. 2015. Membrane recovery of hydrogen from gaseous mixtures of biogenic and technogenic origin. *International Journal of Hydrogen Energy*, 40, 3438-3451.
- SHEN, L., WU, J., GAO, Z. & XIAO, J. 2009. Reactivity deterioration of NiO/Al<sub>2</sub>O<sub>3</sub> oxygen carrier for chemical looping combustion of coal in a 10 kWth reactor. *Combustion and Flame*, 156, 1377-1385.
- SHOKROLLAHI YANCHESHMEH, M., RADFARNIA, H. R. & ILIUTA, M. C. 2016. High temperature CO<sub>2</sub> sorbents and their application for hydrogen production by sorption enhanced steam reforming process. *Chemical Engineering Journal*, 283, 420-444.
- SILABAN, A., NARCIDA, M. & HARRISON, D. 1996. Characteristics of the reversible reaction between CO<sub>2</sub> (g) and calcined dolomite. *Chemical Engineering Communications*, 146, 149-162.
- SILVA, J. M., SORIA, M. A. & MADEIRA, L. M. 2015. Thermodynamic analysis of Glycerol Steam Reforming for hydrogen production with in situ hydrogen and carbon dioxide separation. *Journal of Power Sources*, 273, 423-430.
- SILVESTER, L., ANTZARA, A., BOSKOVIC, G., HERACLEOUS, E., LEMONIDOU, A. A. & BUKUR, D. B. 2015. NiO supported on Al<sub>2</sub>O<sub>3</sub> and ZrO<sub>2</sub> oxygen carriers for chemical looping steam methane reforming. *International Journal of Hydrogen Energy*, 40, 7490-7501.
- SIMONSEN, K., O'KEEFE, L. & FONG, W. 1992. Oil & Gas Journal 45.
- SIMPSON, A. P. & LUTZ, A. E. 2007. Exergy analysis of hydrogen production via steam methane reforming. *International Journal of Hydrogen Energy*, 32, 4811-4820.
- SINHA, N. K. 2003. Petroleum Refining and Petrochemicals. Delhi: Umesh Publications.
- SONG, C. 2002. Fuel processing for low-temperature and high-temperature fuel cells: Challenges, and opportunities for sustainable development in the 21st century. *Catalysis Today*, 77, 17-49.
- SONIBARE, J. A. & AKEREDOLU, F. A. 2004. A theoretical prediction of non-methane gaseous emissions from natural gas combustion. *Energy policy*, 32, 1653-1665.
- SPATH, P. L. & MANN, M. K. 2001. *Life Cycle Assessment of Hydrogen Production via Natural Gas Steam Reforming*. NREL/TP-570-27637 [Online]. US. [Accessed 7 November 2016].
- SPEIGHT, J. G. 1997. *Petroleum Chemistry And Refining*, London, Taylor & Francis.
- SPEIGHT, J. G. 2000. The Desulphurization of Heavy oils and Residua. Second ed. New York: Marcel Dekker Inc.
- SPEIGHT, J. G. c2007. The chemistry and technology of petroleum Fifth ed. Boca Raton: Taylor and Francis Group, LLC.
- SPEIGHT, J. G. & OZUM, B. c2002. *Petroleum Refining Processes*, New York, Marcel Dekker, Inc.
- STEINFELD, A. 2005. Solar thermochemical production of hydrogen—a review. *Solar Energy*, 78, 603-615.
- STORSET, S. O., BRUNSVOLD, A., JORDAL, K., LANGORGE, O., ANANTHARAMAN, R., BERSTAD, D., DITARANTO, M., BAKKAN, J., BLOM, R., PETERS, T., HOFF, K. A., HENRISKSEN, P. P. &

- FONTAINE, M. L. 2013. Technology survey and assessment for piloting of CO<sub>2</sub> capture technologies. *SINTEF Energy Research, Gas Technology*.
- STRATIEV, D., TZINGOV, T., SHISHKOVA, I. & DERMATOVA, P. 2009. Hydrotreating units chemical hydrogen consumption analysis a tool for improving refinery hydrogen management *44th International Petroleum Conference*. Bratislava, Slovak Republic: Lukoil Neftochim Bourgas-R&D Department.
- SUN, P., LIM, C. J. & GRACE, J. R. 2008. Cyclic CO<sub>2</sub> capture by limestone-derived sorbent during prolonged calcination/carbonation cycling. *AIChE Journal*, 54, 1668-1677.
- SWAMINATHAN, J., GUGULOTH, K., GUNJAN, M., ROY, P. & GHOSH, R. 2008. Failure analysis and remaining life assessment of service exposed primary reformer heater tubes. *Engineering Failure Analysis* 15, 311-331.
- TANG, M., XU, L. & FAN, M. 2015. Progress in oxygen carrier development of methane-based chemical-looping reforming: A review. *Applied Energy*, 151, 143-156.
- THRASH, L. A. 1991. Worldwide refining report. *Oil Gas Journal*, 86(51), 39.
- TOWLER, G. P., MANN, R., SERRIERE, A. J.-L. & GABAUDE, C. M. D. 1996. Refinery Hydrogen Management: Cost Analysis of Chemically-Integrated Facilities. *Industrial & Engineering Chemistry Research*, 35, 2378-2388.
- TURPEINEN, E., RAUDASKOSKI, R., PONGRA' CZ, E. & KEISKI, R. L. 2008. Thermodynamic analysis of conversion of alternative hydrocarbon-based feedstocks to hydrogen. *International Journal of Hydrogen Energy*, 33, 6635–6643.
- UDOMCHOKE, T., WONGSAKULPHASATCH, S., KIATKITTIPONG, W., ARPORNWICHANOP, A., KHAODEE, W., POWELL, J., GONG, J. & ASSABUMRUNGRAT, S. 2016. Performance evaluation of sorption enhanced chemical-looping reforming for hydrogen production from biomass with modification of catalyst and sorbent regeneration. *Chemical Engineering Journal*, 303, 338-347.
- VALAVARASU, G. & SAIRAM, B. 2013. Light Naphtha Isomerization Process: A Review. *Petroleum Science and Technology*, 31, 580-595.
- VAN BEURDEN, P. 2004. On the catalytic aspects of steam-methane reforming. *Energy Research Centre of the Netherlands (ECN), Technical Report I-04-003*.
- VAN HOOK, J. P. 1980. Methane-steam reforming. *Catalysis Reviews—Science and Engineering*, 21, 1-51.
- VAN SELOW, E. R., COBDEN, P. D., VERBRAEKEN, P. A., HUFTON, J. R. & VAN DEN BRINK, R. W. 2009. Carbon Capture by Sorption-Enhanced Water–Gas Shift Reaction Process using Hydrotalcite-Based Material. *Industrial & Engineering Chemistry Research*, 48, 4184-4193.
- VELU, S., SATOH, N., GOPINATH, C. S. & SUZUK, K. 2002. Oxidative reforming of bio-ethanol over CuNiZnAl mixed oxide catalyst for hydrogen production. *Catalysis Letters* 82, 145–152.
- VOJVODIC, A., MEDFORD, A. J., STUDDT, F., ABILD-PEDERSEN, F., KHAN, T. S., BLIGAARD, T. & NØRSKOV, J. K. 2014. Exploring the limits: A low-pressure, low-temperature Haber–Bosch process. *Chemical Physics Letters*, 598, 108-112.
- WANG, K., DOU, B., JIANG, B., ZHANG, Q., LI, M., CHEN, H. & XU, Y. 2016. Effect of support on hydrogen production from chemical looping steam reforming of ethanol over Ni-based oxygen carriers. *International Journal of Hydrogen Energy*, 41, 17334-17347.
- WANG, W. 2014. Thermodynamic and experimental aspects on chemical looping reforming of ethanol for hydrogen production using a Cu - based oxygen carrier. *International Journal of Energy Research*, 38, 1192-1200.
- WANG, X., WANG, N. & WANG, L. 2011. Hydrogen production by sorption enhanced steam reforming of propane : A thermodynamic investigation. *International Journal of Hydrogen Energy*, 36, 466-472.

- WATANABE, F., KABURAKI, I., SHIMODA, N. & SATOKAWA, S. 2016. Influence of nitrogen impurity for steam methane reforming over noble metal catalysts. *Fuel Processing Technology*, 152, 15-21.
- WEI, L., XU, S., LIU, J., LIU, C. & LIU, S. 2004. Hydrogen Production in Steam Gasification of Biomass with CaO as a CO<sub>2</sub> Absorbent. *Energy & Fuels*, 22, 1997–2004.
- WEI, Z., SUN, J., LI, Y., DATYE, A. K. & WANG, Y. 2012. Bimetallic catalysts for hydrogen generation. *Chemical Society Reviews*, 41, 7994-8008.
- WESS, R., NORES-PONDAL, F., LABORDE, M. & GIUNTA, P. 2015. Single stage H<sub>2</sub> production, purification and heat supply by means of Sorption-enhanced Steam Reforming of Glycerol. A thermodynamic analysis. *Chemical Engineering Science*, 134, 86–95.
- WHYSALL, M. & PICIOCCIO, K. W. 1999. *Selection and Revamp of Hydrogen Purification Processes*, USA, American Institute of Chemical Engineers.
- WILCHER, F. P., MILLER, G. Q. & MITARITEN, M. 1995. Technologies for the separation and recovery of hydrogen from refinery streams. Washington, DC United States: American Chemical Society.
- WILLIAMS, R. 1933. *Hydrogen production* [Online]. Available: <http://www.google.com/patents/US1938202> [Accessed 12 June 2015].
- XIE, M., ZHOU, Z., QI, Y., CHENG, Z. & YUAN, W. 2012. Sorption-enhanced steam methane reforming by in situ CO<sub>2</sub> capture on a CaO–Ca<sub>9</sub>Al<sub>6</sub>O<sub>18</sub> sorbent. *Chemical Engineering Journal*, 207–208, 142-150.
- XIU, G., LI, P. & RODRIGUES, A. E. 2003. Adsorption-enhanced steam-methane reforming with intraparticle-diffusion limitations. *Chemical Engineering Journal*, 95, 83-93.
- XU, J., CHEN, L., TAN, K. F., BORGNA, A. & SAEYS, M. 2009. Effect of boron on the stability of Ni catalysts during steam methane reforming. *Journal of Catalysis*, 261, 158-165.
- XU, P., ZHOU, Z., ZHAO, C. & CHENG, Z. 2016. Catalytic performance of Ni/CaO–Ca<sub>5</sub>Al<sub>6</sub>O<sub>14</sub> bifunctional catalyst extrudate in sorption-enhanced steam methane reforming. *Catalysis Today*, 259, Part 2, 347-353.
- YAHOM, A., POWELL, J., PAVARAJARN, V., ONBUDDHA, P., CHAROJROCHKUL, S. & ASSABUMRUNGRAT, S. 2014. Simulation and thermodynamic analysis of chemical looping reforming and CO<sub>2</sub> enhanced chemical looping reforming. *Chemical Engineering Research and Design*, 92, 2575-2583.
- YAMIN, J. A. 2007. Heat losses minimization from hydrogen fueled 4-stroke spark ignition engines. *Brazilian Society of Mechanical Sciences and Engineering*, 29, 109- 114.
- YAZDANPANA, M. M., HOTEIT, A., FORRET, A., DELEBARRE, A. & GAUTHIER, T. 2011. Experimental Investigations on a Novel Chemical Looping Combustion Configuration. *Oil & Gas Science Technology*, 66, 265 - 275.
- YILDIRIM, Ö., KISS, A. A., HÜSER, N., LEßMANN, K. & KENIG, E. Y. 2012. Reactive absorption in chemical process industry: A review on current activities. *Chemical Engineering Journal*, 213, 371-391.
- YOUN, M. H., SEO, J. G., CHO, K. M., JUNG, J. C., KIM, H., LA, K. W., PARK, D. R., PARK, S., LEE, S. H. & SONG, I. K. 2008. Effect of support on hydrogen production by auto-thermal reforming of ethanol over supported nickel catalysts. *Korean Journal of Chemical Engineering*, 25, 236-238.
- ZAFAR, Q., MATTISSON, T. & GEVERT, B. 2005. Integrated hydrogen and power production with CO<sub>2</sub> capture using chemical-looping reforming-redox reactivity of particles of CuO, Mn<sub>2</sub>O<sub>3</sub>, NiO, and Fe<sub>2</sub>O<sub>3</sub> using SiO<sub>2</sub> as a support. *Industrial & Engineering Chemistry Research*, 44(10), 3485-3496.
- ZAKKOUR, P. & COOK, G. 2010. *CCS Roadmap for Industry: High-purity CO<sub>2</sub> sources* [Online]. UK: Carbon Counts Company Ltd. Available: <http://hub.globalccsinstitute.com/sites/default/files/publications/15686/ccs->

roadmap-industry-high-purity-co2-sources-sectoral-assessment.pdf [Accessed 23 June 2016].

- ZHANG, H., LIN, G. & CHEN, J. 2010. Evaluation and calculation on the efficiency of a water electrolysis system for hydrogen production. *International Journal of Hydrogen Energy*, 35, 10851-10858.
- ZHANG, L., LU, Y. & ROSTAM-ABADI, M. 2012. Sintering of calcium oxide (CaO) during CO<sub>2</sub> chemisorption: a reactive molecular dynamics study. *Physical Chemistry Chemical Physics*, 14, 16633-16643.
- ZHAO, D. & YANG, C.-F. 2016. Recent advances in the TiO<sub>2</sub>/CdS nanocomposite used for photocatalytic hydrogen production and quantum-dot-sensitized solar cells. *Renewable and Sustainable Energy Reviews*, 54, 1048-1059.
- ZHENG, X., SU, Q., MI, W. & ZHANG, P. 2014. Effect of steam reforming on methane-fueled chemical looping combustion with Cu-based oxygen carrier. *International Journal of Hydrogen Energy*, 39, 9158-9168.
- ZHU, J., ZHANG, D. & KING, K. D. 2001. Reforming of CH<sub>4</sub> by partial oxidation: thermodynamic and kinetic analyses. *Fuel*, 80, 899-905.
- ZHU, L. & FAN, J. 2015. Thermodynamic analysis of H<sub>2</sub> production from CaO sorption-enhanced methane steam reforming thermally coupled with chemical looping combustion as a novel technology. *International Journal of Energy & Research*, 39, 356-369.
- ZIN, R. M., LEA-LANGTON, A., DUPONT, V. & TWIGG, M. V. 2012. High hydrogen yield and purity from palm empty fruit bunch and pine pyrolysis oils. *International Journal of Hydrogen Energy*, 37, 10627-10638.

## Appendix

### Appendix A1: Supplementary data for thermodynamic equilibrium analysis

Table A1.1 Equilibrium outputs comparing C-SR with SE-SR and CL- SR (H<sub>2</sub> yield and purity in the dry gas and selectivity of C to CaCO<sub>3(s)</sub>) for S:C 0,1,2 and 3 at 1 bar. No reg./with reg. mean calculations not including/ including CaCO<sub>3(s)</sub> regeneration back to CaO<sub>(s)</sub>

S:C ratio	Conditions	H <sub>2</sub> yield (wt. % of fuel)	H <sub>2</sub> purity (%)	Selectivity of C to CaCO <sub>3(s)</sub> (%)	Temperature (K)
0	Without Ca	14.2	52.5	n/a	880
		21.2	62.2	n/a	1070
0	With CaO, no reg.	14.2	52.5	0.0	880
		21.2	62.2	0.0	1070
0	With CaO, with reg.	14.2	52.5	0.0	880
		21.2	62.2	0.0	1070
0	With NiO, NiO:C 1.0	13.0	63.0	n/a	880
		21.0	65.0	n/a	1070
1	Without Ca	21.0	67.7	n/a	880
		33.0	72.3	n/a	1070
1	With CaO, no reg.	36.5	75.3	68.3	880
		33.0	72.3	0.0	1070
1	With CaO, with reg.	36.5	75.3	68.3	880
		33.0	72.3	0.0	1070
1	With NiO, NiO:C 1.0	21.0	61.5	n/a	880
		27.0	68.0	n/a	1070
2	Without Ca	28.3	68.8	n/a	880
		38.5	74.9	n/a	1070
2	With CaO, no reg.	37.5	91.7	74.0	880
		38.5	72.9	0.0	1070
2	With CaO, with reg.	37.5	91.7	74.0	880
		38.5	72.9	0.0	1070
2	With NiO, NiO:C 1.0	26.5	67.3	n/a	880
		29.2	69.4	n/a	1070
2	With CaO & NiO no reg. NiO:C 1.0	34.8	97.7	94.0	880
		29.1	69.4	0.0	1070
2	With CaO & NiO with reg. NiO:C 1.0	34.8	97.7	94.0	880
		29.1	69.4	0.0	1070
3	Without Ca	35.0	73.1	n/a	880
		40.5	75.9	n/a	1070
3	With CaO, no reg.	45.5	97.2	90.1	880
		40.5	75.9	0.0	1070

3	With CaO, with reg.	45.5	97.2	90.1	880
		40.5	75.9	0.0	1070
3	With NiO, NiO:C 0.5	33.0	72.0	n/a	880
		36.0	73.4	n/a	1070
3	With NiO, NiO:C 0.76	31.2	71.0	n/a	880
		32.4	72.0	n/a	1070
3	With NiO, NiO:C 1.0	30.0	70.0	n/a	880
		30.5	70.3	n/a	1070
3	With CaO & NiO no reg. NiO:C 1.0	36.0	98.6	96.3	880
		30.5	70.3	0.0	1070
3	With CaO & NiO with reg. NiO:C 1.0	36.0	98.6	96.3	880
		30.5	70.3	0.0	1070

**Table A1.2 Equilibrium outputs of SE-SR at 880 K ( $\Delta H$  Total (kJ/mol H<sub>2</sub>) and  $\Delta H$  ratio) at 1 bar, Ca:C 1, and S:C 0,1,2 and 3. A and B mean without regeneration and with regeneration respectively).**

Conditions	$\Delta H$ total (kJ/mol H <sub>2</sub> )	$\Delta H$ ratio
S:C 0 With CaO A	65	0.20
S:C 0 With CaO B	65	0.20
S:C 1 With CaO A	37	0.11
S:C 1 With CaO B	85	0.27
S:C 2 With CaO A	57	0.18
S:C 2 With CaO B	106	0.33
S:C 3 With CaO A	66	0.21
S:C 3 With CaO B	117	0.37

**Table A1.3 Equilibrium outputs of CL-SR at 880 and 1070 K ( $\Delta H$  total and  $\Delta H$  ratio at 1 bar, NiO:C 0.5-1.0 and varied S:C 0- 3.)**

S:C ratio	Conditions	$\Delta H$ total (kJ/mol H <sub>2</sub> )	$\Delta H$ ratio	Temperature (K)
1	NiO:C 1.00	30	0.09	880
		56	0.17	1070
2	NiO:C 1.00	74	0.24	880
		91	0.28	1070
3	NiO:C 0.50	119	0.38	880
		133	0.41	1070
3	NiO:C 0.75	106	0.34	880
		123	0.38	1070
3	NiO:C 1.00	98	0.31	880
		118	0.37	1070

## Appendix A2: Validation of CEA software results with Aspen Plus results

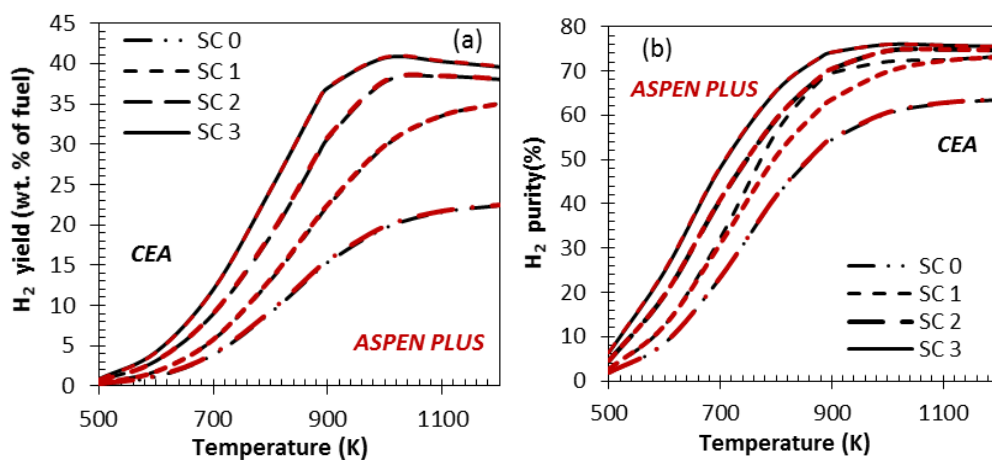


Figure A2.1 C-SR comparison of CEA software and Aspen Plus results at 1 bar and varied S:C ratio (shale gas 1 input): (a) H<sub>2</sub> yield vs temperature (b) H<sub>2</sub> purity vs temperature

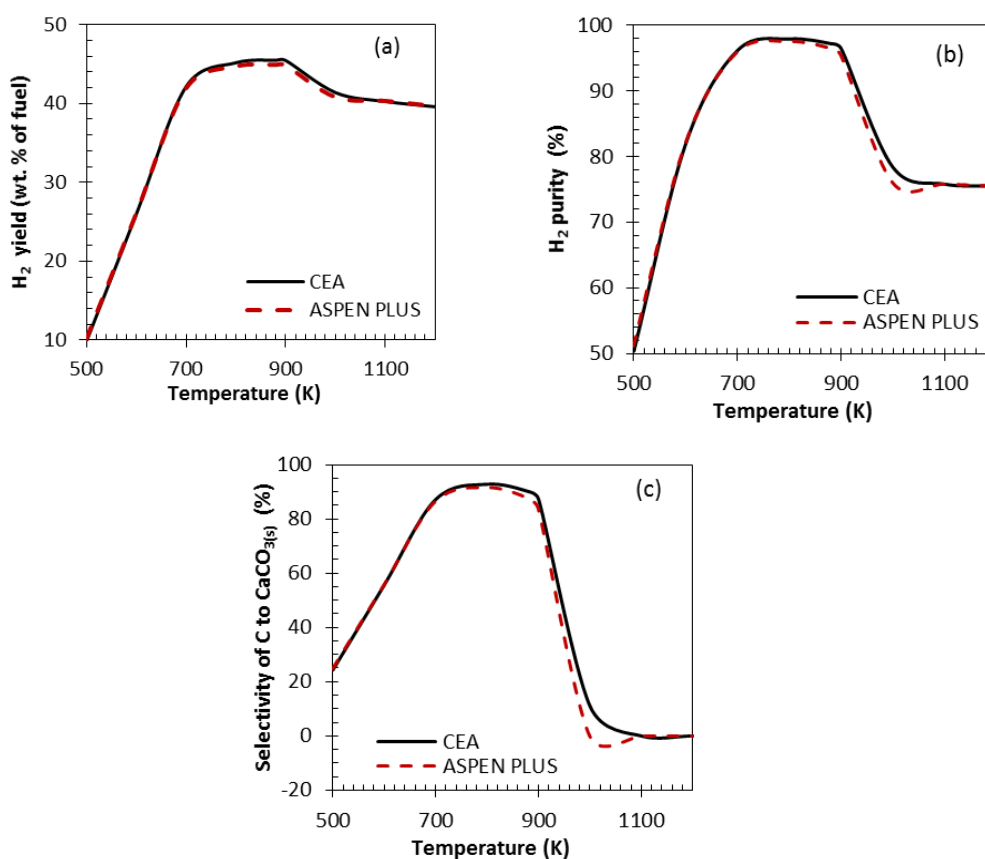


Figure A2.2 SE-SR comparison of CEA software and Aspen Plus results at 1 bar, Ca:C 1 and S:C 3 (shale gas 1 input): (a) H<sub>2</sub> yield vs temperature (b) H<sub>2</sub> purity vs temperature (c) selectivity of C to CaCO<sub>3</sub> vs temperature

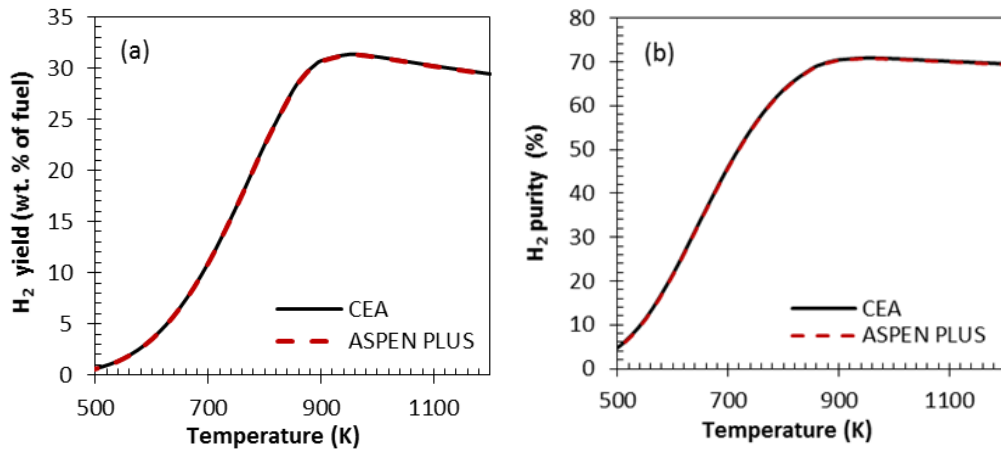


Figure A2.3 CL-SR comparison of CEA software and Aspen Plus results at 1 bar, NiO:C 1 and S:C 3 (shale gas 1 input): (a) H<sub>2</sub> yield vs temperature (b) H<sub>2</sub> purity vs temperature

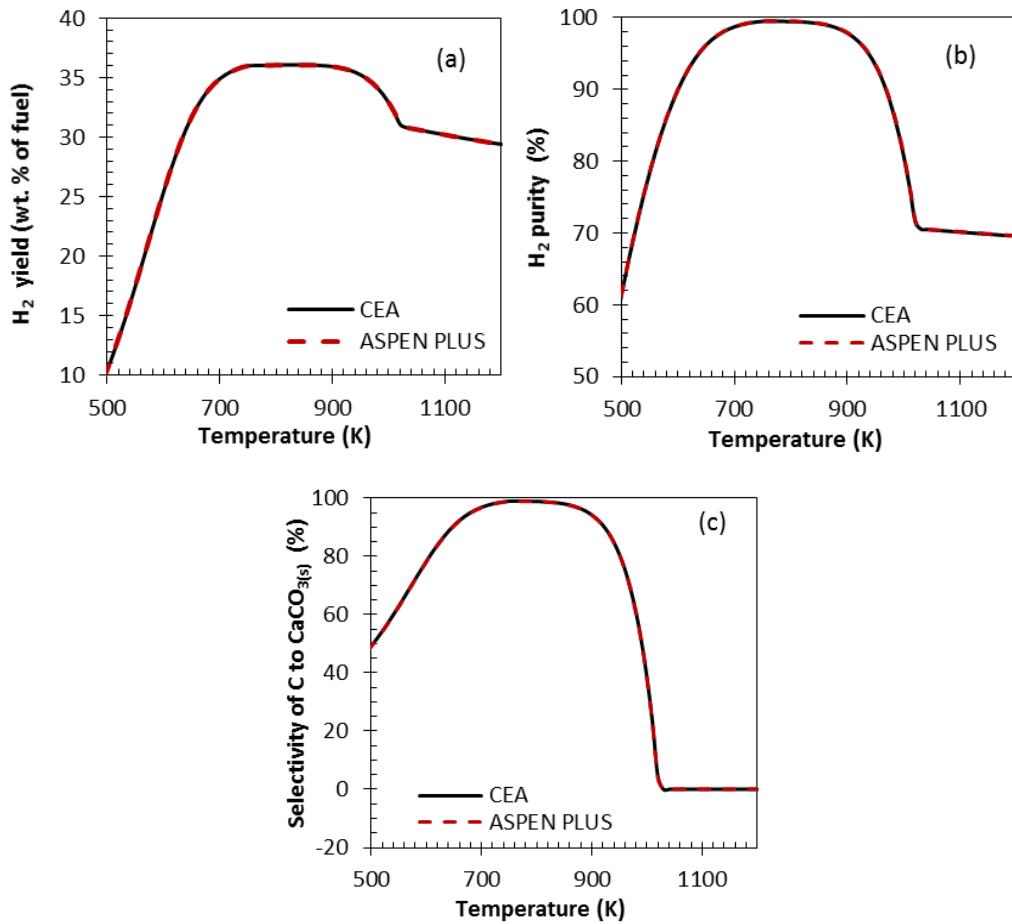


Figure A2.4 SECL-SR comparison of CEA software and Aspen Plus results at 1 bar, Ca:C 1, NiO:C 1 and S:C 3 (shale gas 1 input): (a) H<sub>2</sub> yield vs temperature (b) H<sub>2</sub> purity vs temperature (c) selectivity of C to CaCO<sub>3</sub> vs temperature

## Appendix B1: Calibration results for micro GC

The gas chromatograph used an external standard method to determine the reactor outlet gas composition. Different gases (feeds and expected products) were used for the calibration of the gas chromatograph. The calibration gas was connected to the gas chromatograph and samples were injected to the Column through the sampling pump. Calibration point were taken when the quantity of the sampling gases were constant and there was no residual oxygen from air.

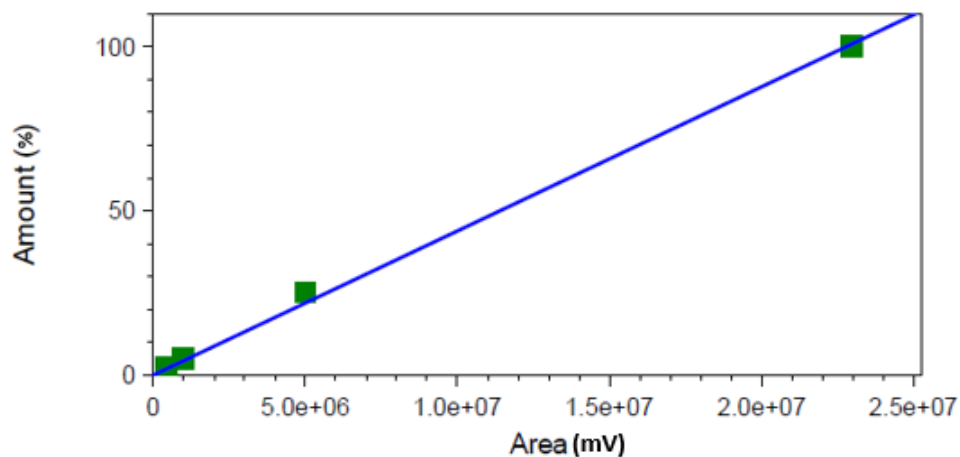


Figure B1.1 Methane (CH<sub>4</sub>) calibration on GC (Channel 1)

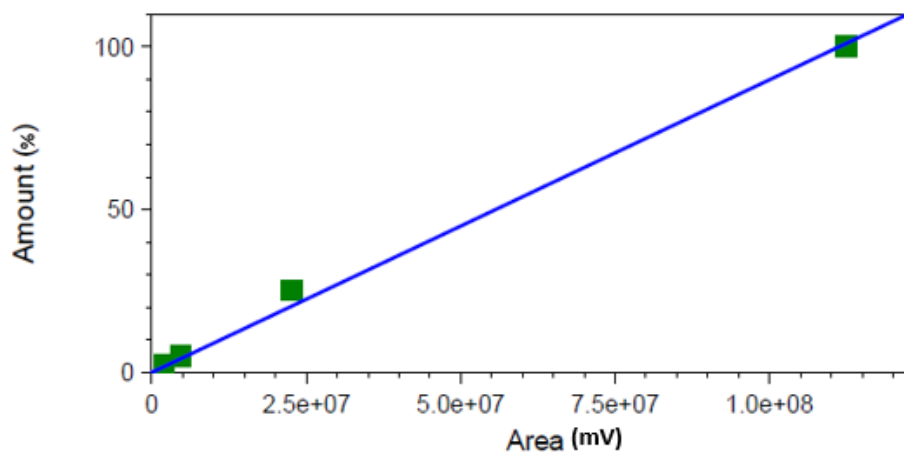


Figure B1.2 Methane (CH<sub>4</sub>) calibration on GC (Channel 2)

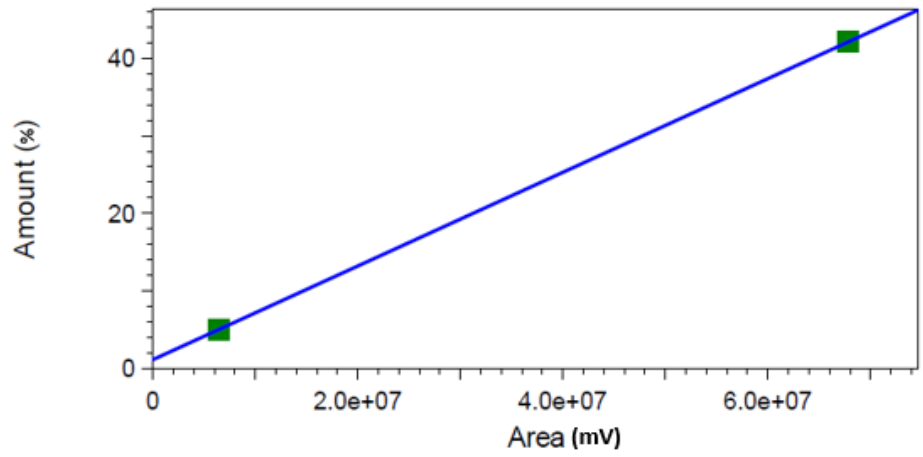


Figure B1.3 Ethane (C<sub>2</sub>H<sub>6</sub>) calibration on GC (Channel 2)

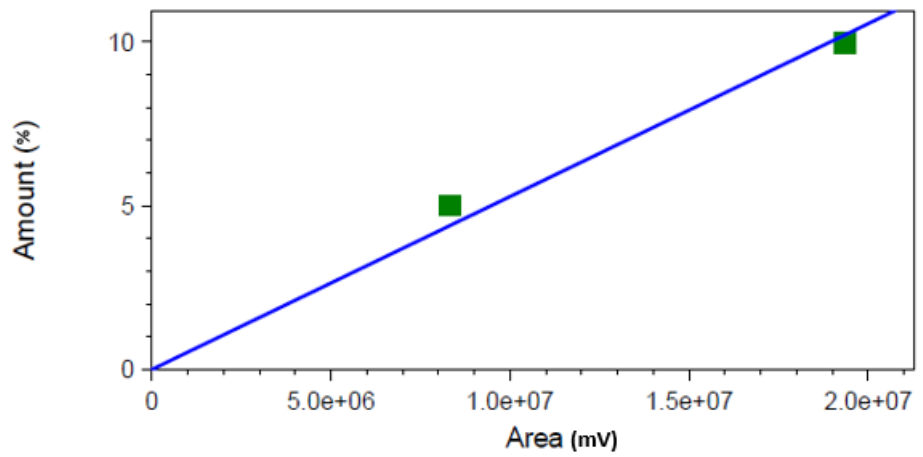


Figure B1.4 Propane (C<sub>3</sub>H<sub>8</sub>) calibration on GC (Channel 2)

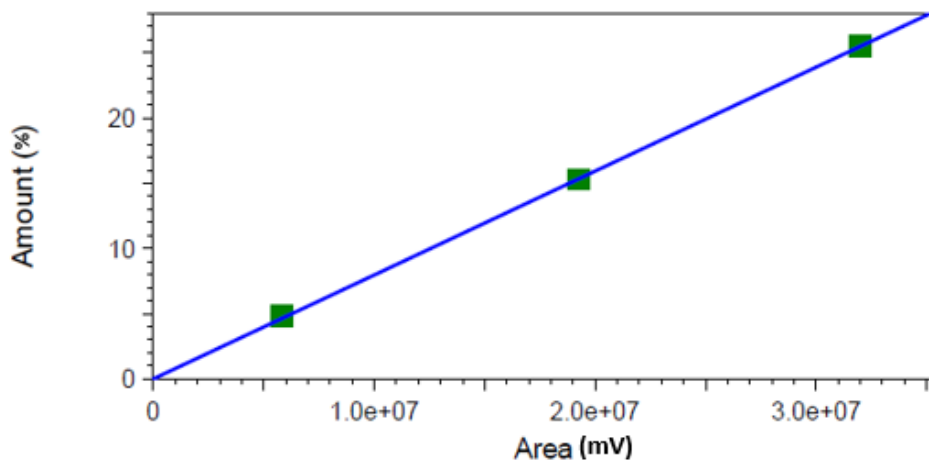


Figure B1.5 Carbon dioxide (CO<sub>2</sub>) calibration on GC (Channel 2)

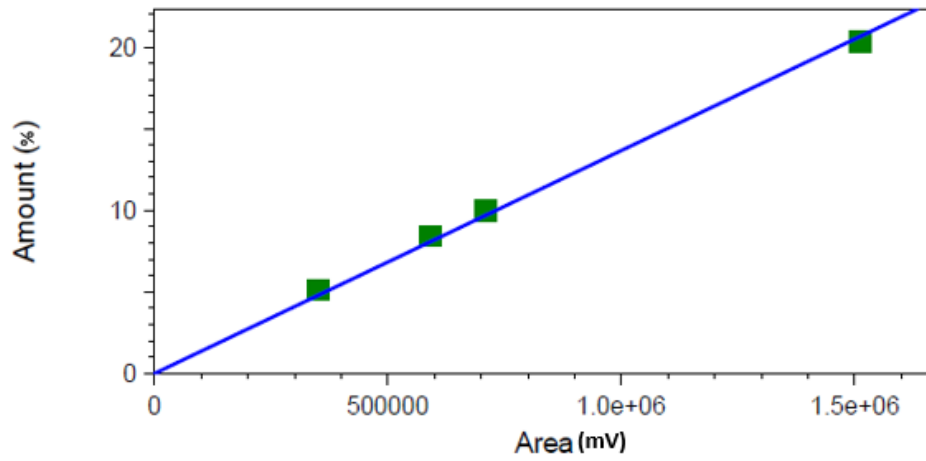


Figure B1.6 Carbon monoxide (CO) calibration on GC (Channel 1)

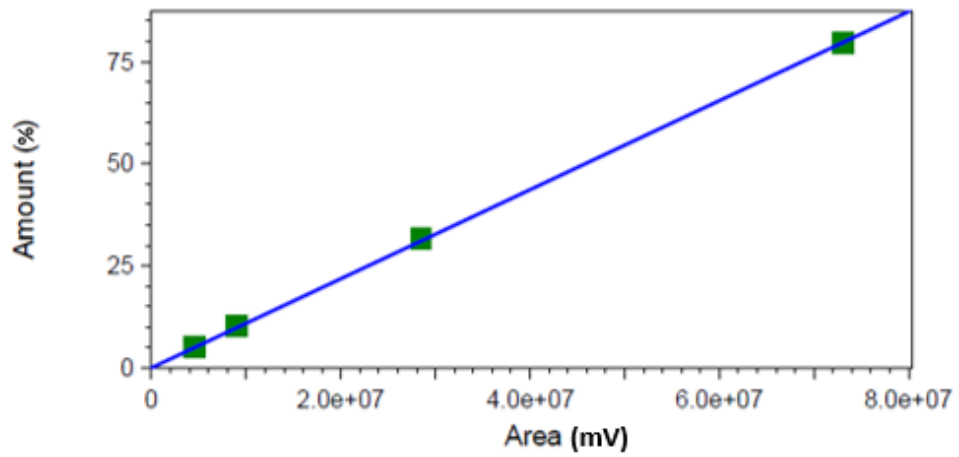


Figure B1.7 Hydrogen (H<sub>2</sub>) calibration on GC (Channel 1)

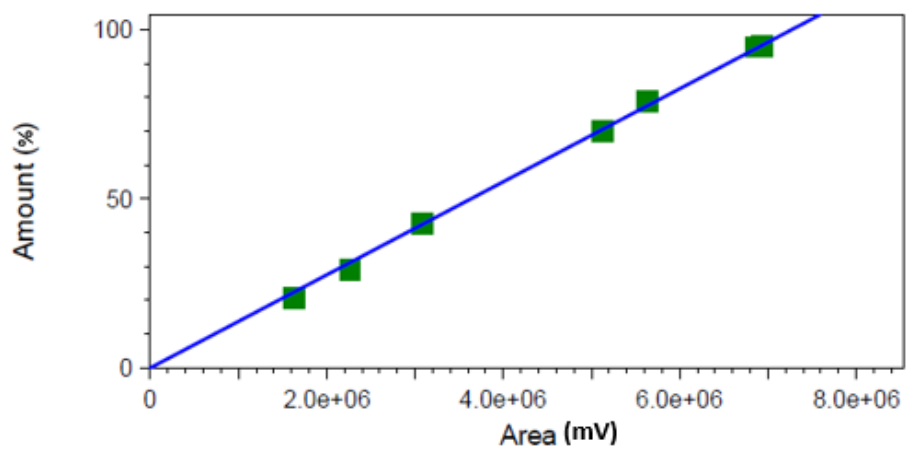


Figure B1.8 Nitrogen (N<sub>2</sub>) calibration on GC (Channel 1)

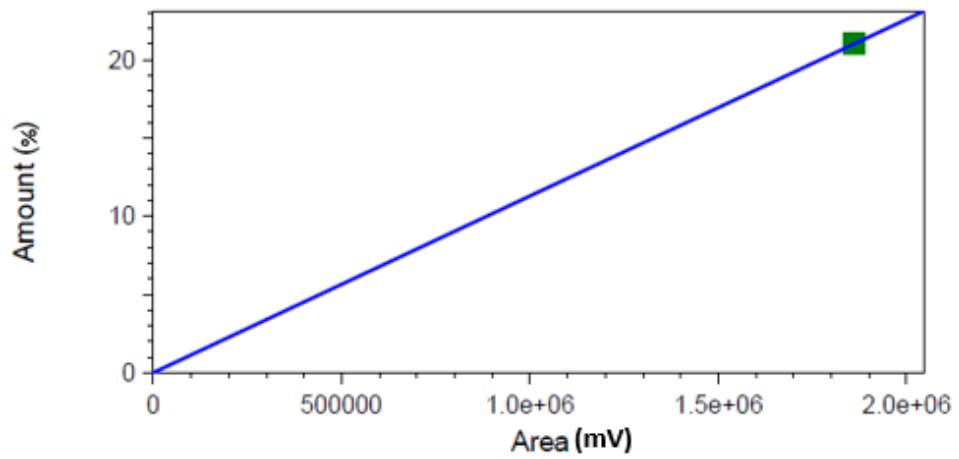


Figure B1.9 Oxygen (O<sub>2</sub>) calibration on GC (Channel 1)

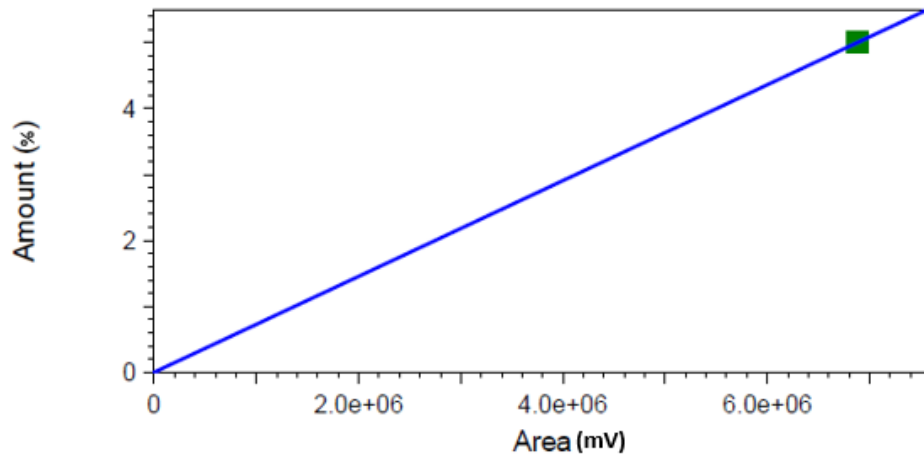


Figure B1.10 Ethylene (C<sub>2</sub>H<sub>4</sub>) calibration on GC (Channel 2) (Note: not detected in experiments)

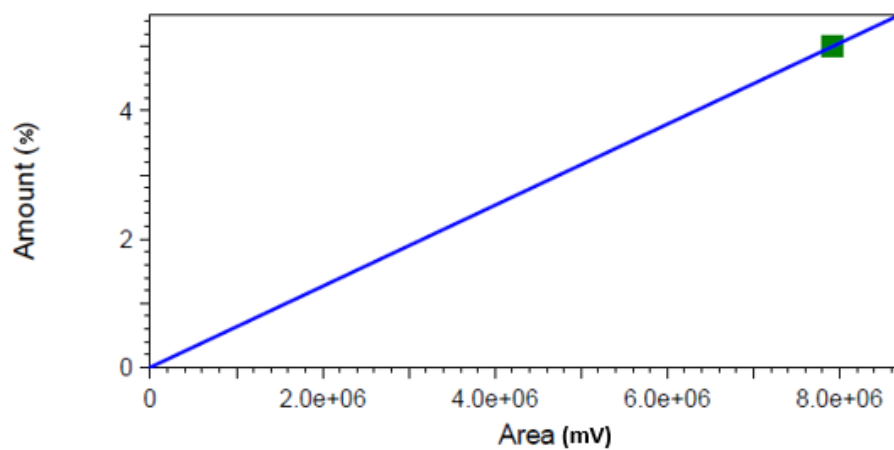


Figure B1.11 Propylene (C<sub>3</sub>H<sub>6</sub>) calibration on GC (Channel 2) (Note: not detected in experiments)

**Table B1.1 Components goodness of fit**

Component	Goodness of fit ( $r^2$ ) Channel 1	Goodness of fit ( $r^2$ ) Channel 2
Methane (CH <sub>4</sub> )	0.997975	0.995915
Ethane (C <sub>2</sub> H <sub>6</sub> )		1.00000
Propane (C <sub>3</sub> H <sub>8</sub> )		0.965270
Carbon dioxide (CO <sub>2</sub> )		0.999868
Carbon monoxide (CO)	0.996690	
Hydrogen (H <sub>2</sub> )	0.999884	
Nitrogen (N <sub>2</sub> )	0.997945	
Oxygen (O <sub>2</sub> )	1.00000	
Ethylene (C <sub>2</sub> H <sub>4</sub> )		1.00000
Propylene (C <sub>3</sub> H <sub>6</sub> )		1.00000

**Appendix B2: ICDD reference code****Table B2.1 ICDD reference code of Ni, Al<sub>2</sub>O<sub>3</sub> and CaO**

Condition	Ni reference code	Al <sub>2</sub> O <sub>3</sub> reference code	CaO reference code
C-SR at 600 °C	04-001-3331	04-014-8419	N/A
C-SR at 650 °C	04-001-1136	04-005-4213	N/A
C-SR at 700 °C	01-071-4653	04-006-9730	N/A
C-SR at 750 °C	01-077-8341	04-006-9359	N/A
SE-SR at 600 °C	04-006-6387	04-015-8609	00-003-1123
SE-SR at 650 °C	00-001-1260	04-006-9730	04-005-4398
SE-SR at 700 °C	00-001-1260	04-006-9730	00-001-1160

## Appendix B3: EDX images

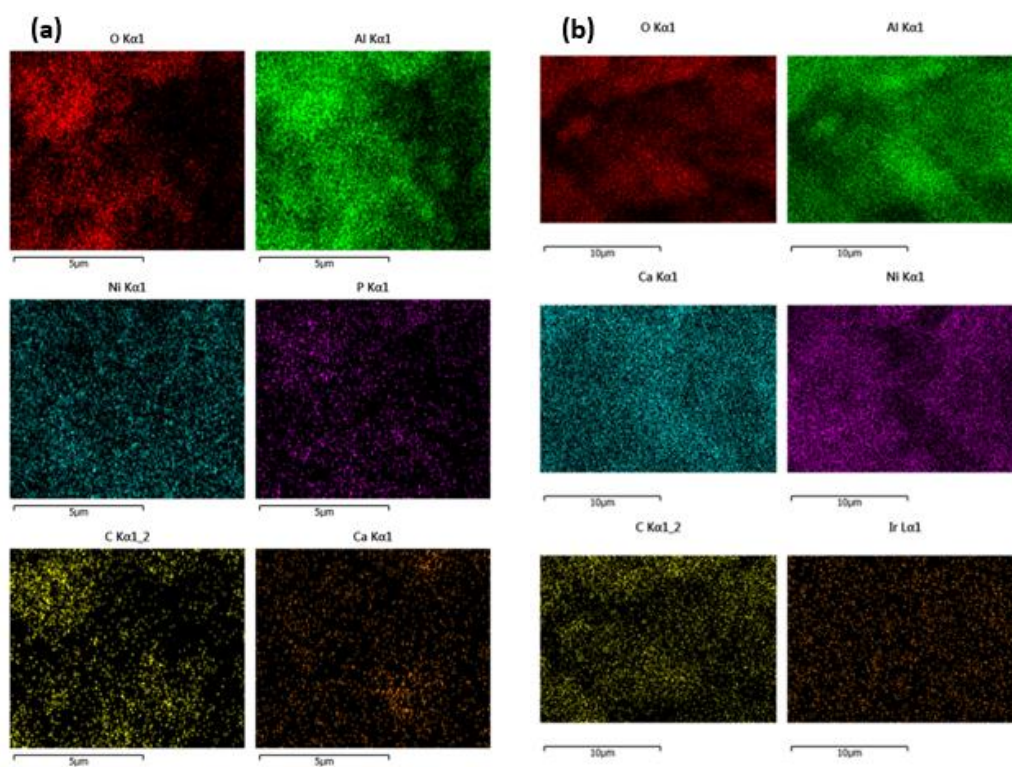


Figure B3.1 (a) C-SR mapping at 650 °C using 18 wt. % NiO on Al<sub>2</sub>O<sub>3</sub> support (b) C-SR mapping at 750 °C using 15 wt. % NiO on CaO/Al<sub>2</sub>O<sub>3</sub> support

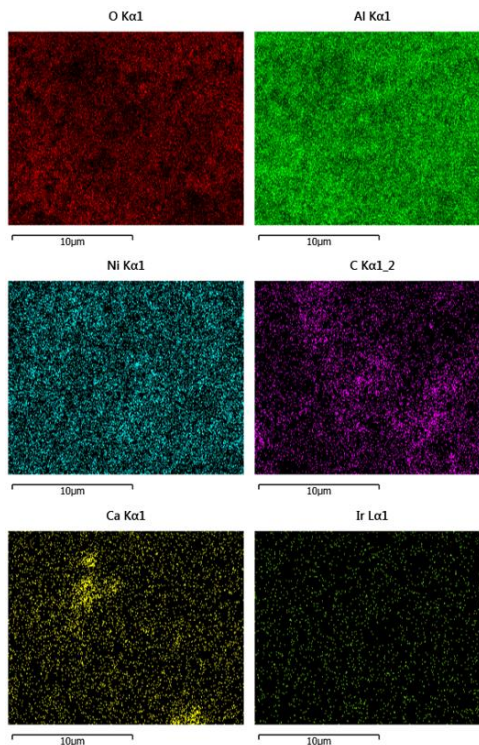


Figure B3.2 SE-SR mapping at 650 °C using 18 wt. % NiO on Al<sub>2</sub>O<sub>3</sub> support

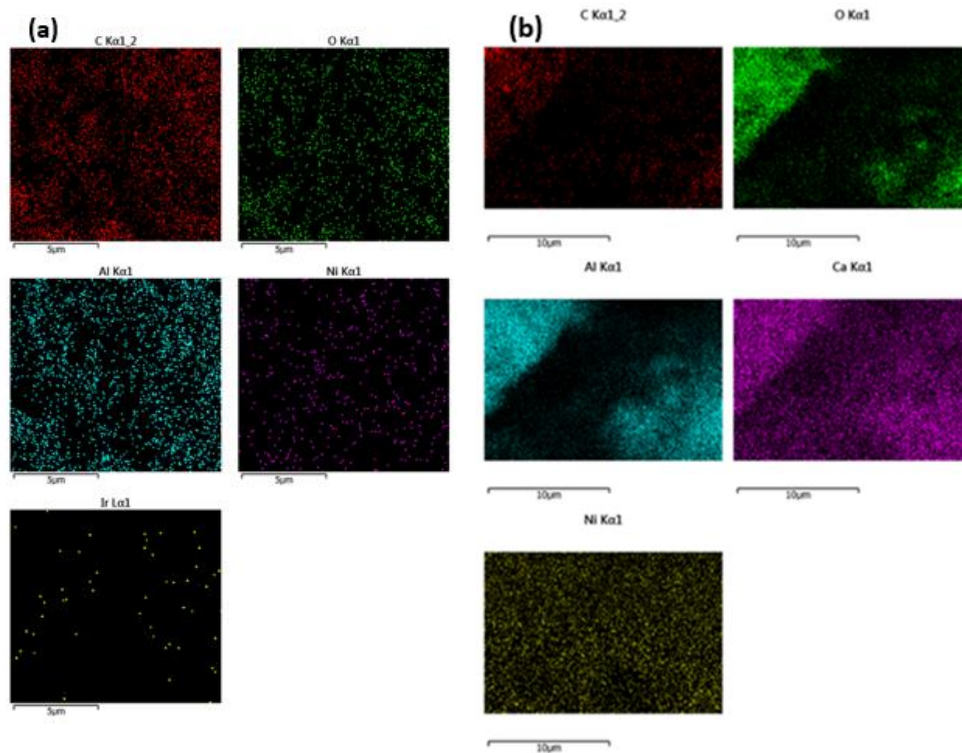


Figure B3.3 (a) CL-SR mapping at 650 °C using 18 wt. % NiO on Al<sub>2</sub>O<sub>3</sub> support (b) CL-SR mapping at 750 °C using 15 wt. % NiO on CaO/Al<sub>2</sub>O<sub>3</sub> support

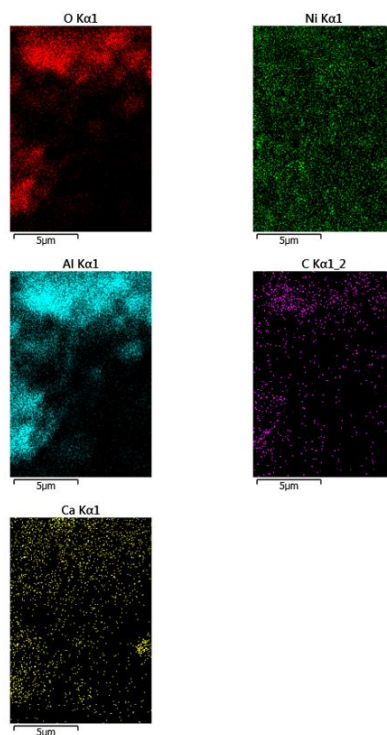


Figure B3.4 SE-CLSR mapping at 650 °C using 18 wt. % NiO on Al<sub>2</sub>O<sub>3</sub> support

## Appendix B4: Carbon balance calculation

Carbon balance is shown below considering NiO on CaO/Al<sub>2</sub>O<sub>3</sub> support as an example;

Input molar flowrate of carbon is  $4.1725 \times 10^{-6}$  mol/s having 3750 s as experiment duration the inlet mole of carbon is calculated to  $4.1725 \times 10^{-6}$  mol/s  $\times$  3750 s =  $1.5647 \times 10^{-2}$  mol.

The feedstock conversion was 81.684 %, thus carbon leaving the reactor with the gases is given by;

$$C \text{ leaving the reactor with gases} = 1.5647 \times 10^{-2} \times 0.8168 = 1.2781 \times 10^{-2} \text{ mol}$$

The amount of C deposited on the catalyst obtained from elemental analysis is calculated as follows;

$$C \text{ on catalyst surface} = \frac{\text{Carbon weight fraction}}{(1 - \text{Carbon weight fraction})} \times \frac{\text{Mass of catalyst}}{\text{Molar mass of carbon}}$$

Using the C-SR process at 750 °C for example: the quantity of carbon obtained from the CHNS analysis is 0.40 wt. % . Thus carbon on the surface of the catalyst is;

$$C \text{ on catalyst surface} = \frac{0.0040}{(1 - 0.0040)} \times \frac{3.0000}{12.0107} = 1.0031 \times 10^{-3}$$

The amount of C in the condensate is calculated as follows;

$$C \text{ in condensate} = \frac{\text{Mass con. of C in condensate}}{1000} \times \frac{\text{Volume of condensate}}{1000} \times \frac{1}{12}$$

Again, Using the C-SR process at 750 °C for example; the quantity of C in the condensate was 39.57 ppm and the quantity of condensate collected was 1 ml, therefore the quantity of C in the condensate would be

$$C \text{ in condensate} = \frac{39.57}{1000} \times \frac{1}{1000} \times \frac{1}{12} = 3.2975 \times 10^{-6}$$

The total output was as follows;

$$\text{Total output } C = \sum C \text{ in gas} + C \text{ on catalyst surface} + C \text{ in condensate}$$

$$\begin{aligned} \text{Total output } C &= (1.2781 \times 10^{-2} + 1.0031 \times 10^{-3} + 3.2975 \times 10^{-6}) \\ &= 1.3788 \times 10^{-2} \end{aligned}$$

$$\text{Unaccounted carbon (\%)} = \frac{\text{Inlet mole of C} - \text{Total output C}}{\text{Total output C}} \times 100$$

$$\text{Unaccounted carbon (\%)} = \frac{1.5647 \times 10^{-2} - 1.3788 \times 10^{-2}}{1.3788 \times 10^{-2}} \times 100 = 13.487 \%$$

$$\text{Carbon in gas} = \frac{\text{C leaving the reactor with gases}}{\text{Total output C}} \times 100$$

$$\text{Carbon in gas} = \frac{1.2781 \times 10^{-2}}{1.3788 \times 10^{-2}} \times 100 = 92.70 \%$$

$$\text{Carbon in catalyst} = \frac{\text{C on catalyst surface}}{\text{Total output C}} \times 100$$

$$\text{Carbon in catalyst} = \frac{1.0031 \times 10^{-3}}{1.3788 \times 10^{-2}} \times 100 = 7.28 \%$$

$$\text{Carbon in condensate} = \frac{\text{C in condensate}}{\text{Total output C}} \times 100$$

$$\text{Carbon in condensate} = \frac{3.2975 \times 10^{-6}}{1.3788 \times 10^{-2}} \times 100 = 0.02$$

## Appendix B5: C-SR process maximum and average process outputs

Table B5.1 Maximum and average process outputs of C-SR process using 18 wt. % NiO on Al<sub>2</sub>O<sub>3</sub> support as catalyst

T(°C)	H <sub>2</sub> yield (wt. % of fuel)	H <sub>2</sub> purity (%)	Fuel conversion (%)	H <sub>2</sub> O conversion (%)
<b>Maximum process outputs</b>				
600	15.045	57.217	50.284	12.442
650	20.035	68.729	62.507	16.478
700	21.027	69.737	63.084	21.207
750	24.159	68.076	65.642	27.684
<b>Average process outputs</b>				
600	14.600	57.525	49.266	11.293
650	17.453	64.396	61.081	10.771
700	19.337	64.884	62.179	19.563
750	23.278	65.955	63.759	24.003

Table B5.2 Maximum and average process outputs of C-SR process using 15 wt. % NiO on CaO/Al<sub>2</sub>O<sub>3</sub> support as catalyst

T (°C)	H <sub>2</sub> yield (wt. % of fuel)	H <sub>2</sub> purity (%)	Fuel conversion (%)	H <sub>2</sub> O conversion (%)
<b>Maximum process outputs</b>				
600	13.389	58.578	45.930	10.395
650	16.632	62.007	50.412	16.48
700	23.012	71.021	67.367	21.596
750	40.933	76.302	90.018	52.012
<b>Average process outputs</b>				
600	12.018	52.451	44.114	8.071
650	15.770	57.983	48.611	14.745
700	21.871	66.723	66.163	18.773
750	31.593	71.318	81.684	33.489

## Appendix B6: SE-SR process maximum and average process outputs

**Table B6.1 Maximum and average process outputs of SE-SR process using CaO sorbent and 18 wt. % NiO on Al<sub>2</sub>O<sub>3</sub> support as catalyst (pre- breakthrough period values). Note: the fuel and water conversion are not reliable**

T (°C)	H <sub>2</sub> yield (wt. % of fuel)	H <sub>2</sub> purity (%)	Fuel conversion (%)	H <sub>2</sub> O conversion (%)
<b>Maximum process outputs</b>				
600	27.311	94.011	61.755	19.212
650	23.005	86.058	60.429	19.136
700	22.966	95.845	53.807	18.085
<b>Average process outputs</b>				
600	21.138	83.946	61.755	13.067
650	20.793	83.966	60.429	13.800
700	20.323	82.961	53.807	13.680

**Table B6.2 Average process outputs of SE-SR process using CaO sorbent and 18 wt. % NiO on Al<sub>2</sub>O<sub>3</sub> support as catalyst (post breakthrough period values)**

T (°C)	H <sub>2</sub> yield (wt. % of fuel)	H <sub>2</sub> purity (%)	Fuel conversion (%)	H <sub>2</sub> O conversion (%)
600	18.041	70.691	61.755	6.868
650	18.892	69.406	60.429	9.771
700	16.559	65.235	53.807	7.131

## Appendix B7: CL-SR process maximum and average process outputs

Table B7.1 Maximum process outputs of CL-SR process using 18 wt. % NiO on Al<sub>2</sub>O<sub>3</sub> support as OTM/catalyst. Reforming/reduction at 650 °C and oxidation at 750 °C

Number of cycle	H <sub>2</sub> yield (wt. % of fuel)	H <sub>2</sub> purity (%)	Fuel conversion (%)	H <sub>2</sub> O conversion (%)
1st	20.340	74.810	72.460	12.750
2nd	19.684	67.804	72.320	11.966
3rd	18.463	66.171	84.319	9.495
4th	18.563	67.991	82.626	8.769
5th	18.843	70.830	88.519	10.069
6th	18.972	68.824	86.503	8.112
7th	19.223	74.229	84.269	12.543
8th	21.030	69.811	71.991	16.288
9th	23.971	77.564	88.296	20.049
10th	21.295	73.815	80.096	15.082
11th	19.743	78.796	88.136	11.365
12th	20.100	71.357	82.969	11.839
13th	20.480	71.220	84.532	13.163
14th	19.693	68.725	88.939	12.880
15th	20.965	69.684	77.193	15.246
16th	19.869	65.484	71.500	12.573
17th	23.971	77.564	88.296	20.049
18th	20.100	71.357	82.969	11.839
19th	19.693	68.725	88.939	12.880
20th	19.684	67.804	72.320	11.966

**Table B7.2 Average process outputs of CL-SR process using 18 wt. % NiO on Al<sub>2</sub>O<sub>3</sub> support as OTM/catalyst. Reforming/reduction temperature at 650 °C and oxidation at 750 °C**

<b>Number of cycle</b>	<b>H<sub>2</sub> yield (wt. % of fuel)</b>	<b>H<sub>2</sub> purity (%)</b>	<b>Fuel conversion (%)</b>	<b>H<sub>2</sub>O conversion (%)</b>
1st	19.165	70.740	71.531	8.218
2nd	17.963	66.137	70.276	5.957
3rd	16.820	63.438	69.758	3.354
4th	17.720	65.475	69.464	5.870
5th	17.773	65.154	69.909	5.712
6th	18.307	66.471	71.205	6.225
7th	18.487	64.162	67.24	9.332
8th	19.470	65.957	68.585	10.970
9th	19.819	66.444	69.951	10.985
10th	19.985	65.879	69.769	11.506
11th	18.268	66.322	71.739	5.766
12th	18.369	65.304	70.262	7.012
13th	19.510	65.287	70.479	9.810
14th	18.616	64.231	68.403	8.889
15th	19.921	65.138	68.496	12.192
16th	19.348	64.459	67.215	11.567
17th	19.819	66.444	69.951	10.985
18th	18.369	65.304	70.262	7.012
19th	18.616	64.231	68.403	8.889
20th	17.963	66.137	70.276	5.957

**Table B7.3 Maximum process outputs of CL-SR process using 15 wt. % NiO on CaO/Al<sub>2</sub>O<sub>3</sub> support as OTM/catalyst. Reforming/reduction temperature at 750 °C and oxidation at 750 °C**

<b>Number of cycle</b>	<b>H<sub>2</sub> yield (wt. % of fuel)</b>	<b>H<sub>2</sub> purity (%)</b>	<b>Fuel conversion (%)</b>	<b>H<sub>2</sub>O conversion (%)</b>
1st	40.933	76.302	90.018	52.012
2nd	30.546	72.052	89.703	32.657
3rd	40.759	77.261	91.460	50.602
4th	39.600	78.714	90.440	49.095
5th	39.476	79.009	89.502	49.241
6th	39.888	76.536	92.720	49.101
7th	40.075	76.413	91.098	49.473
8th	38.861	75.686	87.395	49.710
9th	27.098	69.536	73.740	27.930
10th	25.848	71.795	83.858	25.179
11th	27.617	69.255	72.453	30.986
12th	28.404	70.639	82.116	30.545
13th	28.105	70.158	81.344	31.076
14th	28.149	69.201	77.470	30.507
15th	27.831	69.123	73.101	30.876
16th	28.749	70.189	76.127	30.511
17th	27.810	79.617	91.626	29.615
18th	28.502	70.072	78.315	30.705
19th	28.743	70.194	82.017	31.846
20th	28.404	70.639	81.116	30.545
21st	27.831	69.123	73.101	30.876

**Table B7.4 Average process outputs of CL-SR process using 15 wt. % NiO on CaO/Al<sub>2</sub>O<sub>3</sub> support as OTM/catalyst. Reforming/reduction temperature at 750 °C and oxidation at 750 °C**

<b>Number of cycle</b>	<b>H<sub>2</sub> yield (wt. % of fuel)</b>	<b>H<sub>2</sub> purity (%)</b>	<b>Fuel conversion (%)</b>	<b>H<sub>2</sub>O conversion (%)</b>
1st	31.593	71.318	81.684	33.489
2nd	29.535	69.788	78.398	30.375
3rd	33.239	71.713	82.518	37.176
4th	36.708	73.794	86.778	43.278
5th	37.804	74.484	87.619	45.544
6th	36.727	73.840	87.044	43.151
7th	37.826	74.308	88.274	45.163
8th	37.152	74.033	84.892	45.680
9th	26.019	68.372	72.153	25.473
10th	24.417	67.281	69.445	23.149
11th	26.187	67.828	70.050	27.309
12th	26.595	68.306	72.328	26.842
13th	26.606	68.253	72.084	27.031
14th	26.477	67.842	71.301	27.222
15th	26.479	67.991	71.217	27.284
16th	27.674	69.063	74.817	27.963
17th	26.928	69.036	75.087	25.861
18th	26.741	68.465	73.706	26.300
19th	26.696	68.033	73.553	26.286
20th	26.595	68.306	72.328	26.842

## Appendix B8: SECL-SR process maximum and average process outputs

Table B8.1 Maximum process outputs of SECL-SR process CaO sorbent and using 18 wt. % NiO on Al<sub>2</sub>O<sub>3</sub> support as OTM/catalyst. Reforming/reduction at 650 °C and oxidation at 850 °C (pre-breakthrough period)

Number of cycle	H <sub>2</sub> yield (wt. % of fuel)	H <sub>2</sub> purity (%)
1st	23.146	84.255
2nd	22.396	86.281
3rd	23.977	87.215
4th	37.265	96.508
5th	37.809	97.692
6th	33.988	93.765
7th	29.506	94.079
8th	25.447	89.947
9th	23.031	87.392
10th	26.037	89.602
11th	23.080	86.978
12th	23.312	87.978
13th	19.257	94.231
14th	19.361	90.532
15th	23.417	92.640
16th	23.826	93.464
17th	22.358	84.453
18th	23.428	86.917
19th	29.795	90.282
20th	27.584	87.922

**Table B8.2 Average process outputs of SECL-SR process using CaO sorbent and 18 wt. % NiO on Al<sub>2</sub>O<sub>3</sub> support as OTM/catalyst. Reforming/reduction at 650 °C and oxidation at 850 °C (pre-breakthrough period) Note: the fuel and water conversion are not reliable**

<b>Number of cycle</b>	<b>H<sub>2</sub> yield (wt. % of fuel)</b>	<b>H<sub>2</sub> purity (%)</b>	<b>Fuel conversion (%)</b>	<b>H<sub>2</sub>O conversion (%)</b>
1st	20.046	78.869	39.870	19.046
2nd	20.481	80.884	43.345	17.576
3rd	21.046	80.784	43.831	19.346
4th	31.404	92.039	52.968	34.312
5th	31.796	92.549	57.457	33.558
6th	28.194	89.593	46.011	28.171
7th	23.257	82.965	45.148	20.513
8th	19.694	80.687	42.041	14.080
9th	20.105	82.520	42.742	13.152
10th	19.899	80.637	44.150	13.468
11th	19.693	80.847	44.408	13.167
12th	20.740	83.073	55.416	14.712
13th	17.700	80.897	54.900	6.944
14th	18.251	81.544	61.118	7.747
15th	21.495	85.820	52.010	13.216
16th	21.252	84.506	52.744	14.321
17th	20.662	78.896	69.342	8.389
18th	21.089	78.612	64.016	9.334
19th	23.659	80.606	72.757	14.716
20th	24.344	81.533	72.969	16.792

**Table B8.3 Average process outputs of SECL-SR process using CaO sorbent and 18 wt. % NiO on Al<sub>2</sub>O<sub>3</sub> support as OTM/catalyst. Reforming/reduction at 650 °C and oxidation at 850 °C (Post breakthrough period)**

<b>Number of cycle</b>	<b>H<sub>2</sub> yield (wt. % of fuel)</b>	<b>H<sub>2</sub> purity (%)</b>	<b>Fuel conversion (%)</b>	<b>H<sub>2</sub>O conversion (%)</b>
1st	14.433	59.577	39.870	9.311
2nd	15.566	60.823	43.345	10.367
3rd	15.507	60.589	43.831	9.953
4th	20.411	66.195	52.968	17.693
5th	22.911	68.796	57.457	21.728
6th	16.622	61.924	46.011	11.658
7th	15.863	60.906	45.148	10.165
8th	12.521	59.034	42.041	3.217
9th	11.987	58.218	42.742	1.464
10th	12.956	60.146	44.150	3.205
11th	12.892	60.074	44.408	2.903
12th	19.405	68.574	55.416	13.784
13th	15.164	63.424	54.9	3.130
14th	15.366	63.547	55.862	3.133
15th	15.324	62.469	52.01	5.092
16th	15.759	63.424	52.744	5.821
17th	21.304	74.074	69.342	11.206
18th	23.105	71.204	64.016	18.709
19th	25.173	71.858	72.757	19.846
20th	25.469	71.840	72.969	20.791

## Appendix B9: C-SR process outputs (Repeat experiments)

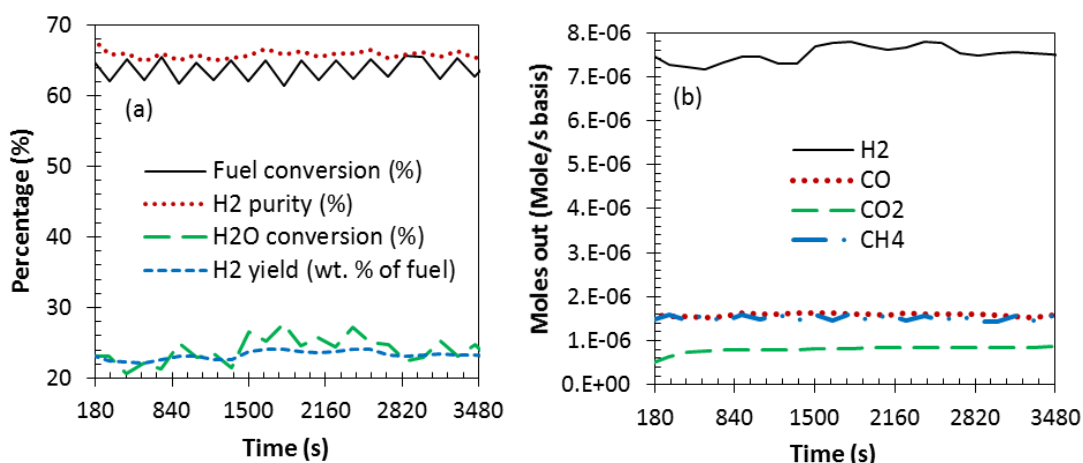


Figure B9.1 Process output vs time at 750 °C , 1 bar, GHSV 0.498 and S:C 3 (a) H<sub>2</sub> yield and purity, fuel and H<sub>2</sub>O conversion vs time using 18 wt. % NiO on Al<sub>2</sub>O<sub>3</sub> support catalyst (b) moles out vs time using 18 wt. % NiO on Al<sub>2</sub>O<sub>3</sub> support catalyst

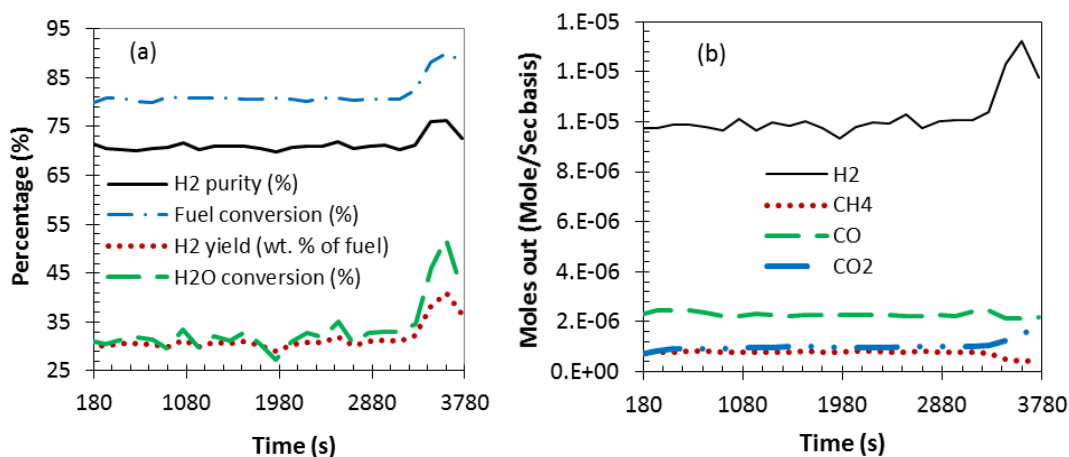


Figure B9.2 Process output vs time at 750 °C , 1 bar, GHSV 0.498 and S:C 3 (a) H<sub>2</sub> yield and purity, fuel and H<sub>2</sub>O conversion vs time using 15 wt. % NiO on CaO/Al<sub>2</sub>O<sub>3</sub> support catalyst (b) moles out vs time using 15 wt. % NiO on CaO/Al<sub>2</sub>O<sub>3</sub> support catalyst

### Appendix B10: SE-SR process outputs (Repeat experiment)

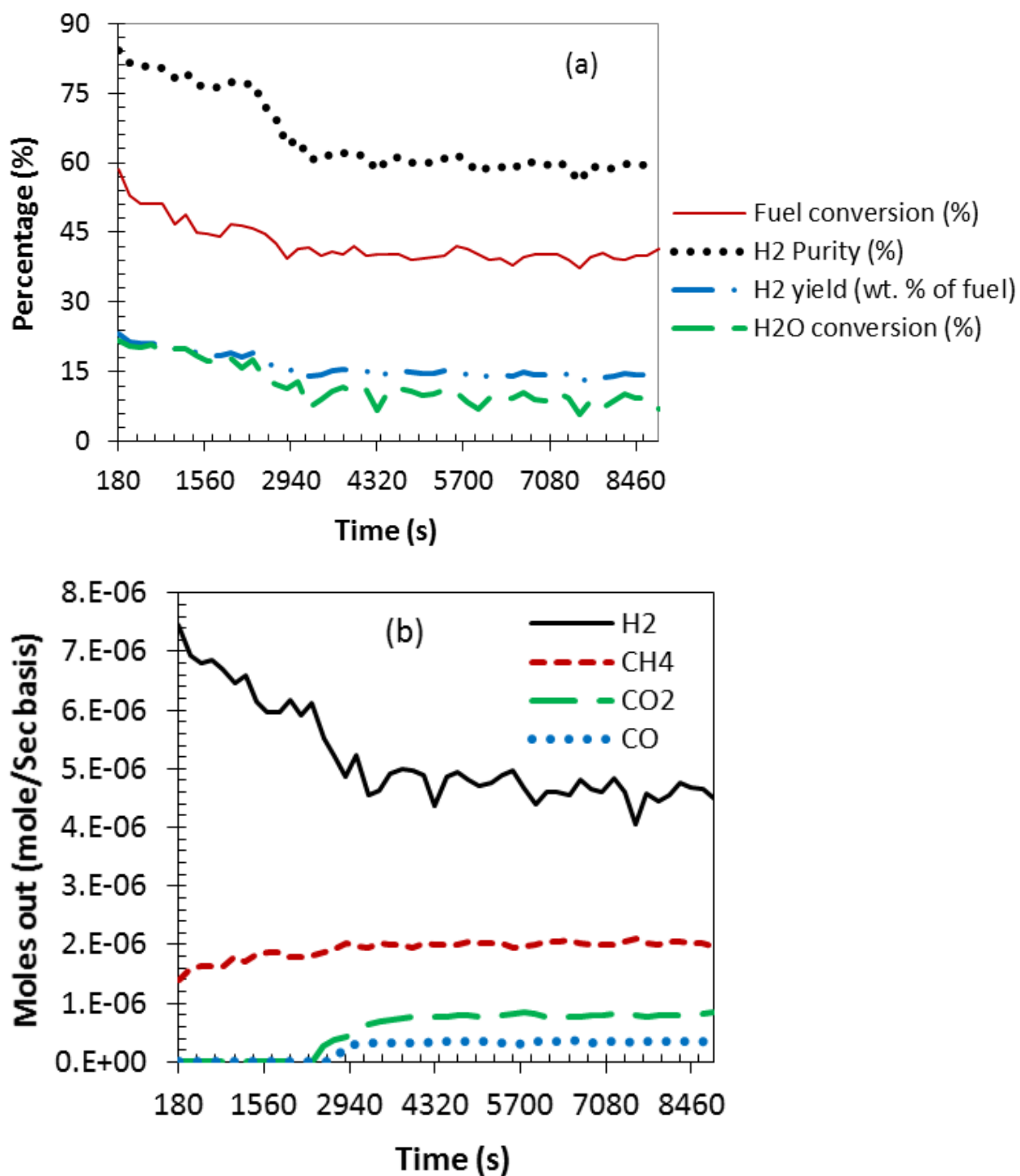


Figure B10.1 Process output vs time at 650 °C, 1 bar, GHSV 0.498 and S:C 3 (a) H<sub>2</sub> yield and purity, fuel and H<sub>2</sub>O conversion vs time using 18 wt. % NiO on Al<sub>2</sub>O<sub>3</sub> support catalyst (b) moles out vs time using 18 wt. % NiO on Al<sub>2</sub>O<sub>3</sub> support catalyst

## Appendix B11: CL-SR process outputs (Repeat experiments)

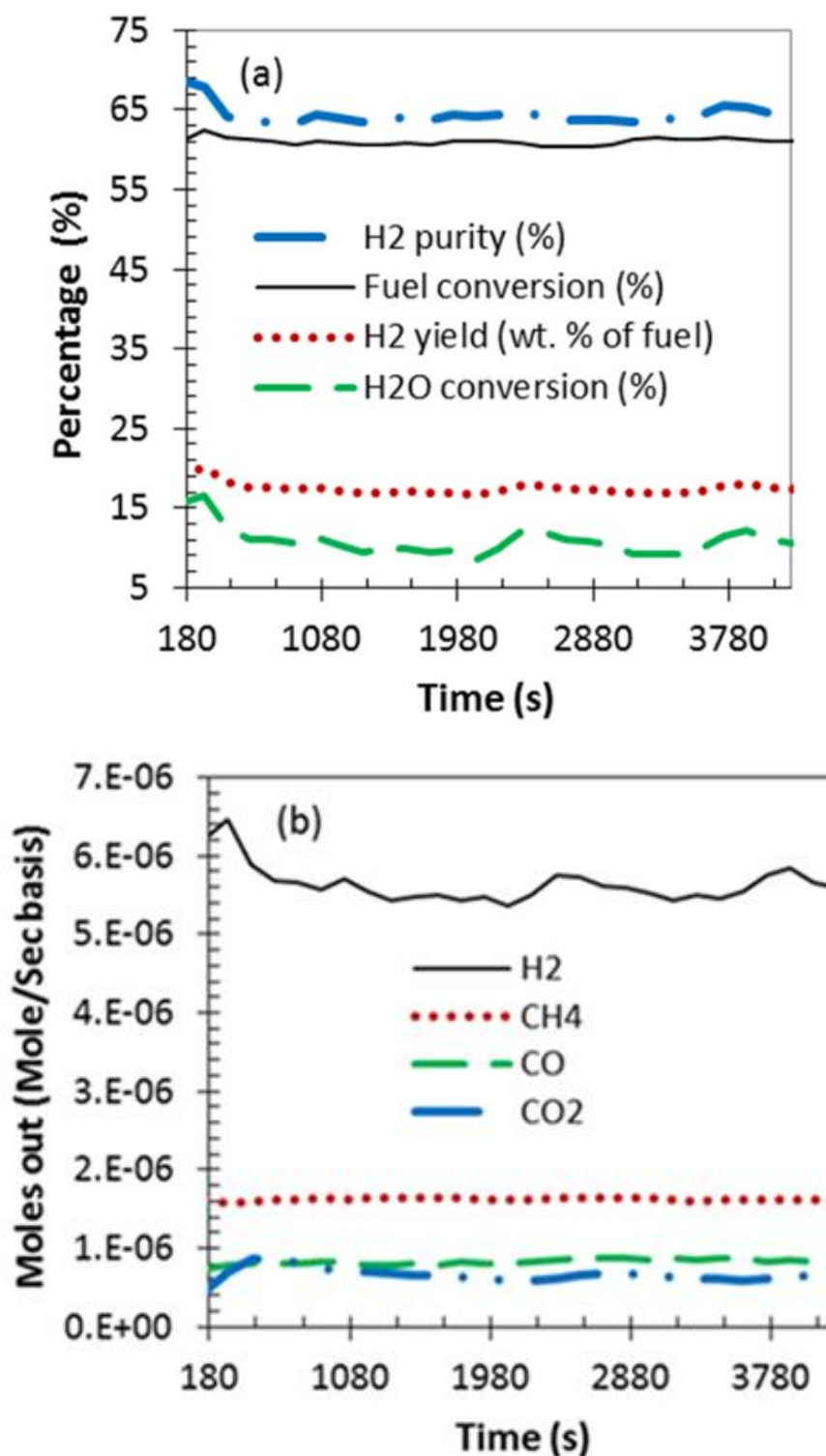


Figure B10.1 First cycle process output vs time at 650 °C, 1 bar, GHSV 0.498 and S:C 3 (a) H<sub>2</sub> yield and purity, fuel and H<sub>2</sub>O conversion vs time using 18 wt. % NiO on Al<sub>2</sub>O<sub>3</sub> support catalyst (b) moles out vs time using 18 wt. % NiO on Al<sub>2</sub>O<sub>3</sub> support catalyst

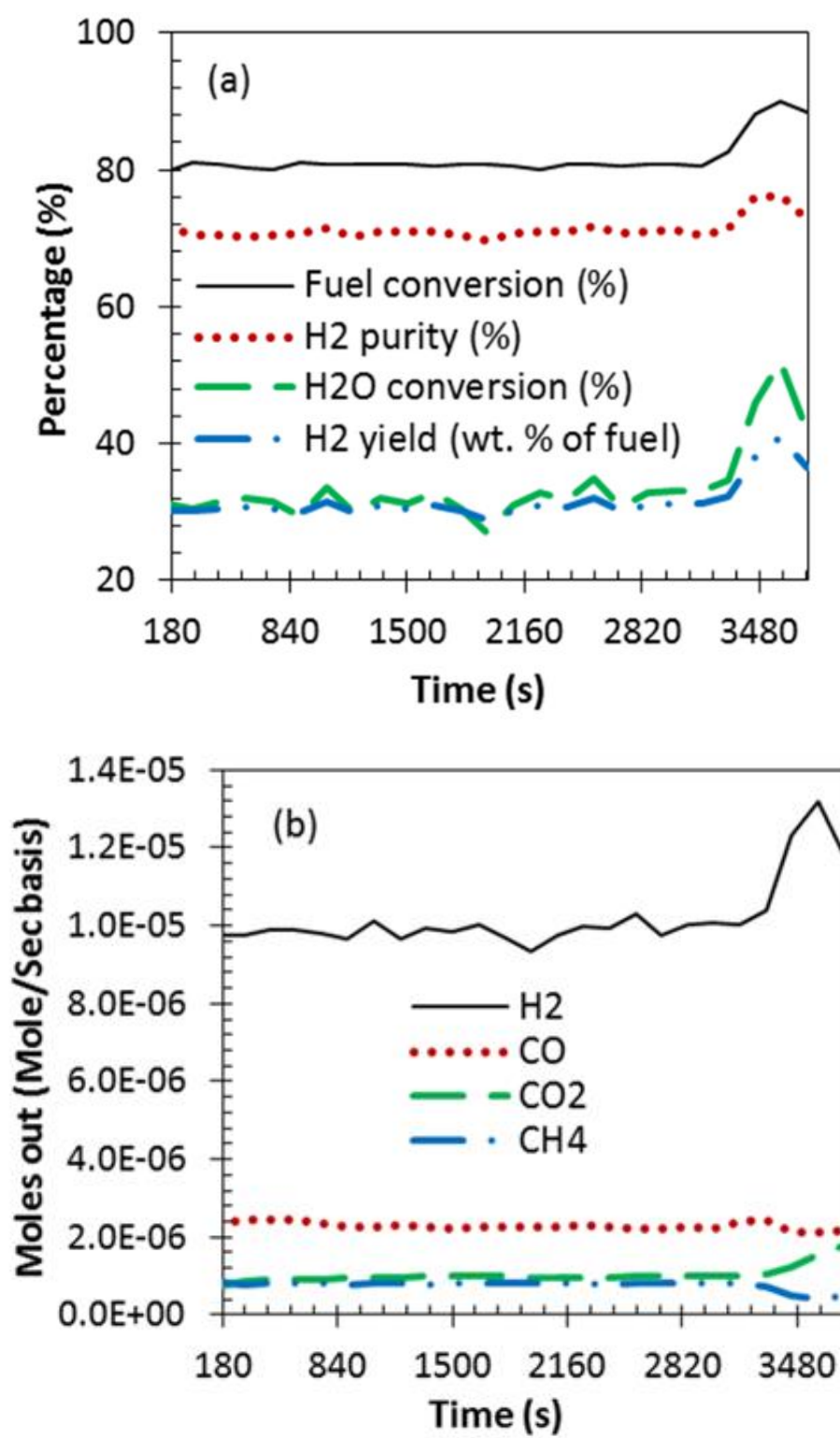


Figure B10.2 First cycle process output vs time at 750 °C , 1 bar, GHSV 0.498 and S:C 3 (a) H<sub>2</sub> yield and purity, fuel and H<sub>2</sub>O conversion vs time using 15 wt. % NiO on CaO/Al<sub>2</sub>O<sub>3</sub> support catalyst (b) moles out vs time using 15 wt. % NiO on CaO/Al<sub>2</sub>O<sub>3</sub> support catalyst

## Appendix B12: SECL-SR process outputs (Repeat experiment)

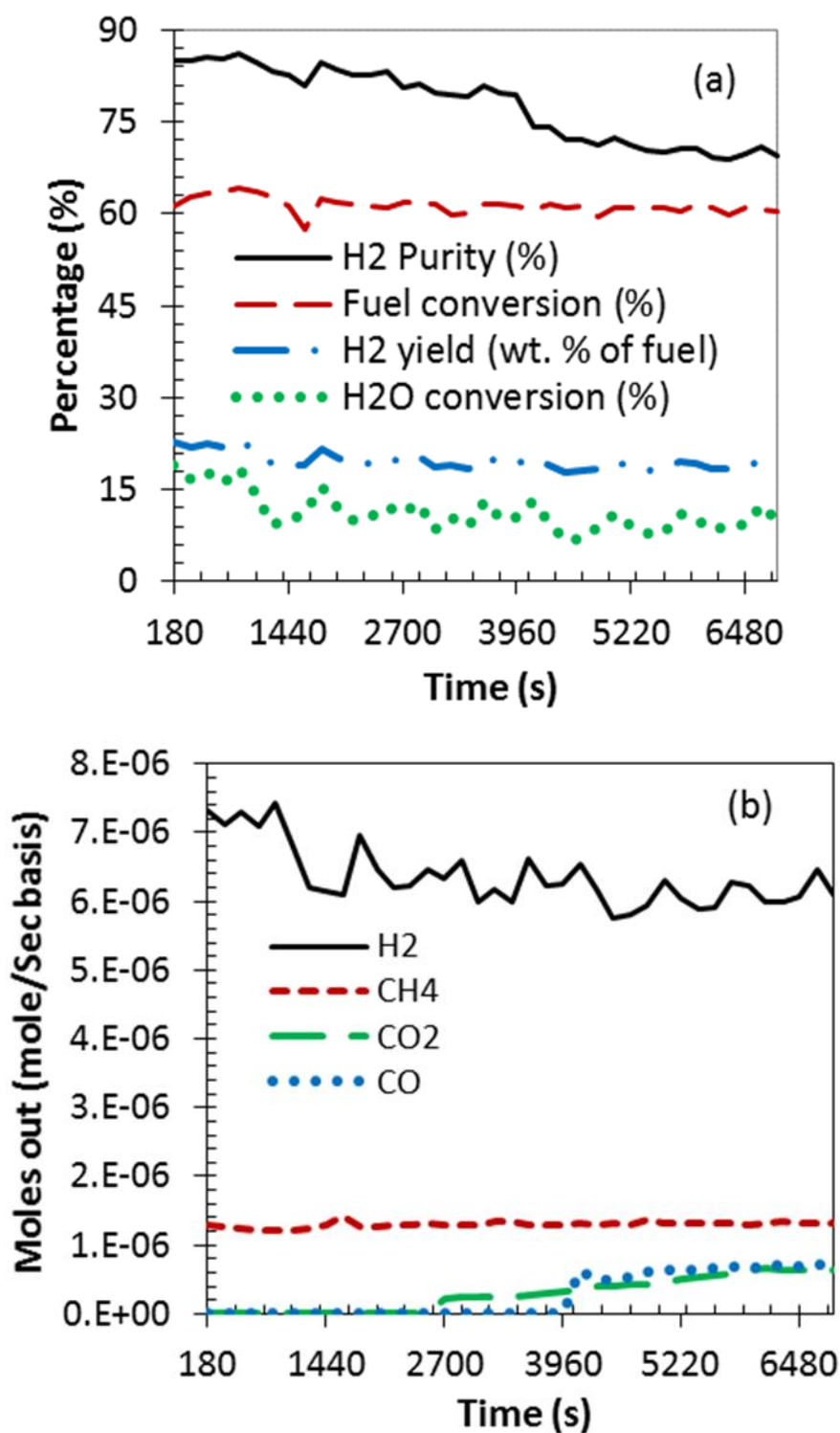


Figure B10.1 First cycle process output vs time at 650 °C, 1 bar, GHSV 0.498 and S:C 3 (a) H<sub>2</sub> yield and purity, fuel and H<sub>2</sub>O conversion vs time using 18 wt. % NiO on Al<sub>2</sub>O<sub>3</sub> support catalyst (b) moles out vs time using 18 wt. % NiO on Al<sub>2</sub>O<sub>3</sub> support catalyst

## Appendix C1: Process description diagrams

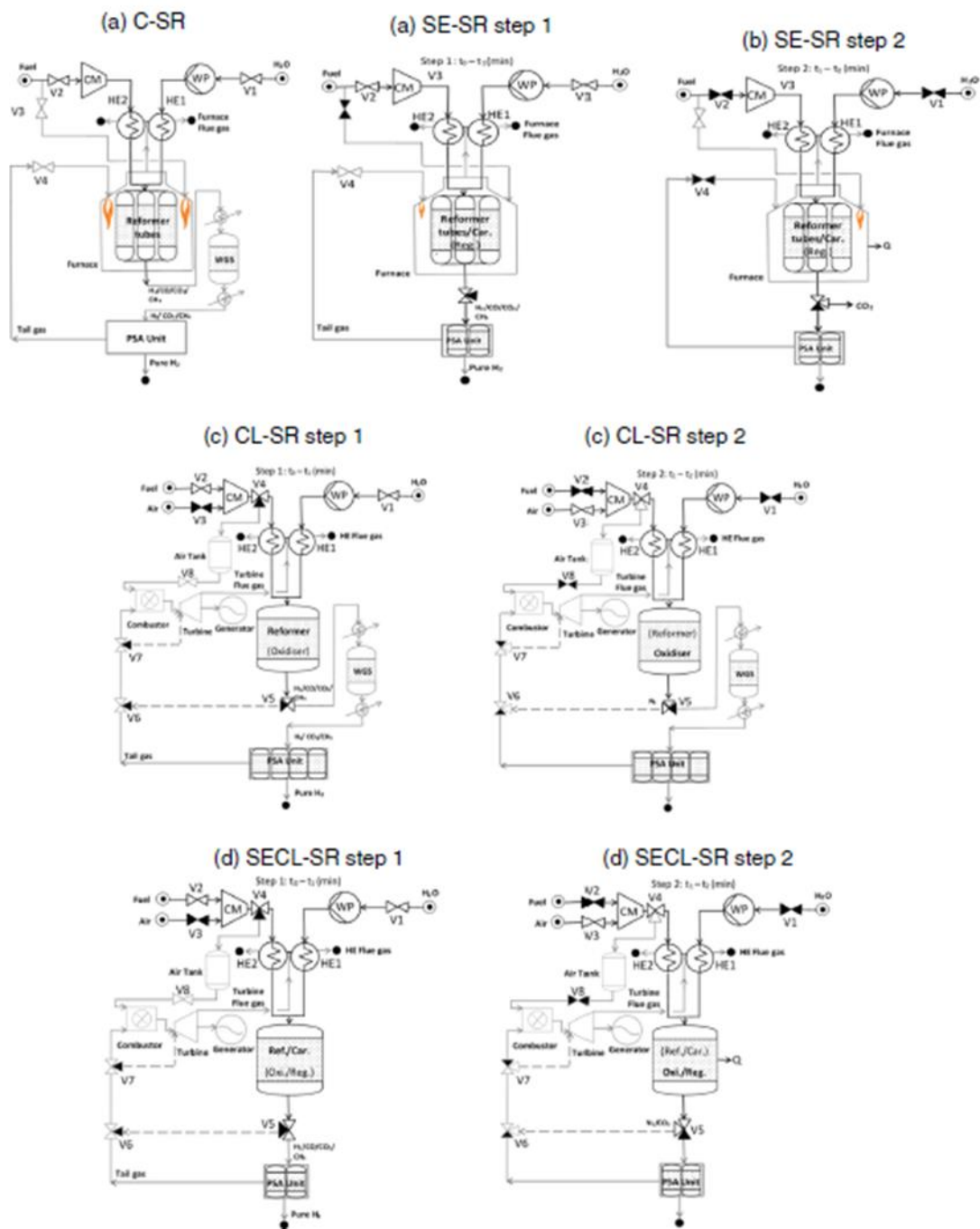


Figure C1.1 Figure 1 (a) C-SR, (b) SE-SR steps 1 & 2, (c) CL-SR steps 1 & 2 and (d) SE-CLSR steps 1 & 2 processes.  $\text{CaCO}_3(\text{S})$  regeneration occurs during step 2 (highlighted in black, using energy from the exothermic oxidation and gas turbine). Units in grey colour are not covered in our calculation. Blacked out valve symbols (if any) represent closed to flow. Size of flames in furnace are commensurate to heat input from relevant combustible flow (fresh fuel vs. separation unit tail gas).